Oxidative Medicine and Cellular Longevity

Oxidative Stress in Muscle Diseases: Current and Future Therapy

Lead Guest Editor: Andrey J. Serra
Guest Editors: Jose R. Pinto, Marko D. Prokić, Hafida Merzouk, and Andrea Vasconsuelo

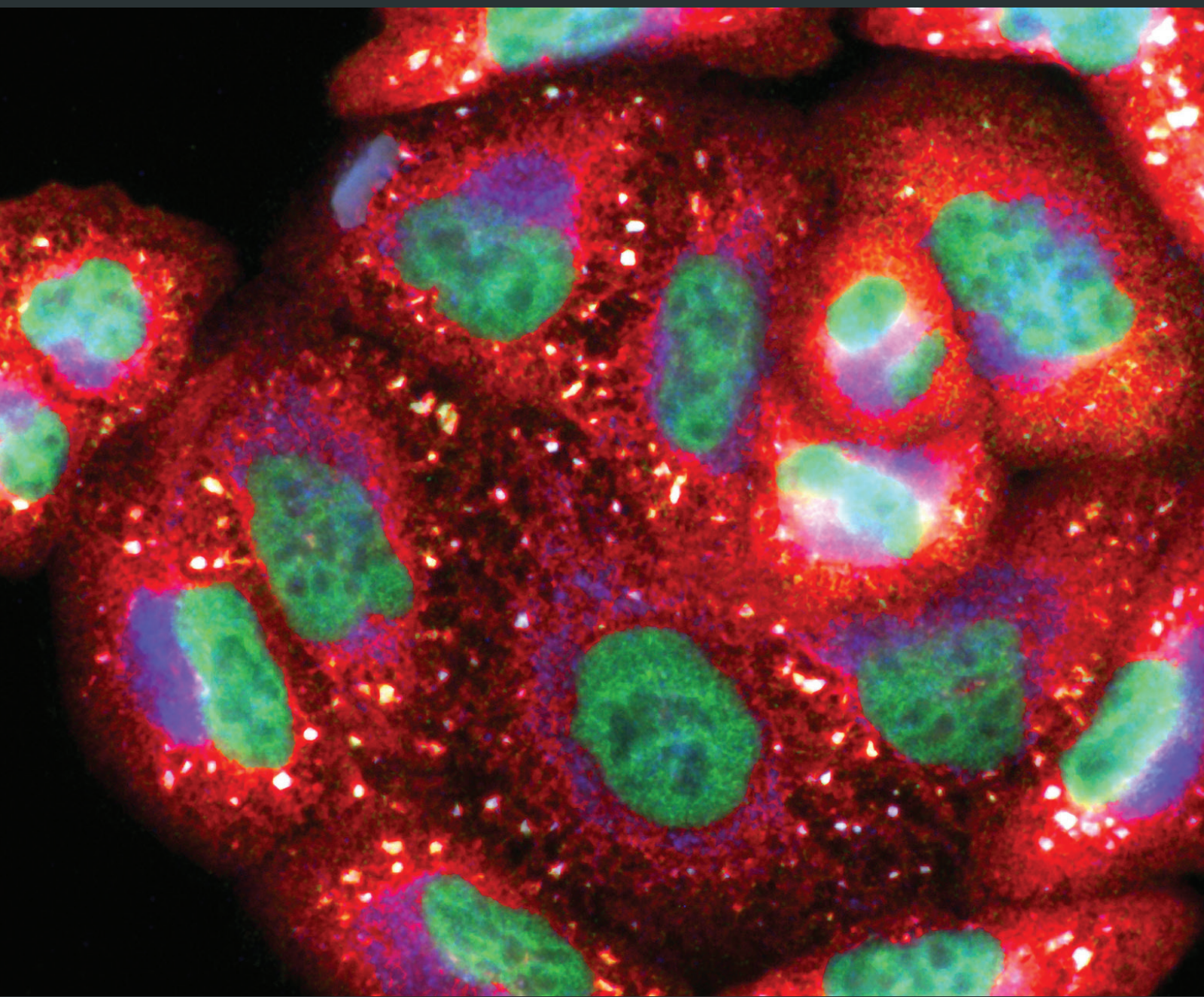

Oxidative Stress in Muscle Diseases: Current and Future Therapy

Oxidative Medicine and Cellular Longevity

Oxidative Stress in Muscle Diseases: Current and Future Therapy

Lead Guest Editor: Andrey J. Serra
Guest Editors: Jose R. Pinto, Marko D. Prokic, and Andrea Vasconsuelo

Editorial Board

Contents

Hindawi
Oxidative Medicine and Cellular Longevity
Volume 2018, Article ID 6439138, 4 pages
https://doi.org/10.1155/2018/6439138

Editorial

Oxidative Stress in Muscle Diseases: Current and Future Therapy

Andrey Jorge Serra,[1] **Marko D. Prokić**,[2] **Andrea Vasconsuelo**,[3] **and José Renato Pinto**[4]

[1]*Universidade Nove de Julho (UNINOVE), São Paulo, SP, Brazil*
[2]*University of Belgrade, Belgrade, Serbia*
[3]*Universidad Nacional del Sur, Bahia Blanca, Argentina*
[4]*Department of Biomedical Sciences, College of Medicine, Florida State University, Tallahassee, FL, USA*

Correspondence should be addressed to Andrey Jorge Serra; andreyserra@gmail.com

Received 14 February 2018; Accepted 18 February 2018; Published 26 April 2018

Oxidative stress can be considered a consequence of imbalance in the formation of reactive oxygen species (ROS) and antioxidant defense systems, in which mitochondria appear to be the main source of ROS production. A key concern is that high levels of ROS can modulate molecular and structural modifications and lead to functional changes within the muscle. In this regard, ROS causes oxidation of biomolecules, in which results in loss of their biological functions and leads to homeostatic imbalance. The main effects mediated by ROS relate to its potential to cause oxidative damage in cells and tissues [1]. Therefore, a ROS burst contributes to cellular dysfunction and can cause a wide range of chronic diseases. Scientific advances have allowed a better understanding of the role of oxidative stress on muscular homeostasis; thereby, deciphering and understanding how ROS regulate specific molecules and processes that alter physiological function could cause development of pathologies. Thus, studying the effects of ROS could assist with the development of new therapeutic avenues that address a wide range of muscle disorders.

This special issue encompasses cutting-edge research and review articles that focus on the role of oxidative stress in both acute and chronic progressive muscle disorders. This special issue provides a platform for sharing recent scientific advancements with researchers and practitioners who work in both skeletal and cardiac muscle scopes, which include clinical diagnostics, basic scientists, and physicians interested in physiology and physiopathology of muscle. Thus, articles included in this special issue address the molecular and cellular mechanisms involved in these processes as well as current therapeutic approaches in human and animals.

Two investigations in this special issue focus on physiological changes induced by acute exercise and subsequent oxidative stress in male runners who completed a marathon race in two different thermal conditions—hot and temperate environments, as well as a rat model of resistance exercise. In these studies, marathon running performance decreased up to 10%, while the wet bulb globe temperature increased from 10 to 25°C [2]. The investigation also highlighted that hot temperature induces pronounced homeostatic alterations, including a proinflammatory response, limited muscle oxygenation, and increased oxidative stress [3, 4]. In the study by H. A. de Oliveira et al., male marathon runners were studied to determine the effects of environmental temperature variation on hematological profiles; tissue damage and oxidative stress markers were investigated in men. The performance of marathon runners was reduced 13.5% in a hot environment (31.4°C) compared when they were performing at a lower temperature (19.8°C). In both environments, marathon racing promotes fluid and electrolyte imbalances, hemolysis, immune activation, tissue damage, and oxidative stress. Moreover, long-term exercise during heat stress conditions worsened running performance by causing hematological changes due to fluid and electrolyte imbalances and purine/protein oxidation of erythrocytes, which lead to renal damage and immune activation. On the other hand, the authors have concluded that reduced performance at hot environment is not associated with muscle damage and lipid peroxidation.

Exercise-induced increases in free radical formation are thought to play a key role in the mechanisms by which skeletal muscle adapts to exercise training [5, 6], whereas aerobic physical exercise appears to be the main trigger of free radical formation. In addition, resistance exercise can also evoke increased free radical production in muscle because of the occurrence of intermittent bouts of hypoxia/reperfusion. An excessive increase in oxidative stress or a free radical burst in working muscles can override the physiological benefits of exercise causing extensive damage to proteins and cellular dysfunction [7, 8]. This is a key concern during intense training stages, in which the burst in free radicals can overcome the existing antioxidant mechanisms. In fact, studies have reported beneficial effects of antioxidant agents used to counteract the increase in oxidative stress induced by exercise. In this special issue, R. A. Oliveira et al. applied low-intensity laser therapy in rat gastrocnemius muscle prior to a high-intensity resistance exercise session. The laser application brought about improvements in lipoperoxidation levels and the oxidized protein content in muscle. Moreover, laser therapy appeared to increase activity of antioxidant enzymes (i.e., superoxide dismutase and glutathione peroxidase) and led to higher total nonenzymatic antioxidant potential. Thus, photobiomodulation could be a promising antioxidant approach to counter risks associated with high-intensity resistance exercises. However, further studies are needed to better understand the influence of different irradiation dosages and the mechanisms that modulate oxidative stress linked to exercise.

Further analysis of the role of photobiomodulation was showed in a review article entitled "Effects of Photobiomodulation Therapy on Oxidative Stress in Muscle Injury Animal Models: A Systematic Review," which moves the focus on from the several models of experimental muscle injury (e.g., fatigue, cryoinjury, and traumatic insult). First, S. A. dos Santos et al. summarized that, despite the limited number of studies in this research area, photobiomodulation could be a factual approach to reduce oxidative stress markers (e.g., thiobarbituric acid reactive) and to increase antioxidant substances (e.g., superoxide dismutase, catalase, and glutathione peroxidase). Second, the authors' advocate "whole mechanisms" by which photobiomodulation could modulate oxidative stress generated during muscle injury. A possible mechanism is the improvement of mitochondrial function, which is associated with reduced free radical formation linked to superoxide dismutase, catalase, and glutathione peroxidase. The primary beneficial effect of photobiomodulation in different muscles may be its anti-inflammatory effects [9, 10]. In this regard, S. A. dos Santos et al. have considered that oxidative muscular homeostasis linked to photobiomodulation may be mediated by its anti-inflammatory action, which mitigates the migration of inflammatory cells (e.g., neutrophils and macrophages) and thus the source of ROS.

This special issue also covers the role of oxidative stress and antioxidants in different disorders using human cells and model organisms. A. J. O'Leary et al. explored the cellular and functional consequences of sustained hypoxic stress in a mouse model of acute hypoxia and the effects of N-acetyl cysteine (NAC) pretreatment. The authors showed that acute hypoxic stress increases the protein content of HIF-1α in the diaphragm as well as activated MAPK, mTOR, Akt, and FoxO3a signaling pathways. Acute hypoxic stress also led to increases in lipid peroxidation and FoxO3 and MuRF-56 1 gene expression in the diaphragm. The treatment with NAC at a dose of 200 mg/kg completely prevented hypoxia-induced diaphragm dysfunction in mouse models studied. NAC substantially enhanced cell survival signaling pathways which, along with its general antioxidant functions, prevented hypoxia-induced diaphragm oxidative stress. These findings may have relevance to develop treatment strategies for hypoxaemic respiratory patients and populations living at high altitudes. NAC treatment was also evaluated in a study conducted by A. Michelucci et al., in which RYR1$^{Y522S/WT}$ knock-in mouse, carrying a human mutation in RYR1 linked to malignant hyperthermia (MH) exhibiting *cores* with a NAC treatment regimen for either two or six months. They found that two months of NAC-treatment initiated at two months of age, when mitochondrial and fiber damage was still minimal, (i) reduced the formation of *unstructured* and *contracture cores*, (ii) improved muscle function, (iii) and decreased mitochondrial damage. The beneficial effects of NAC treatment was also evident following six months of treatment that was initiated later, at four months of age when structural damage was advanced. Likely, NAC exerts its protective effects by lowering oxidative stress, as supported by the reduction of 3-NT and Mn-superoxide dismutase levels. This work suggests that NAC-administration is beneficial and prevents mitochondrial damage and the formation of *cores* and improves muscle function in RYR1$^{Y522S/WT}$ mice. S. C. Khor et al. evaluated the effects of a 24 h treatment with the antioxidant tocotrienol-rich fraction (TRF), with the goal of reestablishing the oxidative status of myoblasts during replicative senescence. The effects of TRF on oxidative status were compared to the effects of other antioxidants (α-tocopherol (ATF) and NAC). Treatment with TRF was associated with diminished ROS production and lipid peroxidation in senescent myoblasts. Moreover, gene expression in senescent myoblasts of Mn-superoxide dismutase, catalase, and glutathione peroxidase was modulated by TRF. Additional parameters were affected by TRF including increased activity of superoxide dismutase and catalase and reduced glutathione peroxidase in senescent myoblasts. In comparison to ATF and NAC, TRF was more efficient at increasing antioxidant capacity and reducing insult caused by free radicals. The authors suggested that TRF can ameliorate antioxidant mechanisms and improve replicative senescence-associated oxidative stress in myoblasts.

An imbalance between oxidant and antioxidant systems has been proposed as a secondary effect in Duchenne muscular dystrophy (DMD, X-linked genetic disease). In this regard, the significance and precise extent of the perturbation in redox signaling cascades are poorly understood. L. Pelosi et al. tried to fill this gap of knowledge. The authors reported that mdx dystrophic mice can trigger a compensatory antioxidant response at the presymptomatic stage of the disease. On

the other hand, increased circulating levels of IL-6 perturb the redox signaling cascade, even prior to the development of necrosis, which is responsible for the severity and progressive nature of DMD disease. Multiple cellular and molecular mechanisms have been implicated in the DMD, which makes the disease complex to study and complicates the development of beneficial interventions. In this regard, M. D'Agostino et al. showed that miR-200c overexpression impaired skeletal muscle differentiation in cultured myoblasts and anti-miR-200c treatment ameliorated myogenic differentiation. Moreover, the authors found that miR-200c and p66Shc Ser-36 phosphorylation was increased in mdx muscles. These findings link miR-200c to muscle wasting in DMD, in which miR-200c overexpression can be evoked by ROS.

Accumulation of reactive oxygen species (ROS) can be mitigated by inbuilt mechanisms that help prevent excessive oxidative stress in cardiomyocytes during hypoxia-reoxygenation. Nitric oxide (NO) can compete successfully with oxygen when the myocardium experiences hypoxia. Therefore, NO accumulation can serve in a protective role by forming NO-Fe^{2+} complexes when chelating iron is released from oxygen complexes [11]. The study by V. I. Kapelko et al. explored the use of a stable NO donor (Oxacom®) (DNIC) dinitrosyle iron complex with glutathione to preserve the integrity of cardiomyocytes and improve functional outcomes in rat hearts after hypoxia-reoxygenation. This study is the first to report antihypoxic cardioprotective potential of Oxacom to counter hypoxic insult, including a reduction in hypoxic contractures, attenuation of cardiac arrhythmias, and an increase of left ventricular pressures during reoxygenation. Oxacom pretreatment substantially reduced ROS accumulation in hypoxia-treated rat cardiomyocytes. The reduction in ROS is expected to improve the performance of ion transporters and regulatory proteins, maintaining their thiol groups in a reduced state and protected by reversible S-nitrosylation [12, 13]. Oxacom eliminates slow sarcoplasmic Ca^{2+} removal as well as delayed relaxation of cardiomyocytes. These findings dovetail well, with the overall view that primary Ca^{2+} removal from the sarcoplasm by the energy-dependent ion transporters/exchangers is slowed down in hypoxia since high-energy phosphates and oxygen are depleted. Some of the protective effects of Oxacom may be derived by its impact on improving mitochondrial function. This will benefit contractile processes overall, which have even greater energy requirements. Overall, the authors conclude that Oxacom positively affects energy production and utilization, which may underlie its ability to prevent hypoxic contractures and the rapid functional recovery seen during reoxygenation.

Mechanisms to protect against oxidative stress appear to diverge between the different sexes. A study by A. Michelucci et al. addresses the unexplained sex differences that underlie vulnerability for developing malignant hyperthermia (MH), which is influenced by oxidative status. MH is a lethal disorder in humans, triggered by halogenated/volatile anesthetics, and caused by the release of excessive calcium in skeletal muscle [14, 15]. Estrogens protect calsequestrin-1 (CASQ1) knockout mice during lethal hyperthermic episodes, and the mechanism of protection relies on a reduction of oxidative stress in muscle. When male CASQ1-null mice are exposed to conditions that resemble human MH (halothane and heat), they experience a high incidence of mortality [16]. To explore the role of sex hormones in development of MH, A. Michelucci et al. treated male and female CASQ1-null mice with Premarin (conjugated estrogens) and Leuprolide (GnRH analog), respectively, for one month. Their findings demonstrate that previously vulnerable CASQ1-null males were largely protected from MH-induced mortality by Premarin treatment prior to exposure to halothane and heat, while CASQ1 females treated with Leuprolide suffered higher mortality rates after losing the protective effects of estrogen. To explore functional changes in these mice due to the hormonal treatments, individual muscles were exposed to temperature and caffeine. The sarcoplasmic Ca^{2+} release was measured in single fibers and levels of oxidative stress, and expression of the main redox regulators was measured. In summary, Premarin treatment in CASQ1-null males reduced muscle temperature and caffeine sensitivity, normalized the release of Ca^{2+} from the sarcoplasmic reticulum (SR), and reduced oxidative stress. Overall, female mice appear to be protected by female sex hormones from lethal hyperthermic episodes by reducing the amount of sarcoplasmic reticulum Ca^{2+} leak and oxidative stress.

An epidemiological study by E. Brunelli et al. examined a healthy population in Italy consisting of woman and man volunteers to look for early indicators of major cardiovascular risk factors [17–19]. Blood plasma from individuals was analyzed for prooxidant and antioxidant molecules. In high cardiovascular risk categories, a significant depletion in total plasma antioxidant barrier efficacy was found. As expected, increasing age correlated with increased oxidative status. In addition, individuals with metabolic disorders including diabetes, obesity, and dyslipidemia displayed significant depletion of the efficacy of total plasma antioxidant barrier. Known risk factors, such as cholesterol imbalance, appear to be the main element leading to depletion of total plasma-antioxidant barrier efficacy. Furthermore, minimal increases in both total serum cholesterol and total serum cholesterol/HDL as well as hypertension and slight increases in systolic blood pressure significantly increase oxidative status. In summary, this study identifies a primary prevention target and depletion of the antioxidant barrier, as the earliest detectable redox disturbance. This redox perturbation appears to pinpoint the likelihood that an individual will develop cardiovascular disease in the future due to overutilization of antioxidant-directed mechanisms.

We hope that this special issue is successful in providing new insights into the impact of oxidative stress in muscle on different physiological and pathological disorders. The findings presented here can be used to improve knowledge and understanding of changes induced by exercise on oxidative stress, in which low-intensity laser therapy is able to modulate excessive oxidative stress after physical effort. We also feel that this is an opportunity to report findings concerning the role of N-acetyl cysteine in different *in vitro* and *in vivo* models. Moreover, the editors considered the

interdisciplinary nature of the papers included as necessary to expand on concepts fundamental to basic research as well as those important to applied science. As a result, papers covering the effects of oxidative stress in Duchenne muscular dystrophy, cardiomyocyte hypoxia-reoxygenation, malignant hyperthermia, and cardiovascular risk were included. Therefore, the readers of this special issue should find information of interest, relevant to their respective area of scientific investigations.

Disclosure

The funding sources listed do not influence the selection of data presented in this editorial.

Acknowledgments

The guest editorial team would like to thank all authors of the contributed papers and review articles submitted to this special issue. We are very grateful to the various reviewers, who have donated their time, knowledge, and experience to review the manuscripts. We hope that you enjoy this special issue, dedicated to the exciting field of oxidative stress with an emphasis on physiology and physiopathology of muscle. Andrey Jorge Serra is a research fellow from the Fundação de Amparo à Pesquisa do Estado de São Paulo (FAPESP) (nos. 2015/11028-9 and 2017/09274-7) and Conselho Nacional de Desenvolvimento Científico e Tecnológico (CNPq) (no. 305527/2017-7). José Renato Pinto is supported by the National Institutes of Health (NIH) Grant R01HL128683.

Andrey Jorge Serra
Marko D. Prokić
Andrea Vasconsuelo
José Renato Pinto

References

[1] B. Halliwell and M. Whiteman, "Measuring reactive species and oxidative damage *in vivo* and in cell culture: how should you do it and what do the results mean?," *British Journal of Pharmacology*, vol. 142, no. 2, pp. 231–255, 2004.

[2] M. R. Ely, D. E. Martin, S. N. Cheuvront, and S. J. Montain, "Effect of ambient temperature on marathon pacing is dependent on runner ability," *Medicine & Science in Sports & Exercise*, vol. 40, no. 9, pp. 1675–1680, 2008.

[3] S. N. Cheuvront, R. W. Kenefick, S. J. Montain, and M. N. Sawka, "Mechanisms of aerobic performance impairment with heat stress and dehydration," *Journal of Applied Physiology*, vol. 109, no. 6, pp. 1989–1995, 2010.

[4] S. K. Gill, A. Teixeira, L. Rama et al., "Circulatory endotoxin concentration and cytokine profile in response to exertional-heat stress during a multi-stage ultra-marathon competition," *Exercise Immunology Review*, vol. 21, pp. 114–128, 2015.

[5] D. M. Bailey, L. Lawrenson, J. McEneny et al., "Electron paramagnetic spectroscopic evidence of exercise-induced free radical accumulation in human skeletal muscle," *Free Radical Research*, vol. 41, no. 2, pp. 182–190, 2007.

[6] M. C. Gomez-Cabrera, E. Domenech, M. Romagnoli et al., "Oral administration of vitamin C decreases muscle mitochondrial biogenesis and hampers training-induced adaptations in endurance performance," *The American Journal of Clinical Nutrition*, vol. 87, no. 1, pp. 142–149, 2008.

[7] L. T. Retamoso, M. E. P. Silveira Junior, F. D. Lima et al., "Increased xanthine oxidase-related ROS production and TRPV1 synthesis preceding DOMS post-eccentric exercise in rats," *Life Sciences*, vol. 152, pp. 52–59, 2016.

[8] M. Wiecek, M. Maciejczyk, J. Szymura, and Z. Szygula, "Effect of maximal-intensity exercise on systemic nitro-oxidative stress in men and women," *Redox Report*, vol. 22, no. 4, pp. 176–182, 2017.

[9] C. Ferraresi, Y. Y. Huang, and M. R. Hamblin, "Photobiomodulation in human muscle tissue: an advantage in sports performance?," *Journal of Biophotonics*, vol. 9, no. 11-12, pp. 1273–1299, 2016.

[10] M. T. Manchini, A. J. Serra, R. . S. Feliciano et al., "Amelioration of cardiac function and activation of anti-inflammatory vasoactive peptides expression in the rat myocardium by low level laser therapy," *PLoS One*, vol. 9, no. 7, p. e101270, 2014.

[11] P. Korge, P. Ping, and J. N. Weiss, "Reactive oxygen species production in energized cardiac mitochondria during hypoxia/reoxygenation: modulation by nitric oxide," *Circulation Research*, vol. 103, no. 8, pp. 873–880, 2008.

[12] S. Gyorke and D. Terentyev, "Modulation of ryanodine receptor by luminal calcium and accessory proteins in health and cardiac disease," *Cardiovascular Research*, vol. 77, no. 2, pp. 245–255, 2008.

[13] C. Figueiredo-Freitas, R. A. Dulce, M. W. Foster et al., "*S*-Nitrosylation of sarcomeric proteins depresses myofilament Ca^{2+} sensitivity in intact cardiomyocytes," *Antioxidants & Redox Signaling*, vol. 23, no. 13, pp. 1017–1034, 2015.

[14] D. MacLennan and M. Phillips, "Malignant hyperthermia," *Science*, vol. 256, no. 5058, pp. 789–794, 1992.

[15] H. Rosenberg, N. Sambuughin, S. Riazi, and R. Dirksen, "Malignant hyperthermia susceptibility," in *GeneReviews*, M. P. Adam, H. H. Ardinger, R. A. Pagon, S. E. Wallace, L. J. H. Bean, K. Stephens, and A. Amemiya, Eds., University of Washington, Seattle, WA, USA, 2003.

[16] M. Dainese, M. Quarta, A. D. Lyfenko et al., "Anesthetic- and heat-induced sudden death in calsequestrin-1-knockout mice," *The FASEB Journal*, vol. 23, no. 6, pp. 1710–1720, 2009.

[17] W. B. Kannel, T. R. Dawber, A. Kagan, N. Revotskie, and J. Stokes 3rd, "Factors of risk in the development of coronary heart disease—six year follow-up experience: the Framingham study," *Annals of Internal Medicine*, vol. 55, no. 1, pp. 33–50, 1961.

[18] D. Levy, P. W. F. Wilson, K. M. Anderson, and W. P. Castelli, "Stratifying the patient at risk from coronary disease: new insights from the Framingham Heart Study," *American Heart Journal*, vol. 119, no. 3, pp. 712–717, 1990.

[19] F. D. R. Hobbs, "Cardiovascular disease: different strategies for primary and secondary prevention?," *Heart*, vol. 90, no. 10, pp. 1217–1223, 2004.

Hindawi
Oxidative Medicine and Cellular Longevity
Volume 2018, Article ID 4805493, 19 pages
https://doi.org/10.1155/2018/4805493

Research Article

Diaphragm Muscle Weakness Following Acute Sustained Hypoxic Stress in the Mouse Is Prevented by Pretreatment with N-Acetyl Cysteine

Andrew J. O'Leary,[1] Sarah E. Drummond,[1] Deirdre Edge,[2] and Ken D. O'Halloran[1]

[1]*Department of Physiology, School of Medicine, University College Cork, Cork, Ireland*
[2]*Department of Physiology, Trinity Biomedical Sciences Institute, Trinity College Dublin, The University of Dublin, Dublin, Ireland*

Correspondence should be addressed to Ken D. O'Halloran; k.ohalloran@ucc.ie

Received 2 June 2017; Revised 29 October 2017; Accepted 12 December 2017; Published 19 February 2018

Academic Editor: Andrey J. Serra

Oxygen deficit (hypoxia) is a major feature of cardiorespiratory diseases characterized by diaphragm dysfunction, yet the putative role of hypoxic stress as a driver of diaphragm dysfunction is understudied. We explored the cellular and functional consequences of sustained hypoxic stress in a mouse model. Adult male mice were exposed to 8 hours of normoxia, or hypoxia ($FiO_2 = 0.10$) with or without antioxidant pretreatment (N-acetyl cysteine, 200 mg/kg i.p.). Ventilation and metabolism were measured. Diaphragm muscle contractile function, myofibre size and distribution, gene expression, protein signalling cascades, and oxidative stress (TBARS) were determined. Hypoxia caused pronounced diaphragm muscle weakness, unrelated to increased respiratory muscle work. Hypoxia increased diaphragm HIF-1α protein content and activated MAPK, mTOR, Akt, and FoxO3a signalling pathways, largely favouring protein synthesis. Hypoxia increased diaphragm lipid peroxidation, indicative of oxidative stress. FoxO3 and MuRF-1 gene expression were increased. Diaphragm 20S proteasome activity and muscle fibre size and distribution were unaffected by acute hypoxia. Pretreatment with N-acetyl cysteine substantially enhanced cell survival signalling, prevented hypoxia-induced diaphragm oxidative stress, and prevented hypoxia-induced diaphragm dysfunction. Hypoxia is a potent driver of diaphragm weakness, causing myofibre dysfunction without attendant atrophy. N-acetyl cysteine protects the hypoxic diaphragm and may have application as a potential adjunctive therapy.

1. Introduction

The diaphragm is the principal muscle of inspiration, an integral part of the thoracic "pump" musculature, responsible for effective lung ventilation. Diaphragm muscle weakness can present in respiratory disease, and it is a strong predictor of poor outcome in clinical patients, particularly those requiring mechanical ventilation [1]. Hypoxia (oxygen deficit) commonly presents as a feature in many acute respiratory conditions including acute respiratory distress syndrome, ventilator-induced lung injury, ventilator-associated lung injury, and acute lung injury, conditions where diaphragm muscle weakness is typically observed [2–6]. Interventions serving to prevent or suppress diaphragm muscle weakness in hypoxaemic respiratory patients could have substantially beneficial effects for patient outcome. Whereas this is an area of intense research, it appears that the potentially deleterious role of hypoxic stress in the development and manifestation of diaphragm muscle weakness has been overshadowed by other factors such as mechanical unloading (inactivity), injury, infection, and sepsis, despite the potential for significant cellular redox modulation during oxygen deficit, and the well-recognized dominant role of oxidative stress as a contributory factor in respiratory and skeletal muscle wasting in critically ill patients [7–12].

It is established that exposure to chronic sustained hypoxia results in respiratory myofibre atrophy and muscle weakness associated with a time-dependent progressive oxidative stress [13–16]. We recently demonstrated that acute sustained hypoxia (8 hours of exposure) is sufficient

to weaken mouse diaphragm peak force-generating capacity by ~30% [17, 18]. Our finding provides a basis for the hypothesis that acute hypoxia-induced diaphragm dysfunction could be an underrecognized and yet major factor contributing to diaphragm weakness in the critical care setting [18], and perhaps during exposure to environmental hypoxia at high altitude [19–21].

It is recognized that antioxidants have considerable therapeutic efficacy in the treatment of respiratory-related disorders featuring redox imbalance and overt oxidative stress, such as acute lung injury, sepsis, chronic obstructive pulmonary disease, chronic bronchitis, lung fibrosis, and cystic fibrosis [22–30]. N-acetyl cysteine (NAC) is a free radical scavenger, which boosts the synthesis of the endogenous antioxidant glutathione as well as other antioxidant systems. Chronic NAC supplementation has been shown to prevent diaphragm muscle weakness in animal models of chronic sustained hypoxia [16] and chronic intermittent hypoxia [31, 32]. Of interest, acute respiratory distress syndrome patients are in a prooxidant state, which can be improved by NAC supplementation, by increasing glutathione, thiol molecules, and antioxidant defences [33]. The muscles of breathing, like other striated muscles, are highly dependent on redox balance for optimal function [15, 16, 34, 35]. We reasoned that acute hypoxic stress is detrimental to muscle function. If so, antioxidant intervention may alleviate acute hypoxia-induced diaphragm dysfunction, a finding which if it translates to humans could prove useful in the treatment of hypoxaemic respiratory patients in the clinic.

Therefore, we sought to further explore the cellular mechanisms underpinning acute hypoxia-induced diaphragm weakness and establish if pretreatment with NAC at the outset of acute hypoxic exposure prevents or ameliorates diaphragm muscle weakness. The aims of our study were to (1) confirm the deleterious effects of acute sustained hypoxia on mouse diaphragm force-frequency relationship; (2) determine the whole body integrative ventilatory and metabolic strategies adopted by mice during acute hypoxic exposure; (3) examine protein signalling pathways in diaphragm muscle, putatively affected by acute hypoxic stress; (4) examine gene expression changes in the diaphragm associated with atrophy and autophagy processes; (5) determine if 20S proteasome activity is increased by acute hypoxic stress in the diaphragm; (6) determine if diaphragm myofibre size and distribution are affected by acute hypoxia; (7) determine if acute hypoxia causes diaphragm oxidative stress; and (8) explore the efficacy of NAC pretreatment in ameliorating diaphragm functional responses to acute sustained hypoxia.

2. Methods

2.1. Ethical Approval. All protocols involving animals described in this study were performed under licence from the Irish Government in accordance with the National and EU legislation following institutional animal research ethics committee approval.

2.2. Animal Model. Models of acute hypoxia were generated using adult male C57BL6/J mice (Envigo, UK). Mice (~14 weeks of age) were placed in environmental plethysmography chambers (Buxco Ltd., USA), at room temperature, in which ambient oxygen levels were measured and adjusted to desired levels (gas analyzer, ML206, AD Instruments, UK). Mice were exposed to one, four, or eight hours of hypoxia (fraction of inspired oxygen, $FiO_2 = 0.10$) or normoxia ($FiO_2 = 0.21$) ($n = 8$ per group). An additional group of mice ($n = 8$) were each given a single injection of N-acetyl cysteine (NAC; 200 mg/kg; i.p.) immediately prior to 8 hours of hypoxia exposure.

2.3. Whole Body Plethysmography. Breathing parameters, including respiratory frequency (f_R), tidal volume (V_T), and minute ventilation ($\dot{V}_E$) were measured on a breath-by-breath basis. O_2 consumption ($\dot{V}O_2$) and CO_2 production ($\dot{V}CO_2$) were monitored over the course of the gas exposure, serving as an index of whole body metabolism. Gas concentrations entering and leaving the plethysmography chambers were sampled using a gas analyzer (ML206, AD Instruments). The respiratory exchange ratio ($\dot{V}CO_2/\dot{V}O_2$) and the ventilatory equivalent for carbon dioxide ($\dot{V}_E/\dot{V}CO_2$) were determined offline. Following 8 hours of gas exposure, animals were euthanized using a rising concentration of CO_2 until narcosis, followed immediately by cervical dislocation to confirm euthanasia. Core body temperature was determined immediately postmortem, via insertion of a probe (TH-8 Thermalert, Physitemp Instruments, Inc., USA); body mass was recorded. Diaphragm muscles were quickly excised and either immediately used for functional analysis or immediately snap frozen in liquid nitrogen and stored at −80°C until further processing for molecular analysis.

2.4. Muscle Physiology: Experimental Setup. Experiments were performed on diaphragm muscle preparations derived from the 3 groups of mice: normoxia, hypoxia, and hypoxia + NAC. Once excised, diaphragm muscles were placed in a holding bath containing continuously gassed (95% O_2/5% CO_2) Krebs solution at room temperature. A longitudinal strip of diaphragm muscle with rib and central tendon intact was prepared and mounted vertically in a tissue holder by attaching the rib to a fixed hook and connecting the tendon to a force transducer (Aurora Scientific, USA) for the assessment of isometric contractile parameters. The preparation was housed in a tissue bath of Krebs solution at 35°C, gassed with 95% O_2/5% CO_2.

2.5. Muscle Physiology: Experimental Protocol. Muscle preparations were set to optimal length by adjusting the length of the tissue bundle between repeated twitch contractions until peak twitch force was determined. The relationship between stimulation frequency and tetanic force generation (force-frequency relationship) was assessed by stimulating the muscle strip at increasing stimulation frequencies from 10 Hz to 160 Hz and recording the force generated at each frequency. Forces recorded at each frequency were then normalized to the estimated cross-sectional area of the muscle tissue bundle, and data were expressed as specific force in N/cm^2.

2.6. Gene Expression: RNA Extraction and Preparation. Total RNA was extracted from 20–70 mg of frozen diaphragm

tissue homogenized using a general laboratory homogenizer (Omni-Inc., USA) in the presence of Tripure Isolation Reagent (Roche Diagnostics Ltd., UK). The manufacturer's instructions were followed with the addition of a chloroform wash step during phase separation. Next, RNA was treated with TURBO DNA-free Kit (Life Technologies, Bio-Sciences, Ireland) in accordance with the manufacturer's instructions. The quantity and purity of RNA were assessed using a Nanodrop 1000 (Thermo Scientific, USA) and spectrophotometry. The integrity of RNA was assessed by visualization of clear 18S and 28S ribosomal RNA bands using an agarose gel electrophoresis system (E-gel, Life Technologies).

2.7. Gene Expression: Reverse Transcription. Diaphragm muscle RNA was reverse transcribed using Transcriptor First Strand cDNA Synthesis Kit (Roche Diagnostics Ltd.) in accordance with the manufacturer's instructions.

2.8. Gene Expression: qRT-PCR. cDNA was amplified using Realtime ready Catalog or Custom Assays (Roche Diagnostics Ltd.) and Fast Start Essential DNA Probe Master (Roche Diagnostics Ltd.) in 20 μl reactions (5 μl cDNA and 15 μl master mix) using the LightCycler 96 (Roche Diagnostics Ltd.) on 96-well plates, in accordance with the manufacturer's instructions. All reactions were performed in duplicate and reverse transcriptase negatives, RNA negatives, and cDNA negatives (no template), and plate calibrator controls were used on every plate. Diaphragm gene expression was normalized to a reference gene, *hprt1*, to compensate for variations in input amounts of RNA/cDNA and the efficiency of reverse transcription. In preliminary studies, several candidate reference genes were screened, and in consideration of temporal and gas (hypoxia) exposures, *hprt1* was found to be most stable. The relative expression of genes was calculated using the $\Delta\Delta$CT method, that is, normalized expression of the gene of interest to that of the reference gene, with changes in expression displayed as a fold change relative to the control group.

2.9. Cell Signalling: Protein Extraction and Quantification. Frozen muscle samples were removed from storage at −80°C, weighed and homogenized on ice in ice-cold 2.5% *w*/*v* modified radioimmunoprecipitation assay (RIPA) buffer (1X RIPA, deionized H_2O, 200 mM sodium fluoride, 100 mM phenylmethylsulfonylfluoride (PMSF), 1X protease inhibitor cocktail, and 2X phosphatase inhibitor cocktail) using a general laboratory homogenizer (Omni-Inc., USA). Following 20-minute lyse time on ice, with vortexing every 4 minutes, samples were centrifuged in a U-320R centrifuge (Boeckel & Co, Germany) at 14,000 RPM at 4°C for 20 minutes to separate insoluble cellular fractions from the protein homogenates. The protein containing supernatant was separated from the insoluble pellet in each sample, and these were stored at −80°C. The pellets were discarded.

The protein concentration of each sample was determined using a bicinchoninic acid (BCA) protein quantification assay (Pierce Biotechnology, (Fisher Scientific), Ireland) as per the manufacturer's instructions, at a dilution of 1 : 3.

2.10. Cell Signalling: Hypertrophy, Atrophy and HIF Signalling, and Protein/Phosphoprotein Content Assays. Cell signalling assays were performed using an Akt signalling panel–phospho-Akt, phospho-p70S6K, phospho-S6RP, and phospho-GSK-3β; Phospho-/Total mTOR; Phospho-FOXO3a; a MAP Kinase phosphoprotein panel–phospho-p-38, phospho-ERK1/2, and phospho-JNK; and total HIF-1α (MesoDiscovery, USA).

The assays measure the protein or phosphorylated protein content of signalling proteins listed above. The sandwich immunoassays were either in multiplex format (Mesoscale Discovery, USA) allowing the measurement of up to 4 proteins/phosphoproteins in one well, or singleplex assay which allowed measurement of the content of one protein/phosphoprotein per well. The assay was carried out in accordance with the manufacturer's instructions. Briefly, samples were loaded onto the 96-well plate and incubated to allow the proteins of interest to be captured by their specific capture antibodies. Each well was then washed and incubated in a detection antibody solution. The detection antibodies, specific for each protein of interest, are conjugated with an electrochemiluminescent compound, or tag. The detection antibodies bind to the captured proteins of interest, which are bound to their specific capture antibodies, on the distinct spots on the bottom surface of the well. This completes the antibody-protein-antibody sandwich. The well was then washed again, and read buffer was added, creating the correct chemical environment for electrochemiluminescence. The plate was loaded into the MSD SECTOR Imager (a specialized spectrophotometer from Mesoscale) where a voltage is rapidly applied to the distinct working electrodes on the plate spots resulting in the tags conjugated to the antibodies attached to those electrodes emitting light, which is read by the imager at 620 nm. The intensity of this emitted light from each spot, separated both temporally and spatially, provides a quantitative measurement for each protein of interest in the sample. This assay was performed on diaphragm samples from control, hypoxia, and hypoxia + NAC groups. A series of dilutions with muscle sample was also assayed as a control to demonstrate increased luminescence with increased protein content added to the well for each assay.

2.11. Thiobarbituric Acid Reactive Substances (TBARS) Assay. TBARS are degradation products of fats which are routinely used as a marker of lipid peroxidation, an indirect measurement of oxidative stress. Malondialdehyde (MDA) of a known concentration was used to generate a standard curve. Next, 50 μl of thiobarbituric acid (TBA, 50 mM) was added to 50 μl of diaphragm muscle homogenate (as described above in section 2.9), and the solution was incubated for 60 mins at 97°C. Samples were subsequently cooled on ice, and 75 μl of methanol : 1 mM NaOH (91 : 9) was added to the solution. Samples were then centrifuged at 704*g*, and 70 μl of the resultant supernatant was added per well in a black 96-well plate. The plate was read in a SpectraMax-M3 spectrophotometer (Molecular Devices, USA) using 523/553 excitation/emission settings, and data were compared with standards. Data are expressed as nM TBARS per mg of protein in the sample, determined by BCA assay.

2.12. Proteasome Activity Assay. Chymotrypsin-like 20S proteasome activity was measured via fluorescence in a spectrophotometric assay as per the manufacturer's instructions (Abcam, UK) using a Spectramax M3 spectrophotometer (Molecular Devices, USA). The assay employs a peptide substrate tagged to AMC. In the presence of proteasome activity, the AMC tag is released and fluoresced. The kit includes a positive control in the form of Jurkat cell lysate with high proteasome activity and a specific proteasome inhibitor MG-132, which suppresses all proteolytic activity attributed to proteasomes, thus allowing the differentiation of proteasome activity from other protease activity in the sample. This assay was performed on diaphragm samples from normoxia, hypoxia, and hypoxia + NAC groups on a white 96-well plate; all samples and positive controls were assayed with and without the proteasome inhibitor. The samples, positive controls, and standards were added to the 96-well plate. Inhibitor was added to assigned wells (an equal volume of assay buffer was added to the uninhibited wells), and proteasome substrate was added to all wells except the standards. The plate was then incubated at 37°C in the spectrophotometer (protected from light) for one hour while fluorometric readings were made kinetically over that time at Ex/Em = 350/440 nm. There was a slight nonlinearity to the reaction kinetics at the beginning due to the lag time it takes for the reaction to mix and warm to 37°C. Readings were made from the linear range of the reaction. Nonproteasome activity was then subtracted from total activity to give proteasome activity. One unit of proteasome activity is defined as the amount of proteasome which generates 1 nmol of AMC per minute at 37°C.

2.13. Muscle Immunohistochemistry. Sections of hemidiaphragm from control ($n = 6$) and hypoxia ($n = 6$) mice were mounted on cubes of liver to facilitate subsequent tissue sectioning. Samples were coated in optimum cutting temperature (OCT; VWR International, Dublin, Ireland) embedding medium and then quickly frozen in isopentane (Sigma Aldrich, Wicklow, Ireland) cooled in liquid nitrogen. Tissue samples were subsequently stored at −80°C for structural analysis at a later time. Serial transverse muscle sections (10 μm) were generated using a cryostat (Leica CM3050; Leica Microsystems, Nussloch, Germany) at −22°C and mounted on polylysine-coated glass slides (VWR International, Dublin, Ireland). Slides were immersed for 15 minutes in phosphate-buffered saline (PBS, 0.01 M) containing 1% bovine serum albumin (BSA). After PBS washes (3 × 5 minute), slides were next immersed for 30 minutes in PBS containing 5% normal goat serum (Sigma Aldrich, Wicklow, Ireland). Slides then underwent PBS washes (3 × 5 minute) prior to the application of the primary antibody (rabbit anti-laminin, 1 : 200; Sigma Aldrich, Wicklow, Ireland), diluted in PBS and 1% BSA. Slides were then incubated overnight at 4°C in a humidity chamber. The following day, slides were washed with PBS (3 × 5 minutes) before application of the secondary antibody (FITC-conjugated goat anti-rabbit; 1.250, Sigma Aldrich, Wicklow, Ireland), which was diluted in PBS and 1% BSA. Slides were incubated for 1 hour at room temperature in the dark.

Using an Olympus BX51 microscope and an Olympus DP71 camera, muscle sections were viewed at ×10 magnification and images were captured for analysis. For each animal, several images from separate muscle sections were captured for analysis. We employed a square test frame of 600 × 600 μm, with inclusion and exclusion boundaries, which was placed randomly over each image [32]. To determine the size of diaphragm muscle fibres, the individual fibre perimeters were manually highlighted using Image J software allowing the determination of fibre cross-sectional area and minimal Feret's diameter. The coefficient of variation of these parameters was also computed. Data generated from multiple sections were first averaged for each animal before computing group means. Relative frequency histograms were constructed to illustrate the distribution of muscle fibre size in sections from control and hypoxia mice.

2.14. Data and Statistical Analysis. GraphPad Prism (GraphPad Software Inc., USA) was used to perform statistical analysis. Following tests for normality and equal variance in the data sets, the Student *t*-tests were performed for comparisons between two groups: normoxia and hypoxia. For multiple groups, one-way or two-way ANOVA (with Tukey's and Bonferroni post hoc tests, resp.) were used as appropriate. Statistical significance was taken at the level of $p < 0.05$.

3. Results

3.1. Diaphragm Force. The mouse diaphragm force-frequency relationship following exposure to 8 hours of normoxia, hypoxia, and hypoxia + NAC is displayed in Figure 1. Specific force-generating capacity of the diaphragm muscle increased as a function of stimulation frequency (10–160 Hz; frequency: $p < 0.0001$, two-way ANOVA). Specific force generation over the range of stimulation frequencies tested was significantly lower in the hypoxia group compared with the normoxia group (gas: $p = 0.0112$); this weakness was most prominent at higher stimulation frequencies. A single i.p. injection of NAC prior to hypoxic exposure completely prevented hypoxia-induced diaphragm muscle weakness ($p < 0.0001$ versus hypoxia). Indeed, the hypoxia + NAC group developed the highest forces, exceeding control values over the range of stimulation frequencies (Figure 1).

3.2. Metabolism and Breathing. CO_2 production over 8 hours of exposure to normoxia (control) and hypoxia is shown in Figure 2(a). CO_2 production was significantly lower in the hypoxia group compared with the normoxia group (two-way ANOVA; gas: $p < 0.0001$) over the duration of the gas exposures, revealing a hypometabolic response to sustained hypoxia in mice.

Postmortem body temperature following gas treatments in all 3 groups is shown in Figure 2(b). Compared with mice in the normoxia group, body temperatures were lower in mice exposed to hypoxia ($p < 0.0001$, unpaired *t* test) and hypoxia + NAC ($p = 0.0105$, unpaired *t* test with Welch's correction). There was no difference in body temperature between hypoxia and hypoxia + NAC groups.

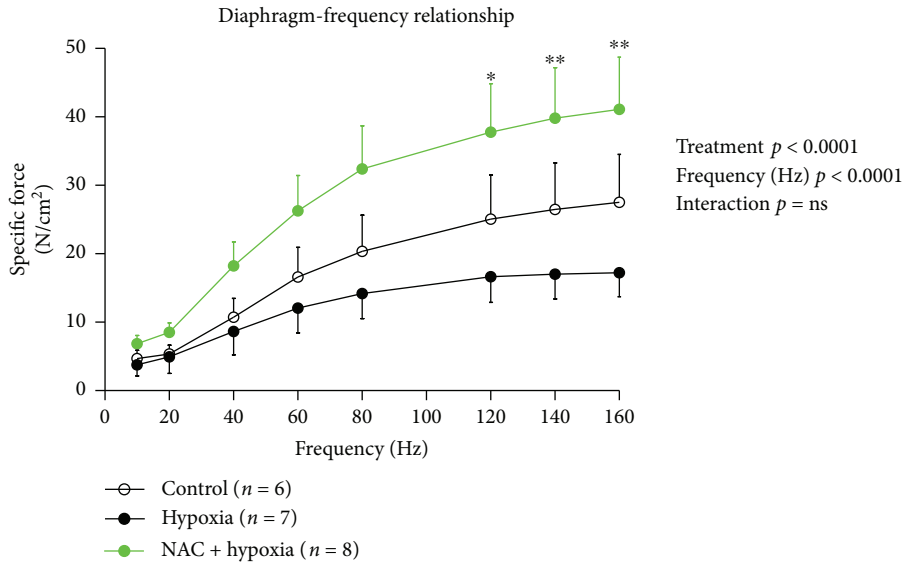

Figure 1: Mouse diaphragm muscle force-frequency relationship following 8 hours of exposure to normoxia (control), hypoxia, or hypoxia + NAC. Diaphragm-specific force (mean ± SEM) expressed as force per unit cross-sectional area of muscle (N/cm^2) as a function of stimulation frequencies ranging between 10 and 160 Hz; $n = 6$–8 per group. Data were compared statistically by two-way (gas treatment × stimulation frequency) ANOVA; $^{*}p < 0.05$ and $^{**}p < 0.01$. Bonferroni's post hoc multiple comparisons test hypoxia + NAC versus hypoxia.

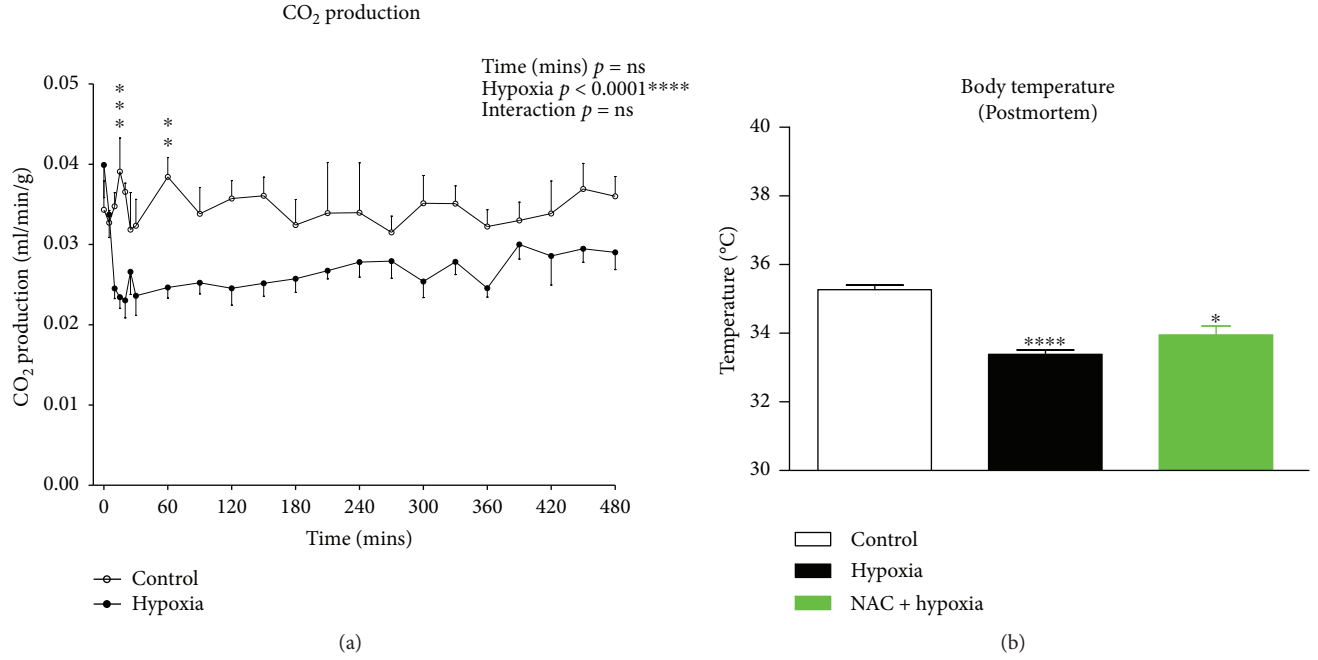

Figure 2: (a) Carbon dioxide production over 8 hours of breathing in mice exposed to normoxia (control) or hypoxia. Carbon dioxide production (mean ± SEM) in mice expressed as ml per minute per gram body mass (ml/min/g) over the 480-minute (8 hour) period of exposure to either normoxia ($FiO_2 = 0.21$, $n = 6$) or hypoxia ($FiO_2 = 0.10$, $n = 7$); two-way (time × gas treatment) ANOVA and Bonferroni's multiple comparisons test. $^{***}p < 0.001$ and $^{**}p < 0.01$ compared with corresponding normoxic values. (b) Postmortem body temperatures in mice following 8 hours of exposure to normoxia (control), hypoxia, or hypoxia + NAC. Postmortem body temperatures (mean ± SEM) of mice exposed to 8 hours of normoxia ($FiO_2 = 0.21$, $n = 6$), hypoxia ($FiO_2 = 0.10$, $n = 7$), or hypoxia + NAC (200 mg/kg i.p. at $FiO_2 = 0.10$, $n = 4$). $^{****}p < 0.0001$, unpaired t test compared with control; $^{*}p = 0.0105$, unpaired t test with Welch's correction compared with control.

Figure 3(a) shows mouse respiratory $\dot{V}_E$, a product of f_R and V_T, throughout the duration of normoxia (control) and hypoxia. $\dot{V}_E$ was increased (two-way ANOVA; gas: $p < 0.001$) after 10 mins of hypoxia compared with normoxia, but returned to levels equivalent to normoxia by 20 mins and remained at levels similar to normoxia for

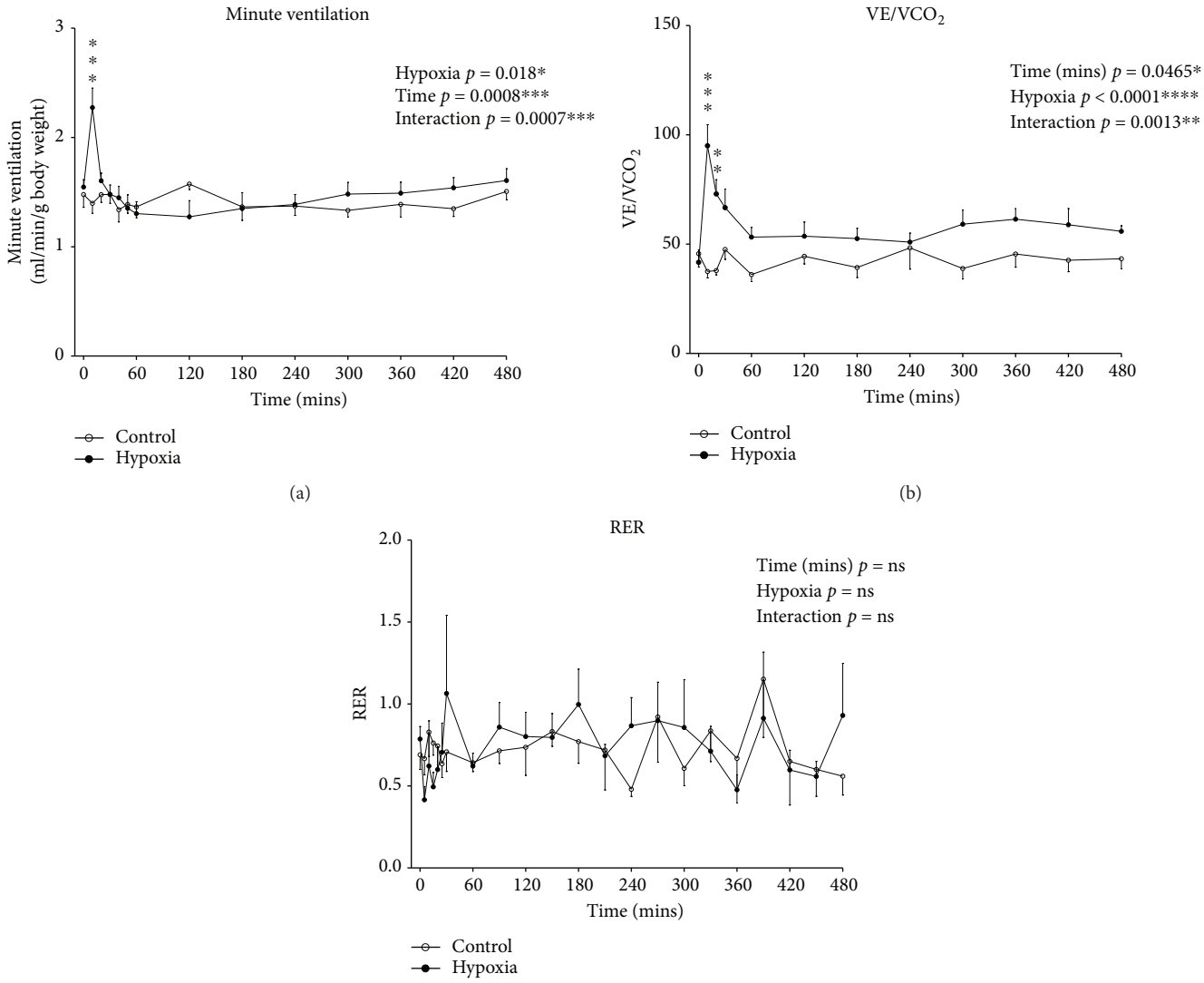

Figure 3: Minute ventilation ($\dot{V}_E$), ventilatory equivalent for carbon dioxide ($\dot{V}_E/\dot{V}CO_2$), and respiratory exchange ratio (RER; $\dot{V}CO_2/\dot{V}O_2$) during 8 hours of exposure to normoxia (control) or hypoxia. (a) Minute ventilation (mean ± SEM) expressed as ml per min per gram body mass (ml/min/g) over the 480-minute (8 hour) period of exposure to either normoxia ($FiO_2 = 0.21$, $n = 6$) or hypoxia ($FiO_2 = 0.10$, $n = 7$); two-way ANOVA (time × gas treatment) and Bonferroni's multiple comparisons test, $^{***}p < 0.001$ compared with corresponding normoxic value. (b) Ventilatory equivalent ratio (mean ± SEM) in mice over the 480-minute (8 hour) period of exposure to either normoxia ($FiO_2 = 0.21$, $n = 6$) or hypoxia ($FiO_2 = 0.10$, $n = 7$); two-way ANOVA (time × gas treatment) and Bonferroni's multiple comparisons test, $^{***}p < 0.001$ and $^{**}p < 0.01$ compared with corresponding normoxic value. (c) Respiratory exchange ratio (mean ± SEM) in mice over the 480-minute (8 hour) period of exposure to either normoxia ($FiO_2 = 0.21$, $n = 6$) or hypoxia ($FiO_2 = 0.10$, $n = 7$); two-way ANOVA (time × gas treatment).

the remainder of the 8-hour exposure to hypoxia. Thus, beyond the initial transient hypoxic ventilatory response, ventilation was largely unchanged during hypoxic exposure in mice.

The ventilatory equivalent for carbon dioxide ($\dot{V}_E/\dot{V}CO_2$) over 8 hours of exposure to normoxia (control) and hypoxia is shown in Figure 3(b). $\dot{V}_E/\dot{V}CO_2$ was significantly increased in the hypoxic group upon gas exposure compared with the control group, and it remained elevated over the course of the 8 hours of gas exposure (two-way ANOVA; gas: $p < 0.0001$), indicative of the development of a hypoxia-induced hyperventilation (arising due to hypometabolism with maintained ventilation).

Figure 3(c) shows the respiratory exchange ratio ($\dot{V}CO_2/\dot{V}O_2$) over 8 hours of exposure to normoxia (control) and hypoxia. There was no significant effect of exposure to hypoxia on $\dot{V}CO_2/\dot{V}O_2$ over the course of the 8 hours of gas exposure compared with control.

3.3. HIF-1α: Gene Expression and Protein Content. There was no significant difference in HIF-1α mRNA expression between groups (data not shown). Figure 4 shows HIF-1α

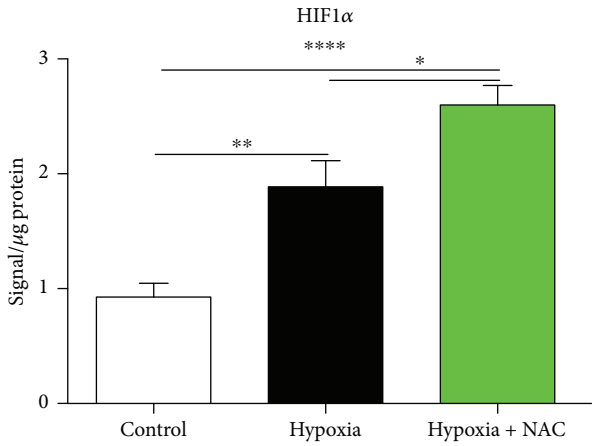

Figure 4: Mouse diaphragm HIF-1α protein content following 8 hours of exposure to normoxia (control), hypoxia, or hypoxia + NAC. Diaphragm HIF-1α protein content (mean ± SEM) expressed as signal/μg of total protein (corrected for background signal) following exposure to either normoxia (control; $FiO_2 = 0.21$, $n = 6$), hypoxia ($FiO_2 = 0.10$, $n = 7$), or hypoxia + NAC (200 mg/kg i.p. at $FiO_2 = 0.10$); $^{*}p = 0.0332$, $^{**}p = 0.0019$, and $^{****}p < 0.0001$; unpaired t tests.

protein content in diaphragm muscle from mice exposed to 8 hours of normoxia, hypoxia, or hypoxia + NAC. Hypoxia significantly increased HIF-1α protein content compared with the control group ($p = 0.0019$; unpaired t test). HIF-1α protein content was further increased in hypoxia + NAC compared with normoxia ($p < 0.0001$) and was also significantly higher in hypoxia + NAC compared with the hypoxia group ($p = 0.0332$).

3.4. Cell Signalling: Akt Pathway. Phospho-Akt protein content in diaphragm muscle from mice exposed to 8 hours of normoxia, hypoxia, or hypoxia + NAC is shown in Figure 5(a). Exposure to hypoxia significantly increased phospho-Akt protein content compared with the control group ($p = 0.0109$; unpaired t test). Phospho-Akt protein content was further increased in hypoxia + NAC compared with normoxia ($p = 0.0001$) and was also significantly higher in hypoxia + NAC compared with the hypoxia group ($p = 0.0004$).

Figure 5(b) shows phospho-p70S6K protein content in diaphragm muscle from mice exposed to 8 hours of normoxia, hypoxia, or hypoxia + NAC. Exposure to hypoxia had no significant effect on phospho-p70S6K protein content compared with normoxia. However, hypoxia + NAC increased phospho-p70S6K protein content compared with the control group ($p = 0.0019$) and also increased phospho-p70S6K protein content above the level of the hypoxia group ($p = 0.0616$).

Figure 5(c) shows phospho-S6RP protein content in diaphragm muscle from mice exposed to 8 hours of normoxia, hypoxia, or hypoxia + NAC. Exposure to hypoxia significantly increased phospho-S6RP protein content compared with the control group ($p = 0.0434$). Hypoxia + NAC also increased phospho-S6RP protein content compared with the control group ($p = 0.0099$), but there was no difference between the hypoxia and hypoxia + NAC groups.

Figure 5(d) shows phospho-GSK-3β protein content in diaphragm muscle from mice exposed to 8 hours of normoxia, hypoxia, or hypoxia + NAC. Exposure to hypoxia significantly increased phospho-GSK-3β protein content compared with the control group ($p = 0.0009$). Hypoxia + NAC increased phospho-GSK-3β protein content further still compared with the control group ($p = 0.0006$), but there was no difference between the hypoxia and hypoxia + NAC groups.

3.5. Cell Signalling: mTOR Pathway. Figure 6(a) shows mTOR protein content in diaphragm muscle from mice exposed to 8 hours of normoxia, hypoxia, or hypoxia + NAC. Exposure to hypoxia significantly increased mTOR protein content compared with the control group ($p = 0.0107$). Hypoxia + NAC, however, did not increase mTOR protein content compared with the control group, and mTOR protein content was significantly lower in the hypoxia + NAC group compared with the hypoxia group ($p = 0.0020$).

Figure 6(b) shows phospho-mTOR protein content in diaphragm muscle from mice exposed to 8 hours of normoxia, hypoxia, or hypoxia + NAC. Exposure to hypoxia significantly increased phospho-mTOR protein content compared with the normoxia group ($p = 0.0123$). Phospho-mTOR protein content was further increased in the hypoxia + NAC group compared with the control group ($p = 0.0001$) and was also significantly higher than the hypoxia group ($p = 0.0067$).

3.6. Cell Signalling: FoxO3a Pathway. Figure 6(c) shows phospho-FoxO3a protein content in diaphragm muscle from mice exposed to 8 hours of normoxia, hypoxia, or hypoxia + NAC. Exposure to hypoxia significantly increased phospho-FoxO3a protein content compared with the normoxia group ($p = 0.0002$). Phospho-FoxO3a protein content was further increased in the hypoxia + NAC group compared with the control group ($p < 0.0001$) and was also significantly higher than the hypoxia group ($p = 0.0024$).

3.7. Cell Signalling: JNK, p38, and ERK1/2 Pathways. Phospho-JNK protein content in diaphragm muscle from mice exposed to 8 hours of normoxia, hypoxia, or hypoxia + NAC is shown in Figure 7(a). Exposure to hypoxia significantly increased phospho-JNK protein content compared with the normoxia group ($p = 0.0120$). Phospho-JNK protein content was further increased in the hypoxia + NAC group compared with the control group ($p = 0.0058$) and was also significantly higher than the hypoxia group ($p = 0.0108$).

Figure 7(b) shows phospho-p38 protein content in diaphragm muscle from mice exposed to 8 hours of normoxia, hypoxia, or hypoxia + NAC. Exposure to hypoxia increased phospho-p38 protein content compared with the normoxia group ($p = 0.0515$). Phospho-p38 protein content was further increased in the hypoxia + NAC group compared with the control group ($p = 0.0030$) and was also significantly higher than the hypoxia group ($p = 0.0092$).

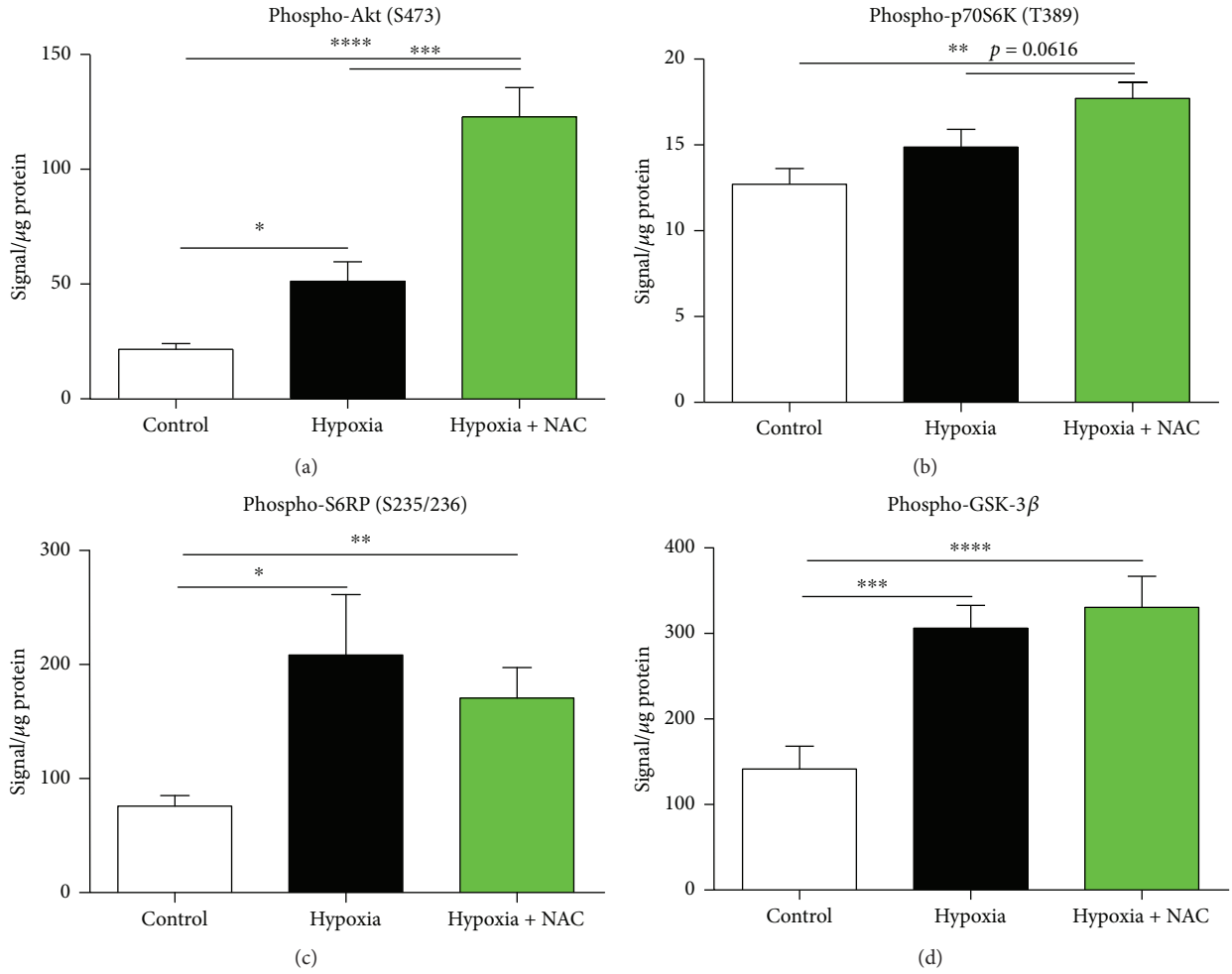

Figure 5: Mouse diaphragm phospho-Akt (S473), phospho-p70S6K (T389), phospho-S6RP (S235/236), and phospho-GSK-3β protein contents following 8 hours of exposure to normoxia (control), hypoxia, or hypoxia + NAC. (a) Diaphragm phospho-Akt (S473) protein content (mean ± SEM) expressed as signal/μg of total protein (corrected for background signal); $n = 8$ per group. $^{*}p = 0.0109$, $^{****}p = 0.0001$, and $^{***}p = 0.0004$; unpaired t tests. (b) Diaphragm phospho-p70S6K (T389) protein content (mean ± SEM) expressed as signal/μg of total protein (corrected for background signal); $n = 8$ per group. $^{**}p = 0.0019$; unpaired t test. (c) Diaphragm phospho-S6RP (S235/236) protein content (mean ± SEM) expressed as signal/μg of total protein (corrected for background signal); $n = 8$ per group. $^{*}p = 0.0434$ and $^{**}p = 0.0099$; unpaired t tests. (d) Diaphragm phospho-GSK-3β protein content (mean ± SEM) expressed as signal/μg of total protein (corrected for background signal); $n = 8$ per group. $^{****}p = 0.0006$ and $^{***}p = 0.0009$; unpaired t tests.

Phospho-ERK1/2 protein content in diaphragm muscle from mice exposed to 8 hours of normoxia, hypoxia, or hypoxia + NAC is shown in Figure 7(c). Hypoxia significantly increased phospho-ERK1/2 protein content compared with the normoxia group ($p = 0.0406$). Phospho-ERK1/2 protein content was increased further in the hypoxia + NAC group compared with the control group ($p = 0.0020$) and was also significantly higher than the hypoxia group ($p = 0.0046$).

3.8. Atrophy and Autophagy Gene Expression. Figure 8 shows expression data in diaphragm muscle for genes related to atrophy and autophagy. There were no significant changes in FoxO-1, Atrogin-1, LC3B, BNIP3, or GABARAPL3 mRNA expression between groups (one-way ANOVA and Tukey's post hoc test). FoxO-1, Atrogin-1, and BNIP3 displayed nonsignificant trends toward increased expression levels following increasing durations of hypoxic exposure (1, 4, and 8 hours). Both FoxO-3 and MuRF-1 mRNA expression was significantly increased following 8 hours of hypoxic exposure compared with control ($p < 0.05$, one-way ANOVA and Tukey's post hoc test) (Figures 8(b) and 8(d), resp.).

3.9. Oxidative Stress: TBARS Concentration. Data for diaphragm TBARS concentration (a marker of lipid peroxidation) in normoxia, hypoxia, and hypoxia + NAC groups are shown in Figure 9. TBARS concentration was significantly increased following exposure to hypoxia compared with normoxia ($p = 0.0076$). TBARS concentration was significantly lower in NAC + hypoxia compared with hypoxia ($p < 0.0001$) and also significantly lower compared with the normoxia group ($p = 0.0030$).

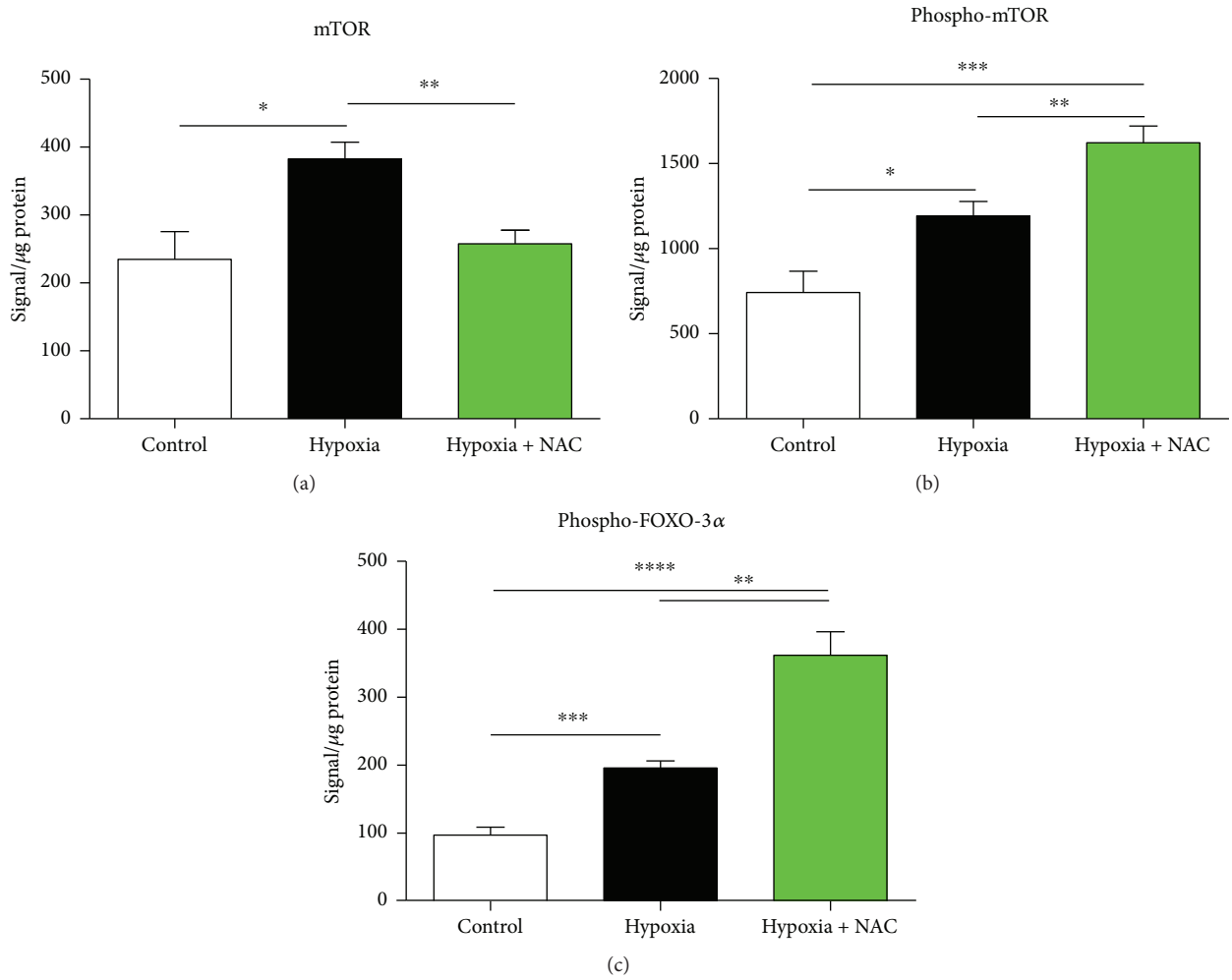

Figure 6: Mouse diaphragm mTOR, phospho-mTOR, phospho-ERK1/2, and phospho-FOXO3a protein contents following 8 hours of exposure to normoxia (control), hypoxia, or hypoxia + NAC. (a) Diaphragm mTOR protein content (mean ± SEM) expressed as signal/μg of total protein (corrected for background signal); $n = 7 - 8$ per group. $^{*}p = 0.0107$ and $^{**}p = 0.0020$; unpaired t tests. (b) Diaphragm phospho-mTOR protein content (mean ± SEM) expressed as signal/μg of total protein (corrected for background signal); $n = 7 - 8$ per group. $^{*}p = 0.0123$, $^{**}p = 0.0067$, and $^{***}p = 0.0001$; unpaired t tests. (c) Diaphragm phospho-FOXO3a protein content (mean ± SEM) expressed as signal/μg of total protein (corrected for background signal); $n = 7 - 8$ per group. $^{**}p = 0.0024$, $^{***}p = 0.0002$, and $^{****}p < 0.0001$; unpaired t tests.

3.10. Chymotrypsin-Like Proteasome Activity. Figure 10 shows diaphragm muscle chymotrypsin-like proteasome activity in normoxia and hypoxia groups. There was no significant difference in chymotrypsin-like proteasome activity between the two groups.

3.11. Diaphragm Muscle Fibre Size and Distribution. Representative immunofluorescence images of diaphragm muscles from mice exposed to normoxia and hypoxia are shown in Figures 11(a) and 11(b). There was no significant difference in the mean minimal Feret's diameter (Figure 11(c)) or mean cross-sectional area of fibres (Figure 11(d)) between the two groups. The coefficient of variation of these indices was also equivalent in control and hypoxia muscles (Figures 11(e) and 11(f)). There was no shift in the relative frequency distribution of fibres in hypoxia compared with normoxia (Figures 11(f) and 11(g)).

4. Discussion

The main findings of this study are the following: (1) Acute hypoxic stress over several hours causes diaphragm muscle weakness; (2) Diaphragm dysfunction is unrelated to enhanced respiratory muscle work during hypoxic exposure, since ventilation is unchanged in mice exposed to sustained hypoxia; (3) Acute hypoxic stress stabilized diaphragm HIF-1α protein and activated MAPK, mTOR, Akt, and FoxO3a signalling pathways, favouring protein synthesis; (4) Autophagy gene expression was unaffected by acute hypoxia, but FoxO3 and MuRF-1 atrogene expression was progressively increased during hypoxic exposure without effect on diaphragm 20S proteasome activity; (5) Acute hypoxia increased diaphragm TBARS concentration indicative of oxidative stress; (6) Acute hypoxia did not affect diaphragm myofibre size or distribution; (7) NAC pretreatment strongly

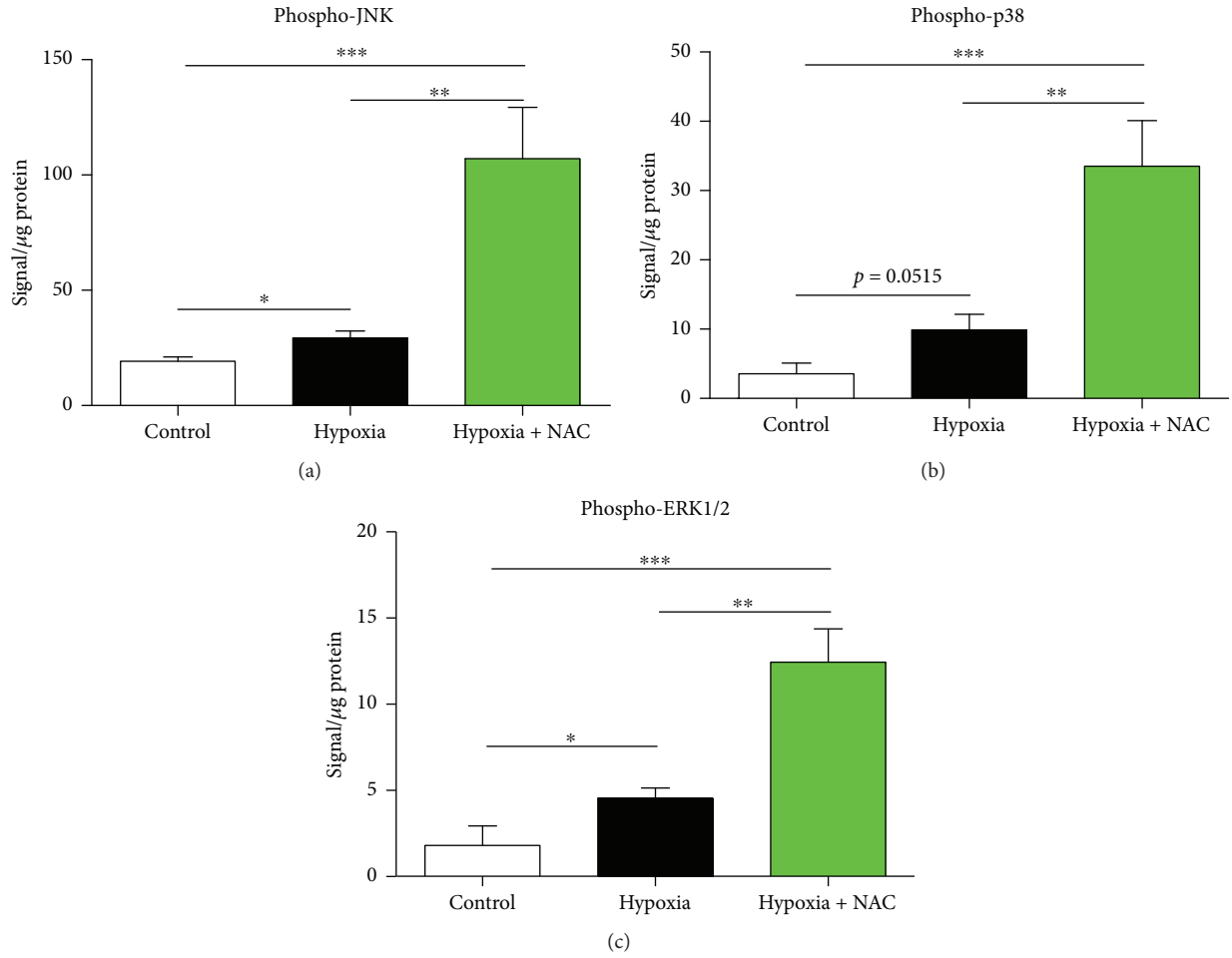

Figure 7: Mouse diaphragm phospho-JNK and phospho-p38 protein contents following 8 hours of exposure to normoxia (control), hypoxia, or hypoxia + NAC. (a) Diaphragm phospho-JNK protein content (mean ± SEM) expressed as signal/μg of total protein (corrected for background signal); $n = 8$ per group. $^{*}p = 0.0120$, $^{**}p = 0.0108$, and $^{***}p = 0.0058$; unpaired t tests. (b) Diaphragm phospho-p38 protein content (mean ± SEM) expressed as signal/μg of total protein (corrected for background signal); $n = 6$–8 per group. $^{**}p = 0.0092$ and $^{***}p = 0.0030$; unpaired t tests. (c) Diaphragm phospho-ERK1/2 protein content (mean ± SEM) expressed as signal/μg of total protein (corrected for background signal); $n = 5$–8 per group. $^{*}p = 0.0406$, $^{***}p = 0.0020$, and $^{**}p = 0.0046$; unpaired t tests.

potentiated many of the endogenous cell survival signalling responses to acute hypoxic stress and reversed diaphragm oxidative stress; (8) Antioxidant pretreatment with NAC prevented acute hypoxia-induced diaphragm dysfunction.

4.1. Muscle Function. This study confirms our previous report [17], revealing that acute sustained hypoxia causes pronounced diaphragm muscle weakness. Our experimental approach was to study diaphragm performance ex vivo under standardized conditions. In this way, we determined that weakness is intrinsic to diaphragm muscle fibres, as we controlled the stimulation frequency. The approach allowed us to reestablish optimal oxygen and acid-base conditions for the study of muscle performance. Therefore, diaphragm function was assessed at normal pH, whereas the persistent hyperventilation associated with hypoxia exposure results in a respiratory alkalosis and elevated blood pH, which are likely to cause further perturbation to respiratory muscle function *in vivo*. Our data reveal that the force-generating capacity of diaphragm from hypoxic animals is intrinsically weak, especially at high stimulation frequencies, which correspond to activation of the muscle during airway protective behaviours [36]. Decreased peak force-generating capacity is linked to poor prognosis in respiratory patients [1]. Oxygen was provided abundantly in the ex vivo preparation allowing comparison of normoxia and hypoxia groups under similar conditions. We concede that whereas the hypoxia group was revealed as having decreased force-generating capacity compared with the normoxia group, we did not extend the study to determine how the hypoxia group would have compared with the normoxia group under conditions of bath hypoxia. For example, exposure to chronic sustained hypoxia has been shown to improve tolerance to a subsequent severe hypoxic stimulus [37] revealing that hypoxic adaptation in respiratory muscle can result in some protective outcomes relevant to the prevailing stimulus of oxygen deficit. Our data highlight the potential for acute hypoxic stress to adversely affect diaphragm performance, which has relevance to respiratory patients, particularly in the critical care setting [1], and may have implications for individuals

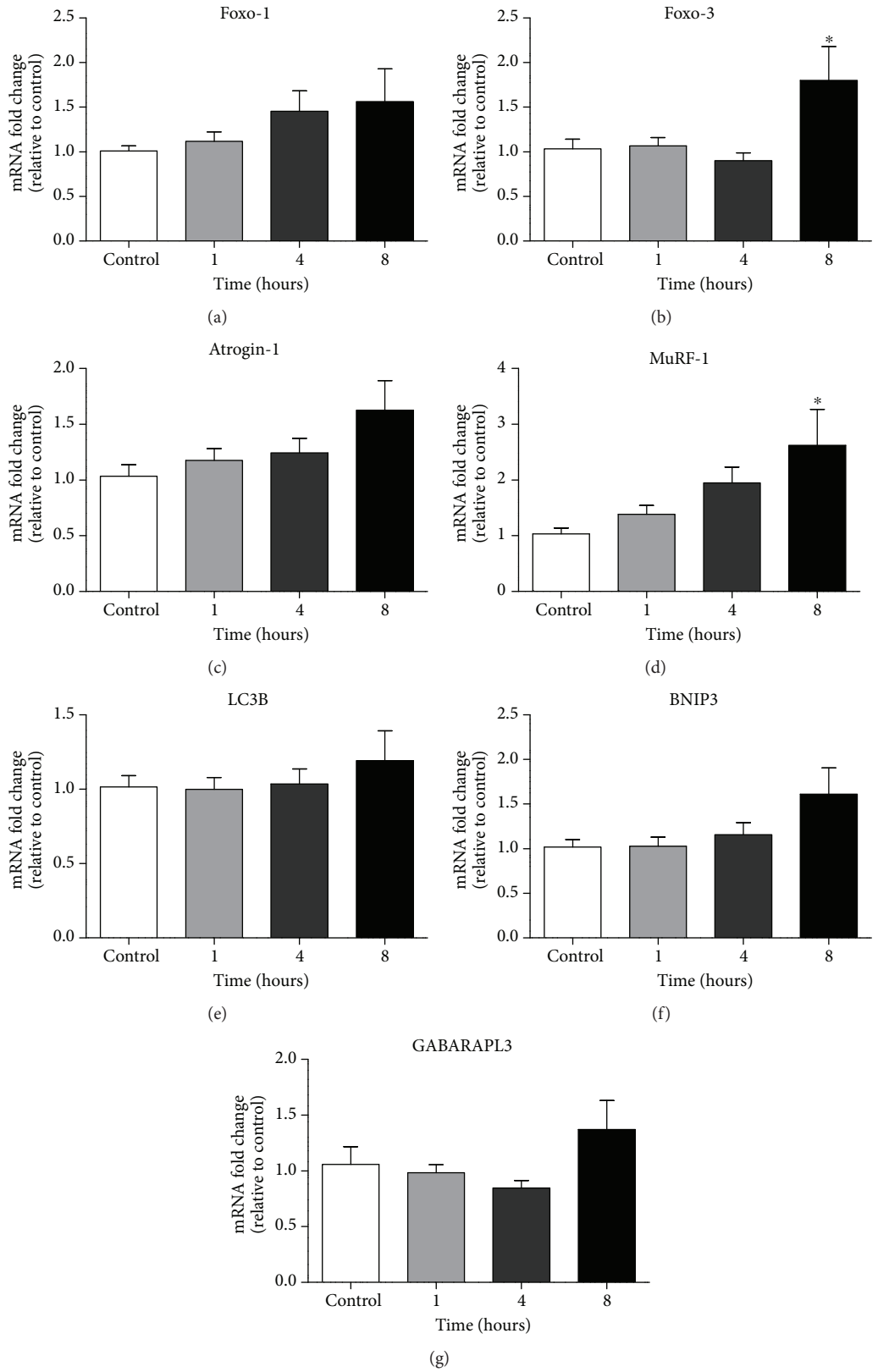

Figure 8: Mouse diaphragm muscle atrophy and autophagy gene expression following exposure to normoxia (control) or 1, 4, or 8 hours of hypoxia. Fold changes in mRNA expression (relative to the control (normoxia) group) for (a) FoxO-1; (b) FoxO-3; (c) Atrogin-1; (d) MuRF-1; (e) LC3B; (f) BNIP3; and (g) GABARAPL3; mean ± SEM, $n = 7$–8 per group. $^{*}p < 0.05$ versus control, one-way ANOVA and Tukey's post hoc test following 8 hours of exposure to normoxia and 1, 4, and 8 hours of exposure to hypoxia.

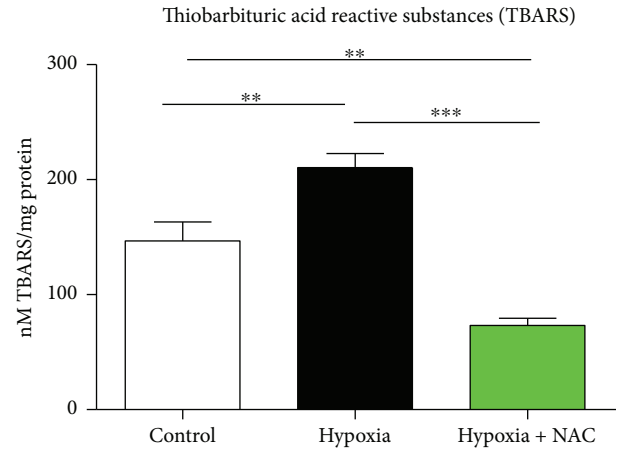

Figure 9: Mouse diaphragm muscle thiobarbituric acid reactive substances (TBARS) concentration following 8 hours of exposure to normoxia (control), hypoxia, or hypoxia + NAC. TBARS concentration in diaphragm muscle (mean ± SEM) expressed as nM TBARS per mg of protein following exposure to either normoxia ($FiO_2 = 0.21$), hypoxia ($FiO_2 = 0.10$), or hypoxia + NAC (200 mg/kg i.p. at $FiO_2 = 0.10$); $n = 8$ per group. $^{**}p < 0.01$ and $^{***}p < 0.0001$; unpaired t test with Welch's correction.

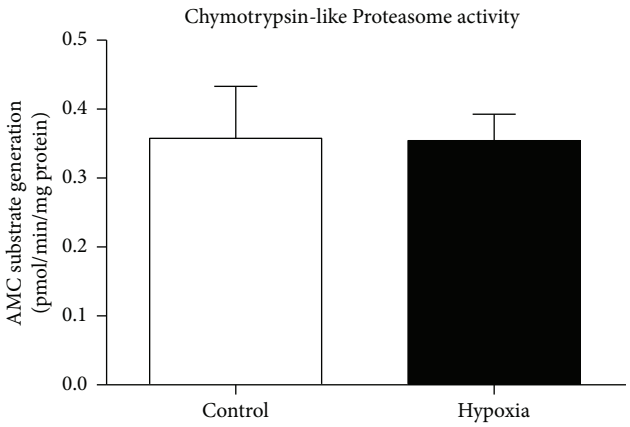

Figure 10: Mouse diaphragm muscle chymotrypsin-like proteasome activity following 8 hours of exposure to normoxia (control) or hypoxia. Chymotrypsin-like proteasome activity in diaphragm muscle (mean ± SEM) expressed as a rate of AMC tag release from peptide substrate (pmol/min/mg of protein) following exposure to either normoxia (control; $FiO_2 = 0.21$) or hypoxia ($FiO_2 = 0.10$); $n = 8$ per group. There was no significant difference between the two groups (unpaired t test).

at high altitude [19, 20]. We acknowledge that further assessments of diaphragm function *in vivo* are required, where respiratory muscle performance can be considered in the context of an integrative multisystem response to hypoxia (e.g., blood flow and neural drive), to lend further credence to our hypothesis that hypoxia is a driver of respiratory muscle dysfunction.

Antioxidant pretreatment with NAC prior to hypoxic exposure completely rescued the diaphragm from acute hypoxia-induced diaphragm weakness. Indeed, notwithstanding hypoxic exposure, NAC supplementation enhanced muscle force-generating capacity above control levels. The finding is reminiscent of a study showing that NAC treatment immediately after the initiation of 6 hours of mechanical ventilation completely prevented the development of mechanical ventilation-induced diaphragmatic weakness [8]. Of interest, in the latter study, NAC did not suppress autophagy, rather it augmented autophagosome formation suggesting that NAC exerts its beneficial effects on ventilator-induced diaphragm dysfunction via stimulation of autophagy (excess ROS can inhibit autophagy), which appears to be a beneficial adaptive response in the diaphragm to the physiological stress of mechanical ventilation, rather than representing a contributing factor to the development of diaphragm dysfunction [8]. NAC has also been shown to protect the diaphragm from the damaging effects of controlled mechanical ventilation including diaphragmatic oxidative stress and proteolysis, as well as controlled mechanical ventilation-induced contractile dysfunction [38]. We have previously reported beneficial effects of NAC in ameliorating diaphragm protein carbonylation, which presents progressively in response to exposure to chronic sustained hypoxia [16]. Indeed, protein carbonylation underpins the loss of skeletal muscle mass in a number of chronic conditions [39] suggesting that NAC and other antioxidants could have widespread utility as adjunctive therapies in skeletal muscle disease. Of interest, NAC also proved efficacious in preventing diaphragm muscle weakness and fatigue in a rat model of chronic intermittent hypoxia modelling sleep apnoea [32].

4.2. Metabolism. Acute hypoxic stress decreased metabolism in mice, as evident from the rapid and sustained reduction in CO_2 production during hypoxia, as well as the reduction in postmortem body temperature following hypoxia. Interestingly, body temperature was reduced to an equivalent level in the hypoxia + NAC group revealing that the beneficial effect of NAC on hypoxic diaphragm performance is unlikely related to an influence on the hypoxic hypometabolic/hypothermic state and associated alkalosis caused by the reduction in CO_2 production concomitant with maintained ventilation, that is, hypoxic hyperventilation. It is therefore conceivable to consider that the beneficial effects of NAC relate instead to direct antioxidant and/or signalling effects in muscle.

It is also noteworthy that minute ventilation was relatively unchanged over the 8 hours of hypoxic exposure in comparison with control animals. This reveals that diaphragm activity is not increased due to a hypoxia-induced increase in ventilatory drive (common to other mammals), and so increased muscle activity during hypoxic stress is not a contributory factor to the development of hypoxia-induced diaphragm weakness, although it may be a further aggravating factor during acute hypoxic stress in humans. Our study in mice reveals the potential for diaphragm muscle weakness related to direct hypoxic (redox) stress of muscle fibres [16]. The hypometabolic response causes a relative hyperventilation evident from the hypoxia-induced increase in the ventilatory equivalent for carbon dioxide. The ensuing alkalosis (which is achieved in humans during exposure to hypoxia by way of enhanced ventilation with no change in

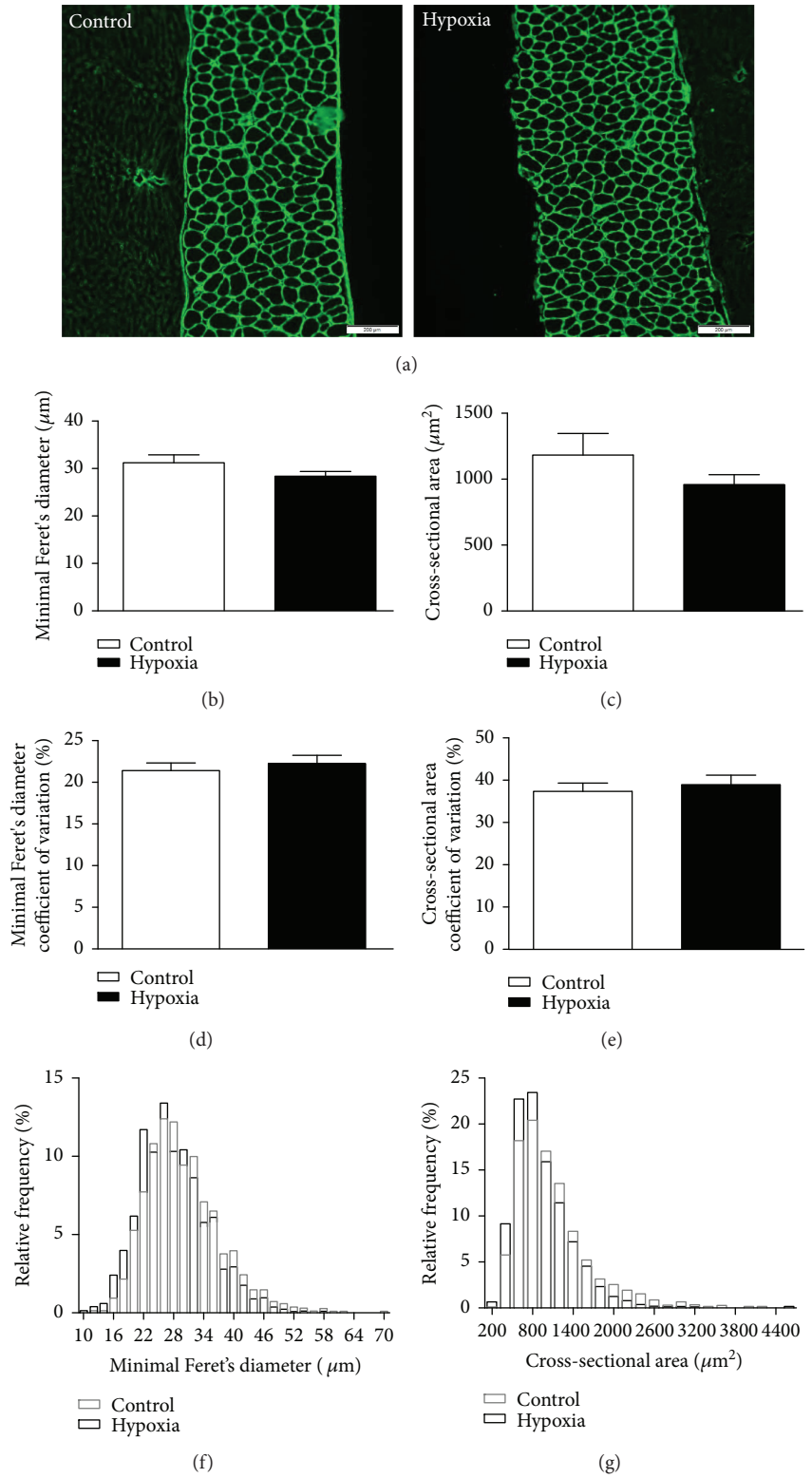

Figure 11: Mouse diaphragm muscle fibre size and distribution following exposure to 8 hours of normoxia (control) or hypoxia. (a) Representative images of mouse diaphragm muscle immunofluorescently labelled for laminin to highlight individual fibres from animals exposed to 8 hours of normoxia (control, $FiO_2 = 0.21$) and hypoxia ($FiO_2 = 0.10$). (b) Group data for mean minimal Feret's diameter. (c) Group data for mean muscle fibre cross-sectional area. (d) Group data for coefficient of variation of diaphragm muscle fibre size measured by minimal Feret's diameter. (e) Group data for coefficient of variation of diaphragm muscle fibre size measured by cross-sectional area. Data in (b–e) expressed as mean ± SEM; there were no significant differences between groups ($n = 6$ per group; unpaired Student's t-tests). (f) and (g) Relative frequency distribution of diaphragm muscle fibres measured by minimal Feret's diameter (f) and cross-sectional area (g).

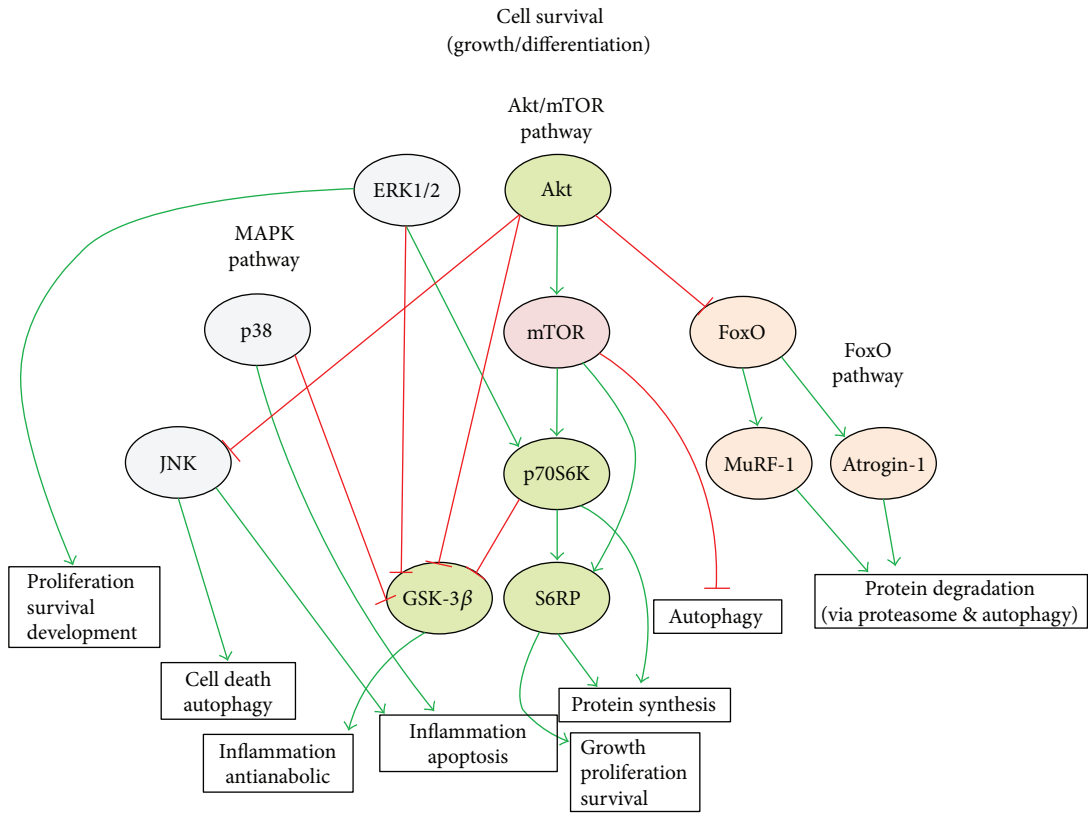

Figure 12: Schematic depicting the various cell survival signalling pathways explored in this study. Green arrows indicate activation, and red lines indicate inhibition in diaphragm muscle following exposure to acute hypoxic stress.

metabolism) may be a factor of relevance for diaphragm performance *in vivo*. Of interest, the respiratory exchange ratio was unchanged during exposure to hypoxia suggesting that there was not a hypoxia-induced switch in metabolic substrate preference away from lipids.

4.3. Hypoxia Signalling. HIF-1α protein content was increased in the diaphragm following 8 hours of hypoxia. This is not altogether surprising given that HIF-1α protein accumulation is indirectly proportional to cytosolic oxygenation, although muscle-specific and temporal responses have been reported in respiratory muscles in response to chronic sustained hypoxia [15, 16]. Reactive oxygen species can induce HIF-1α expression, but this effect can be dependent on exposure time, and reactive oxygen species can exert the opposite effect over prolonged periods, thus creating some uncertainty regarding how swings in cellular redox balance affect HIF-1α expression [40–43]. One might have expected that NAC, as an antioxidant, would influence hypoxia-induced increase in HIF-1α protein content. However, HIF-1α is responsive to redox balance within the intracellular environment and reducing conditions can stabilize HIF-1α. Moreover, NAC-induced increases in cellular glutathione can elevate HIF-1α expression [44–47]. In our study, pretreatment with NAC prior to hypoxic exposure enhanced HIF-1α protein content in diaphragm muscle compared with hypoxia alone. In view of the protective effect of NAC on diaphragm force-generating capacity, this suggests that HIF-1α stabilization was a component of the adaptive response of muscle to hypoxic challenge. Indeed, it has been reported that HIF-1α contributes to the neuroprotective effect of NAC in an ischaemic stroke model of transient cerebral ischaemia in rats [47].

4.4. Hypertrophy/Atrophy Signalling. We examined the protein and/or phosphoprotein content of various proteins associated with signalling pathways involved in the balance between cell survival and death and protein balance (hypertrophy/atrophy) in diaphragm muscle (summarized in Figure 12).

4.5. Prohypertrophy/Cell Survival Signalling

4.5.1. Akt Pathway. Akt, particularly the Akt/mTOR pathway, is central to the control of the hypertrophic/atrophic balance in muscle, acting in a phosphorylation-dependent manner as a key regulator of downstream effectors involved in modulating cell growth and survival. Activated (phosphorylated) Akt is predominantly prohypertrophic, via inhibition of atrophic signals and promotion of hypertrophic signals. In our study, phosphorylated (active) Akt (phospho-Akt) protein content was increased following acute hypoxia exposure and enhanced further still by NAC supplementation. It has been previously demonstrated that under certain conditions hypoxia can activate Akt and it is suggested that hypoxia-induced Akt activation may play a role in protection against apoptosis [48–51]. Similarly, in our model, it would appear that acute hypoxia-induced Akt activation is a beneficial

compensatory mechanism supporting the functional integrity of the diaphragm muscle. NAC pretreatment enhanced the endogenous induction of Akt signalling, potentially bolstering the cellular defences against acute hypoxic stress. This may be (part of) the mechanism by which NAC rescues diaphragm force in acute hypoxia. It is also worth noting that Akt/mTOR signalling can regulate HIF-1α and may play a role in hypoxia-induced HIF-1α expression [52–54]. Akt also exerts prohypertrophic effects via inhibition of atrophic signalling (Figure 12).

Phospho-p70S6K, which is downstream of Akt, was slightly elevated by acute hypoxia in the diaphragm. Its protein content was, however, significantly elevated in the hypoxic diaphragm by NAC supplementation. p70S6k activation by Akt is mediated via the indirect activation of mTOR by Akt. p70S6K, when activated, promotes translation/protein synthesis and cell survival in muscle [55–57]. The fact that the induction of elevated phospho-p70S6K is greater in hypoxia + NAC compared with hypoxia alone is likely due to the greater elevation of phospho-Akt, phospho-mTOR, and phospho-ERK1/2 in hypoxia + NAC, which all activate phospho-p70S6K [58]. Again, this is indicative of prohypertrophy signalling induced by NAC supplementation, a mechanism which appears beneficial in the maintenance of diaphragm muscle performance. Indeed, decreased phospho-p70S6K expression occurs in the diaphragm of mechanically ventilated rats prior to decreased protein synthesis [59].

Phospho-S6RP content, which is a downstream of both Akt/mTOR and p70S6K, was significantly increased in the diaphragm both by hypoxia and hypoxia + NAC. The phosphorylation of S6RP by phospho-p70S6K, driven by Akt/mTOR, drives translation/protein synthesis and growth (Figure 12).

Hypoxia can activate Akt leading to GSK-3 phosphorylation [49]. Phosphorylation negatively regulates GSK-3β, inhibiting it, resulting in the activation of protein synthesis and a cessation of antianabolic signalling from GSK-3β. In our study, phospho-GSK-3β protein content was increased significantly by hypoxia and increased further still by hypoxia + NAC. Again, these data suggest a drive toward a prohypertrophic/proprotein synthesis state in acute hypoxia that is further augmented by NAC pretreatment.

4.5.2. mTOR Pathway. mTOR is a protein kinase functioning in the regulation of growth, survival, and protein synthesis in skeletal muscle. Both mTOR and phospho-mTOR were measured in our study. mTOR mediates its hypertrophic/cell survival signalling effects via its phosphorylated/activated state. Acute hypoxia significantly increased mTOR protein content. Whereas hypoxia and hypoxia + NAC both increased phospho-mTOR protein content, expression was greatest in the hypoxia + NAC group. It appears that hypoxia alone, in the absence of NAC, induces an increase in mTOR protein expression, or indeed a reduction in mTOR degradation, while phosphorylation of mTOR is induced by hypoxia, and to a greater extent by hypoxia concomitant with NAC supplementation. Phospho-p70S6K and phospho-s6RP, discussed above, are also both downstream of, and activated by, mTOR, and so the increase in phospho-mTOR observed in our study likely contributes to the increases in phospho-p70S6K and phospho-s6RP reported above.

4.5.3. MAPK Pathway. ERK1/2 is a member of the MAPK family which positively regulates p70S6K, negatively regulates GSK-3β, and itself positively regulates cellular proliferation, survival, and development. Through these mechanisms, it is procell survival/hypertrophy. Here, acute hypoxia increased diaphragm phospho-ERK1/2 protein content, and NAC pretreatment further augmented phospho-ERK1/2 protein content. This, combined with changes in Akt signalling described above, is further suggestive that NAC pretreatment bolsters the endogenous cellular signalling mechanisms acting to promote protein synthesis and cell survival in the acutely hypoxic diaphragm.

4.5.4. FoxO3a Pathway. The FoxO pathway is generally associated with atrophy and protein degradation in its dephosphorylated state. However, when phosphorylated, FoxO3a is inhibited from translocation into the nucleus and exerting its atrophic effects. One mechanism by which Akt exerts a hypertrophic effect is by the phosphorylation and thus inhibition of FoxO3a, preventing the atrophic action of the atrogenes MuRF-1 and Atrogin-1, which would otherwise be transcriptionally upregulated by FoxO3a. Our study revealed that acute hypoxia increases phospho-FoxO3a protein content in the diaphragm and NAC pretreatment further augmented phosphoprotein content, thus enhancing the prohypertrophic/antiatrophic signalling cascades described above, via the downregulation of FoxO3a-induced proteasomal and autophagy-mediated protein degradation. The acute hypoxia-induced increase in phosphoprotein content is likely mediated via the increase in phospho-Akt.

4.6. Proatrophy/Cell Death Signalling

4.6.1. MAPK Pathway. While there appears to be a predominant drive toward protein synthesis in the acutely hypoxic diaphragm, augmented further by NAC pretreatment, there is also an increase in atrophic signalling via the MAPK pathway. JNK promotes autophagy, apoptosis, inflammation, and cell death and is activated by phosphorylation [60]. We observed that acute hypoxia elevated diaphragm levels of phospho-JNK protein, an effect which is further augmented by NAC supplementation. This is somewhat surprising given that Akt, which is also activated, negatively regulates the JNK pathway via a cross-talk mechanism [61]. JNK phosphorylation in our model is therefore likely induced by some other mechanism/stress affecting the MAPK pathway. p38 can promote inflammation and apoptosis, while also negatively regulating GSK-3β to promote survival [62]. In our study, acute hypoxia increased diaphragm phospho-p38 expression to near significant levels in the diaphragm, while NAC concomitant with acute hypoxia significantly augmented this response. This suggests a proatrophic effect of hypoxia + NAC in the diaphragm. We acknowledge that our assessment of apoptotic pathways is incomplete.

We observed no change in autophagy gene expression. We do not have information on autophagy signalling at the

protein level, but this is an area worthy of further pursuit. We observed no change in the expression of several atrogenes, but there was an increase in the mRNA expression of FoxO3 and MuRF-1 in the diaphragm after 8 hours of hypoxia exposure. Despite this apparent increase in atrophy signalling, there was no downstream change in diaphragm proteasome enzymatic activity, suggesting that protein catabolism did not occur, at least not within 8 hours of hypoxic stress, which suggested that diaphragm muscle weakness in hypoxia is not likely related to muscle fibre atrophy, a phenomenon that has been observed in respiratory muscles following chronic sustained hypoxic exposure [13, 14]. Immunohistochemical analysis of diaphragm muscle fibre size and distribution revealed that acute sustained hypoxia did not cause myofibre atrophy or a shift in the size distribution of fibres. Therefore, we conclude that myofibre contractile dysfunction underpins diaphragm weakness following acute hypoxia, a phenomenon that has been reported, in addition to fibre atrophy, in diaphragm in response to chronic sustained hypoxia [63].

We employed a TBARS assay as a measure of muscle lipid peroxidation. We acknowledge the limitation of this measurement as an index of oxidative stress. Malondialdehyde is generated only by certain lipid peroxidation products, and it is not generated exclusively by lipid peroxidation. Exposure to acute hypoxia resulted in a modest but significant increase in diaphragm malondialdehyde, which we interpret as indicative of oxidative stress, but this needs to be confirmed in future studies. Although the source of reactive oxygen species was not determined in our study, the inhibitory effects of reactive oxygen species on striated muscle force-generating capacity are well described [64–66]. Pretreatment with NAC completely reversed the hypoxia-induced increase in diaphragm lipid peroxidation, decreasing TBARS levels to below control values. This reveals the antioxidant capacity of NAC and suggests that some of its inotropic action in diaphragm muscle exposed to hypoxia most likely related to suppression of hypoxia-induced oxidative stress. We acknowledge that the effects of NAC pretreatment were not determined in all experiments.

5. Conclusions

Figure 12 provides an overview of the effects of acute hypoxia on diaphragm protein signaling pathways pivotal to protein turnover and cell survival. Our study determined that acute hypoxic stress of just several hours is sufficient to cause diaphragm weakness, which may have clinical relevance. Hypoxia-induced diaphragm dysfunction is prevented by NAC pretreatment, via a mechanism independent of hypoxic hypometabolism in mice. We previously demonstrated that exposure to acute hypoxia increases UCP-3 mRNA expression in the mouse diaphragm suggesting an increased reliance on fatty acid metabolism [17, 18]. However, in the present study, we determined that the respiratory exchange ratio is unaffected by acute hypoxia, suggesting that there is no switch in metabolic energy source; the ratio of 0.7 reveals that fatty acids are the primary substrate for oxidative metabolism and energy production in normoxic mice, and this is unaltered by hypoxic exposure. This differs from the pronounced metabolic remodelling that occurs in respiratory muscles exposed to chronic sustained hypoxia [15, 16]. The hypoxia-induced increase in UCP-3 [17] may therefore be a compensatory mechanism to reduce ROS production and oxidative stress. Nevertheless, acute hypoxia results in diaphragm muscle oxidative stress, which is likely implicated in the elaboration of diaphragm weakness. Hypoxia did not cause any persistent change in ventilation (diaphragm muscle activity), and therefore muscle weakness and molecular changes are likely directly related to hypoxic stress per se and unrelated to altered mechanical work in hypoxia, though this may be a factor in other mammals such as humans. NAC pretreatment potentiates endogenous cell survival signalling and prevents hypoxia-induced diaphragm oxidative stress. The drive to increase both hypertrophy and atrophy signalling may be required to increase protein turnover and amino acid-dependent ATP generation, but notably diaphragm myofibre size and distribution are unaffected. NAC appears to boost endogenous cell survival signalling cascades potentiating defence responses, perhaps in this way preserving diaphragm function in the face of redox stress, in addition to established antioxidant actions. Our findings highlight the potentially critical role of hypoxic stress as a contributor to diaphragm myofibre dysfunction in respiratory patients. Our results may also have relevance to respiratory muscle performance at high altitude. On the basis of our findings in an animal model, we conclude that NAC may be a beneficial adjunctive therapy in patients, alleviating hypoxia-induced diaphragm dysfunction, potentially improving patient outcome.

Conflicts of Interest

The authors declare that they have no conflicts of interest.

Authors' Contributions

Andrew J. O'Leary and Ken D. O'Halloran conceived and designed the study. Andrew J. O'Leary performed all experiments and data analysis, except for the TBARS assay, which was performed and analyzed by Sarah E. Drummond, and immunohistochemistry, which was performed and analyzed by Deirdre Edge. All authors approved the final version of the manuscript.

Acknowledgments

Ken D. O'Halloran received a Strategic Research Award from University College Cork. Andrew J. O'Leary was supported by the Department of Physiology, University College Cork. The authors are grateful to the staffs of the Biological Services Unit, UCC, for the support with animal care and welfare. The authors are grateful to Dr. Greg Jasionek, Department of Physiology, UCC, for technical support.

References

[1] G. S. Supinski and L. A. Callahan, "Diaphragm weakness in mechanically ventilated critically ill patients," *Critical Care*, vol. 17, no. 3, article R120, 2013.

[2] M. B. Hudson, A. J. Smuder, W. B. Nelson, C. S. Bruells, S. Levine, and S. K. Powers, "Both high level pressure support ventilation and controlled mechanical ventilation induce diaphragm dysfunction and atrophy," *Critical Care Medicine*, vol. 40, no. 4, pp. 1254–1260, 2012.

[3] A. N. Kavazis, E. E. Talbert, A. J. Smuder, M. B. Hudson, W. B. Nelson, and S. K. Powers, "Mechanical ventilation induces diaphragmatic mitochondrial dysfunction and increased oxidant production," *Free Radical Biology & Medicine*, vol. 46, no. 6, pp. 842–850, 2009.

[4] J. Doorduin, J. Leentjens, M. Kox et al., "Effects of experimental human endotoxemia on diaphragm function," *Shock*, vol. 44, no. 4, pp. 316–322, 2015.

[5] G. S. Supinski, A. P. Alimov, L. Wang, X. H. Song, and L. A. Callahan, "Calcium-dependent phospholipase A_2 modulates infection-induced diaphragm dysfunction," *American Journal of Physiology Lung Cell Molecular Physiology*, vol. 310, no. 10, pp. L975–L984, 2016.

[6] A. H. Jonkman, D. Jansen, and L. M. Heunks, "Novel insights in ICU-acquired respiratory muscle dysfunction: implications for clinical care," *Critical Care*, vol. 21, no. 1, p. 64, 2017.

[7] A. V. Namuduri, G. Heras, J. Mi et al., "A proteomic approach to identify alterations in the SUMO network during controlled mechanical ventilation in rat diaphragm muscle," *Molecular & Cell Proteomics*, vol. 16, no. 6, pp. 1081–1097, 2017.

[8] I. Azuelos, B. Jung, M. Picard et al., "Relationship between autophagy and ventilator-induced diaphragmatic dysfunction," *Anesthesiology*, vol. 122, no. 6, pp. 1349–1361, 2015.

[9] S. K. Powers, M. B. Hudson, W. B. Nelson et al., "Mitochondria-targeted antioxidants protect against mechanical ventilation-induced diaphragm weakness," *Critical Care Medicine*, vol. 39, no. 7, pp. 1749–1759, 20111759, 2011.

[10] J. Wu and S. T. Li, "Dexmedetomidine may produce extra protective effects on sepsis-induced diaphragm injury," *Chinese Medical Journal*, vol. 128, no. 10, pp. 1407–1411, 2015.

[11] G. S. Supinski and L. A. Callahan, "Free radical-mediated skeletal muscle dysfunction in inflammatory conditions," *Journal of Applied Physiology*, vol. 102, no. 5, pp. 2056–2063, 2007.

[12] S. K. Powers, M. P. Wiggs, K. J. Sollanek, and A. J. Smuder, "Ventilator-induced diaphragm dysfunction: cause and effect," *American Journal of Physiology-Regulatory Integrative and Comparative Physiology*, vol. 305, no. 5, pp. R464–R477, 2013.

[13] C. McMorrow, A. Fredsted, J. Carberry et al., "Chronic hypoxia increases rat diaphragm muscle endurance and sodium-potassium ATPase pump content," *European Respiratory Journal*, vol. 37, no. 6, pp. 1474–1481, 2011.

[14] J. L. Gamboa and F. H. Andrade, "Muscle endurance and mitochondrial function after chronic normobaric hypoxia: contrast of respiratory and limb muscles," *Pflügers Archiv - European Journal of Physiology*, vol. 463, no. 2, pp. 327–338, 2012.

[15] P. Lewis, D. Sheehan, R. Soares, A. Varela Coelho, and K. D. O'Halloran, "Chronic sustained hypoxia-induced redox remodeling causes contractile dysfunction in mouse sternohyoid muscle," *Frontiers in Physiology*, vol. 6, p. 122, 2015.

[16] P. Lewis, D. Sheehan, R. Soares, A. V. Coelho, and K. D. O'Halloran, "Redox remodeling is pivotal in murine diaphragm muscle adaptation to chronic sustained hypoxia," *American Journal of Respiratory Cell and Molecular Biology*, vol. 55, no. 1, pp. 12–23, 2016.

[17] A. J. O'Leary and K. D. O'Halloran, "Diaphragm muscle weakness and increased UCP-3 gene expression following acute hypoxic stress in the mouse," *Respiratory Physiology & Neurobiology*, vol. 226, pp. 76–80, 2016.

[18] A. J. O'Leary, *Acute Hypoxia-Induced Diaphragm Dysfunction Is Prevented by Antioxidant Pre-Treatment, [Ph.D. thesis]*, University College Cork, Ireland, 2017, https://cora.ucc.ie/bitstream/handle/10468/3895/O'LearyAJ_PhD2017.pdf.

[19] R. Pellegrino, G. Deboeck, J. J. Moraine, and R. Naeije, "Respiratory muscle strength may explain hypoxia-induced decrease in vital capacity," *Medicine & Science in Sports & Exercise*, vol. 26, pp. 754–758, 2005.

[20] S. Sharma and B. Brown, "Spirometry and respiratory muscle function during ascent to higher altitudes," *Lung*, vol. 185, no. 2, pp. 113–121, 2007.

[21] P. Lewis and K. D. O'Halloran, "Diaphragm muscle adaptation to sustained hypoxia: lessons from animal models with relevance to high altitude and chronic respiratory diseases," *Frontiers in Physiology*, vol. 7, p. 623, 2016.

[22] R. Campos, M. H. M. Shimizu, R. A. Volpini et al., "*N*-acetylcysteine prevents pulmonary edema and acute kidney injury in rats with sepsis submitted to mechanical ventilation," *American Journal of Physiology Lung Cellular and Molecular Physiology*, vol. 302, no. 7, pp. L640–L650, 2012.

[23] M. Cazzola, L. Calzetta, C. Page et al., "Influence of *N*-acetylcysteine on chronic bronchitis or COPD exacerbations: a meta-analysis," *European Respiratory Review*, vol. 24, no. 137, pp. 451–461, 2015.

[24] C. Conrad, J. Lymp, V. Thompson et al., "Long-term treatment with oral N-acetylcysteine: affects lung function but not sputum inflammation in cystic fibrosis subjects. A phase II randomized placebo-controlled trial," *Journal of Cystic Fibrosis*, vol. 14, no. 2, pp. 219–227, 2015.

[25] B. J. Day, "Antioxidants as potential therapeutics for lung fibrosis," *Antioxidant & Redox Signaling*, vol. 10, no. 2, pp. 355–370, 2008.

[26] M. Skov, T. Pressler, J. Lykkesfeldt et al., "The effect of short-term, high-dose oral N-acetylcysteine treatment on oxidative stress markers in cystic fibrosis patients with chronic *P. aeruginosa* infection - a pilot study," *Journal of Cystic Fibrosis*, vol. 14, no. 2, pp. 211–218, 2015.

[27] P. M. Suter, G. Domenighetti, M.-D. Schaller, M.-C. Laverrière, R. Ritz, and C. Perret, "N-acetylcysteine enhances recovery from acute lung injury in man," *Chest Journal*, vol. 105, no. 1, pp. 190–194, 1994.

[28] V. M. Víctor, J. V. Espulgues, A. Hernández-Mijares, and M. Rocha, "Oxidative stress and mitochondrial dysfunction in sepsis: a potential therapy with mitochondria-targeted antioxidants," *Infectious Disorders Drug Targets*, vol. 9, no. 4, pp. 376–389, 2009.

[29] S. Levine, M. H. Bashir, T. L. Clanton, S. K. Powers, and S. Singhal, "COPD elicits remodeling of the diaphragm and vastus lateralis muscles in humans," *Journal of Applied Physiology*, vol. 114, no. 9, pp. 1235–1245, 2013.

[30] M. Klimathianaki, K. Vaporidi, and D. Georgopoulos, "Respiratory muscle dysfunction in COPD: from muscles to cell," *Current Drug Targets*, vol. 12, no. 4, pp. 478–488, 2011.

[31] M. Dunleavy, A. Bradford, and K. D. O'Halloran, "Oxidative stress impairs upper airway muscle endurance in an animal model of sleep-disordered breathing," *Advances in*

Experimental Medicine and Biology, vol. 605, pp. 458–462, 2008.

[32] C. M. Shortt, A. Fredsted, H. B. Chow et al., "Reactive oxygen species mediated diaphragm fatigue in a rat model of chronic intermittent hypoxia," *Experimental Physiology*, vol. 99, no. 4, pp. 688–700, 2014.

[33] M. S. Soltan-Sharifi, M. Mojtahedzadeh, A. Najafi et al., "Improvement by N-acetylcysteine of acute respiratory distress syndrome through increasing intracellular glutathione, and extracellular thiol molecules and anti-oxidant power: evidence for underlying toxicological mechanisms," *Human & Experimental Toxicology*, vol. 26, no. 9, pp. 697–703, 2007.

[34] J. Magalhães, A. Ascensão, J. M. C. Soares et al., "Acute and severe hypobaric hypoxia increases oxidative stress and impairs mitochondrial function in mouse skeletal muscle," *Journal of Applied Physiology*, vol. 99, no. 4, pp. 1247–1253, 2005.

[35] M. A. Smith and M. B. Reid, "Redox modulation of contractile function in respiratory and limb skeletal muscle," *Respiratory Physiology & Neurobiology*, vol. 151, no. 2-3, pp. 229–241, 2006.

[36] Y. B. Seven, C. B. Mantilla, and G. C. Sieck, "Recruitment of rat diaphragm motor units across motor behaviors with different levels of diaphragm activation," *Journal of Applied Physiology*, vol. 117, no. 11, pp. 1308–1316, 2014.

[37] P. Lewis, C. McMorrow, A. Bradford, and K. D. O'Halloran, "Improved tolerance of acute severe hypoxic stress in chronic hypoxic diaphragm is nitric oxide-dependent," *The Journal of Physiological Sciences*, vol. 65, no. 5, pp. 427–433, 2015.

[38] A. Agten, K. Maes, A. Smuder, S. K. Powers, M. Decramer, and G. Gayan-Ramirez, "N-acetylcysteine protects the rat diaphragm from the decreased contractility associated with controlled mechanical ventilation," *Critical Care Medicine*, vol. 39, no. 4, pp. 777–782, 2011.

[39] E. Barreiro, "Role of protein carbonylation in skeletal muscle mass loss associated with chronic conditions," *Proteomes*, vol. 4, no. 2, p. 18, 2016.

[40] S. Bonello, C. Zähringer, R. S. BelAiba et al., "Reactive oxygen species activate the HIF-1α promoter via a functional NFκB site," *Arteriosclerosis Thrombosis, and Vascular Biology*, vol. 27, no. 4, pp. 755–761, 2007.

[41] S. W. Jusman, A. Halim, S. I. Wanandi, and M. Sadikin, "Expression of hypoxia-inducible factor-1α (HIF-1α) related to oxidative stress in liver of rat-induced by systemic chronic normobaric hypoxia," *Acta Medica Indonesia*, vol. 42, pp. 17–23, 2010.

[42] H. Niecknig, S. Tug, B. D. Reyes, M. Kirsch, J. Fandrey, and U. Berchner-Pfannschmidt, "Role of reactive oxygen species in the regulation of HIF-1 by prolyl hydroxylase 2 under mild hypoxia," *Free Radical Research*, vol. 46, no. 6, pp. 705–717, 2012.

[43] M. Schieber and N. S. Chandel, "ROS function in redox signaling and oxidative stress," *Current Biology*, vol. 24, no. 10, pp. R453–R462, 2014.

[44] W. S. Jin, Z. L. Kong, Z. F. Shen, Y. Z. Jin, W. K. Zhang, and G. F. Chen, "Regulation of hypoxia inducible factor-1α expression by the alteration of redox status in HepG2 cells," *Journal of Experimental & Clinical Cancer Research*, vol. 30, no. 1, p. 61, 2011.

[45] M. Nikinmaa, S. Pursiheimo, and A. J. Soitamo, "Redox state regulates HIF-1α and its DNA binding and phosphorylation in salmonid cells," *Journal of Cell Science*, vol. 117, no. 15, pp. 3201–3206, 2004.

[46] J. Sceneay, M. C. P. Liu, A. Chen, C. S. F. Wong, D. D. L. Bowtell, and A. Möller, "The antioxidant N-acetylcysteine prevents HIF-1 stabilization under hypoxia *in vitro* but does not affect tumorigenesis in multiple breast cancer models *in vivo*," *PLoS One*, vol. 8, no. 6, article e66388, 2013.

[47] Z. Zhang, J. Yan, S. Taheri, K. J. Liu, and H. Shi, "Hypoxia-inducible factor 1 contributes to N-acetylcysteine's protection in stroke," *Free Radical Biology & Medicine*, vol. 68, pp. 8–21, 2014.

[48] M. Alvarez-Tejado, S. Naranjo-Suarez, C. Jiménez et al., "Hypoxia induces the activation of the phosphatidylinositol 3-kinase/Akt cell survival pathway in PC12 cells: protective role in apoptosis," *Journal of Biological Chemistry*, vol. 276, no. 25, pp. 22368–22374, 2001.

[49] D. Beitner-Johnson, R. T. Rust, T. C. Hsieh, and D. E. Millhorn, "Hypoxia activates Akt and induces phosphorylation of GSK-3 in PC12 cells," *Cellular Signalling*, vol. 13, no. 1, pp. 23–27, 2001.

[50] T. Dai, H. Zheng, and G. Fu, "Hypoxia confers protection against apoptosis *via* the PI3K/Akt pathway in endothelial progenitor cells," *Acta Pharmacologica Sinica*, vol. 29, no. 12, pp. 1425–1431, 2008.

[51] H. Stegeman, J. H. Kaanders, D. L. Wheeler et al., "Activation of AKT by hypoxia: a potential target for hypoxic tumors of the head and neck," *BMC Cancer*, vol. 12, no. 1, p. 463, 2012.

[52] M. Kilic-Eren, T. Boylu, and V. Tabor, "Targeting PI3K/Akt represses hypoxia inducible factor-1α activation and sensitizes rhabdomyosarcoma and Ewing's sarcoma cells for apoptosis," *Cancer Cell International*, vol. 13, no. 1, p. 36, 2013.

[53] S. C. Land and A. R. Tee, "Hypoxia-inducible factor 1α is regulated by the mammalian target of rapamycin (mTOR) via an mTOR signaling motif," *Journal of Biological Chemistry*, vol. 282, no. 28, pp. 20534–20543, 2007.

[54] X. M. Yang, Y. S. Wang, J. Zhang et al., "Role of PI3K/Akt and MEK/ERK in mediating hypoxia-induced expression of HIF-1α and VEGF in laser-induced rat choroidal neovascularization," *Investigative Ophthalmology & Visual Science*, vol. 50, no. 4, pp. 1873–1879, 2009.

[55] K. Baar and K. Esser, "Phosphorylation of $p70^{S6k}$ correlates with increased skeletal muscle mass following resistance exercise," *American Journal of Physiology Cell Physiology*, vol. 276, no. 1, pp. C120–C127, 1999.

[56] P. Gran, A. E. Larsen, M. Bonham et al., "Muscle p70S6K phosphorylation in response to soy and dairy rich meals in middle aged men with metabolic syndrome: a randomised crossover trial," *Nutrition & Metabolism*, vol. 11, no. 1, p. 46, 2014.

[57] N. E. Zanchi and A. H. Lancha, "Mechanical stimuli of skeletal muscle: implications on mTOR/p70s6k and protein synthesis," *European Journal of Applied Physiology*, vol. 102, no. 3, pp. 253–263, 2008.

[58] J. G. Krolikowski, D. Weihrauch, M. Bienengraeber, J. R. Kersten, D. C. Warltier, and P. S. Pagel, "Role of Erk1/2, p70s6K, and eNOS in isoflurane-induced cardioprotection during early reperfusion in vivo," *Canadian Journal of Anesthesiology*, vol. 53, no. 2, pp. 174–182, 2006.

[59] J. M. McClung, M. A. Whidden, A. N. Kavazis, D. J. Falk, K. C. Deruisseau, and S. K. Powers, "Redox regulation of diaphragm proteolysis during mechanical ventilation," *American Journal*

of Physiology Regulatory, Integrative and Comparative Physiology, vol. 294, no. 5, pp. R1608–R1617, 2008.

[60] A. Berdichevsky, L. Guarente, and A. Bose, "Acute oxidative stress can reverse insulin resistance by inactivation of cytoplasmic JNK," *Journal of Biological Chemistry*, vol. 285, no. 28, pp. 21581–21589, 2010.

[61] V. Levresse, L. Butterfield, E. Zentrich, and L. E. Heasley, "Akt negatively regulates the cJun N-terminal kinase pathway in PC12 cells," *Journal of Neuroscience Research*, vol. 62, no. 6, pp. 799–808, 2000.

[62] T. M. Thornton, G. Pedraza-Alva, B. Deng et al., "Phosphorylation by p38 MAPK as an alternative pathway for GSK3beta inactivation," *Science*, vol. 320, no. 5876, pp. 667–670, 2008.

[63] H. Degens, A. Bosutti, S. F. Gilliver, M. Slevin, A. van Heijst, and R. C. Wust, "Changes in contractile properties of skinned single rat soleus and diaphragm fibres after chronic hypoxia," *Pflügers Archiv - European Journal of Physiology*, vol. 460, no. 5, pp. 863–873, 2010.

[64] T. L. Clanton, "Hypoxia-induced reactive oxygen species formation in skeletal muscle," *Journal of Applied Physiology*, vol. 102, no. 6, pp. 2379–2388, 2007.

[65] L. Zuo, T. M. Best, W. J. Roberts, P. T. Diaz, and P. D. Wagner, "Characterization of reactive oxygen species in diaphragm," *Acta Physiologica*, vol. 213, no. 3, pp. 700–710, 2015.

[66] M. B. Reid and J. S. Moylan, "Beyond atrophy: redox mechanisms of muscle dysfunction in chronic inflammatory disease," *The Journal of Physiology*, vol. 589, no. 9, pp. 2171–2179, 2011.

Hindawi
Oxidative Medicine and Cellular Longevity
Volume 2018, Article ID 4814696, 10 pages
https://doi.org/10.1155/2018/4814696

Research Article

Role of miR-200c in Myogenic Differentiation Impairment via p66Shc: Implication in Skeletal Muscle Regeneration of Dystrophic *mdx* Mice

Marco D'Agostino,[1] Alessio Torcinaro,[2,3] Luca Madaro,[4] Lorenza Marchetti,[5] Sara Sileno,[5] Sara Beji,[5] Chiara Salis,[5] Daisy Proietti,[4] Giulia Imeneo,[3] Maurizio C. Capogrossi,[5,6] Francesca De Santa,[3,4] and Alessandra Magenta[5]

[1]*Department of Experimental Medicine, Sapienza University of Rome, Viale Regina Elena 324, 00161 Rome, Italy*
[2]*Department of Biology and Biotechnology "Charles Darwin", Sapienza University of Rome, Roma, Italy*
[3]*Institute of Cell Biology and Neurobiology (IBCN), Italian National Research Council (CNR), 00143 Rome, Italy*
[4]*Fondazione Santa Lucia IRCCS, 00143 Rome, Italy*
[5]*Vascular Pathology Laboratory, Instituto Dermopatico dell'Immacolata-IRCCS, FLMM, Via dei Monti di Creta 104, 00167 Rome, Italy*
[6]*Department of Cardiology, Ochsner Medical Center, 1514 Jefferson Hwy., New Orleans, LA 70121, USA*

Correspondence should be addressed to Alessandra Magenta; ale.magenta@gmail.com

Received 31 July 2017; Revised 18 December 2017; Accepted 25 December 2017; Published 13 February 2018

Academic Editor: Andrey J. Serra

Duchenne muscular dystrophy (DMD) is a genetic disease associated with mutations of Dystrophin gene that regulate myofiber integrity and muscle degeneration, characterized by oxidative stress increase. We previously published that reactive oxygen species (ROS) induce miR-200c that is responsible for apoptosis and senescence. Moreover, we demonstrated that miR-200c increases ROS production and phosphorylates p66Shc in Ser-36. p66Shc plays an important role in muscle differentiation; we previously showed that p66Shc$^{-/-}$ muscle satellite cells display lower oxidative stress levels and higher proliferation rate and differentiated faster than wild-type (*wt*) cells. Moreover, myogenic conversion, induced by MyoD overexpression, is more efficient in p66Shc$^{-/-}$ fibroblasts compared to *wt* cells. Herein, we report that miR-200c overexpression in cultured myoblasts impairs skeletal muscle differentiation. Further, its overexpression in differentiated myotubes decreases differentiation indexes. Moreover, anti-miR-200c treatment ameliorates myogenic differentiation. In keeping, we found that miR-200c and p66Shc Ser-36 phosphorylation increase in *mdx* muscles. In conclusion, miR-200c inhibits muscle differentiation, whereas its inhibition ameliorates differentiation and its expression levels are increased in *mdx* mice and in differentiated human myoblasts of DMD. Therefore, miR-200c might be responsible for muscle wasting and myotube loss, most probably via a p66Shc-dependent mechanism in a pathological disease such as DMD.

1. Introduction

We previously showed that oxidative stress inhibits myogenic differentiation [1] and in a model of oxidative stress such as acute hind limb ischemia, it was demonstrated that reactive oxygen species (ROS) production plays a causal role in tissue damage, leading to cell death by both apoptosis and necrosis [2].

p66Shc adaptor protein is a redox enzyme implicated in mitochondrial ROS generation and translation of oxidative signals [3]. Under physiological conditions, the phosphorylation of Tyr residues of p66Shc by growth factors mediates the signal transduction to the nucleus, inhibiting the Ras signaling pathway, while phosphorylation of the Ser-36 site is crucial for oxidative stress response [4]. p66Shc once phosphorylated in Ser-36 enhances ROS production by using

three different mechanisms restricted in the nucleus, the plasma membrane, and the mitochondria [4].

In keeping, our previous results demonstrated that p66Shc inhibits myogenic differentiation and p66Shc deletion enhances skeletal muscle regeneration after ischemia [1].

MicroRNAs (miRNAs) are 21–23 nucleotide RNA molecules that regulate stability or translational efficiency of target messenger RNAs [5]. miRNAs control a wide range of cell functions and have been associated with inflammation, oxidative stress, and differentiation [6–8].

We previously showed that the miR-200 family is upregulated upon oxidative stress in different cells, such as endothelial cells, human fibroblasts, murine myoblasts, and myotubes [9]. This miRNA family consists of five members (miR-200c, miR-141, miR-200a, miR-200b, and miR-429). We demonstrated that miR-200c is the most upregulated family member and is responsible for apoptosis and senescence by targeting zinc finger E-box-binding homeobox 1 (ZEB1) protein [9]. We also demonstrated that miR-200c is induced following acute hind limb ischemia in skeletal muscles and this induction was oxidative stress dependent, since in p66Shc$^{-/-}$ mice, which exhibit less oxidative stress than wild-type (*wt*) mice [1], miR-200c increase is significantly attenuated [9].

In a recent publication, we demonstrated that miR-200c increased ROS production and induced p66Shc protein phosphorylation in Ser-36; this mechanism upregulated ROS and inhibited FOXO1 transcription of ROS scavengers, reinforcing this molecular circuitry [10].

Moreover, we showed that anti-miR-200c treatment in hind limb ischemia in mice rescued the decrease of miR-200c protein targets and improved limb perfusion [10].

Herein, we wanted to dissect the role of miR-200c in muscle differentiation and to comprehend whether miR-200c levels were modulated in muscle pathological diseases associated with oxidative stress increase, such as Duchenne muscular dystrophy (DMD) [11, 12].

In keeping with this hypothesis, in the paper of Greco et al., an interesting link between ischemia-, *mdx*-, and DMD-modulated miRNAs associated with apoptosis/myonecrosis was demonstrated [13]. Interestingly, in adductor muscles of *mdx*, a miR-200c upregulation was found in a miRNA screening, although not significantly [13].

Muscular dystrophies are a heterogenous group of genetic disorders characterized by muscle degeneration and associated with mutations of genes that regulate myofiber integrity [14]. The most common dystrophy is the DMD, a lethal X-linked genetic disease characterized by severe muscle degeneration, caused by deficiency of dystrophin, a critical component of the dystrophin glycoprotein complex (DGC), acting as a link between cytoskeleton and extracellular matrix both in skeletal and cardiac muscles [15, 16]. The *mdx* mice strain represents the most used animal model to study DMD [17].

Dystrophic muscles undergo continuous cycles of degeneration and regeneration. Satellite cells (SC), the skeletal muscle stem cells, exit from quiescence and undergo the proliferation phase followed by activation of skeletal muscle differentiation program or return to quiescence to maintain the stem cell pool. Although SC compensate for muscle fiber loss in the early stages of dystrophy leading to muscle compensatory regeneration, eventually, these progenitors become exhausted [18]. As a result, muscles are characterized by necrosis and inflammation culminating in extracellular matrix and fat deposition. Consequently, fibrous and fatty connective tissue overtakes the functional myofibers [15, 19].

Recent papers highlighted new cellular and molecular mechanisms contributing to SC dysfunction in dystrophic muscle. Specifically, SC hold an intrinsic cell dysfunction affecting their polarity and asymmetric division [20]. Moreover, SC can undergo mesenchymal fibrogenic conversion, mediated by TGFbeta signaling, compromising their physiological muscle regenerative functions [21, 22].

The pathology of DMD appears to be exacerbated by oxidative stress, and ROS increase plays a pivotal role in the necrosis of skeletal muscles in DMD and in dystrophic *mdx* mouse [11]. Moreover, since contractile (myofibrillar) proteins such as myosin, actin, troponin, and tropomyosin containing thiol side chains are sensitive to oxidation, these modifications may alter excitation/contraction coupling and cross-bridge cycling, modulating muscle contraction. As a consequence, excessive oxidative stress that occurs in DMD provokes muscle weakness and wasting [11].

The results of the present work show that miR-200c impairs muscle differentiation, whereas miR-200c inhibition ameliorates differentiation; moreover, both miR-200c expression levels and p66Shc phosphorylation in Ser-36 increase in *mdx* mice. Moreover, miR-200c increases also in differentiated human myoblasts of DMD. Therefore, we hypothesized a miR-200c role in muscle wasting and myotube loss via a p66Shc-dependent mechanism in DMD.

2. Materials and Methods

2.1. Cell Line, Culture Conditions, and Transfections. C2.12 (C2C12), a subclone of the C2 mouse myoblast cell line, was obtained from M Buckingham. C2C12 were cultured in growth medium ((GM) DMEM-GlutaMAX complemented with penicillin/streptomycin and 20% FBS). Myogenic differentiation was induced by shifting the cells in differentiation medium ((DM) DMEM-GlutaMAX complemented with penicillin/streptomycin and 2% FBS).

Human myoblasts were derived from muscle biopsies of healthy donors or DMD patients. Human myoblasts were cultured in growth medium (GM) (DMEM-GlutaMAX complemented with penicillin/streptomycin and 20% FBS). Myogenic differentiation was induced by shifting the cells in differentiation medium (DM) (DMEM-GlutaMAX complemented with penicillin/streptomycin, 5% horse serum, and insulin 100 μg/ml).

Transfections were carried out by using Lipofectamine 3000 reagent (Invitrogen) according to the manufacturer's instructions. Cells were seeded at 10^5 per well in six-well dishes and transfected 18 hours (h) later. The amount of plasmid used in transfection assay is indicated in the figure legend.

2.2. Drug Treatments. H_2O_2 (30% (wt/wt) solution; Sigma) was administered to the cells as a 100 mM solution in phosphate-buffered saline (PBS).

2.3. Plasmid Constructs. p66Shc-Ser-36 to Ala mutant was generated using QuickChange Site-Directed Mutagenesis Kit (Stratagene) starting from p66Shc pBABE vector. plko.1-miR-200c and plko.1-anti-miR-200c constructs were described previously [9, 10].

2.4. miRNA Overexpression and Inhibition. Stable expression of miR-200c, anti-miR-200c, or miR-scramble in C2C12 cells was generated by viral infection using lentiviral supernatants. These viruses were produced as previously described [23]. In summary, cells were infected with lentiviral virus for 2 h and then were recovered in complete fresh medium for 24 h. Afterwards, infected cells were selected by puromycin-containing medium (Sigma) for 72 h. miR-200c overexpression was controlled by quantitative real-time PCR (RT-qPCR) (see methods below).

2.5. Immunofluorescence of Cultured Cells. C2C12 in culture were fixed in 4% paraformaldehyde in PBS for 10 minutes at room temperature, incubated with glycine 50 mM in PBS for 10 minutes at room temperature to quench paraformaldehyde, and permeabilized with 0.1% Triton-X in PBS for 10 min at room temperature. Then, cells were blocked with 4% IgG-free bovine serum albumin (BSA) in PBS for 30 minutes. Cells were immune labelled with the antibody against myosin heavy chain (MyHC) (MF20 Hybridoma bank) in 4% BSA overnight at +4°C. Donkey anti-mouse IgG conjugated to Alexa Fluor 488 (Jackson ImmunoResearch #715-545-150) were used to detect the signal. Nuclei were counterstained with DAPI (Sigma D9542). Phase contrast images of C2C12 cells were acquired with Leica microscope (DM-IRB). Immunofluorescence images were acquired with confocal laser scanning microscopy system Zeiss Axiovert 200M or fluorescence microscope Nikon Eclipse TE-2000E. Counts were performed with ImageJ software.

Differentiation index calculations are as follows:

(i) *Differentiation index* was measured as the percentage of all $MyHC^+$ cells, both mononucleated and multinucleated cells.

(ii) *Fusion index* was measured as the percentage of multinucleated $MyHC^+$ cells (≥2 nuclei).

(iii) *Nuclei per myotube* were calculated as the mean of the number of nuclei within myotubes.

2.6. Animal Model. *Mdx* mice (C57BL10J DMD^{mdx}) and wild-type (*wt*) mice (C57BL10J) were purchased from Charles River. All mice handling procedures were approved by the internal Animal Research Ethical Committee according to the Italian Ministry of Health and complied with the NIH Guide for the Care and Use of Laboratory Animals. All the procedures were carried out in accordance with the promise of the three Rs (replacement, reduction, and refinement). The animals were housed in cages with environmental enrichment in order to reduce pain and stress and increase animal welfare. The animals were sacrificed, and hind limb muscles were directly frozen in liquid nitrogen and stored at −80°C.

2.7. RNA Isolation and qPCR Analysis. Hind limb muscles from *mdx* mice were homogenized by a handheld rotor-stator homogenizer (TissueRuptor—Qiagen) in TRIzol reagent (Invitrogen). RNA was extracted following manufacturer's protocol (TRIzol—Invitrogen).

Hind limb muscles were isolated from 3 different animals for each strain and age described in the figures, and RNA was isolated and quantified by NanoDrop (Thermo Scientific 2000C).

miRNA levels were analyzed using the TaqMan RT-qPCR and quantified with the ABI Prism 7000 SDS (Applied Biosystems). miR-200c levels were normalized to U6 small RNA expression as previously reported [24, 25].

Primers for miR-200c, U6, and reagents for reverse transcriptase and RT-qPCRs were all obtained from Applied Biosystems.

2.8. Protein Isolation and Western Blot Analysis. C2C12 cells were lysed in a buffer containing 100 mM Tris (pH 6.8), 20% glycerol, and 4% sodium dodecyl sulfate (SDS). Amounts of protein were determined by bicinchoninic acid protein assay kit (Pierce, Rockford, IL). Then dithiothreitol (DTT) (200 mM) was added and lysates were boiled for 5 min.

Hind limb muscles from *mdx* mice were homogenized by a handheld rotor-stator homogenizer (TissueRuptor—Qiagen; 5–10 seconds, 4 times at +4°C) in protein extraction buffer containing 50 mM Tris-HCl pH 7.5, 0.6 M sucrose, 50% glycerol, 1% Triton, and 50 mM NaCl supplemented with protease (1 mM PMSF, 5 μg/ml aprotinin, 5 μg/ml leupeptin, and 5 μg/ml pepstatin) and phosphatase inhibitors (10 mM NaF, 5 mM β-glycerophosphate, and 1 mM Na-orthovanadate). Lysates were also sonicated (5 seconds, 2 times), incubated on a tube rotator at +4°C for 30 minutes, and cleared of insoluble debris by centrifugation at 13000 rpm for 20 minutes at +4°C and the supernatants were stored at −80°C. Protein concentrations were determined by Bradford assay.

For Western blot analysis, proteins were extracted from gastrocnemius and quadriceps muscles of *wt* and *mdx* animals (3 *wt* mice and 3 *mdx* mice of 4 weeks and 36 weeks, resp.). Proteins were separated on denaturing SDS-polyacrylamide gels, transferred to the nitrocellulose membrane by standard procedures, and blotted with the following primary antibodies: ZEB1 (H-102), myosin heavy chain MyHC (MF20 mouse hybridoma), MyoD (MoAb 5.8A, Dako), myogenin (IF5D mouse hybridoma), p66Shc (Transduction Laboratories), p66Shc-phospho-Ser-36 (Abcam 6E10), tubulin (Oncogene Research Products Ab-1), and GAPDH (Calbiochem CB1001). The antibody binding was revealed by horseradish peroxidase-conjugated secondary antibodies followed by chemiluminescence detection (ECL, Pierce).

Immunoprecipitations were performed as previously described [26]. Cells were resuspended in lysis buffer containing 50 mM HEPES (pH 7.5), 250 mM NaCl, 1 mM DTT, 0.1% Tween 20, 10% glycerol, 5 mM CaCl2, 1 mM phenylmethylsulfonyl fluoride (PMSF), 10 mM Na_3VO_4, 50 mM NaF, and protease inhibitors (complete EDTA-free protease inhibitor mixture tablets; Roche Applied Sciences). Immunoprecipitations were performed for 2 to 3 h at 4°C with protein A/G agarose and 1 μg of relevant antibodies. Immune

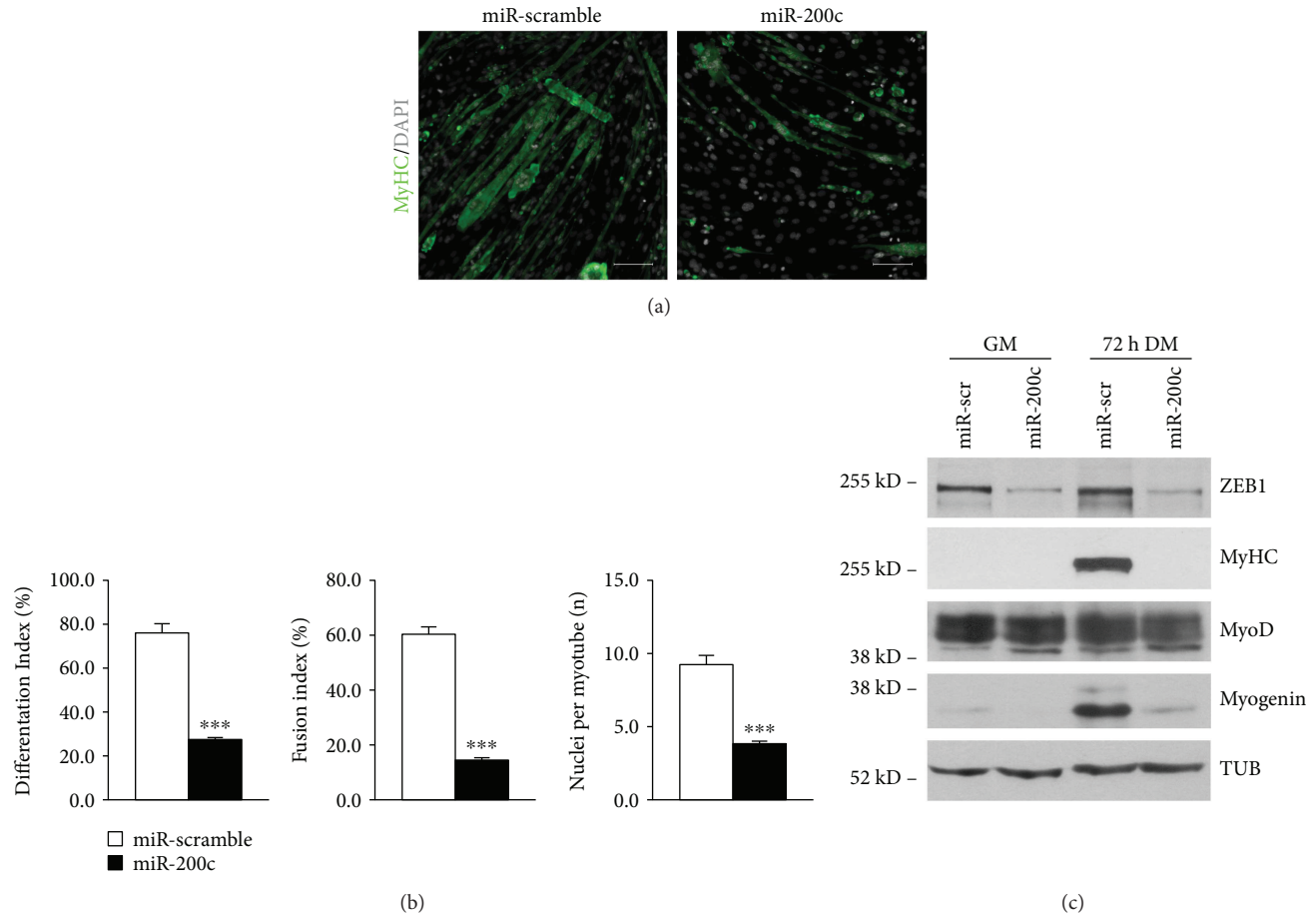

Figure 1: miR-200c overexpression in myoblasts inhibits skeletal muscle differentiation *in vitro*. C2C12 myoblasts were infected either with a lentivirus encoding miR-200c or with a control virus. After selection with puromycin, cells were plated and shifted to differentiation medium for 3 days. (a) Representative images of anti-MyHC staining (green). Nuclei were counterstained with DAPI (grey). Immunofluorescence with anti-MyHC antibody showed a decrease in myotubes in miR-200c-overexpressing cells compared to control. Scale bar: 200 μm. (b) Bar graphs representing differentiation index (percentage of MyHC-positive cells), fusion index (percentage of nuclei within a myotube), and number of nuclei per myotube. miR-200c overexpression decreased all these parameters ($n = 3$ independent experiments; $^{***}p < 0.001$). (c) A representative Western blot using ZEB1, MyHC, myogenin, and antibodies showed that protein levels decreased upon miR-200c overexpression and MyoD expression was not affected. α-Tubulin (TUB) was used as loading control.

complexes were resuspended in 2x Laemmli buffer, separated by SDS-polyacrylamide gel electrophoresis (PAGE), and immunoblotted with relevant antibodies.

2.9. Statistical Analysis. The number of samples or independent experiments and the definition of reported values are indicated in the figure legends as mean ± standard error of the mean (SEM). Statistical analyses were performed using the GraphPad Prism software (Version 5.0). Statistical significance was assessed by unpaired Student's *t*-test or ANOVA. *P* value < 0.05 was considered as statistically significant.

3. Results

3.1. miR-200c Overexpression Inhibits Myogenic Differentiation. We previously showed that oxidative stress inhibits muscle differentiation [1]. We also demonstrated that miR-200c is highly induced upon H_2O_2 treatment in C2C12 in both myoblasts and differentiated myotubes [9]. Therefore, we asked whether miR-200c modulation had an effect on myogenic differentiation.

To this aim, we overexpressed miR-200c in C2C12 myoblasts; then, we shifted the cells to differentiation medium (DM). We found that miR-200c inhibited myotube formation as assessed by MyHC immunofluorescence staining (Figure 1(a)). In addition, a decrease of three muscle differentiation parameters was also observed, specifically differentiation index (percentage of both myotubes and MyHC-positive cells), fusion index (percentage of nuclei within a myotube), and number of nuclei within myotubes (Figure 1(b)). We then analyzed myogenic differentiation by Western blot analysis, and we observed that ZEB1, MyHC, and myogenin proteins were all downregulated upon miR-200c overexpression, whereas MyoD was not affected (Figure 1(c)).

miR-200c overexpression was also performed in C2C12 after 24 hrs of myogenic differentiation. As shown in phase contrast images of Figure 2(a), we started from cells with a similar degree of differentiation prior to infection (upper

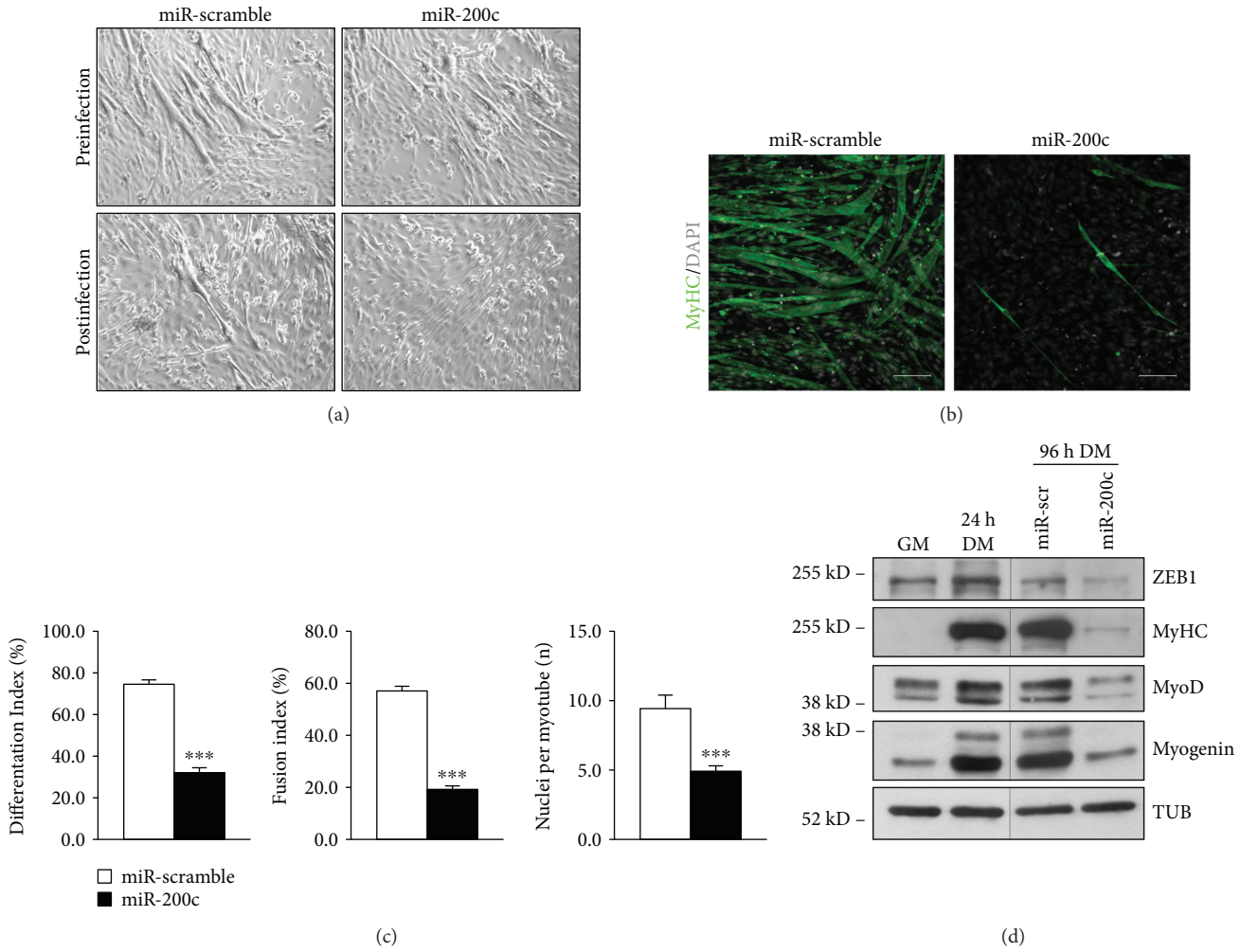

Figure 2: miR-200c overexpression in myotubes inhibits skeletal muscle differentiation *in vitro*. C2C12 myoblasts were shifted to differentiation medium for 24 hrs; then, cells were infected either with a lentivirus encoding miR-200c or with a control virus. Afterwards, cells were selected with puromycin in differentiation medium for 3 days. (a) Representative-phase contrast images of C2C12 myoblasts prior to infection (upper panels) and after infection (lower panels). (b) Representative images of anti-MyHC staining (green). Nuclei were counterstained with DAPI (grey). Scale bar: 200 μm. (c) Bar graphs representing differentiation index, fusion index, and number of nuclei per myotube. miR-200c overexpression decreased all these parameters ($n = 3$ independent experiments; $^{***}p < 0.001$). (d) A representative Western blot using ZEB1, MyHC, myogenin, and MyoD antibodies showed that protein levels decreased upon miR-200c overexpression. α-Tubulin (TUB) was used as loading control.

panels); we found that miR-200c overexpression decreased the myotube number (Figure 2(a) lower panels), assessed also by MyHC immunofluorescence staining (Figure 2(b)). Moreover, a decrease in differentiation index, fusion index, and number of nuclei within myotubes was also observed in differentiated miR-200c-overexpressing cells (Figure 2(c)).

We then analyzed myogenic differentiation by Western blot, and we observed that ZEB1, MyHC, myogenin, and MyoD proteins were all downregulated upon miR-200c overexpression (Figure 2(d)).

All these results suggested a role for miR-200c in myogenic differentiation inhibition and in myotube loss.

3.2. miR-200c Inhibition Enhances Myogenic Differentiation. We then asked whether anti-miR-200c treatment was able to ameliorate myogenic differentiation. Therefore, we transduced C2C12 cells with anti-miR-200c lentiviral particles and we shifted cells to DM for increasing period of times. We found that anti-miR-200c increased myotube formation as assessed by MyHC immunofluorescence staining (Figure 3(a)). In addition, an increase of three muscle differentiation parameters was also observed, specifically differentiation index, fusion index, and number of nuclei within myotubes (Figure 3(b)). We analyzed myogenic differentiation by Western blot, and we found that MyHC, myogenin, and MyoD proteins were increased at 48 h and 72 h of DM upon anti-miR-200c expression at higher levels compared to anti-scramble-treated C2C12 (Figure 3(c)).

3.3. miR-200c Increased p66Shc Phosphorylation in Ser-36 in C2C12 Myoblasts. We previously showed that, in endothelial cells, miR-200c induces p66Shc phosphorylation in Ser-36, a

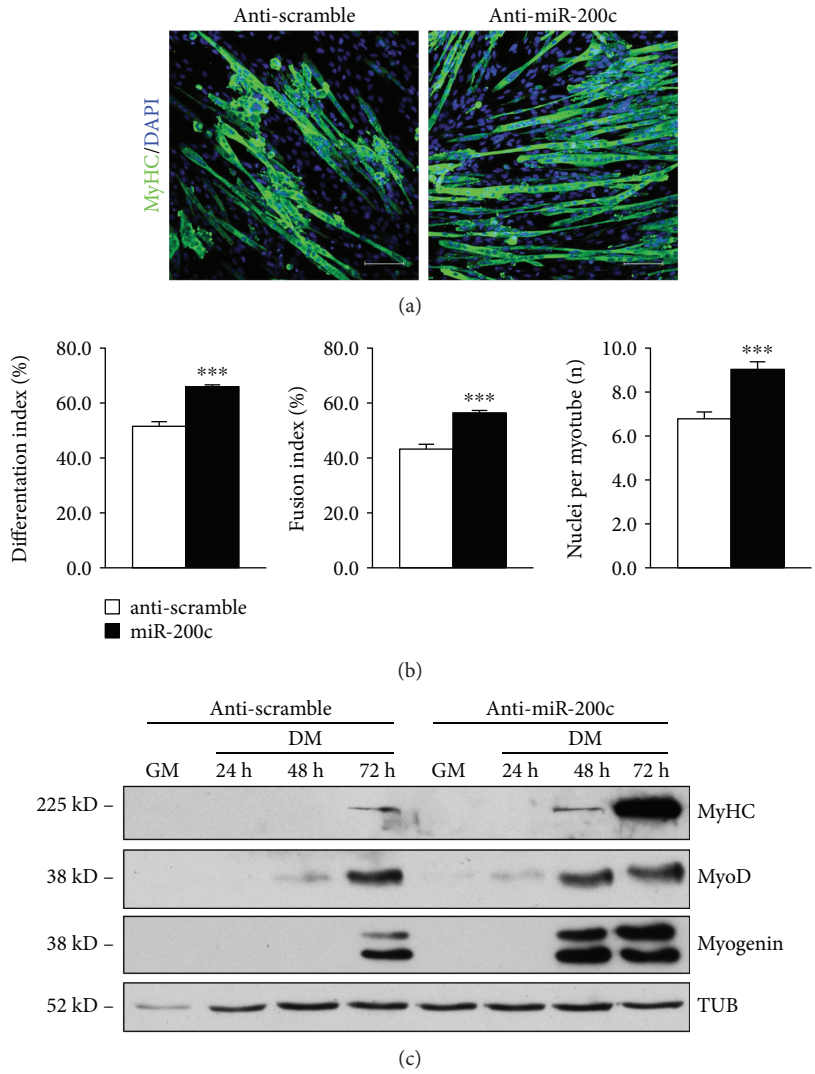

Figure 3: Anti-miR-200c treatment enhances skeletal muscle differentiation *in vitro*. C2C12 myoblasts were infected either with a lentivirus encoding anti-miR-200c or with a control virus. After selection with puromycin, cells were plated and shifted to differentiation medium for the times indicated in the figure. (a) Representative images of anti-MyHC staining (green). Nuclei were counterstained with DAPI (blue). Immunofluorescence with anti-MyHC antibody showed an increase in myotubes in anti-miR-200c-overexpressing cells compared to control at 3 days in DM. Scale bar: 100 μm. (b) Bar graphs representing differentiation index, fusion index, and number of nuclei per myotube. Anti-miR-200c overexpression increased all these parameters ($n = 3$ independent experiments; $^{***}p < 0.001$). (c) A representative Western blot using MyHC, myogenin, and MyoD antibodies showed that all these protein levels increased upon anti-miR-200c overexpression. α-Tubulin (TUB) was used as loading control.

phosphorylation known to be elicited by oxidative stress [10]. We therefore asked whether miR-200c phosphorylated p66Shc in this residue, also in C2C12 myoblasts. To this aim, we transduced C2C12 with miR-200c and scramble control and then transfected the cells with a p66Shc *wt* cells or a mutated p66 (p66mut) plasmid in which Ser-36 was replaced with Ala, that is not phosphorylable. We treated cells with or without 400 μM H_2O_2 for 5 minutes, and we found that Ser-36 phosphorylation increased, as expected, upon H_2O_2 treatment in p66*wt*-transfected cells, but not in the p66mut-transfected ones (Figures 4(a) and 4(b)). Moreover, in C2C12-overexpressing miR-200c, p66*wt* was phosphorylated also in basal conditions, that is, without H_2O_2, and the phosphorylation in Ser-36 increased even further upon H_2O_2 treatment (Figures 4(a) and 4(b)).

Further, we aimed at establishing whether endogenous p66 was phosphorylated in Ser-36 by miR-200c. Unfortunately, we failed to visualize phosphorylation by Western blot analysis; therefore, we immunoprecipitated p66Shc, to enhance the signal of Ser-36 phosphorylation.

As shown in Figure 4c, we found an increase in Ser-36 phosphorylation in the immunoprecipitates of p66 in miR-200c-overexpressing C2C12 compared to scramble control (Figures 4(c) and 4(d)).

Taken together, these results indicate that miR-200c enhances p66Shc phosphorylation in Ser-36 as well as in

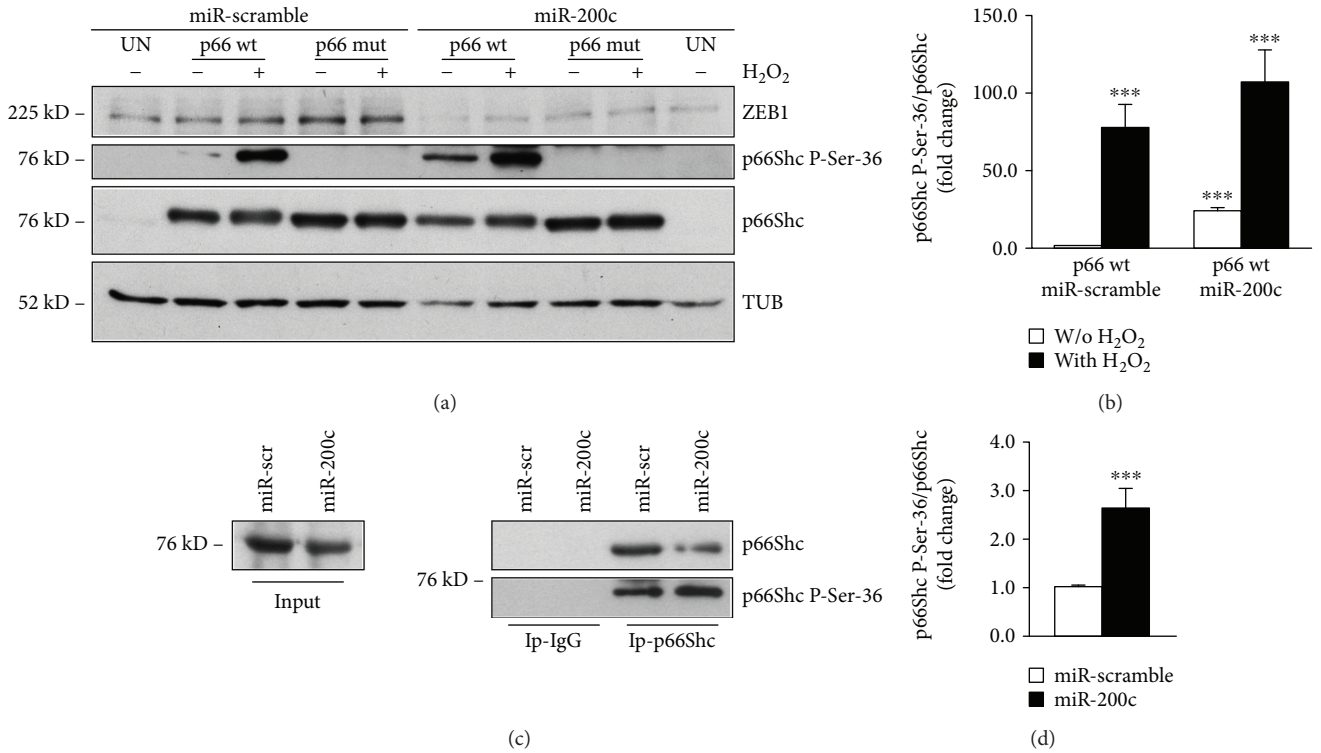

Figure 4: miR-200c overexpression induces p66Shc phosphorylation in Ser-36. C2C12 myoblasts were infected either with a lentivirus encoding miR-200c or with a control virus. After selection with puromycin, cells were transfected with 1 μg of p66*wt* or a mutated version in which Ser-36 was substituted with Ala that was no longer phosphorylable (p66mut). (a) A representative Western blot using p66Shc-Ser-36 antibody showed that p66*wt* phosphorylation was higher in miR-200c-overexpressing cells compared to scramble control both without and with H_2O_2 treatment. Phosphorylation of p66mut was not present, as expected, in any condition. α-Tubulin (TUB) was used as loading control. (b) Bar graph showing the quantification of p66Shc phosphorylation in Ser-36 versus p66*wt* protein levels of C2C12-overexpressing miR-200c compared with control cells ($n = 3$; $^{***}p < 0.001$). (c) C2C12 myoblasts were infected either with a lentivirus encoding miR-200c or with a control virus. After selection with puromycin, cells were immunoprecipitated (Ip) with either an anti-p66 antibody or an irrelevant isotypic antibody (negative control). Western blotting with a p66Shc-phospho-Ser-36 antibody revealed that p66Shc was more phosphorylated in Ser-36 in miR-200c IP-p66 than in scramble control cells. The efficiency of immunoprecipitation was assessed with an anti-p66 antibody. One-twentieth of the immunoprecipitated whole-cell extract (input) was loaded as a reference. (d) Bar graph showing the quantification of p66Shc phosphorylation in Ser-36 versus p66 total protein levels of C2C12-overexpressing miR-200c compared with scramble control cells ($n = 3$; $^{***}p < 0.001$).

C2C12 myoblasts, supporting its role in oxidative stress production [10].

3.4. miR-200c and p66Shc Phosphorylation in Ser-36 Increase in Skeletal Muscles of mdx Mice. Muscle degeneration in *mdx* mice is characterized by high oxidative stress [11]; therefore, we asked whether miR-200c was induced in *mdx* mice compared to *wt* mice.

We analyzed miR-200c expression levels in different muscles, that is, quadriceps (Q), gastrocnemius (GA), tibialis anterior (TA), extensor digitorum longus (EDL), and soleus (SOL), in both young (4-week-old mice (4 w)) and older mice (36-week-old mice (36 w)) (Figures 5(a) and 5(b)). We found that miR-200c was significantly higher in *mdx* mice compared to *wt*, in all muscle groups examined, both in young and older mice (Figures 5(a) and 5(b)); indeed, in Q of young (~6-fold) and in GA of older mice (~12-fold), we found a very high increase of miR-200c expression (Figures 5(a) and 5(b)). An increase of miR-200c expression was also found in human myoblasts derived from muscle biopsies of DMD patients cultured in muscle differentiation medium, compared to human-differentiated myoblasts derived from muscle biopsies of healthy donors (Figure 5(c)).

In light of these results, we examined the levels of p66Shc phosphorylation in Ser-36 in Q and GA.

Interestingly, we found an increase of p66 protein in young *mdx* compared to *wt* mice and a strong upregulation of Ser-36 phosphorylation (Figure 5(d)). Notably, p66 phosphorylation in Ser-36 was increased in older mice also in basal conditions and was even higher in Q and particularly in GA, showing that older mice displayed higher miR-200c (Figure 5(d)).

These results suggest a role for miR-200c in oxidative stress increase in *mdx* mice, mediated, at least in part, by p66Shc-dependent mechanism.

4. Discussion

In this report, we dissected the role of the oxidative stress-induced miR-200c on muscle differentiation, since our and

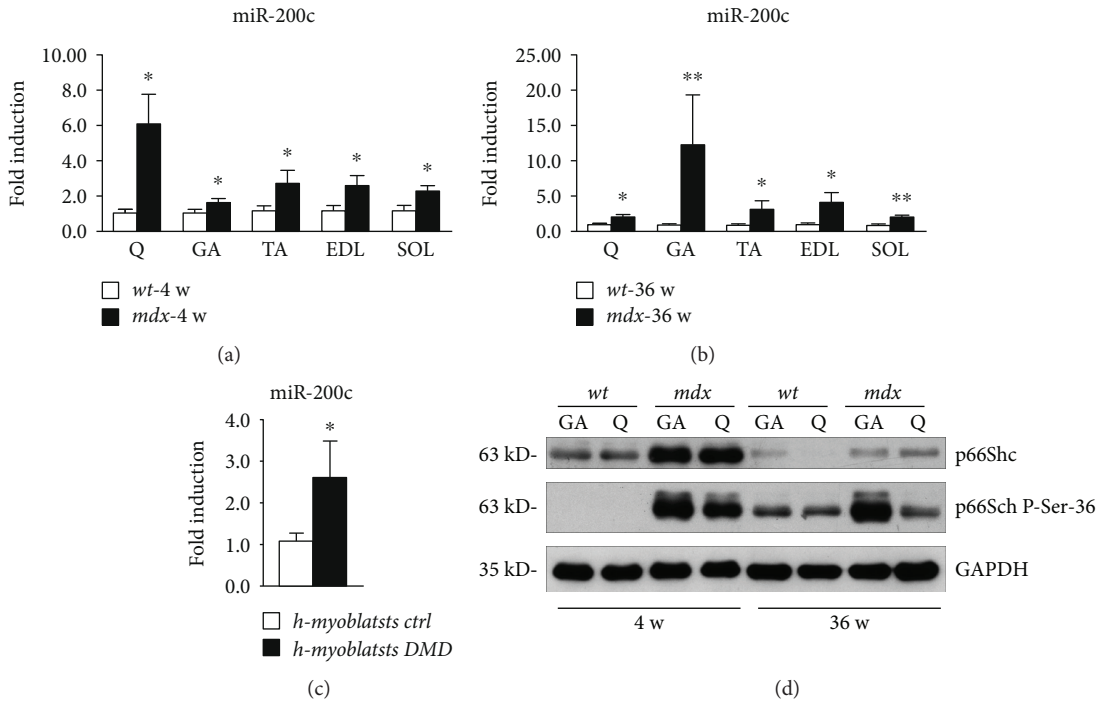

Figure 5: miR-200c and p66Shc phosphorylation in Ser-36 increase in dystrophic muscles of *mdx* mice. (a) The mRNA of quadriceps (Q), gastrocnemius (GA), tibialis anterior (TA), extensor digitorum longus (EDL), and soleus (SOL) muscles isolated from 3 young (4-week-old (4 w)) *mdx* mice were assayed for miR-200c expression. miR-200c increased in young *mdx* mice compared to young *wt* mice ($n = 3$ for each muscle; $^{*}p < 0.05$; the bar graphs are average results of miR-200c expression levels of 3 different mice for each muscle). (b) The mRNA of quadriceps (Q), gastrocnemius (GA), tibialis anterior (TA), extensor digitorum longus (EDL), and soleus (SOL) muscles isolated from 3 old (36-week-old (36 w)) *mdx* mice were assayed for miR-200c expression. miR-200c increased in old *mdx* mice compared to old *wt* mice ($n = 3$ for each muscle; $^{**}p < 0.01$; $^{*}p < 0.05$; the bar graphs are average results of miR-200c expression levels of 3 different mice for each muscle). (c) The mRNA of human myoblasts derived from muscle biopsies of healthy donors or DMD patients and differentiated *in vitro* were assayed for miR-200c expression. miR-200c increased in DMD myoblasts compared to control myoblasts ($n = 3$; $^{*}p < 0.05$; the bar graphs are average results of miR-200c expression levels of 3 different cell populations for control or DMD samples). (d) A representative Western blot of GA and Q protein extracts of both young (4 w) and old *mdx* (36 w) compared to young and old *wt* mice showed that p66 protein was induced in *mdx* mice compared to *wt* mice. Moreover, the phosphorylation in Ser-36 was induced in *mdx* mice compared to *wt* mice in both young and old mice (the experiment was performed on 3 biological replicates; 3 *wt* mice and 3 *mdx* mice of 4 weeks and 36 weeks, resp.). Glyceraldehyde-3-phosphate dehydrogenase (GAPDH) was used as loading control.

other laboratories reported a decrease in myogenic differentiation upon oxidative stress *in vitro* [1, 27–29].

Our results showed that miR-200c inhibits myogenic differentiation when forced miR-200c overexpression was performed in myoblasts; moreover, when miR-200c is overexpressed in differentiated myotubes, a decrease in myotube number and size was also observed. These effects are associated with a decrease in myogenic markers, that is, MyHC and myogenin, both in growing and in differentiating conditions. In keeping, anti-miR-200c treatment in growing myoblasts accelerates myogenic differentiation, increasing myotube numbers and size. We previously found that miR-200c induces oxidative stress and p66Shc phosphorylation in Ser-36 in endothelial cells [10]. In the present study, we confirmed these results also in murine myoblasts. Further, we found that both miR-200c and p66Shc phosphorylation in Ser-36 increase in *mdx* muscles compared to *wt*. Moreover, we found that miR-200c is significantly induced in human-differentiated myoblasts of DMD patients compared to differentiated myoblasts of healthy donors.

Other papers evaluated miRNA expression modulation in *mdx* and DMD muscles and also in sera [13, 30]. Indeed, Greco et al. found that in adductor muscles of *mdx*, a miR-200c upregulation was present, although not significant [13]. Moreover, the authors demonstrated that degenerative miRNAs may regulate, at least in part, critical mediators of cell death, contributing to the apoptotic/necrotic myofiber loss associated with both ischemia and DMD [13]. Our previous data show that miR-200c is highly induced by ischemia and its inhibition is able to increase limb perfusion, reverting the downregulation of its targets responsible of apoptosis, senescence, ROS increase, and nitric oxide (NO) decrease [10]. In keeping, the present study demonstrates that miR-200c that we previously showed to be upregulated upon ischemia [9, 10] is associated with myotube loss and is upregulated in *mdx* and DMD.

Our previous studies demonstrated that p66Shc$^{-/-}$ SC differentiated better than *wt* cells in terms of myogenic marker increase, that is, myogenin and MyHC and myotube numbers, assessed by MyHC fluorescence; further, myogenic

conversion, induced by MyoD overexpression, was more efficient in p66Shc$^{-/-}$ fibroblasts compared to *wt* cells [1]. The explanation for this, was ascribed to lower oxidative stress in p66Shc$^{-/-}$ cells compared to *wt* cells. In addition, it is possible that NO plays a positive role in higher and faster myogenic regeneration potential of p66Shc$^{-/-}$ mice and cells. Indeed, NO mediates SC activation [31] and it is required for myoblast fusion [32]. Since ROS rapidly react with NO, generating nitrogen species, such as peroxynitrite [33], it is conceivable that p66Shc deletion enhances nitric oxide bioavailability [34], thus, favoring myogenic differentiation.

DMD is a genetic disease caused by deficiency of dystrophin, a critical component of the DGC, acting as a link between cytoskeleton and extracellular matrix in skeletal and cardiac muscles [15, 16]. A direct consequence of the DGC inefficiency is muscle fragility, contraction-induced damage, necrosis, reduced NO [35], oxidative stress, and inflammation.

In keeping, different preclinical studies in *mdx* mice report benefits, that is, decreased necrosis and improved muscle pathology, for many antioxidant drugs and interventions [11].

Resveratrol, among others, is an antioxidant drug that has a positive role on DMD [36]; interestingly, it is a potent activator of sirtuin1 (SIRT1). Moreover, SIRT1 overexpression in muscle reverses the phenotype of *mdx* mice [37].

SIRT1 is a NAD^+-dependent deacetylase that displays antioxidant properties and enhances NO bioavailability [38].

Our recent report demonstrated that miR-200c targets directly SIRT1 and also two important proteins that modulate NO production and ROS scavenger transcription, that is, endothelial nitric oxide synthase (eNOS) and FOXO1. Therefore, we showed that miR-200c upregulation decreases NO, increases ROS production, and induces p66Shc protein phosphorylation in Ser-36; this, in turn, induces ROS via different mechanisms, one of which is the inhibition of FOXO1 transcription of ROS scavengers, reinforcing this molecular circuitry [10].

Taken together, these results suggest a pivotal role of miR-200c in oxidative stress induction in DMD via a p66Shc-dependent mechanism. miR-200c upregulation might contribute to the establishment of the negative consequences associated with this muscle disease, such as muscle wasting, lack of muscle regeneration, necrosis, NO decrease, and oxidative stress increase.

5. Conclusion

p66Shc phosphorylation in Ser-36 is increased in *mdx* muscles, and miR-200c expression levels are upregulated both in *mdx* muscles and in differentiated human myoblasts of DMD. Although further experiments should be accomplished in order to point to miR-200c as a therapeutic target, these data strongly suggest its possible involvement in muscle wasting in DMD, through apoptosis and senescence induction, as well as, by the induction of ROS and the decrease of NO.

Conflicts of Interest

The authors declare no conflict of interest.

Authors' Contributions

Marco D'Agostino and Alessio Torcinaro contributed equally to this work. Francesca De Santa and Alessandra Magenta are cosenior authors.

Acknowledgments

In memory of Dr. Fabrizio Carlomosti who passed away in 2015 and initiated this work. This study was supported by Ministero della Salute GR- 2010-2309531 and RC-2017 to Alessandra Magenta; by Ministero della Salute, RF-2010-2318330, to Maurizio C. Capogrossi; by the Italian Ministry of Education, Universities and Research (MIUR) (Grant IRMI: CTN01_00177_888744); by AFM-Telethon, Grant no. 16772; by Duchenne Parent Project-Netherlands (DPP-NL) #DeSanta-DPP-NL to Francesca De Santa; and by Ministero della Salute GR- 2013-02356592 to Luca Madaro.

References

[1] G. Zaccagnini, F. Martelli, A. Magenta et al., "p66^{ShcA} and oxidative stress modulate myogenic differentiation and skeletal muscle regeneration after hind limb ischemia," *The Journal of Biological Chemistry*, vol. 282, no. 43, pp. 31453–31459, 2007.

[2] G. Zaccagnini, F. Martelli, P. Fasanaro et al., "p66^{ShcA} modulates tissue response to hindlimb ischemia," *Circulation*, vol. 109, no. 23, pp. 2917–2923, 2004.

[3] L. Bonfini, E. Migliaccio, G. Pelicci, L. Lanfrancone, and P. G. Pelicci, "Not all Shc's roads lead to Ras," *Trends in Biochemical Sciences*, vol. 21, no. 7, pp. 257–261, 1996.

[4] A. Magenta, S. Greco, M. C. Capogrossi, C. Gaetano, and F. Martelli, "Nitric oxide, oxidative stress, and p66Shc interplay in diabetic endothelial dysfunction," *BioMed Research International*, vol. 2014, Article ID 193095, 16 pages, 2014.

[5] D. P. Bartel, "MicroRNAs: genomics, biogenesis, mechanism, and function," *Cell*, vol. 116, no. 2, pp. 281–297, 2004.

[6] A. Magenta, S. Greco, C. Gaetano, and F. Martelli, "Oxidative stress and microRNAs in vascular diseases," *International Journal of Molecular Sciences*, vol. 14, no. 9, pp. 17319–17346, 2013.

[7] R. M. O'Connell, D. S. Rao, and D. Baltimore, "MicroRNA regulation of inflammatory responses," *Annual Review of Immunology*, vol. 30, no. 1, pp. 295–312, 2012.

[8] M. Horak, J. Novak, and J. Bienertova-Vasku, "Muscle-specific microRNAs in skeletal muscle development," *Developmental Biology*, vol. 410, no. 1, pp. 1–13, 2016.

[9] A. Magenta, C. Cencioni, P. Fasanaro et al., "miR-200c is upregulated by oxidative stress and induces endothelial cell apoptosis and senescence via ZEB1 inhibition," *Cell Death and Differentiation*, vol. 18, no. 10, pp. 1628–1639, 2011.

[10] F. Carlomosti, M. D'Agostino, S. Beji et al., "Oxidative stress-induced miR-200c disrupts the regulatory loop among SIRT1, FOXO1 and eNOS," *Antioxidants & Redox Signaling*, vol. 27, no. 6, pp. 328–344, 2016.

[11] J. R. Terrill, H. G. Radley-Crabb, T. Iwasaki, F. A. Lemckert, P. G. Arthur, and M. D. Grounds, "Oxidative stress and pathology in muscular dystrophies: focus on protein thiol oxidation and dysferlinopathies," *The FEBS Journal*, vol. 280, no. 17, pp. 4149–4164, 2013.

[12] S. Petrillo, L. Pelosi, F. Piemonte et al., "Oxidative stress in Duchenne muscular dystrophy: focus on the NRF2 redox pathway," *Human Molecular Genetics*, vol. 26, no. 14, pp. 2781–2790, 2017.

[13] S. Greco, M. De Simone, C. Colussi et al., "Common micro-RNA signature in skeletal muscle damage and regeneration induced by Duchenne muscular dystrophy and acute ischemia," *The FASEB Journal*, vol. 23, no. 10, pp. 3335–3346, 2009.

[14] I. Dalkilic and L. M. Kunkel, "Muscular dystrophies: genes to pathogenesis," *Current Opinion in Genetics & Development*, vol. 13, no. 3, pp. 231–238, 2003.

[15] N. P. Evans, S. A. Misyak, J. L. Robertson, J. Bassaganya-Riera, and R. W. Grange, "Dysregulated intracellular signaling and inflammatory gene expression during initial disease onset in Duchenne muscular dystrophy," *American Journal of Physical Medicine & Rehabilitation*, vol. 88, no. 6, pp. 502–522, 2009.

[16] C. Pichavant, A. Aartsma-Rus, P. R. Clemens et al., "Current status of pharmaceutical and genetic therapeutic approaches to treat DMD," *Molecular Therapy*, vol. 19, no. 5, pp. 830–840, 2011.

[17] P. Sicinski, Y. Geng, A. S. Ryder-Cook, E. A. Barnard, M. G. Darlison, and P. J. Barnard, "The molecular basis of muscular dystrophy in the mdx mouse: a point mutation," *Science*, vol. 244, no. 4912, pp. 1578–1580, 1989.

[18] A. Sacco, F. Mourkioti, R. Tran et al., "Short telomeres and stem cell exhaustion model Duchenne muscular dystrophy in mdx/mTR mice," *Cell*, vol. 143, no. 7, pp. 1059–1071, 2010.

[19] C. J. Mann, E. Perdiguero, Y. Kharraz et al., "Aberrant repair and fibrosis development in skeletal muscle," *Skeletal Muscle*, vol. 1, no. 1, p. 21, 2011.

[20] N. A. Dumont, Y. X. Wang, J. von Maltzahn et al., "Dystrophin expression in muscle stem cells regulates their polarity and asymmetric division," *Nature Medicine*, vol. 21, no. 12, pp. 1455–1463, 2015.

[21] S. Biressi, E. H. Miyabara, S. D. Gopinath, P. M. M. Carlig, and T. A. Rando, "A Wnt-TGFβ2 axis induces a fibrogenic program in muscle stem cells from dystrophic mice," *Science Translational Medicine*, vol. 6, no. 267, article 267ra176, 2014.

[22] P. Pessina, Y. Kharraz, M. Jardí et al., "Fibrogenic cell plasticity blunts tissue regeneration and aggravates muscular dystrophy," *Stem Cell Reports*, vol. 4, no. 6, pp. 1046–1060, 2015.

[23] A. Follenzi and L. Naldini, "HIV-based vectors. Preparation and use," *Gene Therapy Protocols*, vol. 69, pp. 259–274, 2002.

[24] C. G. Crist, D. Montarras, and M. Buckingham, "Muscle satellite cells are primed for myogenesis but maintain quiescence with sequestration of *Myf5* mRNA targeted by microRNA-31 in mRNP granules," *Cell Stem Cell*, vol. 11, no. 1, pp. 118–126, 2012.

[25] V. Saccone, S. Consalvi, L. Giordani et al., "HDAC-regulated myomiRs control BAF60 variant exchange and direct the functional phenotype of fibro-adipogenic progenitors in dystrophic muscles," *Genes & Development*, vol. 28, no. 8, pp. 841–857, 2014.

[26] A. Magenta, P. Fasanaro, S. Romani, V. Di Stefano, M. C. Capogrossi, and F. Martelli, "Protein phosphatase 2A subunit PR70 interacts with pRb and mediates its dephosphorylation," *Molecular and Cellular Biology*, vol. 28, no. 2, pp. 873–882, 2008.

[27] E. Ardite, J. A. Barbera, J. Roca, and J. C. Fernández-Checa, "Glutathione depletion impairs myogenic differentiation of murine skeletal muscle C2C12 cells through sustained NF-κB activation," *The American Journal of Pathology*, vol. 165, no. 3, pp. 719–728, 2004.

[28] S. Fulle, F. Protasi, G. Di Tano et al., "The contribution of reactive oxygen species to sarcopenia and muscle ageing," *Experimental Gerontology*, vol. 39, no. 1, pp. 17–24, 2004.

[29] J. M. Hansen, M. Klass, C. Harris, and M. Csete, "A reducing redox environment promotes C2C12 myogenesis: implications for regeneration in aged muscle," *Cell Biology International*, vol. 31, no. 6, pp. 546–553, 2007.

[30] N. Vignier, F. Amor, P. Fogel et al., "Distinctive serum miRNA profile in mouse models of striated muscular pathologies," *PLoS One*, vol. 8, no. 2, article e55281, 2013.

[31] J. E. Anderson, "A role for nitric oxide in muscle repair: nitric oxide-mediated activation of muscle satellite cells," *Molecular Biology of the Cell*, vol. 11, no. 5, pp. 1859–1874, 2000.

[32] K. H. Lee, D. G. Kim, N. Y. Shin et al., "NF-κB-dependent expression of nitric oxide synthase is required for membrane fusion of chick embryonic myoblasts," *Biochemical Journal*, vol. 324, no. 1, Part 1, pp. 237–242, 1997.

[33] N. R. Madamanchi and M. S. Runge, "Mitochondrial dysfunction in atherosclerosis," *Circulation Research*, vol. 100, no. 4, pp. 460–473, 2007.

[34] P. Francia, C. delli Gatti, M. Bachschmid et al., "Deletion of p66Shc gene protects against age-related endothelial dysfunction," *Circulation*, vol. 110, no. 18, pp. 2889–2895, 2004.

[35] T. Kasai, K. Abeyama, T. Hashiguchi, H. Fukunaga, M. Osame, and I. Maruyama, "Decreased total nitric oxide production in patients with Duchenne muscular dystrophy," *Journal of Biomedical Science*, vol. 11, no. 4, pp. 534–537, 2004.

[36] A. Kuno and Y. Horio, "SIRT1: a novel target for the treatment of muscular dystrophies," *Oxidative Medicine and Cellular Longevity*, vol. 2016, Article ID 6714686, 11 pages, 2016.

[37] A. Chalkiadaki, M. Igarashi, A. S. Nasamu, J. Knezevic, and L. Guarente, "Muscle-specific SIRT1 gain-of-function increases slow-twitch fibers and ameliorates pathophysiology in a mouse model of Duchenne muscular dystrophy," *PLoS Genetics*, vol. 10, no. 7, article e1004490, 2014.

[38] M. Potente and S. Dimmeler, "Emerging roles of SIRT1 in vascular endothelial homeostasis," *Cell Cycle*, vol. 7, no. 14, pp. 2117–2122, 2008.

Hindawi
Oxidative Medicine and Cellular Longevity
Volume 2018, Article ID 5763256, 9 pages
https://doi.org/10.1155/2018/5763256

Research Article

Photobiomodulation Leads to Reduced Oxidative Stress in Rats Submitted to High-Intensity Resistive Exercise

Helenita Antonia de Oliveira,[1] Ednei Luiz Antonio,[2] Gisela Arsa,[3,4] Eduardo Tadeu Santana,[2] Flávio André Silva,[2] Daniel Arruda Júnior,[2] Simone dos Santos,[1] Paulo de Tarso Camillo de Carvalho,[1] Ernesto Cesar Pinto Leal-Junior,[1] Amanda Araujo,[5] Kátia De Angelis,[5] Danilo Sales Bocalini,[6] José Antonio Silva Junior,[1] Paulo José Ferreira Tucci,[2] and Andrey Jorge Serra[1]

[1]*Biophotonic Department, Universidade Nove de Julho, São Paulo, SP, Brazil*
[2]*Cardiology Division, Escola Paulista de Medicina, Universidade Federal de São Paulo (UNIFESP), São Paulo, SP, Brazil*
[3]*Postgraduate Program of Physical Education, Universidade Federal de Mato Grosso (UFMT), Cuiabá, MT, Brazil*
[4]*Postgraduate Program in Nutrition, Food and Metabolism, Universidade Federal de Mato Grosso (UFMT), Cuiabá, MT, Brazil*
[5]*Laboratory of Translational Physiology, Universidade Nove de Julho, São Paulo, SP, Brazil*
[6]*Centro de Educação Física e Desporto, Universidade Federal do Espírito Santo (UFES), Vitória, ES, Brazil*

Correspondence should be addressed to Andrey Jorge Serra; andreyserra@gmail.com

Received 4 August 2017; Revised 11 November 2017; Accepted 29 November 2017; Published 13 February 2018

Academic Editor: Swaran J. S. Flora

The aim of this study was to determine whether oxidative stress markers are influenced by low-intensity laser therapy (LLLT) in rats subjected to a high-intensity resistive exercise session (RE). Female Wistar rats divided into three experimental groups (Ctr: control, 4J: LLLT, and RE) and subdivided based on the sampling times (instantly or 24 h postexercise) underwent irradiation with LLLT using three-point transcutaneous method on the hind legs, which was applied to the gastrocnemius muscle at the distal, medial, and proximal points. Laser (4J) or placebo (device off) were carried out 60 sec prior to RE that consisted of four climbs bearing the maximum load with a 2 min time interval between each climb. Lipoperoxidation levels and antioxidant capacity were obtained in muscle. Lipoperoxidation levels were increased (4-HNE and CL markers) instantly post-RE. LLLT prior to RE avoided the increase of the lipid peroxidation levels. Similar results were also notified for oxidation protein assays. The GPx and FRAP activities did not reduce instantly or 24 h after RE. SOD increased 24 h after RE, while CAT activity did not change with RE or LLLT. In conclusion, LLLT prior to RE reduced the oxidative stress markers, as well as, avoided reduction, and still increased the antioxidant capacity.

1. Introduction

Free radicals (FR) are molecules regularly produced by the body, leading to tissue injury or toxic compounds to tissues, and its accumulation results in tissue injury, DNA damage, and cellular dysfunction [1, 2]. The FR are responsible for damages caused by the oxidative stress and show accumulative effects that might contribute to the development of diseases such as diabetes, arteriosclerosis, and cancer [3, 4]. Physical exercise promotes the rise on the FR formation in function of the increment on the oxygen intake. Nevertheless, exercise training engenders adaptations able to unstiffen the damaging effects triggered by FR [5].

The FR are naturally formed in organisms through oxidative metabolic events, being extremely convenient as in conditions where the stimulation of the immunologic system is

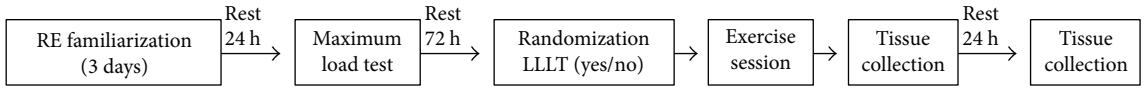

Figure 1: Timeline of experimental procedures.

mandatory (e.g., macrophages utilize the hydrogen peroxide to destroy bacteria), in drug detoxification, and in the production of nitric oxide, an endothelium-derived relaxing factor imperative in processes that mediate the blood vessels relaxation [6, 7]. An excess of FR has been implied as both physiologically beneficial and pathologically harmful in the body. The FR has been demonstrated to act as intracellular signaling molecules for insulin signaling transduction in healthy tissues, and FR produced during exercise is also thought to play a key role in skeletal muscle adaptations associated with exercise training [8, 9]. In contrast to this physiologically beneficial FR, a chronic overproduction of FR systemically in skeletal muscle promotes oxidative stress and might contribute to the pathogenesis of type 2 diabetes [10], aging [11], and cancer cachexia [12].

Several damages can raise the free radical production, in which aerobic physical exercise shows to be a free radical trigger linked to mitochondrial pathway mainly as a result of increased oxygen consumption [13]. On the other hand, resistance exercise evokes temporary blood flow reduction between the concentric and eccentric stages of muscle followed by perfusion reestablishment [14]. This intermittent hypoxia/reperfusion is associated with ATP degradation, xanthine oxidase activation, and a higher production of oxygen-reactive species [15, 16]. In this regard, McBride et al. reported an increased plasmatic malondialdehyde level with 6 and 24 h after a single resistance exercise session [14]. Hudson et al. have shown higher levels of carbonylated protein at healthy men immediately and 60 min postresistance exercise [15]. Lastly, elevated levels of thiobarbituric acid reactive substances, glutathione, and products of protein oxidation were reported in healthy well-trained men with 10 min postresistance exercise [16].

An excessive increase of the oxidative stress during muscle work can cause damage to proteins and cellular dysfunction. Moreover, high-intensity exercises (e.g., upward of the second ventilatory threshold) are marked by decompensated metabolic acidosis and sarcolemma microinjury, which can lead to inflammation and a burst of free radicals [17, 18]. The implication of these findings is a delayed postexercise muscle recovery, hence, impairing the quality of training sessions [19]. This is a key issue mainly during intense training stages, in which the free radical burst can overcome the antioxidant chemical and enzymatic protection [20] to maintain redox homeostasis, inducing oxidative damages as observed by Rietjens et al. and Cakir-Atabek et al. after a single resistance exercise session in men [21, 22].

Several studies have reported beneficial effects of therapy with antioxidant agents, including tocopherol (vitamin E) and other antioxidants [13, 23]. There is a main interest for new strategies as well as for the low-intensity laser therapy (LLLT) [24]. The prior LLLT application to a run exercise was suitable to reduce oxidative stress and muscle damage in trained men [23]. It was shown that six weeks of LLLT treatment was appropriate to mitigate the increased concentration of thiobarbituric acid reactive substances in older rats [25]. In another study, a reduced content of carbonylated protein in the gastrocnemius muscle of the mdx mice with muscular dystrophy that underwent LLLT irradiations prior to a high-intensity exercise on a treadmill was reported [26]. To our knowledge, no existing studies have evaluated the repercussion of LLLT on the oxidative stress induced by a bout of resistance exercise. Therefore, this study was designed to determine if the levels of oxidative stress markers are influenced by LLLT in rats subjected to a high-intensity resistance exercise session.

2. Material and Methods

2.1. Animals and Experimental Design. Forty-eight female Wistar rats (*Rattus norvegicus* Albinus), weighing 200–250 g and aged 12 weeks, were obtained from the animal facility of the Federal University of São Paulo, São Paulo, SP, Brazil, and they were kept under controlled environments of light and temperature, with full water and food (Nuvilab CR-1; Global soluções para biotérios Inc., SP, BRA) access. Based on rats' availability in our animal's facility, several protocols were performed using female rats that have been published recently [27]. However, primarily, the same protocols were performed using both sexes and significant difference was not found between males and females in photobiomodulation experiments. Moreover, in a translational view, the landscape of female athletics has changed dramatically in the past three decades, in which female athletic participation in competitions has drastically increased worldwide [28]. The study protocol was approved by the Institutional Research Ethics Committee (8868250615), and experimental procedures were carried out in accordance with the guidelines stipulated by the Brazilian College of Animal Experimentation and the International Council for Laboratory Animal Science Standards. The rats were assigned for one of the three experimental groups, with some animals allocated per subgroup based on the sampling times (instantly or 24 h postexercise). Thus, three groups were as follows: *Ctr*, comprising rats that did not undergo resistance exercise or LLLT application; *RE*, comprising rats that only underwent a resistance exercise session. These rats were manipulated in the same way as those in the LLLT group, but the equipment was turned off; 4J, rats that were subjected to 4J LLLT prior to a resistance exercise session. Experimental timeline design is illustrated in Figure 1, in which the rats were initially adapted to the act of climbing for three consecutive days and following (post-24 h) the maximum load test. Then, the rats were kept at rest for 72 hours and randomized to undergo or not LLLT prior resistance exercise. Finally, the

rats were euthanized for the removal of the gastrocnemius muscle instantly or 24 h postexercise.

2.2. Resistance Exercise Protocol. Rats were familiar to climb a ladder containing 54 vertical (slope: 80°) steps and a cage at the top as previously described by Sanches et al. [29]. The maximum load supported by the animal was determined as follows: (i) a load of 75% of body weight was attached to the rat's tail base; (ii) an additional load of 15% of the body weight was progressively attached to the tail in subsequent climbs until the animal failed to complete the climb to the top of the ladder. A 2 min rest was given between each climb attempt, and the load of the last complete climb was established as a maximum load. Overall, three climbs were required for the rats to reach maximum load. Resistance exercise session was carried out 72 h after maximum load test, in which this was defined based on a pilot study. It was observed that 72 h of rest between the maximal load test and the resistance exercise session results in the return of muscle injury markers (e.g., creatine kinase and lactic dehydrogenase) to the basal levels (data not shown). Resistance exercise session comprised four climbs bearing the maximum load with a 2 min time interval between each climb.

2.3. LLLT Protocol. A DMC Laser Photon III® model (São Carlos, SP, Brazil) was used as LLLT device. The application used the three-point transcutaneous method on the hind legs, in which the gastrocnemius muscle was irradiated at the distal, medial, and proximal points. Laser or placebo procedure (device off) was carried out 60 sec prior to resistance exercise. The Ctr group experienced the same experimental conditions that RE and 4J groups, but did not receive exercise or laser intervention. The laser device was fixed with the following parameters: wave length (830 nm); laser beam (0.028 cm^2); output power (100 mW); power density (3.57 W/cm^2); energy density (144J/cm^2); total energy per point (4J); and irradiation time per point (40 s). The irradiation parameters were defined based on a previous study of our group (in per review analysis in the *Photochemistry and Photobiology* journal). It was observed that 4J irradiation attenuated muscle injury and inflammation in rats subjected to a resistance exercise session.

2.4. Physical Performance. The load, distance climbed, and time spent to complete each repetition were recorded to evaluate physical performance as previously described for rodents [30]. Thereby, the muscle work (MW) was calculated as follows:

(i) MW (joules) = mgh ("m," comprising the external load fixed on the animal plus the body weight expressed in kg; "g," acceleration due to gravity; "h," climb distance expressed as meters). Results are expressed as mean ± standard error of mean to four climbs.

(ii) Muscle power (MP) = J/s ("J," represents the MW; "s," time to perform the climbs). Results were obtained in milliwatts (mW) and presented for each climb.

2.5. Euthanasia and Tissue Sample. At the end of each experimental period (instantly and 24 h postexercise), the rats were identified, weighed, and then euthanized by intraperitoneal administration of urethane overdose (4.8 g kg^{-1}, i.p.). Then, the gastrocnemius muscles of the right hind paw were quickly removed, rinsed in saline, and trimmed to remove fat tissue and visible connective tissue. The sample was stored at −80°C for further processing.

2.6. Lipid Peroxidation. The muscle was cut into small pieces and homogenized in an Ultra-Turrax blender with 1 g of tissue per 5 mL of buffer (150 mmol/L KCl; 20 nmol/L phosphate; pH 7.4). The homogenates were centrifuged at 600 *g* for 10 min (−2°C), and protein concentration was assessed by the Lowry method. Lipid peroxidation was measured by the tert-butyl hydroperoxide-initiated chemiluminescence assay (CL), as it was previously described [31]. Moreover, 4-hydroxynonenal (4-HNE) expression was also used as a lipid peroxidation marker.

2.7. Western Blot. We followed the methods of Manchini et al. [32] and Melo et al. [33] for the muscle tissue processing and for protein extraction. Protein samples (20 μg) were subjected to SDS-PAGE in 10–12% polyacrylamide gel. Separated proteins were transferred onto hydrophobic membranes (Hybond-P, Amersham Biosciences; Piscataway, NJ, USA), in which they were soaked in a blocking buffer (5% nonfat dry milk and 0.1% Tween 20 in PBS, pH 7.5) for 60 min at room temperature and then incubated overnight at 4°C with primary antibodies: rabbit anti-4-HNE (1 : 2000 dilution; Abcam, Cambridge, MA, USA); rabbit anti-SOD1 (1 : 5000 dilution; Abcam, Cambridge, MA, USA); rabbit anti-CAT (1 : 5000 dilution; Abcam, Cambridge, USA); goat anti-HSP70 (1 : 1000; Abcam, Cambridge, MA, USA); and anti-GAPDH (1 : 500; Santa Cruz Biotechnology, Santa Cruz, CA, USA). Then, membranes were washed five times and incubated for 60 min with horseradish peroxidase-conjugated goat anti-rabbit and rabbit anti-goat secondary antibodies (1 : 2000; Invitrogen, San Diego, CA, USA). Membranes were washed five times again with blocking buffer and then rinsed twice in PBS buffer. Bound antibody was detected by using chemiluminescence reagent for 60 s. The bands were imaged by using Amersham Imager 600 system (GE Health Care, Little Chalfont, UK, USA).

2.8. Oxidized Protein Assay. Measurement of carbonyl groups introduced into proteins by oxidative reactions was evaluated in gastrocnemius muscle with Western blot detection Abcam kit ab178020 (Abcam, Cambridge, MA, USA). An equal protein load (20 μg) was used in all experimental groups, and protein carbonyl groups were measured according to the manufacturer's instructions.

2.9. Antioxidant Enzymes. Superoxide dismutase (SOD) activity was evaluated by the inhibition of the reaction between peroxide anion and pyrogallol, and catalase (CAT) activity was assessed by measuring the decrease in H_2O_2 absorbance at 240 nm [34]. Glutathione peroxidase (GPx) activity was determined by adding to the assay a mixture of 1 U/mL glutathione reductase and 2 mmol/L glutathione in

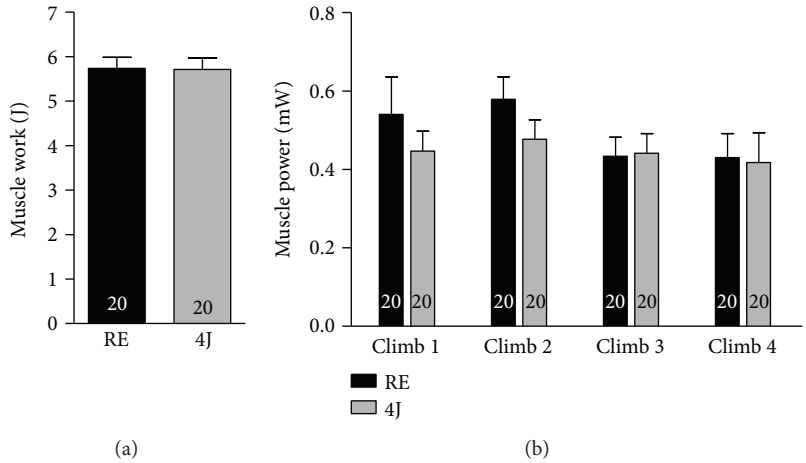

Figure 2: Physical performance data. (a) Muscle work developed by rats that only underwent a resistance exercise session (RE). (b) Muscle power developed by rats that were subjected to 4J LLLT irradiations prior to a resistance exercise session. Representative experiments are shown ($n = 20$ per group, RE and 4J).

1 mL phosphate buffer. Homogenates were preincubated at 37°C for 30 minutes, NADPH and tert-butyl hydroperoxide were added, and the alteration in absorbance at 340 nm was recorded to calculate GPx activity [35].

2.10. Ferric Reduction Ability Power (FRAP). The FRAP assay was applied in the analyses of the total antioxidant capacity of gastrocnemius muscle as adapted from elsewhere [36]. Homogenates tissue proteins were reacted with FRAP solution for 10 min (37°C), and sample absorbance was evaluated at 593 nm. Deionized water and Trolox (6-hydroxy-2,5,8-tetramethylchroman-2-carboxylic acid) were used as blank and standard, respectively. Absorbance readings at 593 nm were taken after 0.5 s and every 15 s thereafter during the monitoring period.

2.11. Statistical Analysis. Data were analyzed using GraphPad Prism software 5.0 (La Jolla, CA, USA). Kolmogorov-Smirnov and Levene tests were applied to verify normality and variance equality of data, respectively. Mann–Whitney test was carried in the analyses of physical performance. Two-way regular ANOVA and Bonferroni post hoc tests were applied to evaluate oxidative stress data. Kruskal-Wallis followed by Dunn's multiple comparison tests was applied to nonnormality data. Statistical significance was set at $p \leq 0.05$. Data are expressed as mean ± standard error of the mean.

3. Results

A positive effect of LLLT was not identified on muscle performance. Thus, there were no significant differences among the experimental groups for total muscle work and muscle power in each climb session (Figure 2).

Lipoperoxidation muscle parameters are shown in Figure 3. As evaluated by CL and 4-HNE expression, there was an elevated lipoperoxidation level post-RE. Both markers indicate a more evident lipoperoxidation increase instantly after exercise, in which LLLT resulted in similar peroxidation levels between 4J and Ctr groups. Exercised rats showed a significant increase in gastrocnemius muscle global protein carbonylation (for both time evaluation (Figure 3(c)). Exercise rats who were previously subjected to LLLT were protected from the increase in global protein carbonylation caused by RE, in which a more pronounced effect was observed 24 hours postexercise.

Regarding antioxidant enzymes, protein expression of SOD, CAT, and HSP70 was not affected by RE or LLLT at any time of analysis (Figure 4).

On the other hand, a higher SOD activity 24 h postexercise has been reported in animals submitted to LLLT (Figure 5). There was no difference in CAT activity between conditions (Ctr versus RE versus 4J) or time (instant versus 24 h). However, a decrease in GPx activity was observed in the RE group compared with Ctr group, in which LLLT has normalized GPx activity in the 4J group to similar levels of the control group in analyses carried out instantly postexercise. In addition, the evaluation of FRAP was significantly increased instantly postexercise in the 4J group.

4. Discussion

There are studies involving animals and humans that show beneficial effects of LLLT on muscle damage and oxidative stress induced by aerobic exercise [23, 24, 26]. However, LLLT repercussion on oxidative stress evoked by RE is still unclear. Thus, our main findings were that oxidative stress and antioxidant capacity after a RE were modulated by the prior LLLT application. The LLLT reduced the oxidative stress and did not only avoid the reductions in antioxidant capacity but increased them.

A controversial issue is whether the LLLT can improve the physical performance. Leal Junior et al. have noticed a higher force peak in anterior tibial muscles of rats subjected to 1 and 3 J LLLT prior muscle fatigue linked to neuromuscular electrical stimulation [37]. On the other hand, Baroni et al. did not observe differences in eccentric peak torque in subjects submitted to LLLT before performing 75 maximal

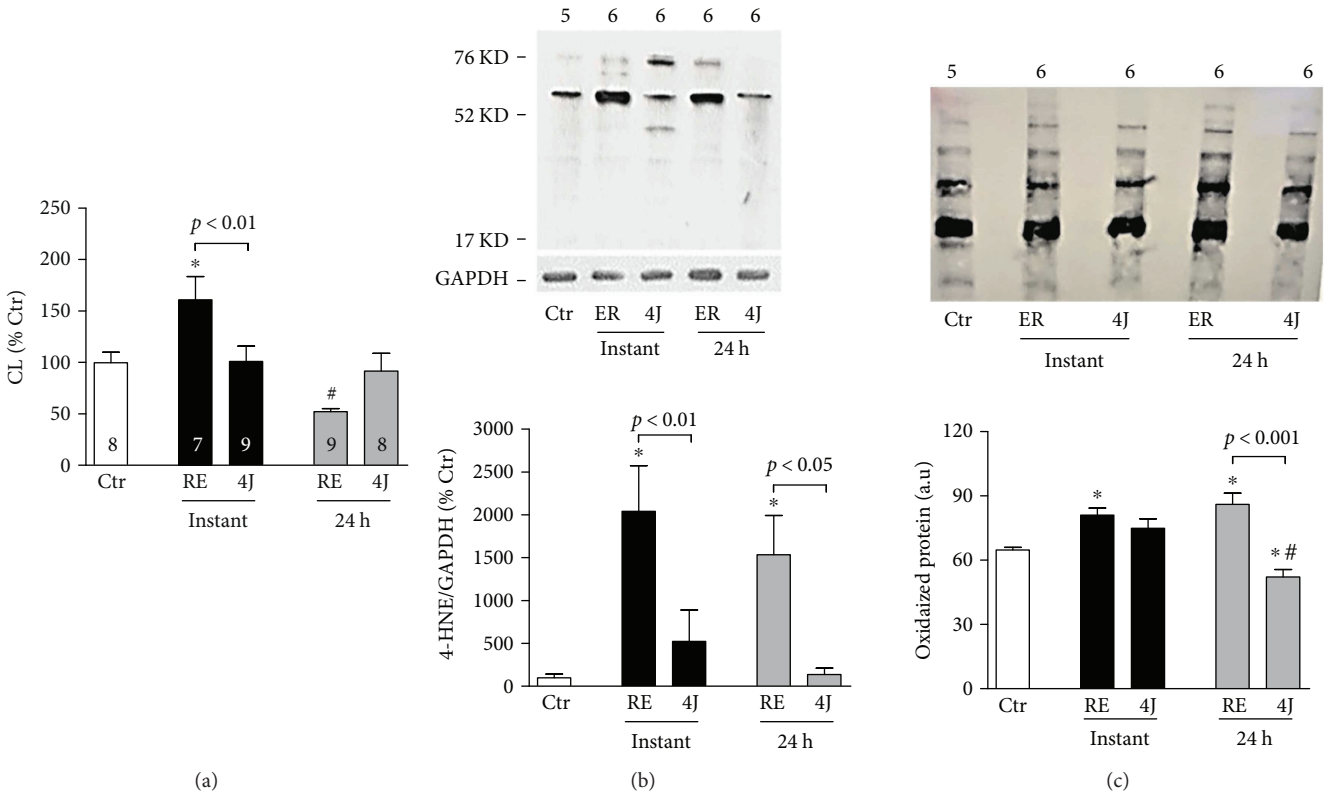

Figure 3: Lipid peroxidation levels in gastrocnemius muscle in control rats (Ctr), rats that only underwent a resistance exercise session (RE), and rats that were subjected to 4J LLLT irradiations prior to a resistance exercise session (4J). Data are representative of samples collected instantly and 24 h after exercise. (a) Chemiluminescence initiated by tert-butil. (b) 4-Hydroxynonenal (4-HNE) expression and (c) carbonyl protein were analyzed by Western blot ($n = 4 - 6$ per group). $^{*}p < 0.05$ versus Ctr group; $^{\#}p < 0.05$ versus instant time. Number of animals for each experiment is shown inside the bars and above the illustrations for (b) and (c).

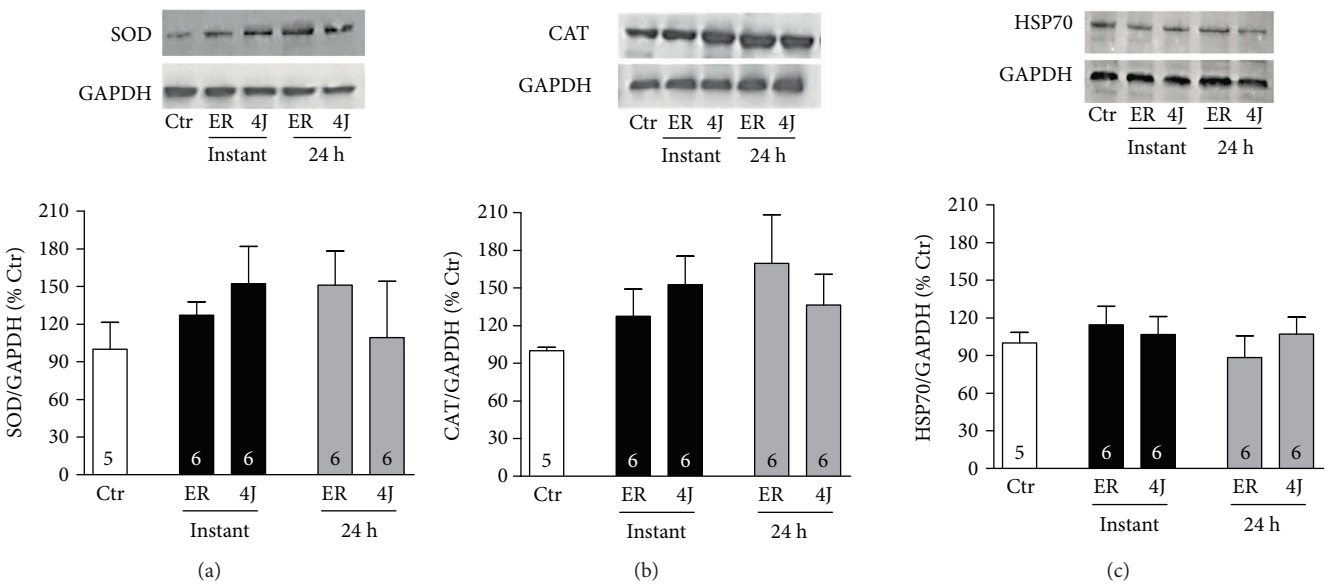

Figure 4: Protein expression of (a) superoxide dismutase (SOD), (b) catalase (CAT), and (c) 70 kilo Dalton heat shock protein (HSP70) in gastrocnemius muscle in control rats (Ctr), rats that only underwent a resistance exercise session (RE), and rats that were subjected to 4J LLLT irradiations prior to a resistance exercise session (4J). Data are representative of samples collected instantly and 24 h after exercise. Kruskal-Wallis and post hoc Dunn's tests were used for multiple comparisons. Number of animals for each experiment is shown inside the bars.

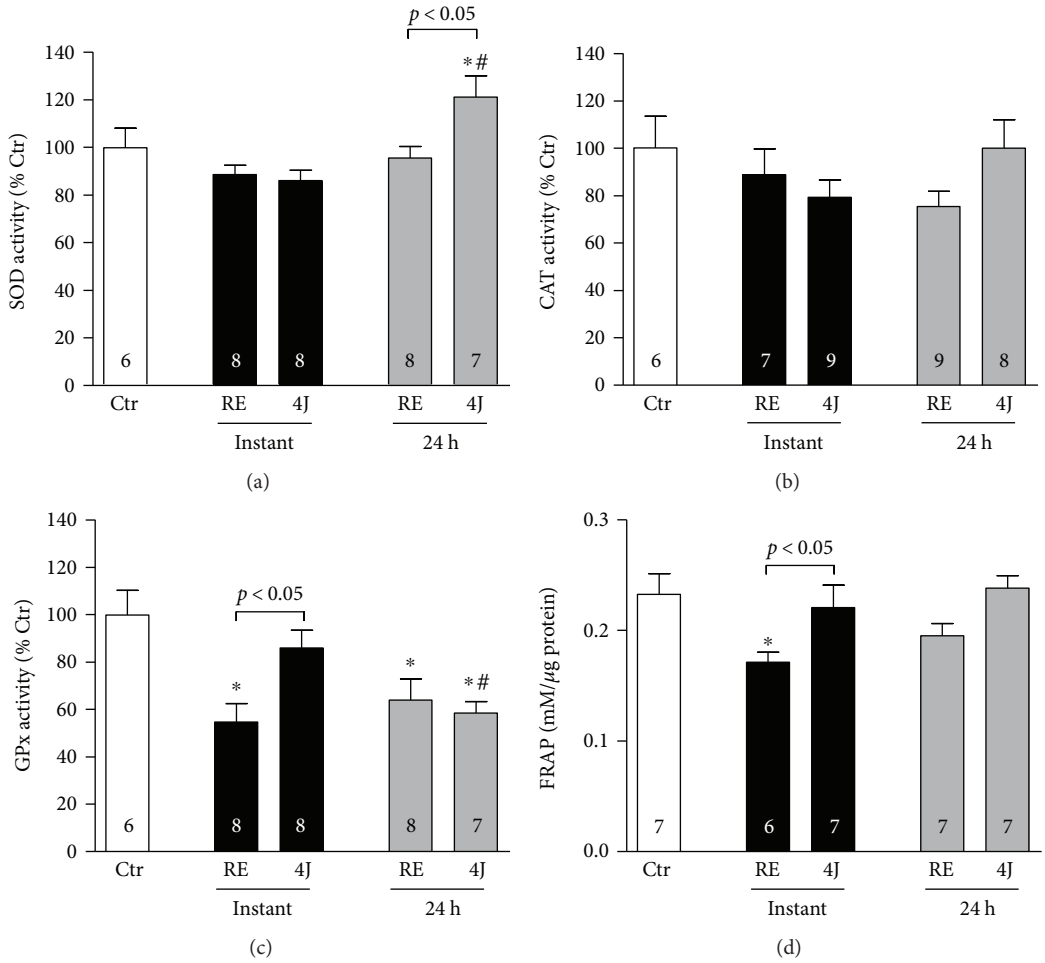

Figure 5: Enzymatic activity of (a) superoxide dismutase (SOD), (b) catalase (CAT), and (c) glutathione peroxidase (GPx) in gastrocnemius muscle in control rats (Ctr), rats that only underwent a resistance exercise session (RE), and rats that were submitted to 4J LLLT irradiations prior to a resistance exercise session (4J). (d) Total antioxidant capacity of gastrocnemius muscle by ferric reduction ability power assay (FRAP). Data are representative of samples collected instantly and 24 h after exercise. ANOVA two-way and Bonferroni post hoc tests were used for multiple comparisons. $^{*}p < 0.05$ versus Ctr group; $^{\#}p < 0.05$ versus instant time. Number of animals for each experiment is shown inside the bars.

knee extensor eccentric contractions compared to the nonirradiated group [38]. Similarly, it was demonstrated by our results that rats irradiated with 4J energy did not show improved performance, as evaluated by muscle work and muscle power compared to nonirradiated rats.

Our resistance exercise protocol was suitable to increase oxidative stress as assessed by lipoperoxidation levels in muscle, corroborating previous data about resistance exercise [14–17, 22]. A decreased oxidative stress in muscles irradiated with 4J energy demonstrates to be of interest, in which more positive results were noticed for analyses of lipid peroxidation performed immediately after RE bout. Moreover, 4J rats exhibited protein oxidation levels similar to the Ctr group. These findings extend previous studies showing an antioxidant effect of LLLT when applied prior to aerobic exercise, as a progressive-intensity running protocol in humans and forced high-intensity treadmill in rats [23, 26]. An important aspect has been reported for our 24 postexercise findings. While the tert-butyl hydroperoxide-initiated chemiluminescence indicated lower lipid peroxidation in the nonirradiated exercised rats, the expression of 4-HNE indicated otherwise. The reasons for these findings are unclear, but may be associated with measurement methods. Some of these findings may be associated with a nonsingular stability of lipid hydroperoxides over time among experimental groups, which also makes it difficult to analyze lipid peroxidation. This chronicity of the process has relevant implications for measurement, in which hydroperoxides are unstable and extensive oxidation of a lipid can occur without a follow-up on the buildup in hydroperoxides [39]. Thus, changes in the mechanism of peroxide decomposition might change the amount generated without a lower lipid peroxidation rate in the RE rats as seen in the chemiluminescence assay. Therefore, we have applied two methods to confirm our findings of lipoperoxidation (i.e., CL and 4-HNE). This route corroborates that two or more different assay methods should be used to evaluate lipid peroxidation [40].

We have extended these analyses to determine whether a lower oxidative stress induced by the LLLT could also be associated with modulation of protein oxidation. Elevated

cellular oxidants can result in posttranslational changes of proteins that can affect muscle function [41]. In fact, a high concentration of carbonyl derivates in gastrocnemius muscle was observed in the nonirradiated rats, mainly in later analyses (i.e., 24 h postexercise).

Reactive oxygen species (e.g., superoxide anions and hydroxyl radicals) cause the oxidation of membrane phospholipids, proteins, and DNA that has been implicated in several physiological disturbances. The adverse effects of an increase in free radicals can be countered by antioxidant enzymes, such as SOD, GPx, and CAT, and by nonenzymatic antioxidants [25]. In our case, antioxidant capacity instantly postexercise (i.e., GPx activity and FRAP) has been reduced in RE rats, but it was not observed when the LLLT was carried out. Moreover, there was an increased antioxidant SOD enzyme activity 24 h postexercise in 4J group when compared with the Ctr group. These results are in line with the findings of other studies showing that LLLT may modulate the antioxidant capacity [42, 43]. In this sense, the experimental results of the present study suggest that LLLT applied prior to resistance exercise session can increase the protection of the cells against oxidative stress induced by exercise. It could delay the impairments of muscle contractility that leads to fatigue [44] and hence contribute to the quality of training program. It should be noted that the CAT activity did not suffer any change with RE or LLLT. Our data agree with a study in which an acute exercise or LLLT [23] was not capable of modulating CAT activity. On the other hand, our data disagree that CAT activity may be reduced after a RE in women [45]. Therefore, the CAT activity affected by the RE remains controversial, and further studies should be performed.

Although the antioxidant enzyme activities have been changed by RE and LLLT, there were no significant changes in the protein expression. A null action of LLLT in the antioxidant protein expression is not a novelty. It has been demonstrated that LLLT does not alter SOD expression in subjects subjected to running [23]. Based on these findings, it may be proposed that LLLT modulate disruption of the physiological balance between the oxidant and antioxidant enzymes in exercised muscle, most likely by favoring increased enzymatic activity. In this context, the data from this study suggest that a comprehensive analysis of antioxidant enzymes should contain their expression as well as activity. Lastly, studies are showing that photobiomodulation can improve mitochondrial function and mitigate FR generated during exercise training [46]. Therefore, the mitochondrial function shows to be a key target, in which the role of photobiomodulation in altering the generation of FR induced by resistance exercise shows to be a goal to be investigated.

A major issue is that the increase in oxidative stress shows to be a common physiological process induced by resistance exercise. Regarding this, our LLLT-induced oxidative stress inhibition findings may fall into the debate whether antioxidant treatment could attenuate or eliminate exercise-induced adaptive response in skeletal muscle [47]. Although some researchers have not reported ablation of beneficial exercise role with an antioxidant treatment [48], it was demonstrated that giving antioxidant (e.g., vitamin C) the whole adaptive response was knocked out [49]. Consequently, the impact of the LLLT-induced oxidative stress prevention in important physiological process as exercise-induced adaptation (e.g., muscle hypertrophy) shows to be investigated.

In conclusion, LLLT prevented the increase of oxidative stress markers in the rats' gastrocnemius muscle subjected to a high-intensity resistance exercise session. The 4J energy irradiation was associated with improvement in the antioxidant defense linked to higher SOD and GPx activities (24 h and instantly postexercise, resp.). Moreover, a significant difference was found in muscle FRAP between RE and 4J rats instantly postexercise, indicating that a nonenzymatic total antioxidant capacity was preserved with LLLT. The ascorbic acid, α-tocopherol, proteins, and bilirubin are the main contributors to FRAP of plasma, detected by the FRAP assay [36, 50]. Thus, the data suggest that LLLT modifies the concentration of these antioxidant molecules in the exercise muscle. Overall, these results indicate that LLLT could be an important approach to counteract the supraphysiological production of reactive oxygen species during RE.

Conflicts of Interest

The authors declare that they have no conflicts of interest.

Acknowledgments

This study was sponsored by Fundação de Amparo à Pesquisa do Estado de São Paulo (FAPESP). Andrey J. Serra is a Research Fellow from São Paulo Research Foundation—FAPESP (no. 2015/11028-9; no. 2017/26113-7; and no. 2017/09274-7) and National Council for Scientific and Technological Development—CNPq (no. 305527/2017-7).

References

[1] B. Halliwell, "Biochemistry of oxidative stress: figure 1," *Biochemical Society Transactions*, vol. 35, no. 5, pp. 1147–1150, 2007.

[2] D. E. Handy and J. Loscalzo, "Redox regulation of mitochondrial function," *Antioxidants & Redox Signaling*, vol. 16, no. 11, pp. 1323–1367, 2012.

[3] I. S. Young and J. V. Woodside, "Antioxidants in health and disease," *Journal of Clinical Pathology*, vol. 54, no. 3, pp. 176–186, 2001.

[4] C. Bisbal, K. Lambert, and A. Avignon, "Antioxidants and glucose metabolism disorders," *Current Opinion in Clinical Nutrition and Metabolic Care*, vol. 13, no. 4, pp. 439–446, 2010.

[5] K. J. Davies, A. T. Quintanilha, G. A. Brooks, and L. Packer, "Free radicals and tissue damage produced by exercise," *Biochemical and Biophysical Research Communications*, vol. 107, no. 4, pp. 1198–1205, 1982.

[6] K. H. Cheeseman and T. F. Slater, "An introduction to free radical biochemistry," *British Medical Bulletin*, vol. 49, no. 3, pp. 481–493, 1993.

[7] D. Knoefler, L. I. Leichert, M. Thamsen et al., "About the dangers, costs and benefits of living an aerobic lifestyle," *Biochemical Society Transactions*, vol. 42, no. 4, pp. 917–921, 2014.

[8] D. M. Bailey, L. Lawrenson, J. McEneny et al., "Electron paramagnetic spectroscopic evidence of exercise-induced free radical accumulation in human skeletal muscle," *Free Radical Research*, vol. 41, no. 2, pp. 182–190, 2007.

[9] M. C. Gomez-Cabrera, E. Domenech, M. Romagnoli et al., "Oral administration of vitamin C decreases muscle mitochondrial biogenesis and hampers training-induced adaptations in endurance performance," *The American Journal of Clinical Nutrition*, vol. 87, no. 1, pp. 142–149, 2008.

[10] C. Bonnard, A. Durand, S. Peyrol et al., "Mitochondrial dysfunction results from oxidative stress in the skeletal muscle of diet-induced insulin-resistant mice," *The Journal of Clinical Investigation*, vol. 118, no. 2, pp. 789–800, 2008.

[11] L. Guarente, "Mitochondria—a nexus for aging, calorie restriction, and sirtuins?," *Cell*, vol. 132, no. 2, pp. 171–176, 2008.

[12] S. Sukhanov, T. Yoshida, A. M. Tabony et al., "Angiotensin II, oxidative stress and skeletal muscle wasting," *The American Journal of the Medical Sciences*, vol. 342, no. 2, pp. 143–147, 2011.

[13] C. K. Sen, "Antioxidants in exercise nutrition," *Sports Medicine*, vol. 31, no. 13, pp. 891–908, 2001.

[14] J. M. McBride, W. J. Kraemer, T. R. Triplett-McBride, and W. Sebastianelli, "Effect of resistance exercise on free radical production," *Medicine and Science in Sports and Exercise*, vol. 30, no. 1, pp. 67–72, 1998.

[15] M. B. Hudson, P. A. Hosick, G. O. McCaulley et al., "The effect of resistance exercise on humoral markers of oxidative stress," *Medicine and Science in Sports and Exercise*, vol. 40, no. 3, pp. 542–548, 2008.

[16] R. Deminice, T. Sicchieri, P. O. Payao, and A. A. Jordao, "Blood and salivary oxidative stress biomarkers following an acute session of resistance exercise in humans," *International Journal of Sports Medicine*, vol. 31, no. 09, pp. 599–603, 2010.

[17] L. T. Retamoso, M. E. J. Silveira, F. D. Lima et al., "Increased xanthine oxidase-related ROS production and TRPV1 synthesis preceding DOMS post-eccentric exercise in rats," *Life Sciences*, vol. 152, pp. 52–59, 2016.

[18] M. Wiecek, M. Maciejczyk, J. Szymura, and Z. Szygula, "Effect of maximal-intensity exercise on systemic nitro-oxidative stress in men and women," *Redox Report*, vol. 22, no. 4, pp. 176–182, 2016.

[19] A. L. Bessa, V. N. Oliveira, G. G. Agostini et al., "Exercise intensity and recovery: biomarkers of injury, inflammation, and oxidative stress," *Journal of Strength and Conditioning Research*, vol. 30, no. 2, pp. 311–319, 2016.

[20] K. Slattery, D. Bentley, and A. J. Coutts, "The role of oxidative, inflammatory and neuroendocrinological systems during exercise stress in athletes: implications of antioxidant supplementation on physiological adaptation during intensified physical training," *Sports Medicine*, vol. 45, no. 4, pp. 453–471, 2015.

[21] S. J. Rietjens, M. Beelen, R. Koopman, L. J. Van Loon, A. Bast, and G. R. Haenen, "A single session of resistance exercise induces oxidative damage in untrained men," *Medicine and Science in Sports and Exercise*, vol. 39, no. 12, pp. 2145–2151, 2007.

[22] H. Cakir-Atabek, F. Ozdemir, and R. Colak, "Oxidative stress and antioxidant responses to progressive resistance exercise intensity in trained and untrained males," *Biology of Sport*, vol. 32, no. 4, pp. 321–328, 2015.

[23] T. De Marchi, E. C. Leal Junior, C. Bortoli, S. S. Tomazoni, R. Á. Lopes-Martins, and M. Salvador, "Low-level laser therapy (LLLT) in human progressive-intensity running: effects on exercise performance, skeletal muscle status, and oxidative stress," *Lasers in Medical Science*, vol. 27, no. 1, pp. 231–236, 2012.

[24] E. M. Amadio, A. J. Serra, S. A. Guaraldo et al., "The action of pre-exercise low-level laser therapy (LLLT) on the expression of IL-6 and TNF-alpha proteins and on the functional fitness of elderly rats subjected to aerobic training," *Lasers in Medical Science*, vol. 30, no. 3, pp. 1127–1134, 2015.

[25] S. A. Guaraldo, A. J. Serra, E. M. Amadio et al., "The effect of low-level laser therapy on oxidative stress and functional fitness in aged rats subjected to swimming: an aerobic exercise," *Lasers in Medical Science*, vol. 31, no. 5, pp. 833–840, 2016.

[26] A. A. Silva, E. C. Leal-Junior, A. D'Avila Kde et al., "Pre-exercise low-level laser therapy improves performance and levels of oxidative stress markers in mdx mice subjected to muscle fatigue by high-intensity exercise," *Lasers in Medical Science*, vol. 30, no. 6, pp. 1719–1727, 2015.

[27] M. T. Manchini, A. J. Serra, S. Feliciano R dos et al., "Amelioration of cardiac function and activation of anti-inflammatory vasoactive peptides expression in the rat myocardium by low level laser therapy," *PLoS One*, vol. 9, no. 7, article e101270, 2014.

[28] M. A. Laframboise, C. Borody, and P. Stern, "The female athlete triad: a case series and narrative overview," *Journal of the Canadian Chiropractic Association*, vol. 57, no. 4, pp. 316–326, 2013.

[29] I. C. Sanches, F. F. Conti, M. Sartori, M. C. Irigoyen, and K. de Angelis, "Standardization of resistance exercise training: effects in diabetic ovariectomized rats," *International Journal of Sports Medicine*, vol. 35, no. 4, pp. 323–329, 2014.

[30] C. Ferraresi, M. V. de Sousa, Y. Y. Huang, V. S. Bagnato, N. A. Parizotto, and M. R. Hamblin, "Time response of increases in ATP and muscle resistance to fatigue after low-level laser (light) therapy (LLLT) in mice," *Lasers in Medical Science*, vol. 30, no. 4, pp. 1259–1267, 2015.

[31] B. Gonzalez Flecha, S. Llesuy, and A. Boveris, "Hydroperoxide-initiated chemiluminescence: an assay for oxidative stress in biopsies of heart, liver, and muscle," *Free Radical Biology & Medicine*, vol. 10, no. 2, pp. 93–100, 1991.

[32] M. T. Manchini, E. L. Antônio, J. A. Junior et al., "Low-level laser application in the early myocardial infarction stage has no beneficial role in heart failure," *Frontiers in Physiology*, vol. 8, p. 23, 2017.

[33] B. L. de Melo, S. S. Vieira, E. L. Antonio et al., "Exercise training attenuates right ventricular remodeling in rats with pulmonary arterial stenosis," *Frontiers in Physiology*, vol. 7, p. 541, 2016.

[34] F. F. Conti, O. Brito Jde, N. Bernardes et al., "Positive effect of combined exercise training in a model of metabolic syndrome and menopause: autonomic, inflammatory, and oxidative stress evaluations," *American Journal of Physiology. Regulatory, Integrative and Comparative Physiology*, vol. 309, no. 12, pp. R1532–R1539, 2015.

[35] D. Farah, J. Nunes, M. Sartori et al., "Exercise training prevents cardiovascular derangements induced by fructose overload in developing rats," *PLoS One*, vol. 11, no. 12, article e0167291, 2016.

[36] I. F. Benzie and J. J. Strain, "The ferric reducing ability of plasma (FRAP) as a measure of "antioxidant power": the

FRAP assay," *Analytical Biochemistry*, vol. 239, no. 1, pp. 70–76, 1996.

[37] E. C. Leal Junior, R. A. Lopes-Martins, P. de Almeida, L. Ramos, V. V. Iversen, and J. M. Bjordal, "Effect of low-level laser therapy (GaAs 904 nm) in skeletal muscle fatigue and biochemical markers of muscle damage in rats," *European Journal of Applied Physiology*, vol. 108, no. 6, pp. 1083–1088, 2010.

[38] B. M. Baroni, E. C. Leal Junior, T. De Marchi, A. L. Lopes, M. Salvador, and M. A. Vaz, "Low level laser therapy before eccentric exercise reduces muscle damage markers in humans," *European Journal of Applied Physiology*, vol. 110, no. 4, pp. 789–796, 2010.

[39] M. Antolovich, P. D. Prenzler, E. Patsalides, S. McDonald, and K. Robards, "Methods for testing antioxidant activity," *Analyst*, vol. 127, no. 1, pp. 183–198, 2002.

[40] M. Repetto, J. Semprine, and A. Boveris, "Chemical Mechanism, Biological Implications and Analytical Determination," in *Lipid Peroxidation*, A. Catala, Ed., InTech, Rijeka, Croatia, 2012.

[41] L. A. Gilliam, D. S. Lark, L. R. Reese et al., "Targeted overexpression of mitochondrial catalase protects against cancer chemotherapy-induced skeletal muscle dysfunction," *American Journal of Physiology. Endocrinology and Metabolism*, vol. 311, no. 2, pp. E293–E301, 2016.

[42] J. L. Costa Carvalho, A. A. Brito, A. P. Oliveira et al., "The chemokines secretion and the oxidative stress are targets of low-level laser therapy in allergic lung inflammation," *Journal of Biophotonics*, vol. 9, no. 11-12, pp. 1208–1221, 2016.

[43] X. G. Liu, Y. J. Zhou, T. C. Liu, and J. Q. Yuan, "Effects of low-level laser irradiation on rat skeletal muscle injury after eccentric exercise," *Photomedicine and Laser Surgery*, vol. 27, no. 6, pp. 863–869, 2009.

[44] F. He, J. Li, Z. Liu, C. C. Chuang, W. Yang, and L. Zuo, "Redox mechanism of reactive oxygen species in exercise," *Frontiers in Physiology*, vol. 7, p. 486, 2016.

[45] A. M. Cardoso, M. D. Bagatini, M. A. Roth et al., "Acute effects of resistance exercise and intermittent intense aerobic exercise on blood cell count and oxidative stress in trained middle-aged women," *Brazilian Journal of Medical and Biological Research*, vol. 45, no. 12, pp. 1172–1182, 2012.

[46] S. A. Dos Santos, A. J. Serra, T. G. Stancker et al., "Effects of photobiomodulation therapy on oxidative stress in muscle injury animal models: a systematic review," *Oxidative Medicine and Cellular Longevity*, vol. 2017, Article ID 5273403, 8 pages, 2017.

[47] Z. Radak, K. Ishihara, E. Tekus et al., "Exercise, oxidants, and antioxidants change the shape of the bell-shaped hormesis curve," *Redox Biology*, vol. 12, pp. 285–290, 2017.

[48] T. Clifford, O. Bell, D. J. West, G. Howatson, and E. J. Stevenson, "Antioxidant-rich beetroot juice does not adversely affect acute neuromuscular adaptation following eccentric exercise," *Journal of Sports Sciences*, vol. 35, no. 8, pp. 812–819, 2017.

[49] D. Morrison, J. Hughes, P. A. Della Gatta et al., "Vitamin C and E supplementation prevents some of the cellular adaptations to endurance-training in humans," *Free Radical Biology and Medicine*, vol. 89, pp. 852–862, 2015.

[50] L. F. Nonato, E. Rocha-Vieira, R. Tossige-Gomes et al., "Swimming training attenuates oxidative damage and increases enzymatic but not non-enzymatic antioxidant defenses in the rat brain," *Brazilian Journal of Medical and Biological Research*, vol. 49, no. 10, article e5310, 2016.

Hindawi
Oxidative Medicine and Cellular Longevity
Volume 2017, Article ID 9824192, 11 pages
https://doi.org/10.1155/2017/9824192

Research Article

Impact of Hot Environment on Fluid and Electrolyte Imbalance, Renal Damage, Hemolysis, and Immune Activation Postmarathon

Rodrigo Assunção Oliveira,[1] Ana Paula Rennó Sierra,[2,3] Marino Benetti,[2] Nabil Ghorayeb,[3] Carlos A. Sierra,[3] Maria Augusta Peduti Dal Molin Kiss,[2] and Maria Fernanda Cury-Boaventura[1]

[1]*Institute of Physical Activity and Sports Sciences, University of Cruzeiro do Sul, São Paulo, SP, Brazil*
[2]*School of Physical Education and Sport, University of São Paulo, São Paulo, SP, Brazil*
[3]*Sports Cardiology Department, Dante Pazzanese Institute of Cardiology, São Paulo, SP, Brazil*

Correspondence should be addressed to Maria Fernanda Cury-Boaventura; maria.boaventura@cruzeirodosul.edu.br

Received 2 June 2017; Revised 9 August 2017; Accepted 26 October 2017; Published 21 December 2017

Academic Editor: Andrey J. Serra

Previous studies have demonstrated the physiological changes induced by exercise exposure in hot environments. We investigated the hematological and oxidative changes and tissue damage induced by marathon race in different thermal conditions. Twenty-six male runners completed the São Paulo International Marathon both in hot environment (HE) and in temperate environment (TE). Blood and urine samples were collected 1 day before, immediately after, 1 day after, and 3 days after the marathon to analyze the hematological parameters, electrolytes, markers of tissue damage, and oxidative status. In both environments, the marathon race promotes fluid and electrolyte imbalance, hemolysis, oxidative stress, immune activation, and tissue damage. The marathon runner's performance was approximately 13.5% lower in HE compared to TE; however, in HE, our results demonstrated more pronounced fluid and electrolyte imbalance, renal damage, hemolysis, and immune activation. Moreover, oxidative stress induced by marathon in HE is presumed to be related to protein/purine oxidation instead of other oxidative sources. Fluid and electrolyte imbalance and protein/purine oxidation may be important factors responsible for hemolysis, renal damage, immune activation, and impaired performance after long-term exercise in HE. Nonetheless, we suggested that the impairment on performance in HE was not associated to the muscle damage and lipoperoxidation.

1. Introduction

Thermoregulation processes maintain the body temperature in a physiological range despite elevated metabolic rates and exposure to hot environments (>30°C); however, marathon running performance decreased by 2–10% approximately as the wet bulb globe temperature (WBGT) increased from 10 to 25°C [1]. The air temperature is the chief weather parameter that correlates to completing the time anomaly and percentage of runners who do not complete the marathon race [2].

Previous studies have demonstrated the physiological changes induced by exercise exposure in hot environments [3, 4]; however, the mechanisms involved in the impaired aerobic exercise performance in warm–hot conditions remain unclear [3–5]. Hypohydration (body water deficit of >2% of body mass) caused by excessive sweat loss begins to impair the aerobic performance when the skin temperatures exceed 27°C and has pronounced influence on impairing the aerobic performance in warm–hot environments [3, 4].

However, the impairment of performance induced by prolonged exercise in hot environments, with or without dehydration (>2% body mass), is associated to one or more alterations in the hematological parameters, redox balance, tissue damage, skeletal muscle metabolism, and cardiovascular system [5].

Endurance exercise in hot environment induces pronounced catecholamine and cortisol, with proinflammatory

and compensatory anti-inflammatory responses, which may influence the tissue damage [6–8]. The environmental heat stress also promotes blood flow and oxygen limitations to the skeletal muscle implicating the impairment of VO_{2max} modifying oxygen metabolism and oxidative stress [5].

Oxidative stress is caused by an imbalance between the generation of reactive oxygen species (ROS) and their clearance by the antioxidant defense system. Endogenous sources of ROS include the mitochondrial respiratory chain, peroxisomes, NADPH oxidase, hemoglobin, myoglobin, and catecholamine autoxidation during exercise [9]. The excessive production of ROS in the hot environment may lead to the oxidative damage of macromolecules, immune dysfunction, and muscle damage. Recently, Mrakic-Sposta et al. [10] demonstrated that endurance exercise induced oxidative stress following transient renal impairment and inflammation; however, in humans, the evidence for oxidative stress-mediated tissue damage following exercise remains unclear [9, 11, 12].

This study aimed to investigate the hematological and oxidative changes and tissue damage induced by the marathon race on amateur runners in different thermal conditions: hot and temperate environment. The combination of heat and endurance exercise could promote pronounced physiological response and influence the athletic performance and disease risk.

2. Methods

2.1. Subjects. Twenty-six Brazilian male endurance runners participated in this study. Volunteers were recruited by e-mail provided by the São Paulo International Marathon Organization (2014 and 2015). After the screening history and medical examination, 71 runners were recruited for the São Paulo International Marathon 2014 (October 19) and 80 runners were recruited for the São Paulo International Marathon 2015 (May 17); however, 26 runners completed both the São Paulo International Marathon 2014 and 2015 and were included in this study. We followed similar experimental procedures and design including the period of blood collection and cardiopulmonary protocol as that of Santos et al. [13].

The exclusion criteria included the use of medication for cardiac, metabolic, pulmonary, or kidney injury and use of alcohol or any kind of drugs and pathologies including systemic arterial hypertension and liver, kidney, metabolic, inflammatory and neoplastic diseases. Subjects were briefed regarding the experimental procedures and the possible risks, and they gave their informed consent before participating, which was approved by the Ethics Committee of Dante Pazzanese Institute of Cardiology, Brazil (permit number: 979/2010), in accordance with the Declaration of Helsinki. Measurements of total body mass (kg), height (cm), and body mass index (BMI, kg/m^2) were conducted according to the International Society for the Advancement of Kinanthropometry, and the values were expressed as the mean ± standard error of mean (SEM).

2.2. Cardiopulmonary Test. Anthropometric parameters were evaluated, and cardiopulmonary exercise test was performed in the same acclimatized room at 21–23°C and 50% relative humidity, 3–21 days before the São Paulo International Marathon 2014 (September 25 to October 16) and 2015 (April 16 to May 14). Functional capacity was assessed by means of cardiopulmonary exercise test (CPET) with expired gas analysis, performed on a treadmill (TEB Apex 200, TEB, São Paulo, Brazil, speed 0–24 km/h, grade 0–35%). A protocol was used, with a starting speed of 8 km/h and grade of 1%; speed was gradually increased by 1 km/h every 1 min. The objective was to achieve fatigue within 8–12 min. Blood pressure was measured with a sphygmomanometer at the commencement of the test. Respiratory gas analysis was performed by the Ergostik (Geratherm, Bad Kissingen, Germany) in breath-by-breath mode.

Tests were considered maximum when at least three of these features were achieved: limiting symptoms/intense physical fatigue, increase in VO_2 lower than $2.1\ mL \cdot kg^{-1} \cdot min^{-1}$ through an increase in speed, attained maximal heart rate, or respiratory quotient higher than 1.1.

2.3. Marathon Races. Both races were commenced at 08:00 a.m. and fluid ingestion was allowed ad libitum during the race. Water was provided at every 2-3 km on the running course, sports drinks at 18 and 36 km, and potato or carbohydrate gel at 30 km. The weather parameters at São Paulo International Marathon in 2014 (HE) between 8 a.m. to 2 p.m. were average temperature of 31.4°C, maximum temperature of 35°C, and minimum temperature of 25.8°C; and average relative humidity of 30.4%, maximum relative humidity of 51%, and minimum relative humidity of 26% (National Institute of Meteorology, Ministry of Agriculture, Livestock, and Supply). The weather parameters at the São Paulo International Marathon in 2015 (TE) between 8 a.m. and 2 p.m. were average temperature of 19.8°C, maximum temperature of 22.6°C, and minimum temperature of 16.7°C; and average relative humidity of 72.8%, maximum relative humidity of 86%, and minimum relative humidity of 61% (National Institute of Meteorology, Ministry of Agriculture, Livestock, and Supply). The air quality in the São Paulo International Marathon 2014 was evaluated as low for sulfur dioxide ($8.5\ \mu g/m^3$), nitrogen dioxide ($9.9\ \mu g/mm^3$), and carbon monoxide (6 ppm) and moderate for particulate matter $_{10}$ ($44\ \mu g/m^3$); whereas, in the São Paulo International Marathon 2015, it was evaluated as low for sulfur oxide ($7\ \mu g/m^3$), nitrogen dioxide ($4.3\ \mu g/mm^3$), carbon monoxide (1.6 ppm), and particulate matter $_{10}$ ($19\ \mu g/m^3$).

2.4. Blood Collection. Blood samples (30 mL) were collected in vacuum tubes containing an anticoagulant (0.004% EDTA) 24 h before, immediately after, 1 day after, and 3 days after the São Paulo International Marathon in 2014 and 2015. Simultaneously, urine samples were also collected. Biochemical analyses were subsequently performed at the Institute of Physical Activity Sciences and Sports of Cruzeiro do Sul University and at the Clinical Laboratory of Dante Pazzanese Institute of Cardiology. After centrifugation,

plasma was aliquoted, frozen, and stored at −80°C for later analysis.

2.5. Biochemical Parameters. The biochemical parameters were evaluated with routine-automated methodology in the Clinical Laboratory of Dante Pazzanese Institute of Cardiology immediately after collection. Plasma calcium, magnesium, iron, and bilirubin were performed by colorimetric method; creatinine, C-reactive protein, alanine transaminase, aspartate transaminase, gamma-glutamyl transferase, lactic dehydrogenase, and creatine kinase were determined by kinetic assay; immunological and hematological parameters (hemoglobin, hematocrit, red blood cell distribution width, mean corpuscular volume, mean corpuscular hemoglobin, mean corpuscular hemoglobin concentration, leukocytes, lymphocytes, monocytes, neutrophils, and eosinophils) were assessed by cytochemical/isovolumetric method; ferritin, troponin, proBNP, myoglobin, and creatine kinase-MB were evaluated by chemiluminescence assay; density urine and pH urine were determined by cytometry; and transferrin and alpha-glycoprotein acid were assessed by immunoturbidimetry. Eventually, sodium and potassium were determined by potentiometric ion-selective electrodes.

2.6. Determination of Blood Levels for TBARs. For TBAR determination, a slightly modified assay was used [14]. Plasma was mixed thoroughly with butylated hydroxytoluene (BHT, 2%) and trifluoroacetic acid (10%) (4 : 1 : 4) and incubated for 10 min at 4°C; 1,1,3,3-tetramethoxypropane (10^{-1} mM) was used as a positive control. The samples were centrifuged for 15 min at 8000 g. Thereafter, the supernatant was collected and mixed with HCl (25%) and thiobarbituric acid (TBA 1%, dissolved in NaOH 0.05 M) (2 : 1 : 2). The reaction mixture was incubated at 100°C for 30 min, and the absorbance of the supernatant was recorded at 535 nm (SpectraMax Plus, Molecular Devices). A baseline absorbance was considered by running a blank along with all samples during the measurement. The TBAR concentration was calculated using the molar extinction coefficient of malondialdehyde (1.56×10^5).

2.7. Superoxide Dismutase 3 Assay. Superoxide dismutase 3 activity was determined by kinetic colorimetric assay on plasma in accordance with the manufacture's protocol (Enzo Life Sciences, NY, USA). The samples and standards were homogenized to SOD Master Mix and xanthine solution was mixed to initiate the reaction. The absorbance readings were recorded at 450 nm at every minute for 10 min at room temperature after 10 s orbital shake prior to the initial read (SpectraMax Plus, Molecular Devices). The slope curve was obtained for each sample and calculated based on the standard curve with sensitivity of 0.1–10 U/L.

2.8. Catalase Activity Assay. Catalase activity was determined according to a slightly modified assay [15]. Briefly, 5 μL of plasma samples were added to 200 μL of a dH_2O and H_2O_2 reagent solution (1 : 1000). The absorbance reading of the samples was recorded at 240 nm for 180 s with 30 s intervals at room temperature (SpectraMax 190 Plus, Molecular Devices). The catalase activity calculation was based on the molar extinction coefficient of H_2O_2 using an equation: (Δ absorbance/0.0218/mg protein).

2.9. Uric Acid Assay. Plasma uric acid was evaluated by enzymatic colorimetric assay and kinetic colorimetric assay in accordance with the manufacture's protocol (Bioclin, MG, Brazil). Standard (6 mg/dL) and plasma samples were mixed with the enzyme reagents and were incubated at 37°C for 5 min. The absorbance readings were recorded at 505 nm (490–540 nm), hitting the zero with the blank (SpectraMax Plus, Molecular Devices). The intensity of the cherry color formed is directly proportional to the concentration of the uric acid in the sample. The uric acid concentration was calculated by the following formula: 6 mg/dL × (sample absorbance/standard absorbance).

2.10. Statistical Analyses. Statistical analyses were performed using the Statistical Package for the Social Sciences (IBM SPSS Statistics for Mac, Version 24.0. Armonk, NY, USA). The normality of the data distribution was determined by the Kolmogorov–Smirnov test and rejects the normality. To compare the general and training characteristics in hot and temperate environment, we performed the paired *t*-test (Wilcoxon test). Differences between the steps (before, immediately after, 1 day after, and 3 days after the race) in the hot and temperate environment were tested for significance with the Friedman test with repeated measures and Müller–Dunn's posttest. Spearman correlation was performed to identify the coefficient correlation between the variables using absolute values and relative changes (Δ) compared to baseline levels. Statistical significance was assumed at p value < 0.05.

3. Results

3.1. Sports Performance and Heat Acclimation. The demographic characteristics of the runners and environment parameters are presented in Table 1. Twenty-six athletes finished the São Paulo International Marathon race in the hot environment (HE, mean 31.4°C, humidity 34.3%) and in the temperate environment (TE, mean 19.8°C, humidity 72.8%). The temperature was higher during the 10 days before the race in HE compared to TE, suggesting possible conditions for acclimatization. The training volume, exhaustion speed, time of exhaustion, anaerobic threshold speed, and respiratory compensation point speed after cardiopulmonary test did not differ from 3 to 21 days before the race in 2014 (HE) and 2015 (TE; Table 1). The peak consumption of oxygen (VO_{2peak}) was higher in 2014 (HE) compared to 2015 (TE); however, the marathon runner's performance during the race was lower by approximately 13.5%, in accordance with the race time and race pace, in HE compared to TE (Table 1).

3.2. Markers of Fluid, Electrolyte Balance, and Kidney Damage. At rest, before the race, we observed that plasma magnesium, sodium concentration, osmolality, and pH urine were greater and plasma potassium and calcium levels were lower for HE indicating fluid and electrolyte imbalance during precompetition (Table 2). The creatinine level

Table 1: General and training characteristics of the marathon runners and environment parameters in the hot and temperate environment.

	Hot environment	Temperate environment
Age (years)	42 ± 2	43 ± 2
Height (m)	1.73 ± 0.01	1.73 ± 0.01
Body mass (kg)	75 ± 2	75 ± 2
BMI (kg/m^2)	25.2 ± 0.2	25.1 ± 0.2
Training experience (years)	6.11 ± 0.22	6.69 ± 0.80
Training volume (km/week)	55.2 ± 3.2	52.03 ± 2.39
Time of exhaustion (min)	10.9 ± 0.4	11.1 ± 0.5
VO_{2peak} (mL·kg^{-1}·min^{-1})	58.6 ± 1.2*	54.6 ± 1.2
Exhaustion speed (km/h)	18.3 ± 0.3	18.4 ± 0.3
AT speed (km/h)	9.3 ± 0.2	9.3 ± 0.2
RCP speed (km/h)	16.6 ± 0.4	16.5 ± 0.5
Race time (min)	276 ± 8*	243 ± 11
Race pace (min/km)	6.54 ± 0.18*	5.75 ± 0.26
Temperature (°C) 10 days before the race	23.4 ± 0.6*	16.3 ± 0.2
Temperature (°C) at race	31.4 ± 0.6*	19.8 ± 0.2
Humidity at race (%)	30.4 ± 7.7*	72.8 ± 7.2

BMI: body mass index; AT: anaerobic threshold; RCP: respiratory compensation point; VO_{2peak}: peak consumption of oxygen. The values presented are the mean ± standard error of mean (SEM) of 26 runners. *$p < 0.05$ for comparison between hot and temperate environment.

also was lower for the HE environment (Table 2). The race time was negatively correlated with urea levels in HE ($r = 0.5$, $p < 0.01$).

In both weathers, marathon race reduces the plasma magnesium concentration (by 20%) and increases the osmolality (by 1.7% to 4%), plasma sodium (by 1% to 3.5%), urea (by 22% to 26%), creatinine (by 50% to 55%), urine density (<1%), hematuria (by 23-fold), and urine WBC (by 6.6-fold), suggesting fluid and electrolyte imbalance and kidney damage. The weight loss was also found to be similar in both 2014 and 2015 marathons (1.8 ± 0.2 kg and 2 ± 0.2 kg in HE and TE, resp.). The osmolality, plasma sodium, and calcium levels were altered 3 days after the race in both the thermal conditions. Moreover, the marathon during HE also promoted elevation of the plasma potassium (by 15%), urine cylinders, and a pronounced physiological response on the osmolality, sodium levels, density urine, urea, hematuria, and urine WBC (Table 2), suggesting exacerbated fluid and electrolyte imbalance, dehydration, and kidney damage in HE. The proteinuria was observed 1 day after the race in HE and 3 days after the race in TE; however, 1 day after the marathon race, creatinine was elevated (by 6%) in TE compared to HE (Table 2).

3.3. Markers of Oxidative Damage in the Peripheral Blood. Plasma superoxide dismutase 3 (SOD3) activity and TBARs were lower in HE before and in the recovery period compared to TE. Moreover, we observed a higher catalase activity in HE; however, it was not significant (Table 3). Plasma uric acid and SOD3 activity elevated immediately after the race only in HE. We observed an increase in the TBAR levels immediately after the race in both climates. Three days after the marathon, TBARs and SOD3 activity returned to the baseline levels in both climates. We did not observe any significant alterations in the CAT values in both environments.

3.4. Hematological Markers. In both the thermal conditions, erythrocytes, hemoglobin, and hematocrit values reduced after the race and maintained altered 3 days after the race indicating hemolysis and/or hemodilution. In TE, the MCV, MCH, MCHC, and RDW values increased after the race as a consequence of fluid and electrolyte imbalance. In HE, the hemoglobin was higher compared to TE by 3-4% after the race; and the MCV, MCH, MCHC, and RDW values were greater in all periods evaluated compared to TE 1 day after the race (by approximately 1%, 3%, 3%, and 16%, resp.; Table 4).

In HE, we observed correlation between race time and erythrocytes, Hb and Ht, ($r = 0.45$, 0.49, 0.47, 0.47, and 0.57, resp., $p < 0.01$) 1 day after the race. In TE, race time was correlated to unconjugated bilirubin only. In addition, race time was correlated to erythrocytes and Ht-relative changes (Δ) 1 day after the race in HE ($r = 0.44$ and 0.4, resp., $p < 0.05$).

After the race, we also demonstrated an increase in the erythropoietin levels (by 16–18%) in both weathers; however, HE promotes a pronounced and earlier response in the erythropoietin levels (Table 4).

3.5. Iron Metabolism Markers. Before competition, we observed higher ferritin and transferrin levels (by 17% and 9%, resp.) and lower transferrin saturation (by 8%) in HE. In the recovery period, transferrin remained higher in HE compared to TE (Table 5).

Immediately after the race, we observed an increase in ferritin (by 13% to 23%) and unconjugated and conjugated bilirubin (by 25 to 40%) in both weathers. However, 3 days after the race, we demonstrated a decrease in the iron (by 8% to 25%) and transferrin levels (by approximately 5%) in both weathers, contributing to hemolysis hypothesis after the race. Moreover, HE promoted an elevation in the iron levels 1 day after the race and a reduction in the ferritin level and transferrin saturation 3 days after the race. However, we observed a higher response for the total and unconjugated bilirubin levels in the TE environment as a result of pronounced muscle damage and myoglobin degradation due to higher exercise intensity (Table 5).

3.6. Immunological Markers. We observed an elevation in the leukocytes, neutrophils, and monocytes (by approximately 2.5-fold, 3.5-fold, and 1.5-fold, resp.) and a decrease in the lymphocytes after the race by 40%, suggesting exacerbated immune activation after competition. In HE, the lymphocyte and leukocyte alterations were more pronounced 1 day after the race. In the recovery period, 3 days after the race, lymphocytes maintained altered in both weathers, even as leukocytes and eosinophils in TE (Table 6). The eosinophil count decreased after the race only in TE. In HE, the eosinophil

Table 2: Fluid, electrolyte balance, and renal function after the marathon race in the temperate and hot environment.

	Reference values	Before	Immediately after	1 day after	3 days after
Sodium (mMol/L)	137–145				
HE		$142 \pm 0.4^{\#\#}$	$147 \pm 0.5^{**\#\#}$	$142 \pm 0.4^{\#}$	$143 \pm 0.3^{*\#}$
TE		139 ± 0.3	140 ± 0.4	$140 \pm 0.3^{*}$	$141 \pm 0.3^{**}$
Magnesium (mg/dL)	1.7–2.5				
HE		$2.5 \pm 0.04^{\#}$	$2 \pm 0.05^{**\#}$	$2.2 \pm 0.03^{**}$	$2.4 \pm 0.03^{*\#}$
TE		2.3 ± 0.1	$1.9 \pm 0.1^{**}$	$2.2 \pm 0.1^{*}$	2.3 ± 0.1
Osmol (mOsm/L)	275–295				
HE		$296 \pm 1^{\#\#}$	$309 \pm 1^{**\#\#}$	$298 \pm 1^{**\#\#}$	$297 \pm 1^{\#\#}$
TE		289 ± 1	$294 \pm 1^{**}$	$293 \pm 1^{**}$	$293 \pm 1^{**}$
Potassium (mMol/L)	3.5–5.6				
HE		$3.9 \pm 0.05^{\#\#}$	$4.5 \pm 0.1^{**}$	$4.4 \pm 0.1^{**}$	$4.3 \pm 0.1^{**\#}$
TE		4.5 ± 0.05	4.4 ± 0.1	4.5 ± 0.1	4.5 ± 0.1
Calcium (mg/dL)	8.4–11				
HE		$9.3 \pm 0.1^{\#\#}$	$9.3 \pm 0.1^{\#\#}$	$9.1 \pm 0.1^{\#\#}$	$8.9 \pm 0.1^{*\#\#}$
TE		9.6 ± 0.1	$9.8 \pm 0.1^{*}$	9.6 ± 0.1	$9.5 \pm 0.1^{*}$
Creatinine (mg/dL)	0.7–1.3				
HE		$0.9 \pm 0.02^{\#\#}$	$1.4 \pm 0.05^{**\#}$	$1 \pm 0.03^{*}$	$0.9 \pm 0.02^{\#}$
TE		1 ± 0.02	$1.5 \pm 0.1^{**}$	1 ± 0.03	1 ± 0.03
Urea (mg/dL)	<40				
HE		40 ± 1	$49 \pm 2^{**}$	$49 \pm 2^{**\#}$	$38 \pm 1^{\#}$
TE		38 ± 1	$48 \pm 1^{**}$	$46 \pm 2^{**}$	35 ± 2
UD (kg/m^3)	1005–1030				
HE		1019 ± 2	$1025 \pm 1^{*\#}$	$1022 \pm 1^{\#}$	$1021 \pm 2^{\#}$
TE		1016 ± 1	$1019 \pm 1^{*}$	$1013 \pm 1^{*}$	1014 ± 1
Urine pH	5-6				
HE		$6 \pm 0.1^{\#}$	$6 \pm 0.1^{\#\#}$	$6 \pm 0.1^{\#\#}$	$6 \pm 0.1^{\#}$
TE		6 ± 0.2	$5 \pm 0.1^{*}$	5 ± 0.1	$6 \pm 0.1^{*}$
Urine WBC (cell/mL)	0–10,000				
HE		1638 ± 314	$10{,}828 \pm 2170^{**\#}$	$4589 \pm 569^{**\#}$	2778 ± 755
TE		2310 ± 598	$4828 \pm 1185^{*}$	2071 ± 230	2250 ± 444
Hematuria (cell/mL)	0–10,000				
HE		3259 ± 1539	$76{,}017 \pm 36{,}939^{**}$	$3679 \pm 736^{\#}$	$4259 \pm 1409^{\#}$
TE		1241 ± 146	$44{,}241 \pm 13{,}538^{*}$	4679 ± 2070	2500 ± 878
Urine cylinders (units/mL)	0				
HE		0 ± 0	$463 \pm 144^{*\#}$	0 ± 0	0 ± 0
TE		69 ± 48	35 ± 35	107 ± 79	0 ± 0
Proteinuria (mg/dL)	0				
HE		3 ± 2	9 ± 5	$1 \pm 1^{\#}$	0 ± 0
TE		3 ± 2	1 ± 1	7 ± 3	2 ± 2

WBC: white blood cells; UD: urine density; Osmol: osmolality; HE: hot environment; TE: temperate environment. The values presented are the mean ± standard error of mean (SEM) of 26 runners. $^{*}p < 0.05$ versus before race; $^{**}p < 0.0001$ versus before race; $^{\#}p < 0.05$; and $^{\#\#}p < 0.0001$ versus temperate environment.

count was lower before the race and elevated immediately after the race compared to TE (Table 6).

3.7. Muscle Damage Markers and Inflammatory Parameters. In HE, the CRP level and LDH, AST, and ALT activities were lower before and after the race (by approximately 50%) compared to TE and GGT was higher before the race compared to TE. In both weathers, the inflammatory markers, CRP and α-1GPA, lactate, and the muscle damage markers, myoglobin, CK, LDH, AST, and ALT increased after the race (by 3 to 4-fold, 1-fold, 2-fold, 5 to 8-fold, 1.8-fold, 23-fold, 2.5-fold, and 1.5-fold, resp.)

Table 3: Redox status after marathon race in temperate and hot environment.

	Before	Immediately after	1 day after	3 days after
Uric acid (mg/dL)				
HE	5.4 ± 0.1	$6.6 \pm 0.3^{**}$	5.7 ± 0.2	5.6 ± 0.3
TE	5.9 ± 0.2	6.3 ± 0.2	6.1 ± 0.2	6.1 ± 0.3
SOD3 (U/mL)				
HE	$2.6 \pm 0.2^{\#}$	$3.2 \pm 0.4^{*}$	$2.4 \pm 0.3^{\#\#}$	$2.6 \pm 0.2^{\#}$
TE	3.3 ± 0.1	3.1 ± 0.1	3.7 ± 0.5	3.1 ± 0.2
TBARs (nMol/mL)				
HE	$2.4 \pm 0.05^{\#}$	$4.1 \pm 0.01^{**\#}$	$3.2 \pm 0.05^{*\#}$	$2.6 \pm 0.2^{\#}$
TE	3.1 ± 0.2	$4.6 \pm 0.1^{**}$	$3.9 \pm 0.1^{*}$	3.3 ± 0.02
CAT (U/mL)				
HE	87.9 ± 8	63.2 ± 9	70.5 ± 8	73.7 ± 8
TE	72.8 ± 9	49.0 ± 5	49.8 ± 6	59.2 ± 5

SOD: superoxide dismutase; CAT: catalase; TBARs: thiobarbituric acid reactive substances; HE: hot environment; TE: temperate environment. The values are presented as mean ± standard error of mean (SEM) of 26 runners. $^{*}p < 0.05$ versus before the race; $^{**}p < 0.0001$ versus before the race; $^{\#}p < 0.05$; and $^{\#\#}p < 0.0001$ versus temperate environment.

Table 4: Hematological parameters after the marathon race in the temperate and hot environments.

	Reference value	Before	Immediately after	1 day after	3 days after
Erythrocytes (10^6/mm^3)	4.5–5.5				
HE		5.2 ± 0.1	5.2 ± 0.1	$4.9 \pm 0.1^{**}$	$4.9 \pm 0.1^{**}$
TE		5.3 ± 0.1	$5.1 \pm 0.1^{*}$	$4.9 \pm 0.1^{**}$	$4.9 \pm 0.1^{**}$
Hemoglobin (g/dL)	13–17				
HE		15.4 ± 0.2	$15.6 \pm 0.2^{\#}$	$14.6 \pm 0.2^{**\#}$	$14.5 \pm 0.1^{**}$
TE		15.2 ± 0.2	15.0 ± 0.2	$14.2 \pm 0.2^{**}$	$14.5 \pm 0.1^{**}$
Hematocrit (%)	40–50				
HE		47 ± 0.5	$46 \pm 0.5^{*}$	$44 \pm 0.5^{**}$	$45 \pm 0.5^{**}$
TE		47 ± 0.5	$46 \pm 0.5^{*}$	$44 \pm 0.7^{**}$	$45 \pm 0.4^{**}$
Erythropoietin (mU/mL)	4.3–29				
HE		12 ± 1	$14 \pm 1^{*\#}$	14 ± 1	$14 \pm 1^{*\#}$
TE		11 ± 1	12 ± 1	12 ± 1	$13 \pm 1^{*}$
MCV (fL)	80–100				
HE		$90 \pm 1^{\#}$	$89 \pm 1^{*}$	$90 \pm 1^{\#}$	89 ± 2
TE		89 ± 1	89 ± 1	89 ± 1	$91 \pm 1^{*}$
MCH (pg)	27–32				
HE		$30 \pm 0.2^{\#\#}$	$30 \pm 0.3^{*\#\#}$	$28 \pm 1^{\#}$	$30 \pm 0.2^{\#}$
TE		29 ± 0.2	$29 \pm 0.2^{*}$	29 ± 0.2	$29 \pm 0.3^{*}$
MCHC (g/dL)	31.5–36				
HE		$33 \pm 0.1^{\#}$	$34 \pm 0.2^{*\#}$	$33 \pm 0.2^{\#}$	$33 \pm 0.1^{\#}$
TE		32 ± 0.1	$33 \pm 0.2^{*}$	32 ± 0.1	$32 \pm 0.2^{*}$
RDW (%)	11.9–15.4				
HE		$14 \pm 0.1^{\#\#}$	$14 \pm 0.1^{\#\#}$	$14 \pm 0.1^{\#\#}$	$14 \pm 0.1^{\#\#}$
TE		12 ± 0.1	$13 \pm 0.1^{**}$	$13 \pm 0.1^{**}$	$13 \pm 0.1^{**}$

MCV: mean corpuscular volume; MCH: mean corpuscular hemoglobin; MCHC: mean corpuscular hemoglobin concentration; RDW: red cell distribution width; HE: hot environment; TE: temperate environment. The values are presented as mean ± standard error of mean (SEM) of 26 runners. $^{*}p < 0.05$ versus before the race; $^{**}p < 0.0001$ versus before the race; $^{\#}p < 0.05$; and $^{\#\#}p < 0.0001$ versus temperate environment.

Table 5: Iron metabolism and hemolysis biomarkers after marathon race in the temperate and hot environments.

	Reference value	Before	Immediately after	1 day after	3 days after
Iron (μg/L)	60–150				
HE		110 ± 8	120 ± 7	142 ± 10*	90 ± 6*
TE		120 ± 9	126 ± 9	130 ± 8	89 ± 6*
Ferritin (ng/L)	23–336.2				
HE		172 ± 23#	194 ± 25*	186 ± 24*#	147 ± 20**
TE		147 ± 20	181 ± 25**	169 ± 21**	152 ± 17
Transferrin (mg/dL)	170–340				
HE		280 ± 4##	277 ± 4	277 ± 4#	266 ± 3*##
TE		257 ± 6	275 ± 7**	248 ± 5	242 ± 4**
Transferrin saturation (%)	20–50				
HE		39 ± 3#	43 ± 3	51 ± 3*	34 ± 2*
TE		47 ± 4	45 ± 3	54 ± 4*	38 ± 3
Total bilirubin (mg/dL)	0.1–1.2				
HE		0.8 ± 0.1	0.9 ± 0.1#	1.1 ± 0.1*	0.7 ± 0.05
TE		0.9 ± 0.1	1.1 ± 0.1*	1.1 ± 0.1*	0.8 ± 0.1*
Unconjugated bilirubin (mg/dL)	0.1–1.2				
HE		0.4 ± 0.04	0.5 ± 0.06*#	0.6 ± 0.1*#	0.4 ± 0.03
TE		0.5 ± 0.1	0.7 ± 0.1*	0.8 ± 0.1*	0.4 ± 0.1*
Conjugated bilirubin (mg/dL)	<0.3				
HE		0.3 ± 0.02	0.4 ± 0.03*	0.4 ± 0.04*#	0.3 ± 0.02
TE		0.3 ± 0.02	0.4 ± 0.03*	0.3 ± 0.01	0.3 ± 0.02

The values are presented as mean ± standard error of mean (SEM) of 26 runners. HE: hot environment; TE: temperate environment. *$p < 0.05$ versus before the race; **$p < 0.0001$ versus before the race; #$p < 0.05$; and ##$p < 0.0001$ versus temperate environment.

Table 6: Immunological parameters after the marathon race in the temperate and hot environments.

	Reference value	Before	Immediately after	1 day after	3 days after
Leukocytes (mil/mm^3)	4.5–11				
HE		6.1 ± 0.4	14.4 ± 0.6**	7.6 ± 0.4*#	5.8 ± 0.2
TE		6.0 ± 0.2	15.3 ± 0.6**	7.1 ± 0.3**	5.4 ± 0.2*
Lymphocytes (mil/mm^3)	1–3.8				
HE		1.8 ± 0.1	1.1 ± 0.1**#	2 ± 0.1#	1.7 ± 0.1*
TE		2 ± 0.1	1.3 ± 0.1**	1.8 ± 0.1	1.7 ± 0.1*
Neutrophils (mil/mm^3)	1.8–7.7				
HE		3.6 ± 0.3	12.4 ± 0.5**	4.9 ± 0.3**	3.4 ± 0.2
TE		3.4 ± 0.2	13.2 ± 0.6**	4.6 ± 0.2**	3.1 ± 0.1
Monocytes (mil/mm^3)	0–0.8				
HE		0.41 ± 0.03	0.60 ± 0.04**	0.49 ± 0.03*	0.39 ± 0.02
TE		0.37 ± 0.02	0.71 ± 0.07**	0.47 ± 0.03**	0.36 ± 0.02
Eosinophils (mil/mm^3)	0–0.45				
HE		0.16 ± 0.02#	0.19 ± 0.02##	0.15 ± 0.03	0.16 ± 0.02
TE		0.23 ± 0.04	0.02 ± 0.01**	0.17 ± 0.03**	0.18 ± 0.03*

The values are presented as mean ± standard error of mean (SEM) of 26 runners. HE: hot environment; TE: temperate environment. *$p < 0.05$ versus before the race; **$p < 0.0001$ versus before the race; #$p < 0.05$; and ##$p < 0.0001$ versus temperate environment.

and maintained altered 3 days after the race, indicating tissue damage. The lactate concentration returned to the basal level 24 h after the race.

The magnitude of changes on the CRP and α-1GPA, CK, LDH, AST, and ALT (by 3 to 4-fold, 1-fold, 1.8-fold, 23-fold, 2.5-fold, and 1.5-fold, resp.) was similar in both

Table 7: Inflammatory mediators and markers of muscle damage after the marathon race in the temperate and hot environments.

	RV	Before	Immediately after	1 day after	3 days after
CRP (mg/dL)	<0.8				
HE		$0.4 \pm 0.01^{\#\#}$	$0.4 \pm 0.01^{\#\#}$	$1.7 \pm 0.2^{**\#}$	$0.6 \pm 0.05^{**\#\#}$
TE		0.8 ± 0.05	$0.6 \pm 0.05^{*}$	$2.5 \pm 0.2^{**}$	$1.3 \pm 0.1^{**}$
α-1GPA (mg/dL)	50–120				
HE		66 ± 3	$77 \pm 3^{**}$	$77 \pm 2^{**}$	$72 \pm 3^{*}$
TE		69 ± 3	$75 \pm 3^{**}$	$77 \pm 3^{**}$	$78 \pm 3^{*}$
Myoglobin (ng/mL)	<106				
HE		44 ± 6	$1016 \pm 126^{**}$	$154 \pm 20^{**}$	$84 \pm 19^{**}$
TE		46 ± 7	$1059 \pm 120^{**}$	$184 \pm 26^{**}$	$96 \pm 35^{*}$
CK (U/L)	<171				
HE		190 ± 28	$481 \pm 56^{**}$	$1427 \pm 246^{**}$	$906 \pm 381^{*}$
TE		393 ± 155	$568 \pm 78^{**}$	$1828 \pm 283^{**}$	$1231 \pm 497^{*}$
LDH (U/L)	120–246				
HE		$252 \pm 12^{\#\#}$	$427 \pm 33^{**\#\#}$	$290 \pm 19^{*\#\#}$	$284 \pm 20^{\#\#}$
TE		500 ± 23	$934 \pm 37^{**}$	$669 \pm 27^{**}$	$625 \pm 32^{**}$
Lactate (mmol/L)	0.5–1.6				
HE		1.1 ± 0.1	$2.4 \pm 0.2^{**}$	1.2 ± 0.1	0.9 ± 0.1
TE		1.2 ± 0.1	$2.8 \pm 0.2^{**}$	0.9 ± 0.1	1.0 ± 0.1
AST (U/L)	<50				
HE		$28 \pm 1^{\#}$	$37 \pm 2^{**\#}$	$75 \pm 10^{**}$	$48 \pm 7^{*\#}$
TE		37 ± 3	$52 \pm 4^{**}$	$85 \pm 7^{**}$	$64 \pm 7^{**}$
ALT (U/L)	<50				
HE		$24 \pm 2^{\#\#}$	$25 \pm 2^{\#\#}$	$29 \pm 3^{*\#\#}$	$34 \pm 4^{*\#}$
TE		39 ± 2	$42 \pm 2^{*}$	$48 \pm 2^{**}$	$52 \pm 2^{**}$
GGT (U/L)	<73				
HE		$34 \pm 4^{\#}$	33 ± 3	$31 \pm 3^{*}$	$30 \pm 3^{*}$
TE		30 ± 3	$32 \pm 3^{*}$	29 ± 3	$28 \pm 3^{*}$

RV: reference value; α-1GPA: alpha 1 acid glycoprotein; CRP: C-reactive protein; LDH: lactate dehydrogenase; CK: creatine kinase; ALT: alanine transaminase; AST: aspartate transaminase; GGT: gamma-glutamyl transferase; HE: hot environment; TE: temperate environment. The values are presented as mean ± standard error of mean (SEM) of 26 runners. $^{*}p < 0.05$ versus before the race; $^{**}p < 0.0001$ versus before the race; $^{\#}p < 0.05$; and $^{\#\#}p < 0.0001$ versus temperate environment.

environments, except for the CK levels, which were 5-fold in HE and 8-fold in TE as a result of the exercise intensity; however, it was not significant (Table 7).

4. Discussion

In both environments, the marathon race promotes fluid and electrolyte imbalance, hemolysis, oxidative stress, immune activation, and tissue damage; however, in HE, we demonstrated more pronounced fluid and electrolyte imbalance, renal damage, hemolysis, and immune activation. Moreover, the oxidative stress induced by the marathon in HE appears to be related more to the protein autoxidation than the other oxidative sources.

The loss of water and electrolytes can directly impact the performance and health. The exercise performance is reduced from 7% to 60% by combining the heat stress up to 30°C and dehydration (about >2% body mass) on aerobic exercise over 90 min [5, 16, 17]. The hot and humid environment could also increase the sweat loss and dehydration [4]; however, in our study, the weather was dry and hot. The high humidity in extreme heat stress demonstrates the influence on the performance and cannot be generalized to different climate [2]; hence, the role of humidity on heat stress induced by exercise remains controversial [18, 19]. In the hot environment, we observed impairment of fluid and electrolytic balance before the competition, and markers of hypohydration, as urea and osmolality, after the marathon were accomplished by lower performance in HE, emphasizing the importance of a redoubled attention regarding hydration in competitions in hot environment. In spite of the VO_2 peak being higher in HE compared to TE, suggesting that the athletes could be more prepared to marathon race in 2014 (HE), the performance on the race was impaired in HE.

The heat acclimatization improves the transpiration capacity, skin blood flow responses, and plasma volume expansion resulting in higher or more stable fluid-electrolyte

balance [16, 20]. This heat acclimation improves the ability to reabsorb electrolytes, calcium, copper, magnesium, and sodium specifically, making acclimatized individuals have a lower mineral concentration in sweat, with lower values than 40%, regardless of the amount of transpiration [20]. In our study, before the race, we observed higher levels of plasma sodium, magnesium, and osmolality in HE as a result of hypohydration and/or heat acclimatization increasing the reabsorbing mineral capacity. In HE, we also observed a pronounced electrolyte imbalance as demonstrated by the high levels of sodium and osmolality after the race and lower levels of potassium and calcium 3 days after the race, increasing the risk to hypokalemia and hypernatremia.

Increased sympathetic tone and intravascular volume depletion, may also contribute to reduced renal perfusion increasing the risk of kidney damage during long-distance exercise [10, 21, 22]. The acute kidney injury could induce greater impairment in renal function after cumulative injuries induced by exercise and incomplete recovery of normal renal function during stress [23]. During exercise and heat stress, we also observed both glomerular filtration and renal blood flow reduction, impairing the urine production [5, 24]. Moreover, in the recovery period, we observed impairment in fluid replacement induced by lower capacity to produce urine [5, 24]. In HE, we demonstrated pronounced kidney damage as demonstrated by the elevation of urine density, urea, presence of cylinders, urine hematuria, and urine WBC after the marathon compared to TE. Nevertheless, the creatinine was higher after the race in TE compared to HE. We suggested that the higher creatinine levels in TE could be related to higher CK activity observed in TE (568 U/L versus 481 U/L). A direct relationship between the postrace serum CK and creatinine levels after long-distance running has been reported [23]. Hence, creatinine levels could not reflect the renal damage under stressed conditions; however, a physiological response to the muscle catabolism and/or prerenal component was observed. The proteinuria and hematuria affect 69% and 22% of the marathon runners, respectively [25]. Proteinuria and hematuria may also indicate kidney disorders; however, the transient changes reported after the marathon race are considered as a physiological compensation. The impact of these alterations in long term for permanent renal damage remains unclear [26].

In long-term exercise, excessive fluid and electrolyte loss may lead to hemolysis and promote changes in the renal damage markers. Hemolysis induced by exercise involves mechanical stress from foot strike, red blood cells passing through capillaries in contracting muscles, plasma volume expansion, alterations of erythrocyte membrane proteins, inflammation, and/or oxidative stress [27–29]. Robach et al. [27] suggested that hypernatremia as well inflammation, as we observed in this study, could induce plasma volume expansion and consequently hemolysis. In accordance with other studies [27, 30–32], we demonstrated that hematological changes were induced by long-distance running; moreover, a worsening response in HE could be related to many factors as hypohydration, electrolyte imbalance, and/or oxidative stress. Hemolysis induces iron release and an imbalance in the iron metabolism [32]. In the present study, hemodilution following the race was suggested by decreases in hematocrit, and hemolysis was demonstrated by hematuria, and higher conjugated bilirubin and ferritin levels immediately after the race follow lower erythrocytes, hemoglobin, iron, and transferrin levels 3 days after race. In HE, we also proposed an exacerbated hematological change, reported by higher hematuria, hemoglobin, conjugated bilirubin, and erythropoietin levels. Changes on erythrocytes and Ht were also correlated to race time suggesting that the combination of heat stress and endurance exercise promoted pronounced hematological changes which contribute to impairment of performance. Elevated erythropoietin and MCV observed in HE can indicate the presence of younger cells and erythropoiesis as a result of the heat stress adaptation/response to pronounced hematological changes [27]. Stress hormones such as catecholamine and cortisol also could stimulate enhanced erythropoiesis [33].

Thermal stress also induces oxidative stress, which may contribute to hemolysis and fatigue [34–36]. Exposure of the red blood cells to free oxygen radicals may promote hemoglobin damage and induce protein degradation, lipid peroxidation, and hemolysis; however, oxidative stress may be more attributed to hypohydration than heat during exercise [37]. The hyperthermia inactivates antioxidative enzymes causing deleterious effects on lipoperoxidation and redox status [34]. In fact, in HE, we observed lower SOD3 activity compared to TE before and in the recovery period; however, we observed an increase in the SOD3 activity after the marathon race in HE reaching the same SOD activity observed in TE environment. A previous study also reported a postexercise antioxidant response in hot and humid environment by elevation of the catalase activity after a treadmill exercise of 45 min at 75–80% of maximal oxygen uptake in well-trained athletes [36]. In HE, we also reported a reduced lipoperoxidation compared to TE; however, a greater uric acid production suggested pronounced purine and protein degradation in erythrocytes or muscle and diffusion of hypoxanthine and uric acid into the bloodstream. Hyperuricemia may induce glomerular hypertension, whereas the increased urinary uric acid may directly injure the renal tubules as a result of exercise and heat stress [24]. Davies and Goldberg [31, 38] described that lipoperoxidation and protein oxidation imply different processes *in vivo* and that protein oxidation occurs more quickly than lipoperoxidation. Maughan et al. [39] demonstrated that lipoperoxidation initiated by free radicals was associated with the muscle damage and its respective markers. In accordance to this study, we demonstrated that TBARs were accomplished by higher levels of muscle markers CK, LDH, ALT, and AST in TE, agreeing that lipoperoxidation initiated by free radicals was associated with muscle damage.

In contrast with our study, after 4 weeks of high-intensity interval training, we observed an increase in protein carbonyls with no changes in TBARs induced by exercise in TE and an increase in TBARs with no changes in protein carbonyls in HE [40].

Inflammatory state also has been associated with oxidative stress and tissue damage [10]. Exercise-induced muscle damage is accompanied by exacerbated immune activation and inflammatory mediators [13]. In this study, the marathon race promoted immune activation and inflammation in both environments. In HE, the leukocytosis and lymphopenia were also more pronounced 1 day after the race. A previous study demonstrated a higher proinflammatory response (MCP-1) following an anti-inflammatory response (IL-6) after the treadmill test in heat stress that could contribute to the understanding of the pronounced inflammatory response (leukocytosis) followed by anti-inflammatory response (lymphopenia) induced by the marathon and the lower levels of CRP in HE [36], in spite of half marathon not demonstrating inflammatory or immunological changes in hot and humid environment [41].

In HE, the enzymes associated to muscle/hepatic damage (LDH, AST, and ALT) and CRP were lower in all periods evaluated suggesting lower exercise or training intensity or inactivation of the metabolic enzyme activity by heat stress. Nevertheless, the magnitude of the change induced long-distance exercise was greater in HE only for the CK levels (5-fold versus 7.5-fold, $p > 0.05$), but was not significant. The CK levels usually maintained altered 3–7 days after intense/prolonged exercise [42], which could explain the values above the reference value in TE. In this study, 13 athletes were above the reference value in TE and 9 athletes were above the reference value in HE before the race indicating less than 1 week of rest before race.

Thus, long-term exercise accomplished by heat stress may compromise the performance by hematological alterations due to fluid and electrolyte imbalance and purine or protein oxidation in erythrocytes, leading to renal damage and immune activation. Nonetheless, we suggested that the impairment on the performance in HE was not associated to the muscle damage and lipoperoxidation. Protein autoxidation and fluid and electrolyte imbalance may be an important factor responsible for hemolysis and impaired performance after long-term exercise in HE.

Conflicts of Interest

No conflicts of interest, financial or otherwise, are declared by the authors.

Authors' Contributions

Rodrigo Assunção Oliveira and Ana Paula Rennó Sierra contributed equally in this paper, they share the first authorship.

Acknowledgments

The authors are indebted to Yescom and IDEEA institute for providing assistance in the São Paulo International Marathon, TEB, Geratherm, AFIP, and Jessica Vieira for technical assistance. This research was supported by the Fundação de Amparo à Pesquisa do Estado de São Paulo (no. 2014/21501-0) and Coordenação de Aperfeiçoamento de Pessoal de Nível Superior.

References

[1] M. R. Ely, D. E. Martin, S. N. Cheuvront, and S. J. Montain, "Effect of ambient temperature on marathon pacing is dependent on runner ability," *Medicine & Science in Sports and Exercise*, vol. 40, no. 9, pp. 1675–1680, 2008.

[2] T. Vihma, "Effects of weather on the performance of marathon runners," *International Journal of Biometeorology*, vol. 54, no. 3, pp. 297–306, 2010.

[3] M. N. Sawka, S. N. Cheuvront, and R. W. Kenefick, "High skin temperature and hypohydration impair aerobic performance," *Experimental Physiology*, vol. 97, no. 3, pp. 327–332, 2012.

[4] M. N. Sawka, S. N. Cheuvront, and R. W. Kenefick, "Hypohydration and human performance: impact of environment and physiological mechanisms," *Sports Medicine*, vol. 45, Supplement 1, pp. S51–S60, 2015.

[5] S. N. Cheuvront, R. W. Kenefick, S. J. Montain, and M. N. Sawka, "Mechanisms of aerobic performance impairment with heat stress and dehydration," *Journal of Applied Physiology*, vol. 109, no. 6, pp. 1989–1995, 2010.

[6] S. K. Gill, A. Teixeira, L. Rama et al., "Circulatory endotoxin concentration and cytokine profile in response to exertional-heat stress during a multi-stage ultra-marathon competition," *Exercise Immunology Review*, vol. 21, pp. 114–128, 2015.

[7] L. M. Cosio-Lima, B. V. Desai, P. B. Schuler, L. Keck, and L. Scheeler, "A comparison of cytokine responses during prolonged cycling in normal and hot environmental conditions," *Open Access Journal of Sports Medicine*, vol. 2, pp. 7–11, 2011.

[8] R. L. Starkie, M. Hargreaves, J. Rolland, and M. A. Febbraio, "Heat stress, cytokines, and the immune response to exercise," *Brain, Behavior, and Immunity*, vol. 19, no. 5, pp. 404–412, 2005.

[9] M. G. Nikolaidis, A. Kyparos, C. Spanou, V. Paschalis, A. A. Theodorou, and I. S. Vrabas, "Redox biology of exercise: an integrative and comparative consideration of some overlooked issues," *The Journal of Experimental Biology*, vol. 215, Part 10, pp. 1615–1625, 2012.

[10] S. Mrakic-Sposta, M. Gussoni, S. Moretti et al., "Effects of mountain ultra-marathon running on ROS production and oxidative damage by micro-invasive analytic techniques," *PLoS One*, vol. 10, no. 11, article e0141780, 2015.

[11] G. G. Duthie, J. D. Robertson, R. J. Maughan, and P. C. Morrice, "Blood antioxidant status and erythrocyte lipid peroxidation following distance running," *Archives of Biochemistry and Biophysics*, vol. 282, no. 1, pp. 78–83, 1990.

[12] R. J. Bloomer, D. E. Larson, K. H. Fisher-Wellman, A. J. Galpin, and B. K. Schilling, "Effect of eicosapentaenoic and docosahexaenoic acid on resting and exercise-induced inflammatory and oxidative stress biomarkers: a randomized, placebo controlled, cross-over study," *Lipids in Health and Disease*, vol. 8, no. 1, p. 36, 2009.

[13] V. C. Santos, A. P. Sierra, R. Oliveira et al., "Marathon race affects neutrophil surface molecules: role of inflammatory mediators," *PLoS One*, vol. 11, no. 12, article e0166687, 2016.

[14] H. Ohkawa, N. Ohishi, and K. Yagi, "Assay for lipid peroxides in animal tissues by thiobarbituric acid reaction," *Analytical Biochemistry*, vol. 95, no. 2, pp. 351–358, 1979.

[15] H. Aebi, "[13] Catalase *in vitro*," *Methods in Enzymology*, vol. 105, pp. 121–126, 1984.

[16] S. N. Cheuvront, R. Carter 3rd, and M. N. Sawka, "Fluid balance and endurance exercise performance," *Current Sports Medicine Reports*, vol. 2, no. 4, pp. 202–208, 2003.

[17] S. Racinais, J. M. Alonso, A. J. Coutts et al., "Consensus recommendations on training and competing in the heat," *Sports Medicine*, vol. 45, no. 7, pp. 925–938, 2015.

[18] M. Hayes, P. C. Castle, E. Z. Ross, and N. S. Maxwell, "The influence of hot humid and hot dry environments on intermittent-sprint exercise performance," *International Journal of Sports Physiology and Performance*, vol. 9, no. 3, pp. 387–396, 2014.

[19] H. E. Wright, T. M. McLellan, J. M. Stapleton, S. G. Hardcastle, and G. P. Kenny, "Cortisol and interleukin-6 responses during intermittent exercise in two different hot environments with equivalent WBGT," *Journal of Occupational and Environmenal Hygiene*, vol. 9, no. 4, pp. 269–279, 2012.

[20] T. D. Chinevere, R. W. Kenefick, S. N. Cheuvront, H. C. Lukaski, and M. N. Sawka, "Effect of heat acclimation on sweat minerals," *Medicine and Science in Sports & Exercise*, vol. 40, no. 5, pp. 886–891, 2008.

[21] G. S. Lipman, B. J. Krabak, S. D. Rundell, K. M. Shea, N. Badowski, and C. Little, "Incidence and prevalence of acute kidney injury during multistage ultramarathons," *Clinical Journal of Sport Medicine*, vol. 26, no. 4, pp. 314–319, 2016.

[22] G. S. Lipman, B. J. Krabak, B. L. Waite, S. B. Logan, A. Menon, and G. K. Chan, "A prospective cohort study of acute kidney injury in multi-stage ultramarathon runners: the biochemistry in endurance runner study (BIERS)," *Research in Sports Medicine*, vol. 22, no. 2, pp. 185–192, 2014.

[23] M. D. Hoffman and R. H. Weiss, "Does acute kidney injury from an ultramarathon increase the risk for greater subsequent injury?," *Clinical Journal of Sport Medicine*, vol. 26, no. 5, pp. 417–422, 2016.

[24] C. Roncal-Jimenez, R. García-Trabanino, L. Barregard et al., "Heat stress nephropathy from exercise-induced uric acid crystalluria: a perspective on Mesoamerican nephropathy," *American Journal of Kidney Diseases*, vol. 67, no. 1, pp. 20–30, 2016.

[25] R. I. Reid, D. H. Hosking, and E. W. Ramsey, "Haematuria following a marathon run: source and significance," *British Journal of Urology*, vol. 59, no. 2, pp. 133–136, 1987.

[26] R. J. Shephard, "Exercise proteinuria and hematuria: current knowledge and future directions," *The Journal of Sports Medicine and Physical Fitness*, vol. 56, no. 9, pp. 1060–1076, 2016.

[27] P. Robach, R. C. Boisson, L. Vincent et al., "Hemolysis induced by an extreme mountain ultra-marathon is not associated with a decrease in total red blood cell volume," *Scandinavian Journal of Medicine and Science in Sports*, vol. 24, no. 1, pp. 18–27, 2014.

[28] M. A. King, T. L. Clanton, and O. Laitano, "Hyperthermia, dehydration, and osmotic stress: unconventional sources of exercise-induced reactive oxygen species," *American Journal of Physiology Regulatory, Integrative and Comparative Physiology*, vol. 310, no. 2, pp. R105–R114, 2016.

[29] H. Mairbaurl, "Red blood cells in sports: effects of exercise and training on oxygen supply by red blood cells," *Frontiers in Physiology*, vol. 4, p. 332, 2013.

[30] D. L. Christensen, D. Espino, R. Infante-Ramírez et al., "Normalization of elevated cardiac, kidney, and hemolysis plasma markers within 48 h in Mexican Tarahumara runners following a 78 km race at moderate altitude," *American Journal of Human Biology*, vol. 26, no. 6, pp. 836–843, 2014.

[31] K. J. Davies and A. L. Goldberg, "Oxygen radicals stimulate intracellular proteolysis and lipid peroxidation by independent mechanisms in erythrocytes," *The Journal of Biological Chemistry*, vol. 262, no. 17, pp. 8220–8226, 1987.

[32] K. A. Shin, K. D. Park, J. Ahn, Y. Park, and Y. J. Kim, "Comparison of changes in biochemical markers for skeletal muscles, hepatic metabolism, and renal function after three types of long-distance running: observational study," *Medicine*, vol. 95, no. 20, article e3657, 2016.

[33] M. Hu and W. Lin, "Effects of exercise training on red blood cell production: implications for anemia," *Acta Haematologica*, vol. 127, no. 3, pp. 156–164, 2012.

[34] S. R. McAnulty, L. McAnulty, D. D. Pascoe et al., "Hyperthermia increases exercise-induced oxidative stress," *International Journal of Sports Medicine*, vol. 26, no. 3, pp. 188–192, 2005.

[35] S. Palazzetti, M. J. Richard, A. Favier, and I. Margaritis, "Overloaded training increases exercise-induced oxidative stress and damage," *Canadian Journal of Applied Physiology*, vol. 28, no. 4, pp. 588–604, 2003.

[36] A. Sureda, A. Mestre-Alfaro, M. Banquells et al., "Exercise in a hot environment influences plasma anti-inflammatory and antioxidant status in well-trained athletes," *Journal of Thermal Biology*, vol. 47, pp. 91–98, 2015.

[37] A. R. Hillman, R. V. Vince, L. Taylor, L. McNaughton, N. Mitchell, and J. Siegler, "Exercise-induced dehydration with and without environmental heat stress results in increased oxidative stress," *Applied Physiology, Nutrition, and Metabolism*, vol. 36, no. 5, pp. 698–706, 2011.

[38] K. J. Davies and A. L. Goldberg, "Proteins damaged by oxygen radicals are rapidly degraded in extracts of red blood cells," *The Journal of Biological Chemistry*, vol. 262, no. 17, pp. 8227–8234, 1987.

[39] R. J. Maughan, A. E. Donnelly, M. Gleeson, P. H. Whiting, K. A. Walker, and P. J. Clough, "Delayed-onset muscle damage and lipid peroxidation in man after a downhill run," *Muscle & Nerve*, vol. 12, no. 4, pp. 332–336, 1989.

[40] A. A. Souza-Silva, E. Moreira, D. de Melo-Marins, C. M. Scholer, P. I. de Bittencourt Jr., and O. Laitano, "High intensity interval training in the heat enhances exercise-induced lipid peroxidation, but prevents protein oxidation in physically active men," *Temperature*, vol. 3, no. 1, pp. 167–175, 2016.

[41] Q. Y. Ng, K. W. Lee, C. Byrne, T. F. Ho, and C. L. Lim, "Plasma endotoxin and immune responses during a 21-km road race under a warm and humid environment," *Annals of the Academy of Medicine, Singapore*, vol. 37, no. 4, pp. 307–314, 2008.

[42] P. Brancaccio, N. Maffulli, and F. M. Limongelli, "Creatine kinase monitoring in sport medicine," *British Medicine Bulletin*, vol. 81-82, no. 1, pp. 209–230, 2007.

Hindawi
Oxidative Medicine and Cellular Longevity
Volume 2017, Article ID 6480145, 11 pages
https://doi.org/10.1155/2017/6480145

Research Article

Impaired Oxidative Status Is Strongly Associated with Cardiovascular Risk Factors

E. Brunelli, D. La Russa, and D. Pellegrino

Department of Biology, Ecology and Earth Sciences, University of Calabria, 87036 Cosenza, Italy

Correspondence should be addressed to D. Pellegrino; danielapellegrino@unical.it

Received 26 June 2017; Revised 27 September 2017; Accepted 18 October 2017; Published 12 December 2017

Academic Editor: Andrey J. Serra

The main target of primary prevention is the identification of cardiovascular risk factors aimed at reducing of the adverse impact of modifiable factors, such as lifestyle and pharmacological treatments. In humans, an alteration of the oxidative status has been associated with several pathologies, including diabetes and cardiovascular diseases. However, the prognostic relevance of circulating oxidative stress biomarkers remains poorly understood. Our study explored, in a healthy population ($n = 322$), the relationship between oxidative status and cardiovascular risk factors. Here, we were successful in demonstrating that plasmatic oxidative status is significantly associated with traditional cardiovascular risk factors. We revealed a significant depletion in the efficacy of total plasma antioxidant barrier in high cardiovascular risk categories, and we confirmed an age-related alteration of oxidative status. The efficacy of total plasma antioxidant barrier is significantly depleted in relation to metabolic disorders. Interestingly, the cholesterol imbalance is the main factor in depleting the efficacy of total plasma antioxidant barrier. The oxidative status is also influenced by hypertension, and a slight increase in systolic blood pressure determines a highly significant effect. We showed that the first detectable event of a redox disturbance is the repairing intervention of the antioxidant barrier that is thus decreased as overutilized.

1. Introduction

Cardiovascular diseases (CVDs) are a group of diseases that share the principal risk factors and often the aetiology. The main manifestations of CVDs are coronary heart disease and stroke that represents the world's primary cause of death and disability and the most important cause of premature death, in agreement with the World Health Organization. CVDs represent a major health problem worldwide that causes a great public financial effort due to both inability to work and higher pharmaceutical expenditure. Therefore, for their broad and well-recognized importance, strategies to prevent CVDs should be considered as a priority for all citizens and healthcare systems.

The main target of primary prevention is the identification of cardiovascular risk factors aimed at reducing of the adverse impact of modifiable factors, such as lifestyle and pharmacological treatments. Furthermore, the evaluation of early and reliable risk factors can be used to identify high-risk subjects before the irreversible effects of the disease (early diagnosis). A growing number of scientific evidence suggests that effective prevention strategies are feasible and useful, also from the economic viewpoint [1].

A series of risk factors with pathogenic implication for CVDs have been identified and summarized in the Framingham study [2]. The main risk factors included smoking, hypertension, dyslipidemia, and diabetes. Over the years, several epidemiological studies validated the prediction models of cardiovascular diseases based on these risk factors, thus contributing to a steady decrease in CVD mortality [3], and the prediction models based on Framingham risk score are still used all over the world. Since the publication of results from Framingham study [2], other important predisposing factors with pathogenic implication for CVDs have been identified, including a high-fat diet, low physical activity, obesity, and genetic influences [4].

Currently, the ongoing studies are aimed at improving the risk algorithms through the individuation of new

biomarkers strongly associated with CVDs (even if devoid of a direct relationship with these pathologies) also in order to define the appropriate preventive therapy of asymptomatic individuals [5, 6].

There are several clinical and experimental evidences supporting the hypothesis of a link between the oxidative status alteration and the development and progression of many health problems, such as neurodegenerative conditions, cardiovascular and inflammatory diseases, and cancer [7–9]. The predictive value of circulating oxidative stress biomarkers is poorly understood, despite the modified oxidative status has been associated with over 100 diseases. In particular, the ability of oxidative stress biomarkers to predict CVDs has been widely studied but remains largely unclear [10].

Oxidative stress is referred to the disproportion between free radicals and antioxidant system to counteract or detoxify their detrimental effects. The direct detection of free radicals is made complex by the nonspecificity and the high reactivity of these molecules. It takes, therefore, evaluating oxidative damage by measurement of secondary products, although the limited evidence that it reflects is oxidative status *in vivo* [11]. Epidemiological investigations have considered just a few of the numerous oxidant species as a biomarker relating them with cardiovascular dysfunctions, such as homocysteine, nitrosated tyrosines, and isoprostanes [12].

An alternative approach to investigate oxidative imbalance is the assessment of antioxidant enzymes (superoxide dismutase, catalase, and ascorbate peroxidase) and antioxidative defense, as well as nonenzymatic ascorbate, glutathione, flavonoids, tocopherols, and carotenoids [12, 13]. However, the predictive ability of these biomarkers and their usefulness to the definition of cardiovascular risk scores are underinvestigated. In the last years, several researchers are using two simple methods for detecting in vivo reactive oxygen species (ROS) using derivatives of reactive oxygen metabolites (dROMs) and biological antioxidant potential (BAP) [14–17]. For instance, in Japanese and Korean epidemiological trials, a significant correlation between oxidative balance and lifestyle-related diseases was found through these new methods [18, 19]. Hence, it is evident that there is a need for more extensive studies on large cohorts and under different clinical situations, including preclinical stages.

In view of this background, our research was designed to investigate, in a Mediterranean population, whether the oxidative balance is related to traditional cardiovascular risk factors. We evaluate, through a cross-sectional analysis on 322 healthy subjects, the global plasmatic oxidant/antioxidant ability by measuring reactive oxygen metabolite and biological antioxidant potential by photometric measurement. This study is of emerging interest in CVD research since the analysis of new biomarkers could improve the predictive role of CVD risk factors.

2. Subjects and Methods

2.1. Subjects. Our study involved 322 healthy Italian volunteers (work suitable) of both sexes and aged between 25 and 69 years (190 males, mean age: 51.42 ± 11.08 years and 132 female subjects, mean age: 46.11 ± 10.40 years) recruited from University of Calabria (UNICAL) staff during the annual visit performed by "UNICAL Prevention and Protection Service". The volunteers were subjected to a "health check" by filling in a form (information on health status and lifestyle), by physical measurements (body mass index, systolic, and diastolic blood pressure), and by blood tests (blood glucose, lipoprotein panel, prooxidant, and antioxidant status). All subjects were studied in the morning and in a fasting state. Blood samples were taken from the antecubital vein and immediately centrifuged (2500g for 15 min at 4°C), and the plasma obtained was stored at 4°C until measurements (maximum 6 hours of venous blood collection). Baseline characteristics of the cohort are shown in Table 1.

2.2. Cardiovascular Risk Chart. The cardiovascular risk charts, based on the global absolute risk, are a simple and verified way of assessing the probability of experiencing a first major cardiovascular event (myocardial infarction or stroke) over the following ten years, by using the values of six risk factors: gender, diabetes, smoking, age, systolic blood pressure, and total serum cholesterol. When applied to the population from which they derive, they provide the best estimate of CVD risk. Therefore, in this study, we used Italian cardiovascular risk chart of The CUORE Project (http://www.cuore.iss.it). The risk charts are four: diabetic man, nondiabetic man, diabetic woman, and nondiabetic woman. For each of these four categories, the charts are further divided into smokers and nonsmokers, and the risk is calculated on the basis of age decade, serum cholesterol, and arterial pressure values. Six cardiovascular risk categories were constructed, called MCV (from I to VI): the CVD risk category indicates how many persons out of 100 with the same characteristics will fall ill over the next 10 years.

2.3. Oxidative Status and Biological Antioxidant Potential Measurements. Oxidative status and biological antioxidant potential determination were performed by using photometric measurement kits and a free radical analyzer system provided with spectrophotometric device reader (FREE Carpe Diem, Diacron International, Grosseto, Italy). All analyses were performed on ice-stored samples within maximum 6 hours of venous blood collection to prevent auto-oxidation phenomenon. We used Diacron reactive oxygen metabolite (dROM) and biological antioxidant potential (BAP) tests to evaluate plasma levels of reactive oxygen metabolites and antioxidant capacity. The dROM test helps to determine the oxidant ability of a plasma sample measuring the presence of reactive oxygen metabolites derivatives, in particular, hydroperoxides. By means of an appropriate acidic buffer, transition metal ions (essentially iron), originating by protein, are converted to alkoxy and peroxy radicals that react with hydroperoxides thus forming new radicals; aromatic amine (N,N-diethylparaphenylene-diamine) reacts with these new radicals originating a colored cation radical spectrophotometrically detectable at 505 nm [14, 15]. Results

Table 1: Baseline characteristics of the cohort ($n = 322$; data are expressed as mean ± SD).

		Normal range
Age (years)	49.24 ± 11.10	
BMI (body weight/height^2)	25.95 ± 9.19	18.50–24.99
Systolic blood pressure (mmHg)	123.07 ± 16.08	<120
Diastolic blood pressure (mmHg)	76.31 ± 9.44	<80
Blood glucose (mg/dL)	97.22 ± 22.54	70–99
Total cholesterol (mg/dL)	206.12 ± 40.45	<240
HDL cholesterol (mg/dL)	54.76 ± 14.37	>60
LDL cholesterol (mg/dL)	132.03 ± 32.22	<115
Triglycerides (mg/dL)	119.01 ± 61.76	<150
Smokers	55 (17%)	

are expressed in Carratelli units (UC; 1 UC = 0.8 mg/L of hydrogen peroxide). The BAP test provides an overall measure of the biological antioxidant potential measuring the blood concentration of antioxidants (such as bilirubin, uric acid, vitamins C and E, and proteins) capable of reducing iron from ferric to the ferrous form; in fact, when the plasma is mixed with a colored solution (ferric chloride and thiocyanate), a decoloration occurs whose intensity is related to the ability of the plasma to reduce the ions of iron [16, 17]. The intensity of decoloration is spectrophotometrically detectable at 505 nm. Results are expressed in μmol/L of the reduced ferric ions.

2.4. Statistical Analysis. Data have been analyzed using GraphPad/Prism version 5.01 statistical software (SAS Institute, Abacus Concept Inc., Berkeley, CA, USA). Differences between groups were examined using the unpaired t-test, or the Mann–Whitney test, or the Dunn's test, or the Kruskal-Wallis test, or the ANOVA test. A p value of < 0.05 was considered to be statistically significant. Data are expressed as the mean ± standard deviation.

2.5. Ethics Statement. All investigations have been conducted according to the Declaration of Helsinki principles and have been approved by Local Ethical Committee (n°8/2016, Regione Calabria, Sezione Area Nord). All subjects have provided written informed consent that, as guarantor, is retained by the corresponding author.

3. Results

Our study population consists of 322 subjects (190 males and 132 females) aged between 25 and 69 years (25–39, $n = 79$; 40–49, $n = 71$; 50–59, $n = 107$; and 60–69, $n = 65$).

Baseline characteristics of the cohort are shown in Table 1. These data are comparable to the results of the second population survey of Cardiovascular Epidemiologic Observatory (The CUORE Project—Istituto Superiore Sanità—Italy) relative to a population sample from Calabria monitored in the period 2008–2012 (http://www.cuore.iss.it/eng/factors/south.asp). In the whole sample, oxidative status and antioxidant barrier efficacy values are the following: dROM test = 333.80 ± 72.94 UC and BAP test = 1968.96 ± 412.21 μmol/L. By suitable statistical tools, we analyzed the trend of both oxidative status and antioxidant barrier efficacy in order to identify possible correlations with MCV and traditional cardiovascular risk factors: gender, diabetes, smoking, age, systolic blood pressure, and total serum cholesterol. We also considered further determinants that may predispose to cardiovascular risk as menopausal status, obesity, and the ratio of total cholesterol to HDL (high-density lipoproteins).

3.1. MCV. We calculated the total CVD risk of our cohort using the Italian cardiovascular risk chart of The CUORE Project. MCV category (from I to VI) has been assigned to subjects aged between 40 and 69 years ($n = 243$) based on parameters described in http://www.cuore.iss.it/eng/assessment/risk_assessment.asp. We analyzed the trend of both oxidative status and antioxidant barrier efficacy by comparing subjects with low (MCV I-II; $n = 180$) medium (MCV III-IV; $n = 45$), and high (MCV V-VI; $n = 18$) total CVD risk. We found no significant differences in ROM values between MCV categories (Figure 1(a)), while we showed a significant decrease in antioxidant barrier efficacy in high (MCV V-VI) CVD risk categories (Dunn's test, $p < 0,005$; Figure 1(b)).

3.2. Cardiovascular Risk Factor: Gender. We found a significant difference between males ($n = 190$) and females ($n = 132$) in the values of both oxidative status (Mann–Whitney test, $p < 0.0001$; Figure 2(a)) and antioxidant barrier efficacy (Mann–Whitney test, $p < 0.001$; Figure 2(b)). In particular, females present high ROM (364.70 ± 85.96 UC) and BAP (2035.74 ± 412.28 μmol/L) values, while males show ROM values close to the normal values (312.00 ± 52.30 UC) and low BAP values (1915.03 ± 406.64 μmol/L). Within the female group, no significant difference was observed in premenopausal ($n = 87$) and postmenopausal ($n = 45$) subjects (ROM values: premenopausal 366.49 ± 50.83 UC and postmenopausal 361.22 ± 45.92 UC; BAP values: premenopausal 2079.32 ± 441.73 μmol/L and postmenopausal 1951.49 ± 337.15 μmol/L).

3.3. Cardiovascular Risk Factor: Diabetes and Obesity. In our study population, only 14 people, all males, had a diagnosis of diabetes and were undergoing insulin or oral hypoglycemic agent treatment. Therefore, we analyzed the values of oxidative status and antioxidant barrier efficacy by comparing nondiabetic males ($n = 176$) with respect to diabetic males ($n = 14$). Despite the small sample size, we found a significant decrease in antioxidant barrier efficacy in diabetic subjects (Mann–Whitney test, $p < 0.05$; Figure 3(b)) while no differences were evidenced in oxidative status (Figure 3(a)). Body mass index (BMI) is a simple index of weight-for-height that is commonly used to classify underweight, overweight, and obesity in adults. To analyze the trend of both oxidative status and antioxidant barrier efficacy in relation to BMI, we divided our study population according to this international classification: underweight (UW, <18.50 BMI, $n = 0$); normal range (N, 18.50–24.99 BMI, $n = 150$);

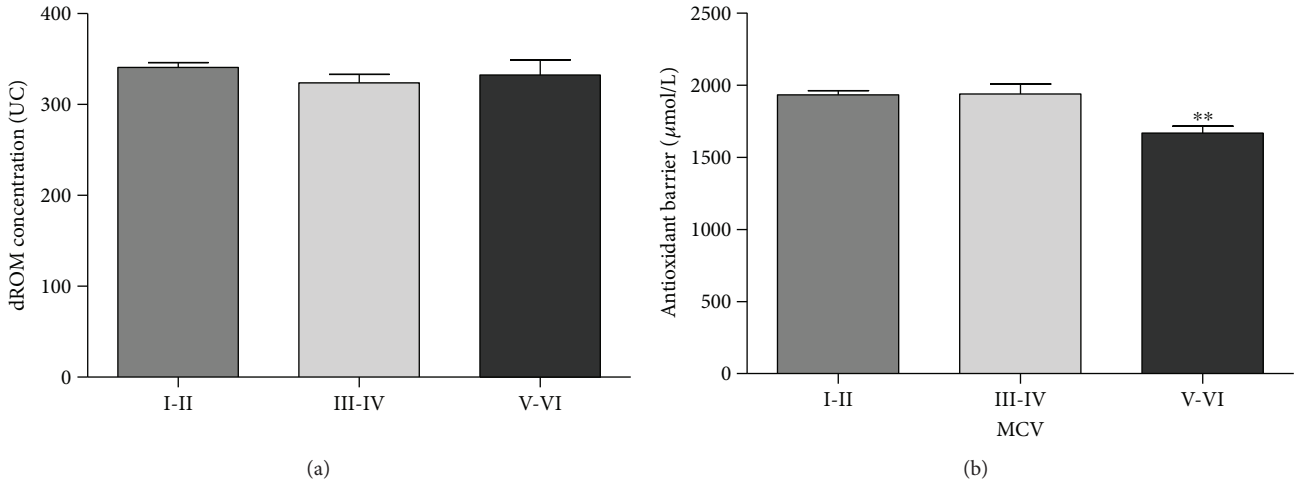

Figure 1: Values of dROM (a) and BAP (b) tests by MCV (data are expressed as mean ± SE; Dunn's test, $^{**}p < 0.005$).

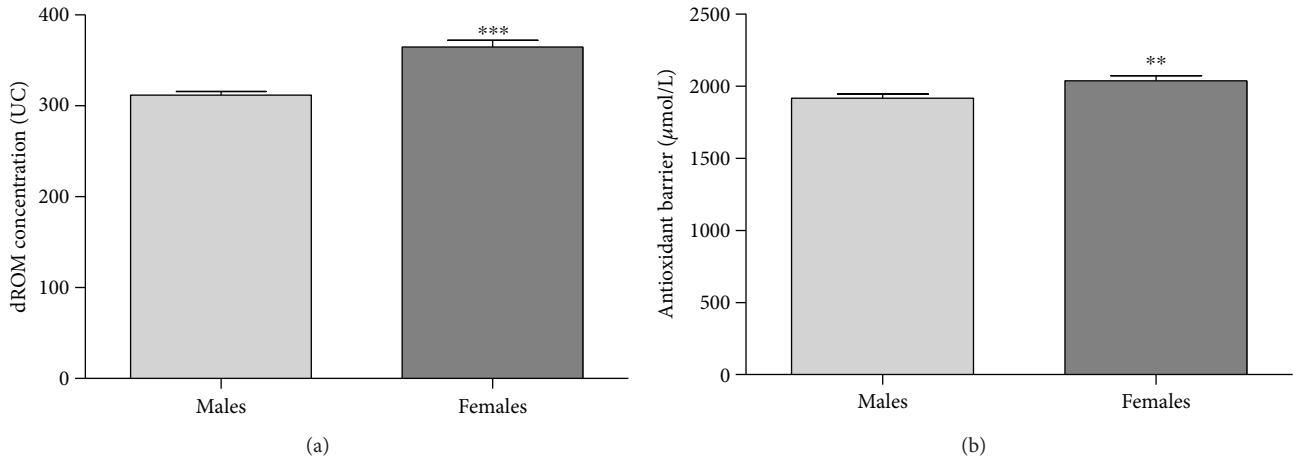

Figure 2: Values of dROM (a) and BAP (b) tests by gender (data are expressed as mean ± SE; Mann–Whitney test, $^{***}p < 0.0001$; $^{**}p < 0.005$).

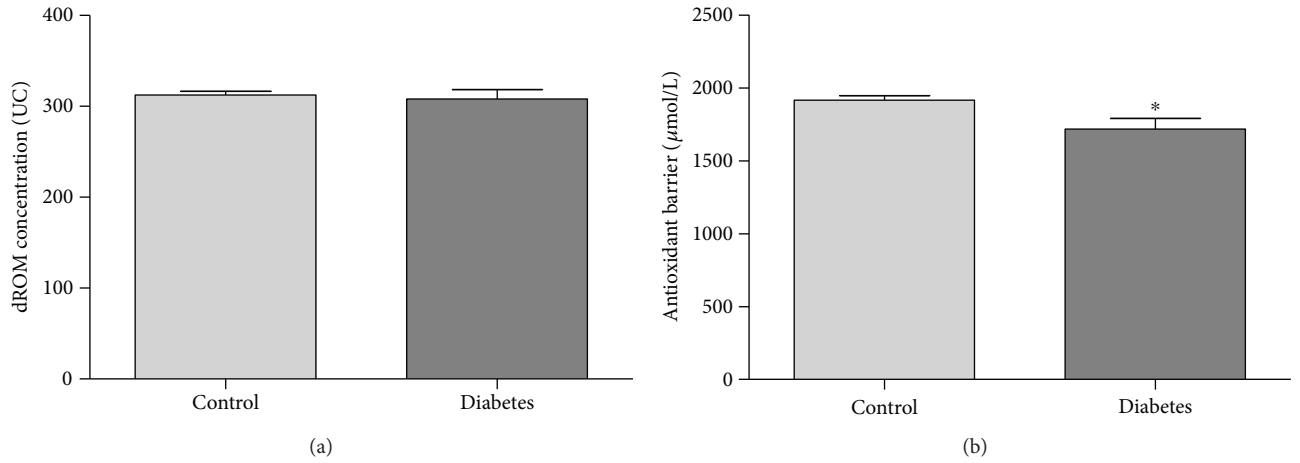

Figure 3: Values of dROM (a) and BAP (b) tests by diabetes status (data are expressed as mean ± SE; Mann–Whitney test, $^{*}p < 0.05$).

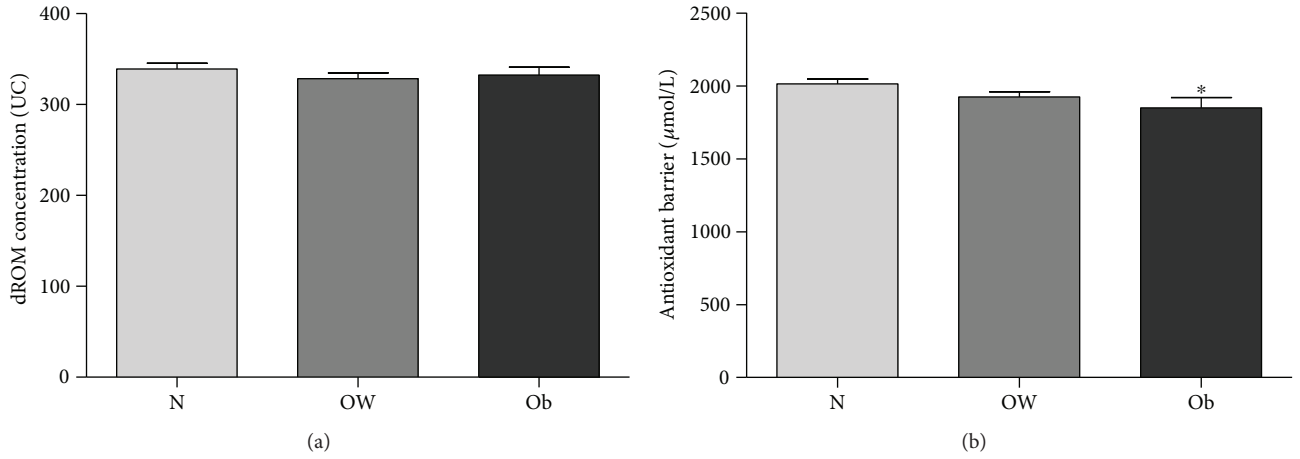

Figure 4: Values of dROM (a) and BAP (b) tests by BMI (data are expressed as mean ± SE; Kruskal-Wallis test, $^{*}p < 0.025$).

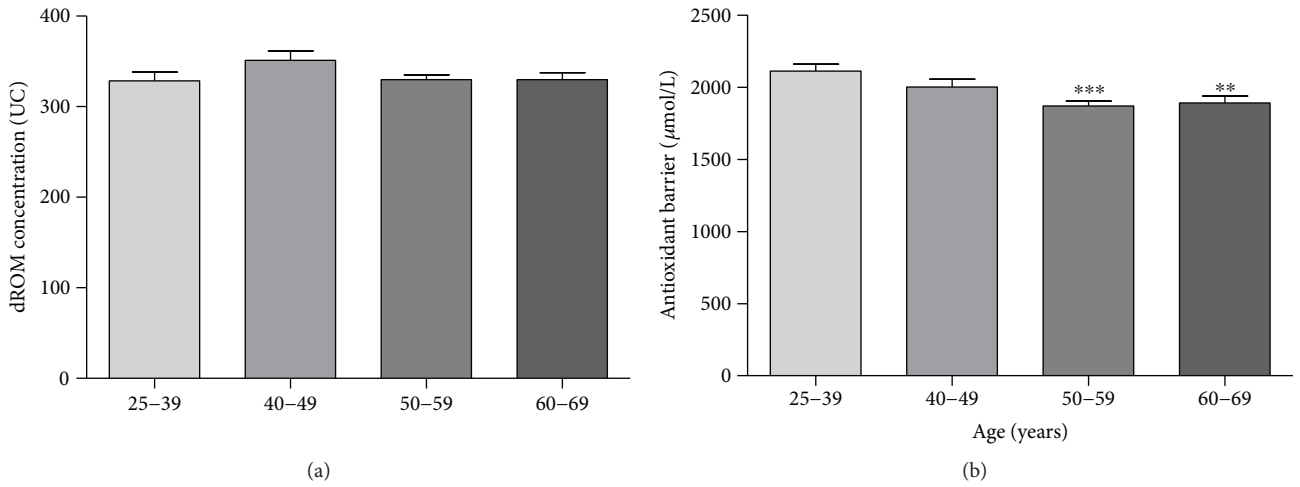

Figure 5: Values of dROM (a) and BAP (b) tests by age (data are expressed as mean ± SE; Kruskal-Wallis test, $^{***}p < 0.0005$; $^{**}p < 0.005$).

overweight (OW, ≥25.00 BMI, $n = 126$); and obese (Ob, ≥30.00 BMI, $n = 35$). Our results showed that there were no differences in ROM values among N, OW, and Ob groups (Figure 4(a)) as a decrease in antioxidant barrier efficacy can be observed already in OW subjects, reduction statistically significant in Ob subjects (Figure 4(b); Kruskal-Wallis test, $^{*}p < 0.025$).

3.4. Cardiovascular Risk Factor: Smoking. Concerning smoking habits, equally distributed between sex (17%), we found no significant differences between nonsmoker ($n = 267$) and smoker ($n = 55$) subjects in the values of both oxidative status and efficacy of antioxidant barrier (ROM values: nonsmokers 335.03 ± 76.23 UC and smokers 329.05 ± 55.06 UC; BAP values: nonsmokers 1968.14 ± 415.10 μmol/L and smokers 1944.09 ± 405.46 μmol/L). However, it should be noted that the smoker sample consists mainly of moderate smokers (less than ten cigarettes daily).

3.5. Cardiovascular Risk Factor: Age. We divided our study population into four age groups: the first group (25–39 years, $n = 78$) not provided for cardiovascular risk chart and used herein as controls and three groups according to the age decades of cardiovascular risk chart (40–49 years, $n = 71$; 50–59 years, $n = 105$; and 60–69 years, $n = 63$). The ROM values remain at a constant level in all groups (Figure 5(a)), while a constant reduction of antioxidant barrier efficacy was observed with increasing age (Figure 5(b)). This reduction is remarkable and highly statistically significant starting from 50 years of age (Kruskal-Wallis test, 50–59 years $p < 0.0005$ and 60–69 years $p < 0.005$).

3.6. Cardiovascular Risk Factor: Systolic Blood Pressure. To analyze the systolic blood pressure values in relation to oxidative status and antioxidant barrier efficacy, we divided our study population into three groups according to the range of cardiovascular risk chart (90–129 mmHg, $n = 174$; 130–149 mmHg, $n = 103$; and 150–169 mmHg, $n = 26$). The ROM values remain at a constant level in all groups (Figure 6(a)), while a statistically significant reduction of antioxidant barrier efficacy was observed starting from 150 mmHg of systolic blood pressure values (Figure 6(b); Kruskal-Wallis test, $p < 0.0005$).

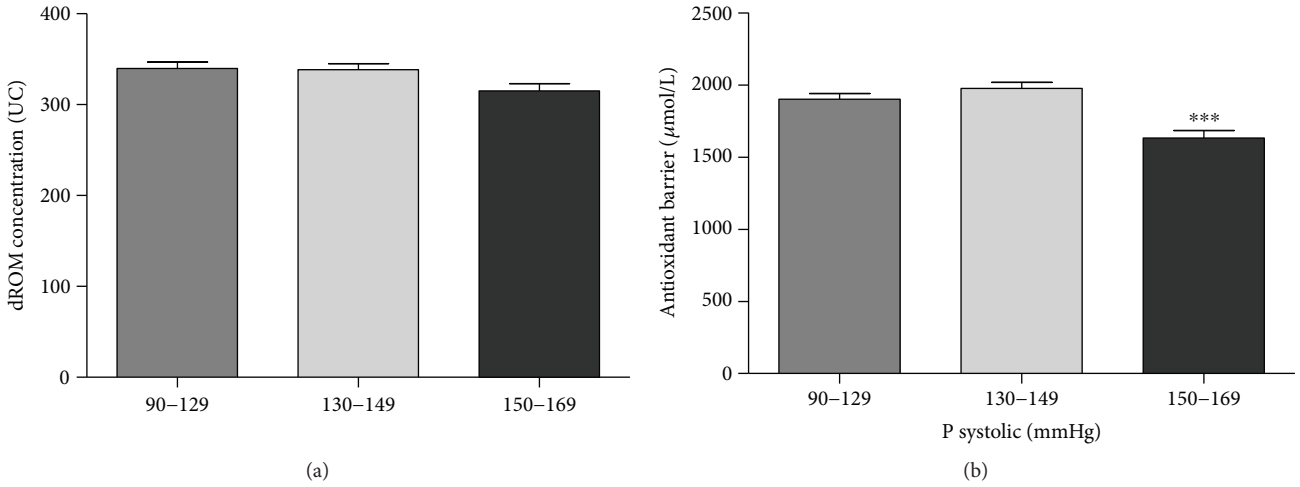

Figure 6: Values of dROM (a) and BAP (b) tests by systolic pressure (data are expressed as mean ± SD; Kruskal-Wallis test, $^{***}p < 0.0005$).

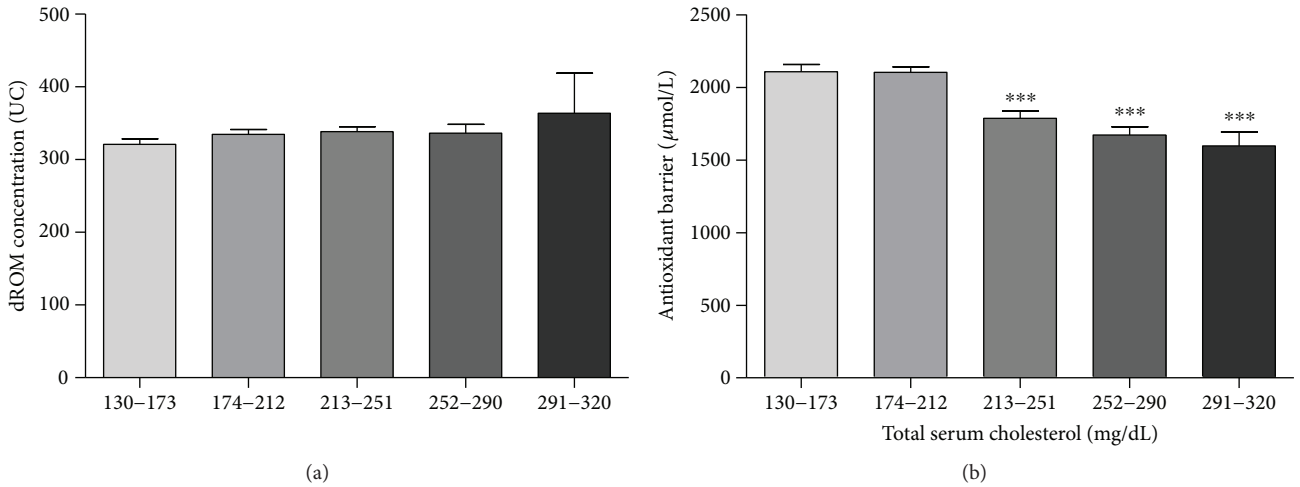

Figure 7: Values of dROM (a) and BAP (b) tests by total serum cholesterol (data are expressed as mean ± SD; Kruskal-Wallis test, $^{***}p < 0.0001$).

3.7. Cardiovascular Risk Factor: Total Serum Cholesterol and Ratio of Total to HDL. We analyzed both total serum cholesterol values and the ratio of total to HDL fraction in relation to oxidative status and antioxidant barrier efficacy. In relation to total serum cholesterol values, we divided our cohort in five groups according to the range of cardiovascular risk chart (130–173 mg/dL, $n = 56$; 174–212 mg/dL, $n = 124$; 213–251 mg/dL, $n = 91$; 252–290 mg/dL, $n = 30$; and 291–320 mg/dL, $n = 9$). The ROM values remain at a constant level in all groups (Figure 7(a)), while a constant reduction of antioxidant barrier efficacy was observed with increasing total serum cholesterol values (Figure 7(b)). This reduction is remarkable and highly statistically significant starting from 213 mg/dL of total serum cholesterol (Kruskal-Wallis test, $p < 0.0001$). Concerning the ratio of total cholesterol to HDL fraction, we divided the study population into five groups: ratio of less than 3 (<3, $n = 59$); ratio of less than 4 (<4, $n = 107$); ratio of less than 5 (<5, $n = 93$); ratio of less than 6 (<6, $n = 33$); and ratio greater than 6 (>6, $n = 7$). Even in this case, the ROM values remain at a constant level in all groups (Figure 8(a)), while a remarkable and highly statistically significant reduction of antioxidant barrier efficacy was observed with increasing ratio of total cholesterol to HDL fraction (Figure 8(b); Kruskal-Wallis test, $p < 0.0001$).

4. Discussion

Our research focused on identifying the putative relationship between oxidative imbalance and cardiovascular risk factors through a cross-sectional analysis on a large healthy population. We clearly showed that the oxidative status is significantly associated with MCV, diabetes, obesity, age, high systolic blood pressure, serum cholesterol, and total cholesterol/HDL. In particular, we reported, for the first time, that the early warning alteration at a systemic level is the reduction of antioxidant capacity.

It is noteworthy that these results have been achieved using a noninvasive method to detect total plasma redox

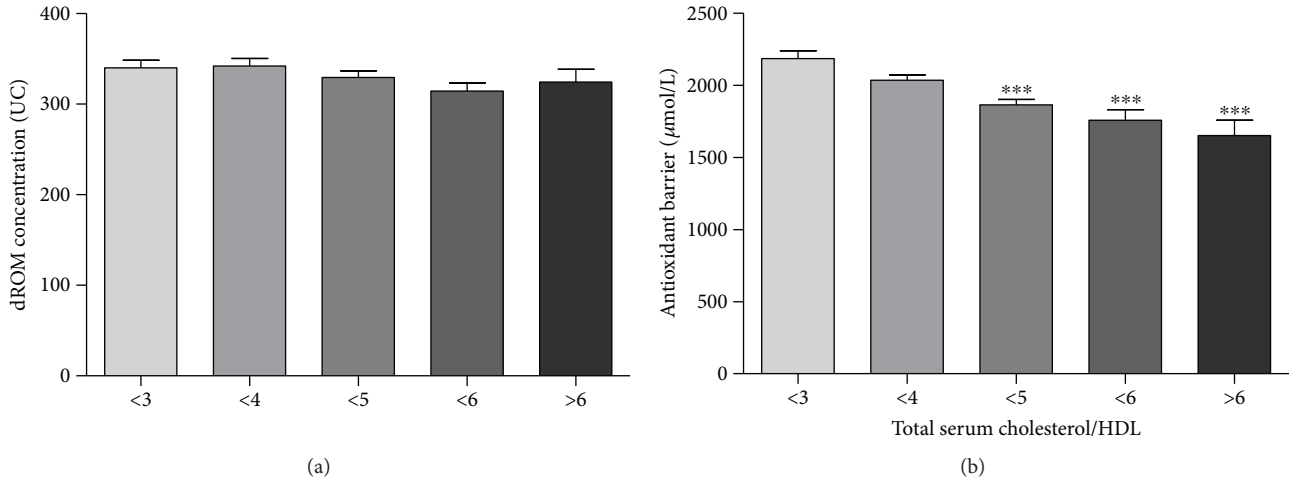

Figure 8: Values of dROM (a) and BAP (b) tests by total serum cholesterol/HDL (data are expressed as mean ± SD; Kruskal-Wallis test, $^{***}p < 0.0001$).

balance, which is of particular importance when analyzing the healthy subject. The analysis of the overall redox balance does not identify the impaired system/s, but it provides an evaluation of the imbalance induced by the alteration of individual parameters.

To the best of our knowledge, this is the first cross-sectional study that investigated, on a healthy cohort, the oxidative status taking into account all the cardiovascular risk factors. Although a direct causality cannot be inferred from such kind of correlative investigations, our data provide an important contribution to understanding the cross-talk between oxidative imbalance and cardiovascular risk factors also representing a point of departure to address further investigation.

4.1. MCV. Global comparative risk assessment and associated health effect studies have estimated that hundreds of thousands or millions of CVD deaths are attributable to established CVD risk factors and other putative, emerging, risk factors that are the subject of extensive research. In particular, several studies suggested a positive correlation between CVDs/CVD risk factors and an increased oxidative stress [7–9]. However, information on healthy populations are scarce, and most of the available data derive from trials conducted on subjects with very high cardiovascular risk [20]. In these situations, it becomes difficult to establish a clear understanding of the relative influence of the different factors in determining oxidative imbalance and then to evaluate the synergic or independent action of CVD risk factors.

Because traditional risk factors account for only a fraction of CVDs, the importance of alternate and additional predictors is evident [21, 22]. Our results, exploring the oxidative status of healthy subjects (without previous cardiovascular events), show a significant association between the high cardiovascular risk (MCV V-VI) and the depletion in the efficacy of total plasma antioxidant barrier despite the normal values of oxidative status. Recently, some authors found a significant correlation between ROM values and age [18] or lipid profile [19], but our study remains the only considering overall CVD risk factors.

Antioxidant deficiencies may be the result of a decreased antioxidant intake, a reduced synthesis of endogenous enzymes, or an increased antioxidant utilization [22]. Since the antioxidant species are numerous and they operate synergistically, evaluating the activity of each antioxidant species may underestimate the association among different effects and probably do not reflect the physiological conditions. Moreover, for each antioxidant compound, a specific test is needed thus making the evaluation of antioxidant capacity extremely complex [23, 24].

We recognize that there are currently no validated methods for quantifying the oxidative status but certainly, the total antioxidant capacity is indicative of both organism antioxidant protection and oxidative stress amount.

4.2. Gender. According to our previous findings [25], we showed that the oxidative status was significantly higher in females than in males and we also demonstrate that this result is not related to the level of circulating hormones since no differences have been detected between pre- and post-menopausal women. The physiological significance of this gender-related difference remains unclear, and research on both animals and humans have shown contrasting results ([25] and references therein). Another interesting finding in our study was the more effective antioxidant barrier detected in females compared to males suggesting that, in healthy subjects, the altered oxidative status is balanced by an enhancement in the antioxidant barrier effectiveness.

4.3. Diabetes and Obesity. Obesity is an important cause of CVDs, and it promotes a cluster of risk factors including dyslipidemia, type 2 diabetes, and hypertension [26]. Several pieces of evidence support the role of oxidative stress in obesity and diabetes metabolic perturbations (and subsequent cardiovascular pathogenesis) [27, 28]. The proinflammatory and prooxidant effects of an increased adiposity represent a potential link between obesity and CVDs, even in the absence

of other risk factors [29, 30]. The positive association between indices of obesity and oxidative stress biomarkers is well acknowledged [20], but the underlying mechanisms are complex and not yet fully identified. In the obese-diabetic patients, the excessive uric acid has been shown to induce CVDs through the generation of ROS and subsequent endothelial dysfunction [31]. Recent studies have emphasized the importance of antioxidant defense in type 2 diabetes patients. In these subjects, the excessive ROS stimulation leads to a progressive deterioration of the antioxidant system that tends to crumble [31]. In our cohort, we found a significant decrease in antioxidant barrier efficacy in both diabetic and obese subjects; these results contribute to emphasize the importance of antioxidant barrier effectiveness in countering the deleterious effects of ROS overproduction.

4.4. Smoking. Smoking is an important risk factor for cardiovascular disease development. Cigarette smoke is a complex mixture of chemical compounds, containing many free radicals and oxidants [32, 33], and it can be associated with oxidative stress in smokers [34, 35]. It has also been highlighted a direct correlation between oxidative index and number of cigarettes smoked [36]. In our cohort, we found no significant differences in the oxidative status between nonsmokers and smokers. However, the smoker sample in our study was small and consisted mainly of moderate smokers (less than ten cigarettes daily). Moreover, the ex-smokers were very few and all of them had stopped smoking for more than ten years.

4.5. Age. The oxidative stress theory of aging postulates that reactive oxygen species play a key role in the aging process through an age-related accumulation of oxidative damages in macromolecules, resulting in a progressive loss of cellular function and senescence [37]. Over the past two decades, several lines of evidence supported this theory [38] and a number of experimental studies, in both humans and animals, showed a linear correlation between age and oxidative stress [39]. In our study, we detected no difference in ROM values in the different age groups whereas a regular reduction of antioxidant barrier efficacy was observed with increasing age. It is well known that antioxidants delay or protect against the damage produced by free radical reactions and are consumed during this process. In fact, global antioxidant status is even used to indirectly evaluate free radical activity [24].

4.6. Blood Pressure. Endothelial dysfunction, the initial stage in the pathogenesis of several cardiovascular diseases including hypertension, is associated with increased vascular ROS production, oxidative stress, and vascular inflammation [40]. Clinical studies, in patients with essential hypertension, demonstrated that systolic and diastolic blood pressure correlate positively with oxidative stress biomarkers [41, 42], and similar results have been found in rats [43]. Direct measurements of ROS vascular production in hypertensive subjects demonstrated higher levels of O_2 and H_2O_2 and an enhanced angiotensin II-stimulated redox signaling compared with cells from normotensive counterparts [44, 45]. In our study, we divided the healthy population into three groups, according to the range of cardiovascular risk charts (90–129 mmHg; 130–149 mmHg; and 150–169 mmHg), and we did not observe any change in the ROM values. On the contrary, we found a statistically significant reduction of antioxidant barrier efficacy in the group with systolic blood pressure higher than 150 mmHg. Several observational studies have reported an inverse relationship between blood pressure and antioxidant levels [46–48]. A decreased antioxidant activity and reduced levels of ROS scavengers might contribute to induce oxidative stress in hypertensive subjects, but also an increase in vascular ROS production has been hypothesized to reduce the antioxidant efficacy [8].

4.7. Lipidic Profile. Lipid metabolism disorders are associated with the overproduction of reactive oxygen species and have been shown to affect the antioxidant status and the lipoprotein levels in different organs [49, 50]. Dyslipidemia in combination with endothelial damage is a crucial event in the most common pathological processes underlying CVDs [51, 52]. In addition, endothelial dysfunction can be started/supported by several factors, including an excess of ROS and the exposure to harmful agents such as oxidized LDL [53]. In our study, we did not find a significant relationship between changes in oxidative status and total cholesterol values whereas a regular and significant reduction of antioxidant barrier efficacy was observed in subjects with pathological cholesterol values (total serum cholesterol values > 213 mg/dL).

We observed a similar result by relating oxidative status with total cholesterol/HDL cholesterol ratio. According to evidence from large observational studies, total cholesterol/HDL cholesterol ratio seems to be a more powerful risk predictor than isolated parameters used independently ([54] and references therein). Indeed, both diagnosis and treatment of dyslipidemia, including instruments for calculating cardiovascular risk factors, nowadays include the lipoprotein ratios that, in view of the evidence-based results, present greater predictive power [54].

Interestingly, in a recent paper, Yagi and colleagues [55] demonstrated that BAP was strongly correlated with carotid artery IMT suggesting that it may be considered a suitable risk marker for carotid atherosclerosis; moreover, they postulate that the measurements of BAP may be superior to the measurements of glutathione peroxidase, superoxide dismutase, catalase, and total antioxidant status for the assessment of antioxidant potential. Our results emphasize that the first detectable event of a redox disturbance is the repairing intervention of the antioxidant barrier that is thus decreased as overutilized.

5. Conclusion

In the present study, we showed through a cross-sectional analysis on a large healthy population that a reduced antioxidant capacity is significantly associated with cardiovascular risk factors. In epidemiological studies, the magnitude of the cohort is a key factor for the validity of

the results. Our numbers reach an average value; therefore, our research can be considered as a pilot study and as the first application of a protocol aimed to verify the validity of the experimental design. Moreover, we assessed the oxidative status through indirect determinations thus providing an overall measure of many oxidants/antioxidants, also without identifying the molecules involved in the perturbation of normal homeostasis. The assessment of both validity and reproducibility of such indirect determinations is important as they represent an analytical tool not many invasive and easy to perform which allows an application on a large scale. Further studies are needed to clarify better how these new putative biomarkers and the traditional risk factors are related and how they can improve the prediction of cardiovascular risk.

Conflicts of Interest

The authors declare that there is no conflict of interest regarding the publication of this article.

Authors' Contributions

D. Pellegrino developed and led the project. All of the authors designed, performed the experiments, and analyzed the results. D. Pellegrino wrote the paper with input from E. Brunelli and D. La Russa. E. Brunelli and D. La Russa equally contributed to this research.

Acknowledgments

This work was supported by the University of Calabria.

References

[1] L. Mosca, C. L. Banka, E. J. Benjamin et al., "Evidence-based guidelines for cardiovascular disease prevention in women: 2007 update," *Circulation*, vol. 115, no. 11, pp. 1481–1501, 2007.

[2] W. B. Kannel, T. R. Dawber, A. Kagan, N. Revotskie, and J. Stokes 3rd, "Factors of risk in the development of coronary heart disease—six-year follow-up experience," *Annals of Internal Medicine*, vol. 55, no. 1, pp. 33–50, 1961.

[3] D. Levy, P. W. F. Wilson, K. M. Anderson, and W. P. Castelli, "Stratifying the patient at risk from coronary disease: new insights from the Framingham heart study," *American Heart Journal*, vol. 119, no. 3, pp. 712–717, 1990.

[4] F. D. R. Hobbs, "Cardiovascular disease: different strategies for primary and secondary prevention?," *Heart*, vol. 90, no. 10, pp. 1217–1223, 2004.

[5] J. S. Berger, C. O. Jordan, D. Lloyd-Jones, and R. S. Blumenthal, "Screening for cardiovascular risk in asymptomatic patients," *Journal of the American College of Cardiology*, vol. 55, no. 12, pp. 1169–1177, 2010.

[6] E. M. deGoma, R. L. Dunbar, D. Jacoby, and B. French, "Differences in absolute risk of cardiovascular events using risk-refinement tests: a systematic analysis of four cardiovascular risk equations," *Atherosclerosis*, vol. 227, no. 1, pp. 172–177, 2013.

[7] A. M. Pisoschi and A. Pop, "The role of antioxidants in the chemistry of oxidative stress: a review," *European Journal of Medicinal Chemistry*, vol. 97, pp. 55–74, 2015.

[8] A. C. Montezano, M. Dulak-Lis, S. Tsiropoulou, A. Harvey, A. M. Briones, and R. M. Touyz, "Oxidative stress and human hypertension: vascular mechanisms, biomarkers, and novel therapies," *The Canadian Journal of Cardiology*, vol. 31, no. 5, pp. 631–641, 2015.

[9] C. Ceconi, A. Boraso, A. Cargnoni, and R. Ferrari, "Oxidative stress in cardiovascular disease: myth or fact?," *Archives of Biochemistry and Biophysics*, vol. 420, no. 2, pp. 217–221, 2003.

[10] N. A. Strobel, R. G. Fassett, S. A. Marsh, and J. S. Coombes, "Oxidative stress biomarkers as predictors of cardiovascular disease," *International Journal of Cardiology*, vol. 147, no. 2, pp. 191–201, 2011.

[11] R. Kohen and A. Nyska, "Oxidation of biological systems: oxidative stress phenomena, antioxidants, redox reactions, and methods for their quantification," *Toxicologic Pathology*, vol. 30, no. 6, pp. 620–650, 2002.

[12] R. Schnabel and S. Blankenberg, "Oxidative stress in cardiovascular disease: successful translation from bench to bedside?," *Circulation*, vol. 116, no. 12, pp. 1338–1340, 2007.

[13] S. Blankenberg, H. J. Rupprecht, C. Bickel et al., "Glutathione peroxidase 1 activity and cardiovascular events in patients with coronary artery disease," *The New England Journal of Medicine*, vol. 349, no. 17, pp. 1605–1613, 2003.

[14] U. Cornelli, R. Terranova, S. Luca, M. Cornelli, and A. Alberti, "Bioavailability and antioxidant activity of some food supplements in men and women using the D-Roms test as a marker of oxidative stress," *The Journal of Nutrition*, vol. 131, no. 12, pp. 3208–3211, 2001.

[15] M. Carratelli, L. Porcaro, M. Ruscica, E. De Simone, A. A. Bertelli, and M. M. Corsi, "Reactive oxygen metabolites and prooxidant status in children with Down's syndrome," *International Journal of Clinical Pharmacology Research*, vol. 21, no. 2, pp. 79–84, 2001.

[16] J. Martinovic, V. Dopsaj, M. J. Dopsaj et al., "Long-term effects of oxidative stress in volleyball players," *International Journal of Sports Medicine*, vol. 30, no. 12, pp. 851–856, 2009.

[17] A. Pasquini, E. Luchetti, V. Marchetti, G. Cardini, and E. L. Iorio, "Analytical performances of d-ROMs test and BAP test in canine plasma. Definition of the normal range in healthy Labrador dogs," *Veterinary Research Communications*, vol. 32, no. 2, pp. 137–143, 2008.

[18] T. Fukui, K. Yamauchi, M. Maruyama, T. Yasuda, M. Kohno, and Y. Abe, "Significance of measuring oxidative stress in lifestyle-related diseases from the viewpoint of correlation between d-ROMs and BAP in Japanese subjects," *Hypertension Research*, vol. 34, no. 9, pp. 1041–1045, 2011.

[19] M. K. Kim, S. W. Cho, and Y. K. Park, "Long-term vegetarians have low oxidative stress, body fat, and cholesterol levels," *Nutrition Research and Practice*, vol. 6, no. 2, pp. 155–161, 2012.

[20] J. F. Keaney, M. G. Larson, R. S. Vasan et al., "Obesity and systemic oxidative stress: clinical correlates of oxidative stress in the Framingham study," *Arteriosclerosis, Thrombosis, and Vascular Biology*, vol. 23, no. 3, pp. 434–439, 2003.

[21] U. N. Khot, M. B. Khot, C. T. Bajzer et al., "Prevalence of conventional risk factors in patients with coronary heart disease," *JAMA*, vol. 290, no. 7, pp. 898–904, 2003.

[22] E. B. Kurutas, "The importance of antioxidants which play the role in cellular response against oxidative/nitrosative stress: current state," *Nutrition Journal*, vol. 15, no. 1, p. 71, 2016.

[23] E. M. Berry and R. Kohen, "Is the biological antioxidant system integrated and regulated?," *Medical Hypotheses*, vol. 53, no. 5, pp. 397–401, 1999.

[24] B. Palmieri and V. Sblendorio, "Oxidative stress tests: overview on reliability and use. Part I," *European Review for Medical and Pharmacological Sciences*, vol. 11, no. 5, pp. 309–342, 2007.

[25] E. Brunelli, F. Domanico, D. Russa, and D. Pellegrino, "Sex differences in oxidative stress biomarkers," *Current Drug Targets*, vol. 15, no. 8, pp. 811–815, 2014.

[26] W. B. Kannel, P. W. F. Wilson, B. H. Nam, and R. B. D'Agostino, "Risk stratification of obesity as a coronary risk factor," *The American Journal of Cardiology*, vol. 90, no. 7, pp. 697–701, 2002.

[27] I. Savini, M. Catani, D. Evangelista, V. Gasperi, and L. Avigliano, "Obesity-associated oxidative stress: strategies finalized to improve redox state," *International Journal of Molecular Sciences*, vol. 14, no. 5, pp. 10497–10538, 2013.

[28] P. Manna and S. K. Jain, "Obesity, oxidative stress, adipose tissue dysfunction, and the associated health risks: causes and therapeutic strategies," *Metabolic Syndrome and Related Disorders*, vol. 13, no. 10, pp. 423–444, 2015.

[29] J. V. Higdon and B. Frei, "Obesity and oxidative stress: a direct link to CVD?," *Arteriosclerosis, Thrombosis, and Vascular Biology*, vol. 23, no. 3, pp. 365–367, 2003.

[30] C. Vassalle, L. Vigna, S. Bianchi et al., "A biomarker of oxidative stress as a nontraditional risk factor in obese subjects," *Biomarkers in Medicine*, vol. 7, no. 4, pp. 633–639, 2013.

[31] U. C. Yadav, V. Rani, G. Deep, R. K. Singh, and K. Palle, "Oxidative stress in metabolic disorders: pathogenesis, prevention, and therapeutics," *Oxidative Medicine and Cellular Longevity*, vol. 2016, Article ID 9137629, 3 pages, 2016.

[32] C. Mur, J. Clària, S. Rodela et al., "Cigarette smoke concentrate increases 8-epi-$PGF_{2\alpha}$ and $TGF\beta_1$ secretion in rat mesangial cells," *Life Sciences*, vol. 75, no. 5, pp. 611–621, 2004.

[33] R. Miri, H. Saadati, P. Ardi, and O. Firuzi, "Alterations in oxidative stress biomarkers associated with mild hyperlipidemia and smoking," *Food and Chemical Toxicology*, vol. 50, no. 3-4, pp. 920–926, 2012.

[34] B. Pignatelli, C. Q. Li, P. Boffetta et al., "Nitrated and oxidized plasma proteins in smokers and lung cancer patients," *Cancer Research*, vol. 61, no. 2, pp. 778–784, 2001.

[35] Y. Yamaguchi, J. Haginaka, S. Morimoto, Y. Fujioka, and M. Kunitomo, "Facilitated nitration and oxidation of LDL in cigarette smokers," *European Journal of Clinical Investigation*, vol. 35, no. 3, pp. 186–193, 2005.

[36] C. Vassalle, C. Novembrino, S. Maffei et al., "Determinants of oxidative stress related to gender: relevance of age and smoking habit," *Clinical Chemistry and Laboratory Medicine*, vol. 49, no. 9, pp. 1509–1513, 2011.

[37] R. S. Sohal and R. Weindruch, "Oxidative stress, caloric restriction, and aging," *Science*, vol. 273, no. 5271, pp. 59–63, 1996.

[38] Y. Zhang, A. Unnikrishnan, S. S. Deepa et al., "A new role for oxidative stress in aging: the accelerated aging phenotype in $Sod1^{-/-}$ mice is correlated to increased cellular senescence," *Redox Biology*, vol. 11, pp. 30–37, 2016.

[39] K. Hensley and R. A. Floyd, "Reactive oxygen species and protein oxidation in aging: a look back, a look ahead," *Archives of Biochemistry and Biophysics*, vol. 397, no. 2, pp. 377–383, 2002.

[40] N. C. Ward, J. M. Hodgson, I. B. Puddey, T. A. Mori, L. J. Beilin, and K. D. Croft, "Oxidative stress in human hypertension: association with antihypertensive treatment, gender, nutrition, and lifestyle," *Free Radical Biology & Medicine*, vol. 36, no. 2, pp. 226–232, 2004.

[41] A. Ahmad, U. Singhal, M. M. Hossain, N. Islam, and I. Rizvi, "The role of the endogenous antioxidant enzymes and malondialdehyde in essential hypertension," *Journal of Clinical and Diagnostic Research*, vol. 7, no. 6, pp. 987–990, 2013.

[42] R. Rodrigo, M. Libuy, F. Feliú, and D. Hasson, "Oxidative stress-related biomarkers in essential hypertension and ischemia-reperfusion myocardial damage," *Disease Markers*, vol. 35, no. 6, pp. 773–790, 2013.

[43] J. F. Reckelhoff, H. Zhang, K. Srivastava, L. J. Roberts, J. D. Morrow, and J. C. Romero, "Subpressor doses of angiotensin II increase plasma F_2-isoprostanes in rats," *Hypertension*, vol. 35, no. 1, pp. 476–479, 2000.

[44] R. M. Touyz, G. Yao, and E. L. Schiffrin, "c-Src induces phosphorylation and translocation of p47phox: role in superoxide generation by angiotensin II in human vascular smooth muscle cells," *Arteriosclerosis, Thrombosis, and Vascular Biology*, vol. 23, no. 6, pp. 981–987, 2003.

[45] R. M. Touyz, G. Yao, M. T. Quinn, P. J. Pagano, and E. L. Schiffrin, "p47phox associates with the cytoskeleton through cortactin in human vascular smooth muscle cells: role in NAD(P)H oxidase regulation by angiotensin II," *Arteriosclerosis, Thrombosis, and Vascular Biology*, vol. 25, no. 3, pp. 512–518, 2005.

[46] J. González, N. Valls, R. Brito, and R. Rodrigo, "Essential hypertension and oxidative stress: new insights," *World Journal of Cardiology*, vol. 6, no. 6, pp. 353–366, 2014.

[47] S. Eslami and A. Sahebkar, "Glutathione-S-transferase M1 and T1 null genotypes are associated with hypertension risk: a systematic review and meta-analysis of 12 studies," *Current Hypertension Reports*, vol. 16, no. 6, p. 432, 2014.

[48] B. Ge, Y. Song, Y. Zhang, X. Liu, Y. Wen, and X. Guo, "Glutathione S-transferase M1 (GSTM1) and T1 (GSTT1) null polymorphisms and the risk of hypertension: a meta-analysis," *PLoS One*, vol. 10, no. 3, article e0118897, 2015.

[49] S. V. Singh, A. Shrivastava, Jyotshna et al., "A mechanism-based pharmacological evaluation of efficacy of *Flacourtia indica* in management of dyslipidemia and oxidative stress in hyperlipidemic rats," *Journal of Basic and Clinical Physiology and Pharmacology*, vol. 27, no. 2, pp. 121–129, 2016.

[50] D. Pellegrino, "Antioxidants and cardiovascular risk factors," *Diseases*, vol. 4, no. 1, p. 11, 2016.

[51] R. O. Halperin, H. D. Sesso, J. Ma, J. E. Buring, M. J. Stampfer, and J. Michael Gaziano, "Dyslipidemia and the risk of incident hypertension in men," *Hypertension*, vol. 47, no. 1, pp. 45–50, 2006.

[52] H. A. Hadi, C. S. Carr, and J. Al Suwaidi, "Endothelial dysfunction: cardiovascular risk factors, therapy, and outcome," *Vascular Health and Risk Management*, vol. 1, no. 3, pp. 183–198, 2005.

[53] M. Navab, J. A. Berliner, G. Subbanagounder et al., "HDL and the inflammatory response induced by LDL-derived oxidized

phospholipids," *Arteriosclerosis, Thrombosis, and Vascular Biology*, vol. 21, no. 4, pp. 481–488, 2001.

[54] J. Millán, X. Pintó, A. Muñoz et al., "Lipoprotein ratios: physiological significance and clinical usefulness in cardiovascular prevention," *Vascular Health and Risk Management*, vol. 5, pp. 757–765, 2009.

[55] H. Yagi, H. Sumino, K. Yoshida et al., "Biological antioxidant potential negatively correlates with carotid artery intima-media thickness," *International Heart Journal*, vol. 57, no. 2, pp. 220–225, 2016.

Hindawi
Oxidative Medicine and Cellular Longevity
Volume 2017, Article ID 5273403, 8 pages
https://doi.org/10.1155/2017/5273403

Review Article

Effects of Photobiomodulation Therapy on Oxidative Stress in Muscle Injury Animal Models: A Systematic Review

Solange Almeida dos Santos,[1] Andrey Jorge Serra,[2] Tatiane Garcia Stancker,[1] Maíra Cecília Brandão Simões,[1] Marcia Ataíze dos Santos Vieira,[1] Ernesto Cesar Leal-Junior,[1] Marko Prokic,[3] Andrea Vasconsuelo,[4] Simone Silva Santos,[2] and Paulo de Tarso Camillo de Carvalho[1,2]

[1]*Postgraduate Program in Rehabilitation Sciences, Universidade Nove de Julho (UNINOVE), São Paulo, SP, Brazil*
[2]*Postgraduate Program in Biophotonics, Universidade Nove de Julho (UNINOVE), São Paulo, SP, Brazil*
[3]*Department of Physiology, Institute for Biological Research "Siniša Stanković", University of Belgrade, Bulevar despota Stefana 142, 11060 Belgrade, Serbia*
[4]*Department of Biology, Biochemistry and Pharmacy, Universidad Nacional del Sur, San Juan 670, 8000 Bahia Blanca, Argentina*

Correspondence should be addressed to Paulo de Tarso Camillo de Carvalho; ptpaulo@terra.com.br

Received 13 April 2017; Accepted 4 July 2017; Published 17 September 2017

Academic Editor: Valentina Pallottini

This systematic review was performed to identify the role of photobiomodulation therapy on experimental muscle injury models linked to induce oxidative stress. EMBASE, PubMed, and CINAHL were searched for studies published from January 2006 to January 2016 in the areas of laser and oxidative stress. Any animal model using photobiomodulation therapy to modulate oxidative stress was included in analysis. Eight studies were selected from 68 original articles targeted on laser irradiation and oxidative stress. Articles were critically assessed by two independent raters with a structured tool for rating the research quality. Although the small number of studies limits conclusions, the current literature indicates that photobiomodulation therapy can be an effective short-term approach to reduce oxidative stress markers (e.g., thiobarbituric acid-reactive) and to increase antioxidant substances (e.g., catalase, glutathione peroxidase, and superoxide dismutase). However, there is a nonuniformity in the terminology used to describe the parameters and dose for low-level laser treatment.

1. Introduction

Muscle injuries are frequent in sports and workplace; more than 30% of the injuries seen in the physician's office are related to skeletal muscle. These injuries can occur through a variety of mechanisms, including those arising through direct trauma (e.g., laceration and contusion) and those through indirect trauma (e.g., ischemia, denervation, and strain), but the general process of muscle repair is similar in most cases [1]. After injury, the muscle repair process begins and is divided into interdependent phases: degeneration/inflammation, regeneration, fibrosis/scar formation, and remodeling [2]. In addition, muscle damage causes an immediate acute ischemic response releasing reactive oxygen species (ROS) including superoxide anion, hydroxyl radical, and hydrogen peroxide. Moreover, ROS may also be released due to the migration, accumulation, and activation of polymorphonuclear cells. These events will finally provoke oxidation of cell membrane lipids, protein oxidation, proteolysis, and DNA fragmentation. Disruption of muscle structural integrity and function will induce changes in transport capacity, energy production, and ionic balance [3].

The oxidative stress has been reported to be involved in several diseases such as diabetes mellitus, neurodegenerative disorders (Parkinson's disease (PD), Alzheimer's disease (AD), and multiple sclerosis (MS)), cardiovascular diseases (atherosclerosis and hypertension), respiratory diseases (asthma), cataract development, and rheumatoid arthritis

[4]. Many studies showed an increase ROS and oxidative damage markers in blood and tissues of humans and animals during and after muscle damage [1, 2, 5, 6]. After muscle injury, oxidative stress could be increased due to a number of potential sites for the ROS generation within the traumatized muscle.

Since the mid-1960s, the use of light energy as a therapy for inflammation and cell trophism has opened up a new research field to understand interaction between electromagnetic energy and biological tissue [7]. More recently, photobiomodulation therapy (PBMT) has been used to mitigate and delay muscle fatigue [8] in clinical [9, 10] and experimental [11] condition. There are studies showing that PBMT can improve mitochondrial function and mitigate ROS as well as reactive nitrogen species (RNS) generated during exercise training [12]. Thus, PBMT has been reported to modulate oxidative events, reducing oxidative stress in different situations [5, 13–15]. We performed this systematic review to identify animal research defining the effects of PBMT on experimental models of muscle injury and the impact of PBMT dosage.

2. Materials and Methods

2.1. Search Strategy. This search strategy was in accordance with the SYstematic Review Center for Laboratory animal Experimentation—SYRCLE guidelines for systemic review. For identification of studies included or considered for this review, from January 2006 to January 2016: EMBASE (Excerpta Medica Database), PubMed (Public/Publisher MEDLINE), and CINAHL (Cumulative Index to Nursing and Allied Health Literature). First, we selected key words from related articles. MeSH and SCOPUS international data lines were used to find more related key words with close meanings: ("oxidative stress"[MeSH Terms] OR ("oxidative"[All Fields] AND "stress"[All Fields]) OR "oxidative stress"[All Fields]) AND ("low-level light therapy"[MeSH Terms] OR ("low-level"[All Fields] AND "light"[All Fields] AND "therapy"[All Fields]) OR "low-level light therapy"[All Fields] OR "PBMT"[All Fields]) AND ("low-level light therapy"[MeSH Terms] OR ("low-level"[All Fields] AND "light"[All Fields] AND "therapy"[All Fields]) OR "low-level light therapy"[All Fields] OR ("low"[All Fields] AND "level"[All Fields] AND "laser"[All Fields] AND "therapy"[All Fields]) OR "low level laser therapy"[All Fields]) ("oxidative stress"[MeSH Terms] OR ("oxidative"[All Fields] AND "stress"[All Fields]) OR "oxidative stress"[All Fields]) AND ("phototherapy"[MeSH Terms] OR "phototherapy"[All Fields]) AND ("low-level light therapy"[MeSH Terms] OR ("low-level"[All Fields] AND "light"[All Fields] AND "therapy"[All Fields]) OR "low-level light therapy"[All Fields] OR ("photobiomodulation"[All Fields] AND "therapy"[All Fields]) OR "photobiomodulation therapy"[All Fields]) AND Photobiomodulation[All Fields].

The search was repeated following review of the eligible papers to specifically search for experimental methodologies and outcomes and parameters of photobiomodulation. We also reviewed the retrieved articles to identify possible additional studies (Figure 1).

2.2. Study Selection. We examined the title list and abstracts identified by the literature searches for potentially relevant studies. Two independent reviewers (SAS and AJS) applied a predetermined inclusion criterion to the full studies. Conflicts were resolved through a third independent researcher (PTC). The inclusion criteria of this systematic search were as follows:

(1) Live animal subjects

(2) Experimental muscle injury model to induce oxidative stress

(3) Random allocation of treatment

(4) Type of low-level laser irradiation was provided as an intervention to at least one of the treatment groups

(5) A quantitative or semiquantitative measure

(6) English language, abstracts were reviewed by at least two raters to determine if they met eligibility criteria.

Exclusion criteria:

(1) *In vitro* clinical studies and systematic review articles with or without meta-analysis.

(2) Papers not published in the English language.

2.3. Assessment of Study Quality. Potentially eligible articles were printed, reviewed, and critically appraised for quality rating by two independent reviewers. Systematic reviews are commonly performed in human research but rarely in animal research. Quality rating scales commonly used in human research may not be appropriate for animal studies, given that they do not consider issues like the appropriateness of the animal model being evaluated. For assessment of appropriateness, we used a quality scale developed by Tajali Bashardoust et al. [16]; this is a quality rating scale for an animal/tissue research scale (QATRS) questionnaire designed to assess the quality of animal studies. The QATRS is a 20-point scaled evaluation chart designed to assess randomization, blinding, similarity of the animal/tissue model with human applications, standardization and reliability of measurement techniques, management of study withdrawals, and appropriateness of statistical methods (Table 1).

3. Results

We found 68 articles in the databases. Abstracts were used to identify research that repeatedly appeared in more than 1 database (duplication of the same study) ($n = 48$). Thus, we prescreened 20 studies for full review. Among the 20 studies analyzed, 12 were excluded for not meeting the inclusion criteria of this systematic review: in vitro study ($n = 1$), clinical study ($n = 4$), systematic review ($n = 4$), abstract only ($n = 1$), and study not written in English ($n = 2$). We included 8 studies for critical evaluation of the effectiveness of PBMT in muscle injury, in which there are diverse treatment parameters of injuries were

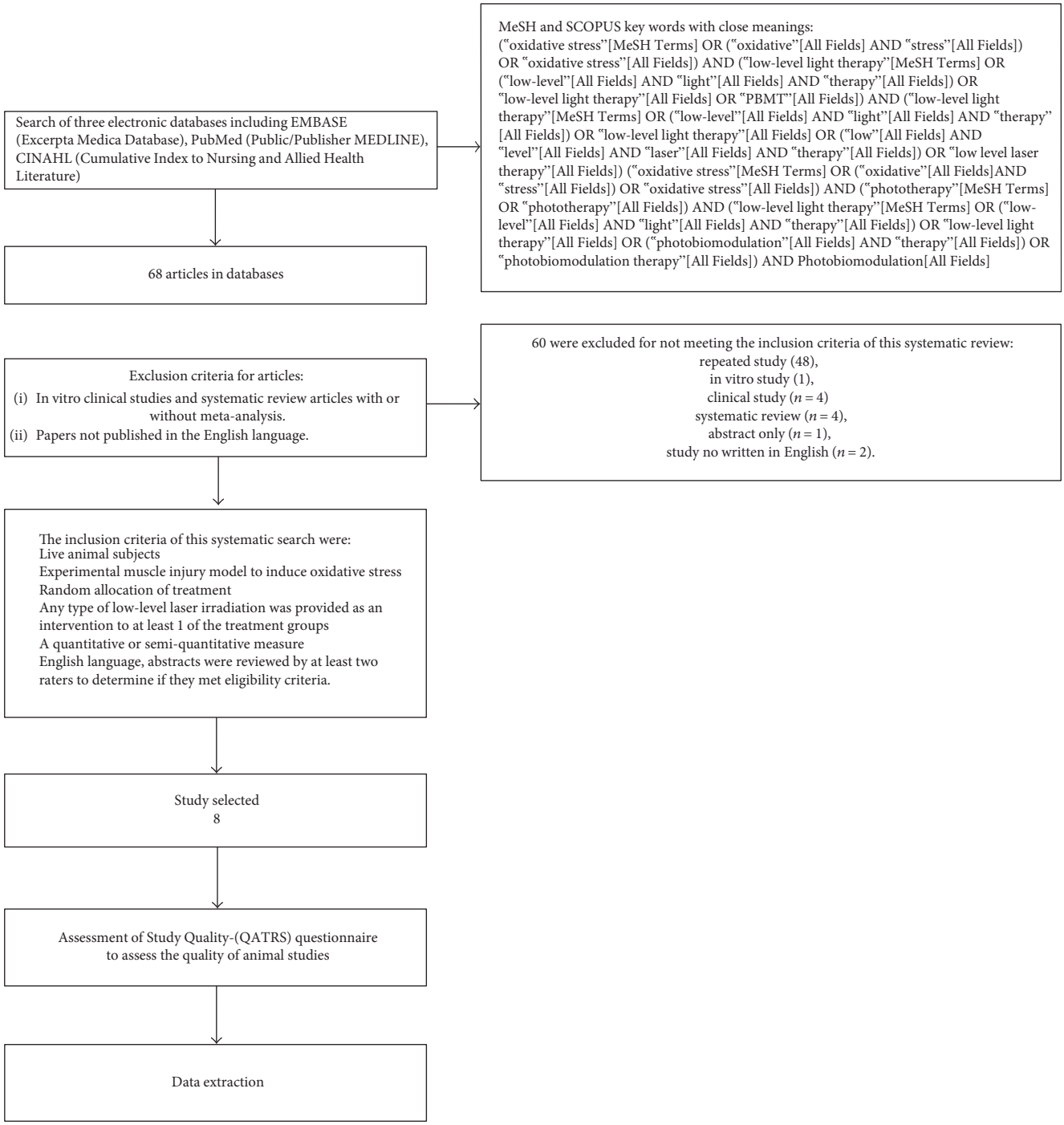

Figure 1: Flow diagram of the results of the study selection procedure.

carried out. Table 2 shows data extracted from the papers. The composition of samples from the 8 studies ranged from 18 to 90 animals, distributed randomly into 3–7 groups, with different studies presenting various primary outcomes; the most frequent oxidative stress biomarkers were catalase (CAT), superoxide dismutase (SOD), glutatione peroxidase (GPX), and biomarkers of lipid peroxidation ($n = 4$) (Table 3).

The studies used several models of experimental injury induction, and all of them were distributed in fatigue [5, 15], cryoinjury [2, 6], traumatic injury [1, 3], and in lesser occurrence Carrageenan [17] and adrenaline [14]. Six studies used male animals and two used female animals. The studies were analyzed by a range of methodological rigor called the QATRS encompassing various aspects that enable better quality control of the experimental studies. Study scores ranged from 17 to 19 points on a scale of 0–20 (Tables 4 and 1). When analysis of the positive effects was statistically significant, eight studies found positive effects (Table 5).

Table 1: Representation of the quality rating scale items for animal/tissue research scale (QATRS).

Item	Rating		
	Yes (2)	Partial (1)	No (0)
(1) Animals/tissue samples were randomly allocated to groups.			
(2) The animals/tissue samples were similar across comparison groups.			
(3) The tissue/animal model study was appropriate for the biological properties/questions being evaluated.			
(4) The animal model used was appropriate to make inferences in terms of human application? (tissue similar to, or is human tissue).			
(5) Objective measurements were performed using sufficient standardization of measurement techniques and appropriate instrumentation.			
(6) Reliability of measurements was reported or referenced to indicate sufficient consistency of the outcomes analyzed.			
(7) Are all animals entered into the study accounted for? (All were analyzed or reasons for withdrawal were noted).			
(8) 90% of the animals entered were included in the data analysis.			
(9) The between group/time statistical comparisons used appropriate statistical methods.			
(10) Measures of variability and confidence intervals were provided to indicate the range/size of the effects observed.			
Total score (/20)			

Table 2: Study characteristics of selected experimental controlled animal studies on low-level laser irradiation effects on oxidative stress.

Authors	Animal type	Gender	Animal race	Age (months)	Weight (g)	Induction model	Site injury	QATRS
Guaraldo et al. [5]	Rat	Male	Wistar	24	517.7 ± 27.54	Fatigue	Gastrocnemius	17
Ribeiro et al. [2]	Rat	Male	Wistar	—	250 ± 15	Cryolesion	Tibialis anterior	19
Oliveira Silva et al. [15]	Mice		Mdx/C57 BL	4	—	Fatigue	Gastrocnemius/Soleus	19
Silveira et al. [3]	Rat	Male	Wistar	Adult	250–300	Trauma	Gastrocnemius	19
Assis et al. [6]	Rat	Male	Wistar	Adult	300	Cryolesion	Tibialis anterior	19
Davila et al. [17]	Rat	Female	Wistar	5	200 ± 20	Carrageenan λ (type IV)	Gastrocnemius	19
Servetto et al. [14]	Rat	Female	—	—	250–300	Adrenaline	Left posterior limb muscle	19
Rizzi et al. [1]	Rat	Male	Wistar	—	250–300	Impact blunt trauma	Gastrocnemius	19

4. Discussion

In this review, articles focusing primarily on the effects of PBMT on oxidative stress in experimentally muscle injury were analyzed; for all articles, there was no unanimity regarding the outcome measures, nor the methods used to measure these outcomes. Frequently, different classifications and evaluations were used to designate similar variables. This may be due to the multifactorial etiology of the disease and the fact that its pathogenesis is still unknown [6]. Enwemeka et al. [18] stated that such failures are the causes of inconsistencies in the literature, especially with PBMT.

The most frequently analyzed variables were histology, creatine kinase, CAT, SOD, GPX, oxide nitric production, and TBARS. Based on the outcomes listed (Table 3), positive outcomes depend on the proper use of two key factors: an experimental model that mimics muscle injury and the use of the intervention employed.

Possibly LLLT and LEDT improves mitochondrial function, $O_2^{\bullet-}$ dismutation via SOD and decreases formation of $ONOO^-$. In addition, LLLT can reduce H_2O_2 via CAT and GPX and can reduce the formation of hydroxyl radicals, which contribute to lower muscle cell membrane damage, as evidenced by a lower lipid peroxidation [19]. The reviewed studies had focused on the analysis of only one muscle, and 60% of these investigated the alterations suffered in the gastrocnemius muscle [1, 3, 5, 17] and the induction medium was distributed in 25% fatigue [5], traumatic lesion 25% [1, 3], and in lesser occurrence Carrageenan [17] and adrenaline [14] with 12.25% (Table 2).

According to Assis et al. [6], the inflammatory phase of the muscle injury is accompanied by an increased ROS and RNS production and a reduced activity in antioxidant enzymes. This imbalance between prooxidants and antioxidants, in favor of prooxidants, can generate oxidative and nitrative stress in the tissue that contributes to

Table 3: Study characteristics of selected experimental controlled animal studies on low-level laser irradiation effects on oxidative stress.

Authors	Sample size	Group number	Number of animals/group	Dependent variables
Guaraldo et al. [5]	30	05	06	Biomarkers of oxidative stress (CAT, SOD, and GPX); biomarkers of lipid peroxidation.
Ribeiro et al. [2]	80	06	05/15	Chemoluminescence; protein oxidation; antioxidant enzyme activity
Oliveira Silva et al. [15]	28	04	07	Histology; quantification total creatine kinase; protein carbonyl; detection of superoxide dismutase
Silveira et al. [3]	18	03	06	Serum creatine kinase activity; hydroxyproline measurement; superoxide anion production; lipid peroxidation assay; superoxide dismutase; protein determination
Assis et al. [6]	60	03	20	Muscle evaluation; muscle morphological analysis; lipid peroxidation; NO production; immunoblotting; dot blot (for detection of nitrotyrosine formation); cytokine measurements (ELISA); total RNA isolation and real-time PCR
Davila et al. [17]	70	07	10	Histological analysis; plasma collection; muscle tissue collection
Servetto et al. [14]	48	06	08	Plasma collection; muscle tissue collection; spectrophotometry in plasma
Rizzi et al. [1]	90	3	30	Histology; collagen quantification; TBARS analysis; Western blot analysis; electrophoretic mobility shift assay

Table 4: Study characteristics of selected experimental controlled animal studies on low-level laser irradiation effects on oxidative stress.

Authors	Wavelength (nm)	Energy density (J/cm^2)	Energy (J)	Power density (W or mW/cm^2)	Spot size (cm^2)	Irradiation time per point (sec)	Duration of treatments (days)	Treatment frequency (days)	Laser frequency (Hz)	Power (mW or W)
Guaraldo et al. [5]	808	144	4	1.071	0.028	40	—	6 weeks	—	100 W
Ribeiro et al. [2]	780/660	10	3.2	1	—	10	7	1, 3, and 7 after the induction of injury	—	40 mW
Oliveira Silva et al. [15]	808	107	—	1027	0,028	100	3	Consecutive days	—	30 mW
Silveira et al. [3]	904	5	2.5	400	0.10	12.5	5	2, 12, 24, 48, 72, 96, and 120 hours after the trauma	9.500	40 mW (peak power 70 W)
Assis et al. [6]	808	180	1.4	3.8	0.00785	47	4	Consecutive days	—	30 mW
Davila et al. [17]	632.8/904	9.5	—	—	—	60/47	10	Consecutive days	—	5/12 mW
Servetto et al. [14]	632.8/904	9.5	—	—	—	60/47	7	Consecutive days	—	5/12 mW
Rizzi et al. [1]	904	5 J	—	—	—	35	7 or 14	Daily	—	45 mW

activate NF-κB, a pleiotropic transcription factor responsible for multiple changes in gene expression in the inflammatory process.

The muscle traumatic injuries especially in the acute phase benefited from the ROS, which in combination with growth factors and cytokines, are important to the muscle repair due to the redirection of myogenic precursor cells (satellite cells to the injury site). Cause apoptosis in satellite cells [20] as differentiated adult skeletal muscle fibers has scarce ability to repair and regenerate themselves when a cellular injury exists; satellite cells have the capacity to proliferate and differentiate, with vital properties to repair the injured tissue [21]. In this context, satellite cells and their response to oxidative stress are important to mature skeletal muscle performance. In addition, photobiomodulation with low-level laser caused a protective effect on myoblasts [22].

Table 5: Study characteristics of selected experimental controlled animal studies on low-level laser irradiation effects on oxidative stress.

Authors	Positive effects: statistically significant	Positive effects: not significant	No effect
Guaraldo et al. [5]		X	
Ribeiro et al. [2]		X	
Oliveira Silva et al. [15]	X		
Silveira et al. [3]	X		
Assis et al. [6]		X	
Davila et al. [17]		X	
Servetto et al. [14]	X		
Rizzi et al. [1]		X	

However, high levels of ROS for a long period in the injured area can cause oxidative harm (secondary damage) by directly reaching vital cell constituents, such as lipids, proteins, and DNA, in addition to interfering negatively in the differentiation of muscle cells [2].

Therefore, we can verify that both the traumatic lesions induced by the use of cold are adequate as models of ROS generation and consequently oxidative stress. The literature has also demonstrated the use of exercise of high intensity [15] with the aim of generating muscle fatigue and consequently oxidative stress can be good indicators for this type of analysis.

Although the focus of the current review is centered on the parameters of dosimetry used during photobiomodulation, it aims to mitigate the oxidative stress and improve the antioxidant ability of the skeletal muscle. In this respect, we realized that there is an agreement on the type of wavelength used in studies ranging from red (632,8 nm) [14, 17] to the infrared (780, 808, and 904 nm) [1–3, 5, 6, 14, 17], being that 30% of the studies offered to make a comparison between the wavelengths (780/660 nm) [2] and (632.8/904 nm) [14, 17], being that in three comparisons these studies obtained better results in the use of infrared (Table 4).

The effective tissue penetration of light and specific wavelength of light absorbed by photoacceptors are two of the major parameters to be considered in light therapy. In the tissue, there is an "optical window" that runs approximately from 650 nm to 1200 nm where the effective tissue penetration of light is maximized [15].

Regarding the power of light used in the studies, we also observed a wide variation between 5 mW and 100 mW, being that 60% of these studies ranged between 35 and 45 mW. Regarding the energy densities (fluence), 100% of the studies described the dose that ranged between 180 and 5 Jcm^2. If on the one hand, all the studies analyzed described the parameters mentioned above, on the other hand 50% did not describe what area of the laser beam [1, 2, 14, 17] was used, as well as power density (irradiance) 30% [1, 14, 17] and energy in Joules 50% [1, 14, 17] (Table 4). The absence of these parameters weakens the studies once the literature has shown that the results of photobiomodulation depends on the irradiation time and dose used. If we take into account that different areas of beam and powers propose different irradiation times and densities of different energies, the reproducibility of these studies are threatened. This can be verified at the great variations presented in the irradiation time per point.

The fluence (energy density) used is generally between 1 and 20 J/cm^2 while the irradiance (power density) can vary widely depending on the actual light source and spot size; values from 5 to 50 mW/cm^2 are common for stimulation and healing, while much higher irradiances (up to W/cm^2) can be used for nerve inhibition and pain relief. PBMT is typically used to promote tissue regeneration, reduce swelling and inflammation, and relieve pain and is often applied to the injury for 30 seconds to a few minutes or so, a few times a week for several weeks [23]. According to Araruna Alves et al. [24], all these aspects must be disclosed in scientific research so that the study becomes reproducible and has measurable outcomes. Therefore, with standardization of the use of the laser, its mechanism of action and its results would be clarified, thus ensuring positive results with the use of photobiomodulation and advances in rehabilitation sciences.

It is accepted that the migration of inflammatory cells (such as neutrophils and macrophages) to the muscle site required during exercise and under this condition cells of inflammatory cells are a source of ROS. Thus, it is possible to imagine that the oxidative muscular homeostasis linked to PBMT could be mediated by its anti-inflammatory action, inhibiting/attenuating the of inflammatory cell migration, then, the ROS source. In addition, PBMT application has been reported to induce superoxide dismutase (SOD) increases, in which could contribute to alleviate the muscle damage by reducing oxidative stress. In fact, SOD is an enzyme with elevated capacity of scavenging O_2 radicals. It has also been shown that some light wavelengths are absorbed by hemoglobin, releasing nitric oxide from the nitrosothiols in the beta chain of the hemoglobin molecule (Mittermayr et al. [25]; Vladimirov et al. [26]; and Vladimirov et al. [27]. Since during exercise (mainly aerobic) there is a greater influx of blood to the active muscle, LLLT could potentialize the release of nitric oxide to modulate oxidative stress (Figure 2).

Based on the results of the studies included in this review, there is sufficient evidence to suggest that photobiomodulation is an effective short-term approach for reducing TBARS levels and antioxidants levels (Table 5). Furthermore, the parameters used for PBMT in the studies examined, such as laser output, irradiation distance, irradiation frequency per day, number of treatment sessions, irradiated energy per day, and the total energy irradiated, did not meet the current recommendations for reproducible studies. It is necessary to establish the optimal dosage and exposure levels necessary for achieving results in decreased oxidative stress in muscle injury.

5. Conclusions

Although the small number of studies limits the systematic review on photobiomodulation, evidence was found to

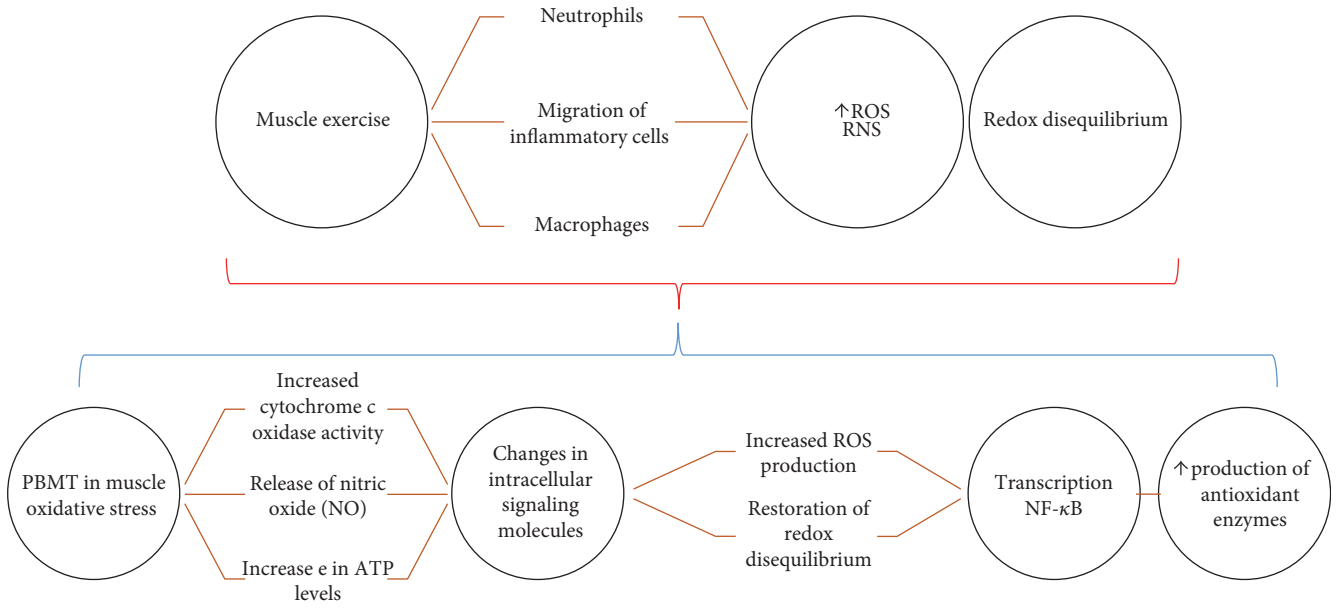

Figure 2: Schematic representation of mechanisms of photobiomodulation- PBMT action on muscle oxidative stress—the oxidative stress generated during exercise or injury is linked to the migration of cells of inflammatory cells (such as neutrophils and macrophages) to the source of ROS. The increase of the reactive oxygen species triggers a redox state de-balancing. Basic biological mechanism behind the effects of PBMT: red and infrared light is absorbed by cytochrome c oxidase (IV complex of the mitochondrial respiratory chain). PBMT triggers increased ROS production, such as superoxide (O_2) and hydrogen peroxide (H_2O_2), leading to the restoration of redox imbalance because of higher production of antioxidant enzymes. Altering the redox state in the cells induces the activation of intracellular signaling, increasing the activation of the transcription factor redox sensitive.

suggest que PBMT is an effective short-term approach for reducing oxidative stress in muscle injury. However, lack of uniformity in the terminology used to describe parameters and the dose used for PBMT limits the ability to reach firm conclusions.

Conflicts of Interest

The authors declare that there is no conflict of interest regarding the publication of this article.

Acknowledgments

Special acknowledgements are given to São Paulo Research Foundation—FAPESP (Grant no. 15/13677-4; 15/11028-9).

References

[1] C. F. Rizzi, J. L. Mauriz, D. S. Freitas Corrêa et al., "Effects of low-level laser therapy (LLLT) on the nuclear factor (NF)-kappaB-signaling pathway in traumatized muscle," *Lasers in Surgery and Medicine*, vol. 38, no. 7, pp. 704–731, 2006.

[2] B. G. Ribeiro, A. N. Alves, L. A. Dos Santos et al., "Red and infrared low level laser therapy prior to injury with or without administration after injury modulate oxidative stress during the muscle repair process," *PLoS One*, vol. 11, no. 4, article e0153618, 2006.

[3] P. C. Silveira, L. A. da Silva, C. A. Pinho et al., "Effects of low-level laser therapy (GaAs) an animal model of muscular damage induced by trauma," *Lasers in Medical Science*, vol. 28, no. 2, pp. 431–436, 2013.

[4] A. Phaniendra, D. B. Jestadi, and L. Periyasamy, "Free radicals: properties, sources, targets, and their implication in various diseases," *Indian Journal of Clinical Biochemistry*, vol. 30, no. 1, pp. 11–26, 2015.

[5] S. A. Guaraldo, A. J. Serra, E. M. Amadio et al., "The effect of low-level laser therapy on oxidative stress and functional fitness in aged rats subjected to swimming: an aerobic exercise," *Lasers in Medical Science*, vol. 31, no. 5, pp. 833–840, 2016.

[6] L. Assis, A. I. Moretti, T. B. Abrahão et al., "Low-level laser therapy (808 nm) reduces inflammatory response and oxidative stress in rat tibialis anterior muscle after cryolesion," *Lasers in Surgery and Medicine*, vol. 44, no. 9, pp. 726–735, 2012.

[7] S. A. dos Santos, M. A. dos Santos Vieira, M. C. B. Simões, A. J. Serra, E. C. Leal-Junior, and P. T. C. de Carvalho, "Photobiomodulation therapy associated with treadmill training in the oxidative stress in a collagen-induced arthritis model," *Lasers in Medical Science*, vol. 32, no. 5, pp. 1071–1079, 2017.

[8] E. C. Leal-Junior, A. A. Vanin, E. F. Miranda, T. de Carvalho Pde, S. Dal Corso, and J. M. Bjordal, "Effect of phototherapy (low-level laser therapy and light-emitting diode therapy) on exercise performance and markers of exercise recovery: a systematic review with meta-analysis," *Lasers in Medical Science*, vol. 30, no. 2, pp. 925–939, 2015.

[9] E. C. Leal-Junior, R. A. Lopes-Martins, L. Frigo et al., "Effects of low-level laser therapy (LLLT) in the development of exercise-induced skeletal muscle fatigue and changes in

biochemical markers related to postexercise recovery," *The Journal of Orthopaedic and Sports Physical Therapy*, vol. 40, no. 8, pp. 524–532, 2010.

[10] P. de Almeida, R. A. Lopes-Martins, T. D. Marchi et al., "Red (660 nm) and infrared (830 nm) low-level laser therapy in skeletal muscle fatigue in humans: what is better?," *Lasers in Medical Science*, vol. 27, no. 2, pp. 453–458, 2012.

[11] L. A. Santos, R. L. Marcos, S. S. Tomazoni et al., "Effects of pre-irradiation of low-level laser therapy with different doses and wavelengths in skeletal muscle performance, fatigue, and skeletal muscle damage induced by tetanic contractions in rats," *Lasers in Medical Science*, vol. 29, no. 5, pp. 1617–1626, 2014.

[12] L. I. Fillipin, J. L. Mauriz, K. Vedovelli et al., "Low-level laser therapy (LLLT) prevents oxidative stress and reduces fibrosis in rat traumatized Achilles tendon," *Lasers in Surgery and Medicine*, vol. 37, no. 4, pp. 293–300, 2005.

[13] E. T. Firat, A. Dağ, A. Günay et al., "The effect of low-level laser therapy on the healing of hard palate mucosa and the oxidative stress status of rats," *Journal of Oral Pathology & Medicine*, vol. 43, no. 2, pp. 103–110, 2014.

[14] N. Servetto, D. Cremonezzi, J. C. Simes et al., "Evaluation of inflammatory biomarkers associated with oxidative stress and histological assessment of low-level laser therapy in experimental myopathy," *Lasers in Surgery and Medicine*, vol. 42, no. 6, pp. 577–583, 2010.

[15] A. A. Oliveira Silva, E. C. Leal-Junior, A. D'Avila Kde et al., "Pre-exercise low-level laser therapy improves performance and levels of oxidative stress markers in mdx mice subjected to muscle fatigue by high-intensity exercise," *Lasers in Medical Science*, vol. 30, no. 6, pp. 1719–1727, 2015.

[16] S. Tajali Bashardoust, J. C. MacDermid, P. Houghton, and R. Grewal, "Effects of low power laser irradiation on bone healing in animals: a meta-analysis," *Journal of Orthopaedic Surgery and Research*, vol. 5, no. 1, pp. 2–10, 2010.

[17] S. Dávila, M. B. Vignola, D. Cremonezzi, J. C. Simes, F. Soriano, and V. R. Campana, "Low-level laser therapy on experimental myopathy," *Laser Therapy*, vol. 20, no. 4, pp. 287–292, 2011.

[18] C. S. Enwemeka, J. C. Parker, D. S. Dowdy, E. E. Harkness, L. E. Sanford, and L. D. Woodruff, "The efficacy of low-power lasers in tissue repair and pain control: a meta-analysis study," *Photomedicine and Laser Surgery*, vol. 22, no. 4, pp. 323–329, 2004.

[19] C. Ferraresi, M. R. Hamblin, and N. A. Parizotto, "Low-level laser (light) therapy (LLLT) on muscle tissue: performance, fatigue and repair benefited by the power of light," *Photonics & Lasers in Medicine*, vol. 1, no. 4, pp. 267–286, 2012.

[20] A. Vasconsuelo, L. Milanesi, and R. Boland, "17Beta-estradiol abrogates apoptosis in murine skeletal muscle cells through estrogen receptors: role of the phosphatidylinositol 3-kinase/Akt pathway," *The Journal of Endocrinology*, vol. 196, no. 2, pp. 385–397, 2008.

[21] N. Yoshida, S. Yoshida, K. Koishi, K. Masuda, and Y. Nabeshima, "Cell heterogeneity upon myogenic differentiation: down-regulation of MyoD and Myf-5 generates 'reserve cells'," *Journal of Cell Science*, vol. 111, Part 6, pp. 769–779, 1998.

[22] L. M. Silva, C. A. Silva, Ad da Silva et al., "Photobiomodulation protects and promotes differentiation of C2C12 myoblast cells exposed to snake venom," *PLoS One*, vol. 11, no. 4, article e0152890, 2016.

[23] Y. Y. Huang, S. K. Sharma, J. Carroll, and M. R. Hamblin, "Biphasic dose response in low-level light therapy - an update," *Dose Response*, vol. 9, no. 4, pp. 602–618, 2011.

[24] A. C. Araruna Alves, A. A. Silva, C. S. d. Melo Rambo et al., "Effects of low-level laser irradiation on cartilage injury in animal models: a systematic review," *Medical Science and Technology*, vol. 54, pp. 35–42, 2012.

[25] R. Mittermayr, A. Osipov, C. Piskernik et al., "Blue laser light increases perfusion of a skin flap via release of nitric oxide from hemoglobin," *Molecular Medicine*, vol. 13, pp. 22–29, 2007.

[26] IuA Vladimirov, G. I. Klebanov, G. G. Borisenko, and A. N. Osipov, "Molecular and cellular mechanisms of the low intensity laser radiation effect," *Biofizika*, vol. 49, no. 2, pp. 339–350, 2004.

[27] Y. A. Vladimirov, A. N. Osipov, and G. I. Klebanov, "Photobiological principles of therapeutic applications of laser radiation," *Biochemistry (Moscow)*, vol. 69, pp. 81–90, 2004.

Hindawi
Oxidative Medicine and Cellular Longevity
Volume 2017, Article ID 6792694, 15 pages
https://doi.org/10.1155/2017/6792694

Research Article

Antioxidant Treatment Reduces Formation of Structural Cores and Improves Muscle Function in RYR1$^{Y522S/WT}$ Mice

Antonio Michelucci,[1,2] Alessandro De Marco,[1,2] Flavia A. Guarnier,[3] Feliciano Protasi,[1,4] and Simona Boncompagni[1,2]

[1]*Center for Research on Aging and Translational Medicine (CeSI-MeT), University G. d'Annunzio of Chieti, 66100 Chieti, Italy*
[2]*Department of Neuroscience, Imaging, and Clinical Sciences (DNICS), University G. d'Annunzio of Chieti, 66100 Chieti, Italy*
[3]*Department of General Pathology, University Estadual de Londrina, 86057-970 Londrina, PR, Brazil*
[4]*Department of Medicine and Aging Science (DMSI), University G. d'Annunzio of Chieti, 66100 Chieti, Italy*

Correspondence should be addressed to Simona Boncompagni; simona.boncompagni@unich.it

Received 6 April 2017; Accepted 13 June 2017; Published 10 September 2017

Academic Editor: Marko D. Prokić

Central core disease (CCD) is a congenital myopathy linked to mutations in the ryanodine receptor type 1 (RYR1), the sarcoplasmic reticulum Ca^{2+} release channel of skeletal muscle. CCD is characterized by formation of amorphous *cores* within muscle fibers, lacking mitochondrial activity. In skeletal muscle of RYR1$^{Y522S/WT}$ knock-in mice, carrying a human mutation in RYR1 linked to malignant hyperthermia (MH) with *cores*, oxidative stress is elevated and fibers present severe mitochondrial damage and *cores*. We treated RYR1$^{Y522S/WT}$ mice with N-acetylcysteine (NAC), an antioxidant provided *ad libitum* in drinking water for either 2 or 6 months. Our results show that 2 months of NAC treatment starting at 2 months of age, when mitochondrial and fiber damage was still minimal, (i) reduce formation of *unstructured* and *contracture cores*, (ii) improve muscle function, and (iii) decrease mitochondrial damage. The beneficial effect of NAC treatment is also evident following 6 months of treatment starting at 4 months of age, when structural damage was at an advanced stage. NAC exerts its protective effect likely by lowering oxidative stress, as supported by the reduction of 3-NT and SOD2 levels. This work suggests that NAC administration is beneficial to prevent mitochondrial damage and formation of *cores* and improve muscle function in RYR1$^{Y522S/WT}$ mice.

1. Introduction

Central core disease (CCD), one of the most common human congenital myopathies, is an inherited neuromuscular disorder characterized by hypotonia and proximal muscle weakness, which cause motor developmental delay in children [1, 2]. Diagnosis of CCD is confirmed by histological examination of muscle biopsies showing amorphous central areas (i.e., *cores*) lacking glycolytic/oxidative enzymes and mitochondria [3]. Disorganization of contractile and sarcotubular systems is also typical in *cores* [4]. To date, management of patients/children is essentially supportive and based on physiotherapic approaches and no curative treatments are available. Hence, a deeper understanding of the molecular mechanisms underlying mitochondrial damage and formation of *cores* in CCD is needed to develop effective therapeutic interventions.

In humans, about 90% of CCD cases are linked to mutations in the ryanodine receptor type 1 (RYR1) gene [5], encoding for the sarcoplasmic reticulum (SR) Ca^{2+} release channel of skeletal muscle. RYR1 is a large protein of about 2200 kDa specifically localized in calcium release units (CRUs), the intracellular junctions formed by the close apposition of transverse-tubules (TT) to the SR. RYR1 in CRUs is part of macromolecular complex deputed to excitation-contraction (EC) coupling, the mechanism that allows transduction of the action potential into Ca^{2+} release from the SR [6, 7]. Mutations in RYR1 gene, which causes abnormalities in the opening probability of the Ca^{2+} channel, are also often associated to malignant hyperthermia (MH) susceptibility,

an inherited pharmacogenetic subclinical myopathy, characterized by a life-threatening hypermetabolic response to commonly used halogenated/volatile anesthetics (i.e., halothane, isofluorane) [8, 9]. An association between CCD and MH exists as individuals with MH may have muscle biopsies with *cores* [10, 11], while CCD patients may be at risk for hyperthermic episodes during anesthetic procedures, as also confirmed by *in vitro* caffeine-halothane contracture testing (either IVCT, *in vitro* contracture test, or the CHCT, caffeine-halothane contracture test), performed on muscle biopsies [2, 12–14].

In the 2006, an animal model (RYR1-Y522S knock-in mice) carrying a human gain-of-function mutation associated to MH, skeletal muscle weakness, and formation of *cores* was generated and characterized [10]. Heterozygous Y522S mice ($RYR1^{Y522S/WT}$) suffer lethal MH crises when acutely exposed to both anesthetics and heat [15, 16] and develop structural *cores* [17]. Muscles of $RYR1^{Y522S/WT}$ mice also exhibit a marked temperature-dependent increase in resting myoplasmic Ca^{2+}, excessive oxidative stress [16], and enhanced mitochondrial superoxide flashes activity [18]. The current view of the molecular mechanisms underlying the phenotype of $RYR1^{Y522S/WT}$ mice is that the Y522S mutation promotes a significant increase of the opening probability of the RYR1 channel, which causes SR Ca^{2+} leak and overproduction of reactive oxygen and nitrogen species (ROS and RNS), as a consequence of the increased Ca^{2+}-dependent mitochondrial activity. In turn, excessive ROS and RNS would determine nitrosylation/glutathionylation of RYR1, oxidative modifications responsible of further increase of RYR1 opening probability [16]. The feed-forward mechanism triggered by ROS/RNS would in principle play a pivotal role: (i) acutely, in anesthetic- and heat-induced lethal MH episodes and (ii) chronically, in mitochondrial damage and development of *cores*, two types of structural alterations that resemble CCD in humans [17].

Here, we treated $RYR1^{Y522S/WT}$ mice with N-acetylcysteine (NAC), a potent antioxidant provided *ad libitum* in drinking water (1% *w*/*v*) for either 2 months (2–4 months of age, starting when mitochondrial and fiber damage was still minimal) or 6 months (4–10 months of age; starting when structural damage was already at an advanced stage) [17], and evaluated the effect of this pharmacological treatment on formation of *cores*, muscle function, mitochondrial damage, and levels of oxidative stress in *extensor digitorum longus* (EDL) muscles. The results collected in this study indicate that NAC administration is beneficial to prevent/reduce mitochondrial damage and formation of *cores* and improve muscle function in $RYR1^{Y522S/WT}$ mice.

2. Materials and Methods

2.1. $RYR1^{Y522S/WT}$ Mice. Heterozygous Y522S mice were generated as previously described [15]. Mice were housed in microisolator cages at 20°C in a 12 hr light/dark cycle and provided free access to water and food. Animals used in this study were all males, and analyses were carried out in EDL muscles. All experiments were conducted according to the Directive of the European Union 2010/63/UE, and animal protocols were approved by the Committee on the Ethics of Animal Experiments of the University of Chieti (15/2011/CEISA/COM). All surgeries were made to minimize animal suffering; animals were anesthetized and then sacrificed by cervical dislocation.

2.2. NAC Treatment. $RYR1^{Y522S/WT}$ mice were randomly assigned to the experimental groups: untreated or NAC-treated $RYR1^{Y522S/WT}$ mice. NAC (Sigma-Aldrich, Milan, Italy) was provided *in vivo* in drinking water at the final concentration of 1% weight/volume (1% *w*/*v*) as previously described [19] for either 2 months (from 2–4 months of age) or 6 months (from 4–10 months of age).

2.3. Preparation and Analysis of Samples in Light and Electron Microscopy (EM). EDL muscles were dissected, fixed at room temperature with 3.5% glutaraldehyde in 0.1 M NaCaCo buffer (pH 7.2), and kept at 4°C in fixative until further use. Small bundles of fixed muscles were then postfixed, embedded, stained en-block, and sectioned as previously described [17, 20]. For EM, ultrathin sections (~50 nm) were examined after staining in 4% uranyl acetate and lead citrate, with a Morgagni Series 268D electron microscope (FEI Company, Brno, Czech Republic), equipped with Megaview III digital camera (Olympus Soft Imaging Solutions GmbH, Munster, Germany) at 60 kV. For histology, 700 nm thick sections were stained in a solution containing 1% Toluidine blue O and 1% sodium borate tetra in distilled water for 3 min on a hot plate at 55–60°C. After washing and drying, sections were finally mounted with mounting medium (DPX Mountant for histology, Sigma-Aldrich, Milan, Italy).

2.4. Quantitative Analysis in Histology and EM Preparations. Consider the following:

(1) Histological sections were examined under direct illumination and/or phase contrast optics with a Leica DMLB fluorescence microscope (Leica Microsystem, Vienna, Austria), and individual EDL fibers were visually scored for the presence of either *unstructured* or *contracture cores* as in [17].

(2) Number/area, size, and volume of mitochondria (and number/area of CRUs and mitochondria CRU pairs) were determined in EDL fibers as follows: (a) Mitochondrial volume was determined using the well-established stereology point-counting technique [21, 22] in micrographs taken from transversal sections at magnification 7100x. Briefly, after superimposing an orthogonal array of dots at a spacing of 0.20 μm to the electron micrographs, ratio between numbers of dots falling within mitochondrial profiles and total number of dots covering the whole image was used to calculate the relative fiber volume occupied by mitochondria. (b) Number of severely damaged mitochondria was counted in longitudinal sections, and their frequency was reported as an average number in 100 μm^2 and as % of mitochondria evaluated. Mitochondria were classified as severely damaged as previously described [17]. (c) Average mitochondrial size (nm^2) of apparently normal

mitochondria was measured in longitudinal sections using the analysis software of the EM digital camera (Olympus Soft Imaging Solutions GmbH, Munster, Germany). Severely damaged mitochondria, included in (b), were excluded from this analysis. (d) Number/area of CRUs, mitochondria, and mitochondria CRU pairs was also evaluated in longitudinal sections and reported as the average number in 100 μm^2.

2.5. Immunolabeling and Confocal Microscopy (CM). EDL muscles were dissected from sacrificed mice and fixed with paraformaldehyde 2% for 1-2 hrs at room temperature. Small bundles of muscles were processed for double immunostaining as previously described [23]. Primary antibodies used (a) mouse monoclonal anti-RyR1/RyR3 34C (1 : 20) (Developmental Studies Hybridoma Bank, University of Iowa, Iowa, USA) and (b) rabbit polyclonal antimitochondrial preprotein translocases of the outer membrane, TOM20 (1 : 50) (Santa Cruz Biotechnology, Inc., Dallas, TX, USA). Secondary antibodies used (a) Cy5-labeled goat anti-mouse IgG and (b) Cy3-labeled goat anti-rabbit IgG (Jackson ImmunoResearch Laboratories, West Grove, PA, USA). Images were acquired using a Zeiss LSM510 META laser-scanning confocal microscope system (Zeiss, Jena, Germany) equipped with Zeiss Axiovert 200 inverted microscope and a Plan Neofluar oil-immersion objective (63X/1.3 NA). Negative controls for each immunostaining assay were performed by immunolabeling of samples with only secondary antibodies.

2.6. Quantitative Plasma and Serum Analyses. Blood levels of creatine kinase (CK) and lactate dehydrogenase (LDH), markers of fiber damage, were spectrophotometrically measured in serum (CK) and plasma (LDH) samples obtained from mice as previously described [19], by using a Screen Touch Master spectrophotometer (Hospitex Diagnostic, Sesto Fiorentino, Italy).

2.7. Calpain Activity. The activity of calpain was measured in total hind limb muscle homogenates, by a chemiluminescence assay using a Calpain Protease Assay kit (Calpain-Glo Protease Assay®, Promega; Madison, WI, USA). The assay provides a proluminescent calpain substrate, in a buffer system optimized for calpain and luciferase activities. During the assay, calpain cleavage of the substrate generates a *glow-type* luminescent signal produced by the luciferase reaction. In this homogeneous, coupled-enzyme format, the signal is proportional to the amount of calpain activity present in the sample [24]. In this study, total hind limb muscle homogenates were prepared at a concentration of 6.25 mg/mL in 10 mM KH_2PO_4 buffer, pH 7.4 in 0.9% NaCl and finally processed according to the manufacturer's instructions. Results are expressed as calpain activity/mg of muscle tissue.

2.8. Carbonyl Protein Content. Protein carbonyl group formations are classic and immediate biomarkers of oxidative modification to proteins, which may promote disorganization of contractile structures [25, 26]. 2,4-Dinitrophenylhydrazine (DNPH) tagging of protein carbonyls has been one of the most common measures of oxidative stress and consequent protein damage. Carbonyl protein content was measured as previously described [25], with modifications. Briefly, a mix of total hind limb muscles (50 mg/mL) was homogenized in 50 mM phosphate buffer, 1 mM ethylenediamine tetraacetic acid, pH 7.4, and tissue samples were centrifuged at 600g/10 min/4°C. A volume of 200 μL of DNPH was added to 200 μL of supernatant and incubated at room temperature. After a 30 min incubation, 100% trichloroacetic acid (TCA) was added and samples were placed on ice for 5 min and then spinned at maximal speed for 2 min. Supernatants were discarded without disturbing pellets, which were washed in cold acetone and placed at −20°C for 5 min. Then, acetone was carefully removed, and pellets were dissolved in 0.5 mL 6 M guanidine hydrochloride to be read at 375 nm. To calculate the protein carbonyl content, the following formula was used: $C = [(OD\ 375\ nm)/6.364 \times (100)]$ nmol/well, where 6.364 is the extinction coefficient using the enclosed 96-well plates in mM (=22 mM-1 cm-1 × 0.2893 cm path length in well). Results were expressed as nmol carbonyl/mg of total protein, which were quantified in each sample at 280 nm.

2.9. Western Blot Analyses. For assessment of 3-nitrotyrosyne (3-NT) content, mixed muscles from hind limb were homogenized on ice in a buffer containing 50 mM Tris-HCl, pH 7.4; 1% NP-40; 0.25% sodium deoxycholate; 150 mM NaCl; 1 mM EDTA; 1 mM PMSF; protease inhibitors. After centrifugation at 10000g for 15 min at 4°C, supernatants were collected and total protein concentration was determined using Bio-Rad Protein assay (Bio-Rad laboratories, CA). 40 μg of total proteins was separated by SDS-PAGE in a 10% polyacrylamide gel, followed by western blotting using anti 3-NT mouse monoclonal antibody (1 : 500, Merk Millipore, Milan, Italy) and a horseradish peroxidase-(HRP-) conjugated anti-mouse secondary antibody (Merck Millipore, Darmstadt, Germany). Visualization and densitometric quantification of signals were done using the imaging system Alliance Mini 4 with Alliance 1D MAX software (UVItec, Cambridge, UK). After measuring 3-NT, the membranes were stripped by Tris/SDS buffer with 2-mercaptoethanol. After blocking, the membranes were incubated with anti-glyceraldehyde-3-phosphate dehydrogenase (GAPDH) antibody (OriGene, Rockville, MD, USA) for normalization to the protein content within each band.

For assessment of Cu/Zn-superoxide dismutase (SOD1) and Mn-superoxide dismutase (SOD2) protein levels, western blot experiments were performed as follows: mixed muscles from hind limb were homogenized on ice in RIPA buffer (50 mM Tris-HCl, pH 8.0; 150 mM NaCl; 0.5% sodium deoxycholate; 0.1% SDS; 1% NP-40; 0.1 mM PMSF; protease inhibitors). Homogenates were centrifuged at 10000g for 15 min at 4°C, supernatants were collected, and total protein concentration was determined using Bio-Rad Protein assay (Bio-Rad laboratories, Hercules, CA, USA). Protein samples (5 μg), solubilized in 2× sample buffer (125 mM Tris-HCl, pH 6.8; 4% SDS; 20% glycerol; 0.004% bromophenol blue; 10% 2-mercaptoethanol), were loaded on a 12% acrylamide gel, separated by SDS-PAGE, and transferred to nitrocellulose membrane. Membranes were probed using primary

antibodies against SOD1 (1 : 1000, Santa Cruz Biotechnology, Dallas, TX, USA), SOD2 (1 : 2000, Santa Cruz Biotechnology, Dallas, TX, USA), and GAPDH (1 : 10000, OriGene, Rockville, MD, USA) overnight at 4°C. HRP-conjugated anti-mouse or rabbit (1 : 10000, Merck Millipore, Darmstadt, Germany) was used as a secondary antibody, and peroxidase activity was detected using an enhanced chemiluminescence (ECL) kit (Perkin Elmer, Waltham, MA, USA). The bands were visualized, and densitometric quantification of signals was performed using the imaging system Alliance Mini 4 with Alliance 1D MAX software (UVItec, Cambridge, UK).

2.10. Grip Strength Test. Strength developed by mice during instinctive grasp was measured as previously described [27]. Briefly, mice were held by the tail and allowed to firmly grasped to a metal grating, connected to the shaft of a Shimpo Fgv 0.5X force transducer (Metrotec Group, Lezo, Spain), with fore and hind limbs before a gentle pull was exerted on the tail. Measurements of peak force generated by each mouse were repeated three times with appropriate intervals (at least 30 sec) to avoid fatigue, and the highest value of peak force (normalized to total body mass) measured before each experiment was used.

2.11. Force and Contraction Kinetics of Intact EDL Muscles. EDL muscles were dissected from WT, untreated RYR1$^{Y522S/WT}$, and NAC-treated RYR1$^{Y522S/WT}$ mice and placed in a dish containing Krebs solution with the following composition in mM: 118 NaCl, 4.7 KCl, 1.2 $MgSO_4$, 2.5 $CaCl_2$, 1.2 KH_2PO_4, 25 $NaHCO_3$, and 11 glucose. Individual EDLs were then pinned, tied with fine silk sutures at each end, and mounted vertically between two platinum electrodes immersed in an organ chamber filled with Krebs solution and attached to a servo motor and force transducer (model 1200A, Aurora Scientific, ON, Canada). Temperature was kept between 23–25°C. Before starting the experimental protocol, stimulation level and optimal muscle length (L_0) were determined using a series of 80 Hz-tetani in order to stretch the muscle to the length that generated maximal force (F_0). After optimization of the stimulation conditions, EDL muscles were subjected to a force-frequency protocol based on a series of train pulses of 500 ms duration each as follows (in Hz): 1, 5, 10, 20, 40, 60, 80, 100, 120, and 140. After 5 min at rest, the same EDL muscles were subjected to a single-sustained high frequency tetanus (120 Hz, 2 sec). Muscle force was recorded using a dynamic muscle control (DMC) software and analyzed using dynamic muscle analysis (DMA) software (both from: Aurora Scientific, ON, Canada). Specific force (mN/mm^2) was calculated by normalizing the absolute force (mN) to the cross sectional area (CSA, mm^2) obtained as the following: muscle wet weight (mg)/L_0 (mm) $*$ 1.06 (mg/mm^3).

2.12. Statistical Analyses. Statistical significance for the quantitative analysis of fibers presenting structural alterations (i.e., *unstructured* and *contracture cores*) was evaluated using two-tailed Fisher's exact test. One-way ANOVA followed by post hoc Tukey test was used for statistical analyses of all other experiments except for those regarding the time courses of *in vivo* grip strength and the force-frequency of intact EDL muscles, in which repeated measures ANOVA was used followed by post hoc Tukey test for the pairwise comparisons. In all cases, differences were considered statistically significant at $p < 0.05$. Two-tailed Fisher's exact tests were performed using GraphPad software, whereas one-way ANOVA and repeated measures ANOVA were performed using Origin 8.0 software.

3. Results

The effect of NAC treatment on structure, function, and oxidative stress levels of EDL muscles from RYR1$^{Y522S/WT}$ mice was evaluated at (a) 4 months of age after 2 months of treatment (starting when mitochondrial and fiber damage was still minimal) and at (b) 10 months of age after 6 months of treatment (starting when mitochondrial damage was already at an advanced stage) [17]. In the manuscript, we will refer to 2 and 6 months of treatment as *short-term* and *long-term* NAC treatments, respectively.

3.1. NAC Treatment Reduces Formation of Structural Cores, Fiber Damage, and Proteolytic Degradation in EDL Muscles of RYR1$^{Y522S/WT}$ Mice. Skeletal fibers from RYR1$^{Y522S/WT}$ mice develop *unstructured* and *contracture cores* [17]. To evaluate the effect of NAC in reducing formation of *cores*, using histological sections, we analyzed and classified fibers in three different categories, as previously described [17]: (a) *normal fibers*, presenting a well-preserved cross striation pattern (Figure 1(a)); (b) fibers with *unstructured cores*, presenting extensive areas lacking cross striation (Figure 1(b), asterisks); and (c) fibers with *contracture cores*, exhibiting areas of extreme sarcomere shortening (Figure 1(c), arrows). Quantitative analysis of the relative percentage of fibers, presenting the different features, indicates that NAC treatment was effective in preventing the formation of structural *cores* (Figure 1(d) and Table S1 available online at https://doi.org/10.1155/2017/6792694). Specifically, *unstructured* and *contracture cores*, which are not present in WT fibers, were found, respectively, in 14% and 23% of fibers in RYR1$^{Y522S/WT}$ EDL muscles (Figure 1(d)). However, following NAC treatment, the number of RYR1$^{Y522S/WT}$ EDL fibers containing *unstructured* and *contracture cores* was significantly reduced to 6% and 3%, respectively (Figure 1(d)). The decrease in the number of fibers containing *cores* results in a parallel increase in the percentage of normal fibers (from 63 to 92%). Data plotted in Figure 1 are available in Table S1.

As fiber damage results in changes in blood parameters, we performed biochemical measurements of markers of muscle damage in blood samples. Specifically, we evaluated serum and plasma levels of the muscle-specific isoforms of creatine kinase (CK, in serum) and lactate dehydrogenase (LDH, in plasma) [28]. Consistent with the higher percentage of fibers presenting structural alterations, in RYR1$^{Y522S/WT}$ samples, both CK and LDH levels were about ~30% higher than those in aged-matched WT mice (Figures 1(e) and 1(f)). The protective effect of NAC was confirmed by these experiments: 2 months of NAC treatment was effective in

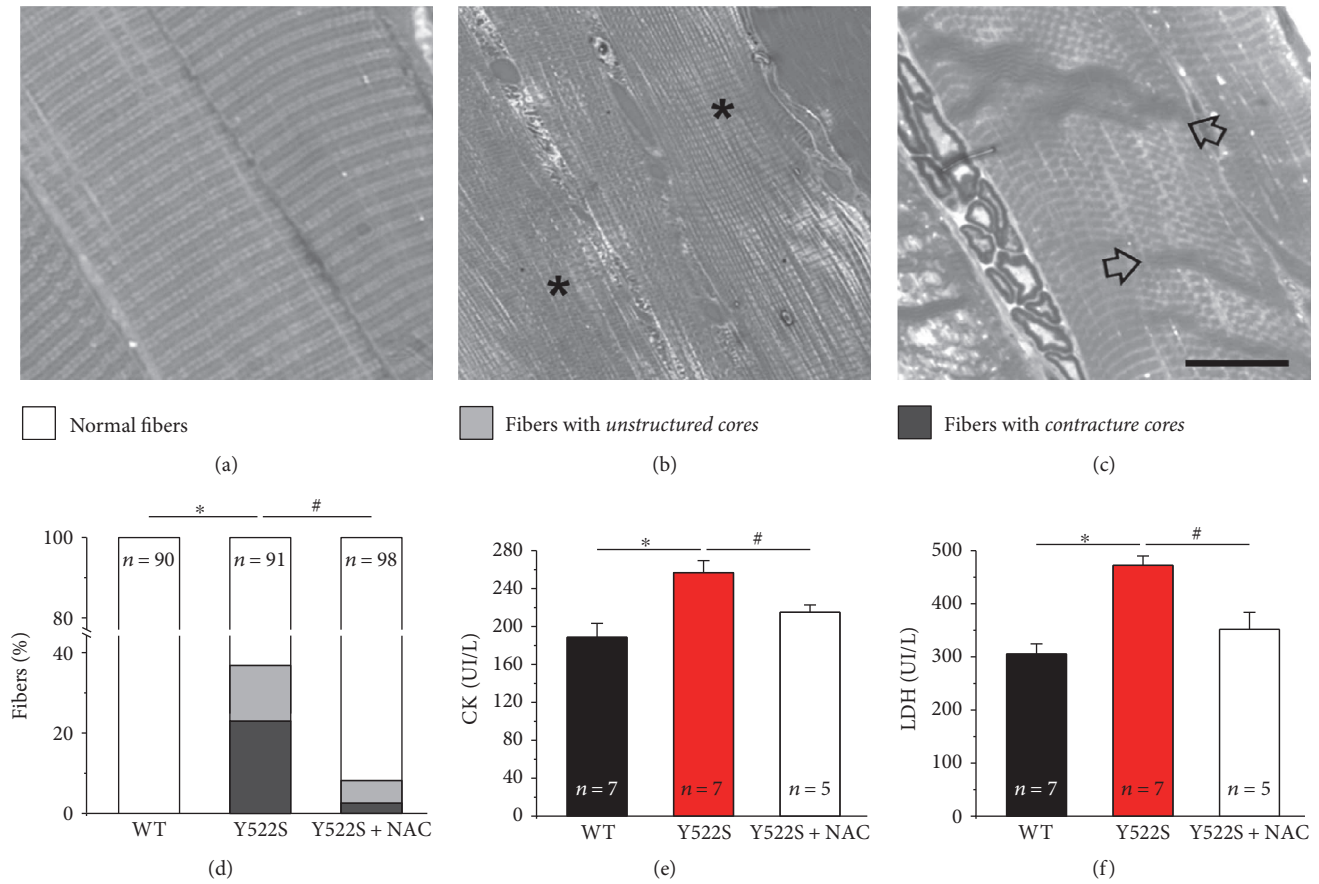

FIGURE 1: Structural *cores* and blood markers of muscle damage (CK and LDH) at 4 months of age. (a–c) Representative histological images of normal fibers (a), fibers with *unstructured cores* (b), and fibers with *contracture cores* (c). (d) Percentage of EDL fibers presenting the features classified in (a–c) (white: *normal fibers*; grey: *fibers with unstructured cores*; and dark grey: *fibers with contracture cores*). See also Table S1. (e and f) Serum levels of creatine kinase (CK) and lactate dehydrogenase (LDH). In (e) and (f), data are given as mean ± SEM; $^{*}p < 0.05$, WT versus RYR1$^{Y522S/WT}$ mice; $^{\#}p < 0.05$, untreated RYR1$^{Y522S/WT}$ versus NAC-treated RYR1$^{Y522S/WT}$ mice. In (d), n = number of fibers analyzed; in (e-f), n = number of mice. *Scale bar: 10 μm*.

reducing the amount of both CK and LDH in blood samples from RYR1$^{Y522S/WT}$ mice to values closer to that of WT (Figures 1(e) and 1(f)), a result consistent with the significant reduction in the incidence of fibers presenting *unstructured* and *contracture cores* (Figure 1(d)).

We also analyzed EDL muscles using a combination of immunofluorescence for CM and EM and assessed proteolytic degradation by measuring calpain activity and carbonyl protein content (Figure 2). In adult EDL fibers from WT mice, both CRUs, marked with an antibody that recognized RYR1, and mitochondria, marked with an antibody that labels translocase of outer mitochondrial membrane 20 homolog (TOM20), form double rows of cross striation (Figure 2(a) and inset). This fluorescence pattern is consistent with positioning of both CRUs and mitochondria at the I band, on either side of the *Z*-line (pointed by arrows in Figures 2(b) and 2(f); see [20] for additional detail on the specific disposition of CRUs and mitochondria in adult skeletal fibers). In RYR1$^{Y522S/WT}$ EDL fibers, this precise cross striation pattern was often compromised (arrow in Figure 2(c) and inset). These areas lacking staining (pointed by arrows in Figure 1(c)) reflect the presence of *contracture cores*, visible in EM as regions with shortened sarcomeres (arrow in Figure 2(d)). NAC treatment in RYR1$^{Y522S/WT}$ mice restored the cross striation pattern in the large majority of fibers (consistent with reduction of fibers with *cores*; Figure 1(d)): both red and green staining were perfectly transversal (Figure 2(e)), while ultrastructure of myofibrils and sarcomeres at the EM examination was virtually indistinguishable from that of WT fibers (compare Figures 2(b) and 2(f)).

The RYR1-Y522S mutation causes leak of Ca^{2+} from the SR [16]. As excessive myoplasmic Ca^{2+} concentration activates calpains that cleave a variety of substrates, including myofibrillar proteins [24, 29, 30], calpain-mediated degradation could contribute to the ultrastructural alterations observed in RYR1$^{Y522S/WT}$ muscle fibers. We measured the total calpain activity, which was markedly elevated in muscles from RYR1$^{Y522S/WT}$ compared to that from WT (Figure 2(g)), but lowered to levels very similar to those from WT following NAC treatment (Figure 2(g)). In addition, we also evaluated the total carbonyl protein content in the same muscle homogenates, an important biomarkers of oxidative modification of proteins [25, 26]. Also in this

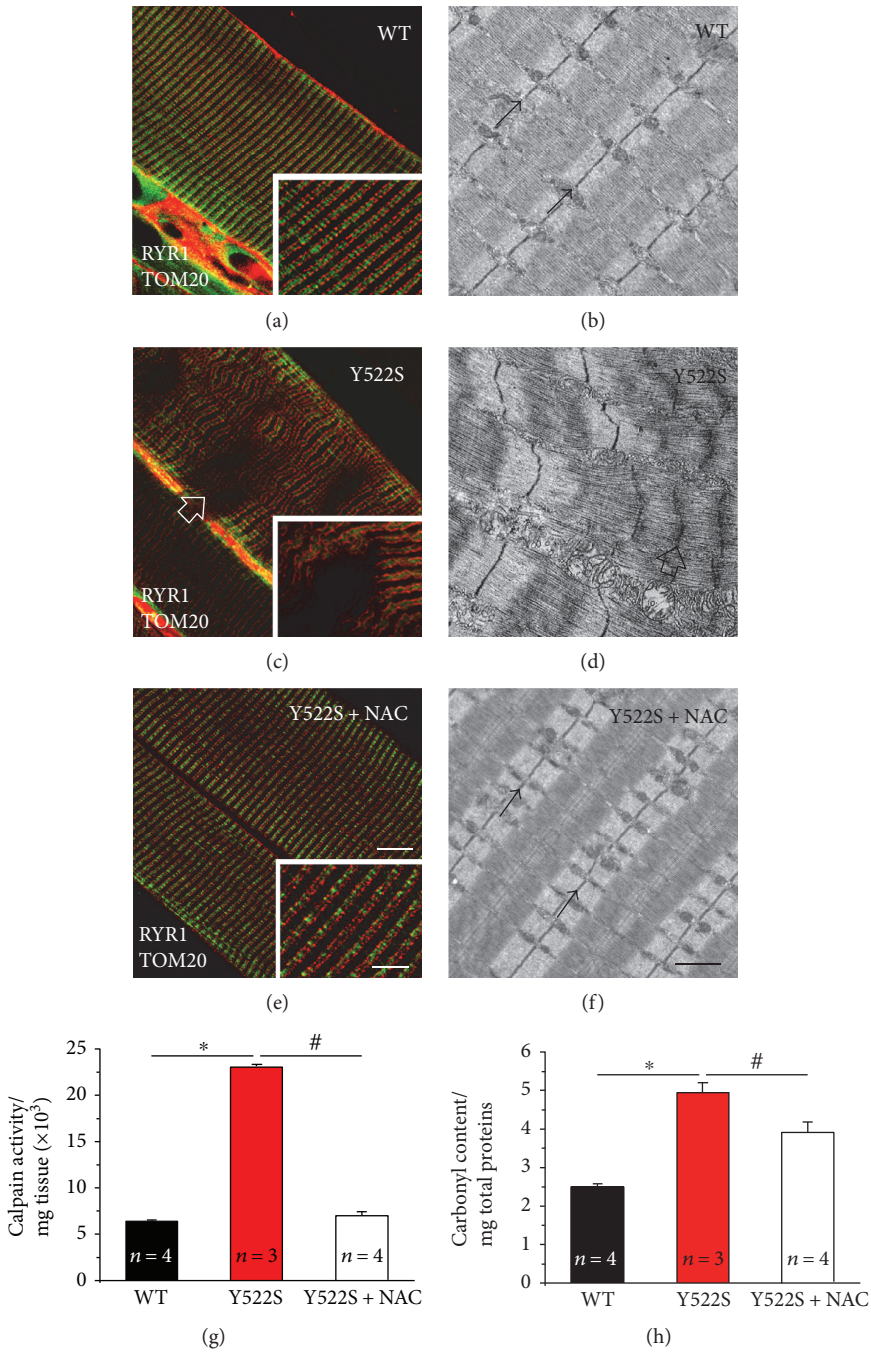

Figure 2: Fiber ultrastructure, calpain activity, and carbonyl protein content at 4 months of age. (a–f) Representative immunofluorescence and EM images showing fluorescent cross striation (a, c, and e) and myofibrillar/sarcomeric organization (b, d, and f) in EDL fibers. In (b) and (f), small arrows point at *Z*-lines, while in (c and d) large arrows point to areas in which cross striation and sarcomeric structure are compromised. (g) Calpain activity expressed in total hind limb muscle homogenates. (h) Carbonyl protein content in EDL muscle homogenates. In (g and h), data are given as mean ± SEM; $^{*}p < 0.05$, WT versus RYR1$^{Y522S/WT}$ mice; $^{\#}p < 0.05$, untreated RYR1$^{Y522S/WT}$ versus NAC-treated RYR1$^{Y522S/WT}$ mice. In (g and h), n = number of mice. *Scale bars* in (a, c, and e) 10 μm (insets 5 μm); in (b, d, and f) 1 μm.

case, the total amount of carbonyl proteins, which was abnormally elevated in RYR1$^{Y522S/WT}$, was lowered of about 20% by NAC treatment, although it remained still higher than that in WT (Figure 2(h)).

3.2. NAC Treatment Improves In Vivo Grip Strength and Ex Vivo Muscle Contractile Function in RYR1$^{Y522S/WT}$ Mice. As NAC treatment was very effective in protecting muscle fibers of RYR1$^{Y522S/WT}$ mice from structural damage, we performed *in vivo* grip strength test and ex vivo contractile experiments on intact EDL muscles, to evaluate whether NAC was also able to improve muscle function of RYR1$^{Y522S/WT}$ knock-in mice. Grip strength was evaluated at 3 different time points between 2 (beginning of the *short-*

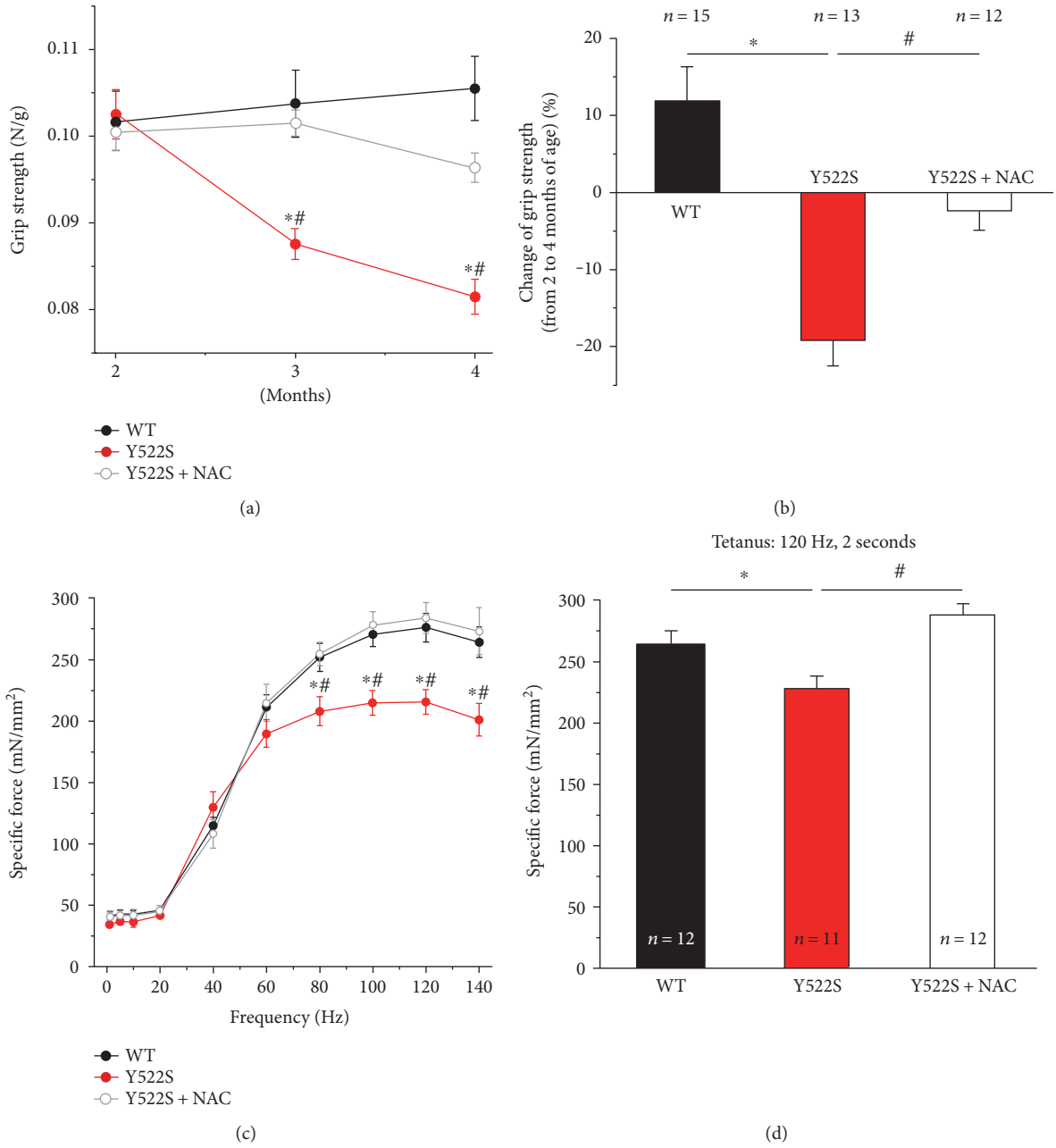

Figure 3: *In vivo* grip strength and ex vivo specific force at 4 months of age. (a) Time-course of grip strength from 2 (beginning of short-term NAC treatment) to 4 months (end of short-term NAC treatment) of age expressed as force on body weight (N/g). (b) Change in grip strength from 2 to 4 months of age (shown as a percentage). (c and d) Force-frequency (1–140 Hz) relationship curves of specific force (c) and specific force during a single 2 s, 120 Hz stimulation train (d) recorded for the same EDL muscles. Data are given as mean ± SEM; $^{*}p < 0.05$, WT versus RYR1$^{Y522S/WT}$ mice; $^{\#}p < 0.05$, untreated RYR1$^{Y522S/WT}$ versus NAC-treated RYR1$^{Y522S/WT}$ mice. In (b), n = number of mice; in (d), n = number of EDL muscles.

term NAC treatment) and 4 months of age (end of *short-term* NAC treatment). Results of these evaluations of force are plotted in Figures 3(a) and 3(b). While no significant difference was found among the three groups of mice tested at 2 months of age, in the following 2 months, (a) WT mice showed a small, but progressive, rise in grip strength of about 10%; (b) untreated RYR1$^{Y522S/WT}$ mice exhibited a pronounced decay, with a force reduction of about 20%; and finally (c) NAC-treated RYR1$^{Y522S/WT}$ mice displayed an ameliorated muscle function compared to untreated RYR1$^{Y522S/WT}$ mice, with a reduction in grasp force of only 4%. To verify if NAC treatment directly improved muscle function, we evaluated ex vivo force-frequency and 2-second tetanic force in isolated EDL muscles at 4 months of age using an *in vitro* setting (Figures 3(c) and 3(d)). The force-frequency relationship curves during high-frequency stimulation (from 80 Hz to 140 Hz) plotted in Figure 3(c) showed that EDL muscles from RYR1$^{Y522S/WT}$ mice

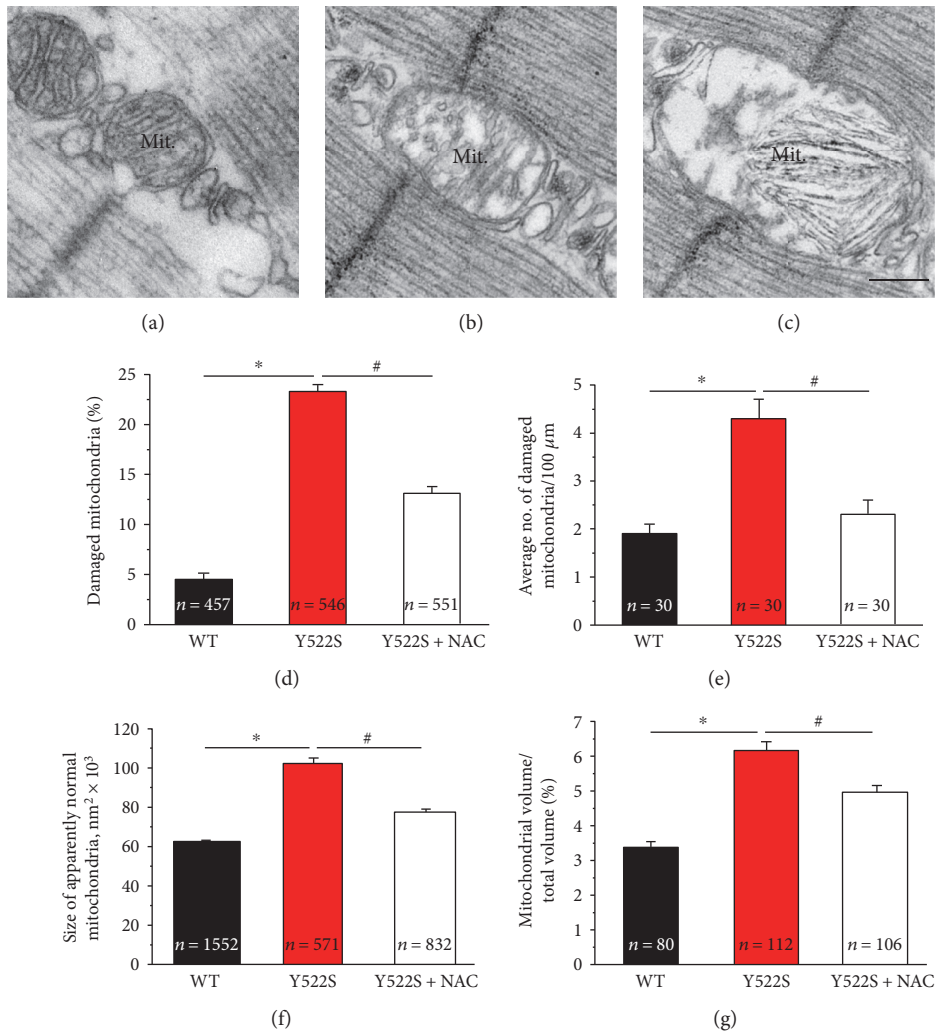

FIGURE 4: Mitochondrial damage, size, and volume at 4 months of age. (a–c) Representative EM images displaying apparently normal (a) and damaged mitochondria (b and c). (d) Percentage of damaged mitochondria. (e) Average number of damaged mitochondria/area of EM section. (f) Average size of apparently normal mitochondria (i.e., mitochondria not included in the quantitative analysis of (d and e)). (g) Percentage of fiber volume occupied by mitochondria. See also Table S2. Data are given as mean ± SEM; $^{*}p < 0.05$, WT versus RYR1$^{Y522S/WT}$ mice; $^{\#}p < 0.05$, untreated RYR1$^{Y522S/WT}$ versus NAC-treated RYR1$^{Y522S/WT}$ mice. In (d and f), n = number of measurements; in (e and g), n = number of fibers analyzed. *Scale bar:* 0.1 μm.

developed a specific force (mN/mm^2) significantly lower than that from WT, force that was efficiently rescued by NAC treatment. Interestingly, the percentage of relative force, normalized to the maximum (F_0), for the half-maximal frequency (Hz_{60}) was significantly higher in RYR1$^{Y522S/WT}$ muscles (87.7 ± 2.8) than that in the WT (74.8 ± 7.4) and NAC-treated RYR1$^{Y522S/WT}$ (77.0 ± 5.6) muscles (Supplementary Figure S2 A). We also evaluated the maximal force developed by the same EDL muscles by applying a single train stimulus (120 Hz for 2 seconds) to generate a fused tetanus (Figure 3(d)). EDL muscles from RYR1$^{Y522S/WT}$ mice exhibited a maximal specific tetanic force significantly lower to that developed by EDL muscles from WT mice (227.2 ± 11.6 versus 264.0 ± 10.6 mN/mm^2); while following two months of NAC treatment, maximal specific tetanic force expressed by EDL muscles from RYR1$^{Y522S/WT}$ mice was rescued to values similar to those of WT muscles (287.7 ± 8.8 mN/mm^2) (Figure 3(d)).

3.3. NAC Treatment Reduces Mitochondrial Swelling and Damage in EDL Muscle of RYR1$^{Y522S/WT}$ Mice. As previously reported, mitochondrial damage underlies formation of *cores* in RYR1$^{Y522S/WT}$ mice [17]. Here, we confirmed previous findings: (a) damaged mitochondria (such as those in Figures 4(b) and 4(c)) were significantly more frequent in EDL fibers from RYR1$^{Y522S/WT}$ mice than in WT (Figures 4(d) and 4(e)); (b) also, mitochondria that are apparently normal (dark appearance, such as that in Figure 4(a)) were larger in size, suggesting that the organelles are swollen (Figure 4(f)); (c) total mitochondrial volume was increased in fibers from RYR1$^{Y522S/WT}$ (Figure 4(g)). *Short-term* NAC treatment significantly rescued all these

features: (a) the number of mitochondria presenting structural damage was decreased in fibers from mice treated with NAC (Figures 4(d) and 4(e)); (b) treatment of RYR1$^{Y522S/WT}$ mice with NAC was also effective in reducing the size of apparently normal mitochondria and the relative fiber volume occupied by these organelles (Figures 4(f) and 4(g)). Data plotted in Figures 4(d), 4(e), 4(f), and 4(g) are reported in Table S2.

As in adult skeletal muscle, mitochondria are usually closely associated with CRUs [20]; here, we verified whether NAC exert a beneficial effect on the CRU-mitochondrial interaction. We evaluated the frequency of mitochondria, CRUs, and mitochondria-CRU pairs (Supplementary Figure S1): (a) number/area of both mitochondria and CRUs is decreased in RYR1$^{Y522S/WT}$ compared to that in WT (Supplementary Figure S1 B and C), which in turn causes a great reduction in the number/area of mitochondria-CRU pairs (Supplementary Figure S1 D). Treatment with NAC was able to partially rescue the number/area of mitochondria (Supplementary Figure S1 B) and of mitochondria-CRU pairs (Supplementary Figure S1 D). However, NAC was not able to rescue the number/area of CRUs (Supplementary Figure S1 C). Data plotted in Supplementary Figure S1 B-C are reported in Table S3.

3.4. NAC Was Effective in Preventing Decay of Muscle Structure/Function in RYR1$^{Y522S/WT}$ Mice Also during Long-Term Treatment. We have previously shown that fiber damage in RYR1$^{Y522S/WT}$ mice becomes quite severe with increasing age [17]. Here, we tested the *long-term* efficacy of NAC in reducing/preventing structural and functional decay of RYR1$^{Y522S/WT}$ fibers by treating mice for 6 months with NAC, starting at 4 months of age when structural damage was already at an advanced stage. Results of these experiments are shown in Figure 5: (a) the percentage of fibers presenting *unstructured* and *contracture cores* (resp., 18% and 30% in RYR1$^{Y522S/WT}$ mice) was significantly reduced (10% and 13%, resp.) by NAC administration (Figure 5(a)). Data plotted in Figure 5(a) are reported in Table S4. As done in samples from 4-month-old mice treated for 2 months, we also measured blood levels of CK and LDH at 10 months of age following 6 months of NAC treatment: both CK and LDH were significantly elevated in RYR1$^{Y522S/WT}$ muscles compared to WT, but significantly lowered by NAC (Figures 5(b) and 5(c)).

Rescue of muscle damage by the *long-term* NAC treatment was also accompanied by functional improvements (Figures 5(d), 5(e), 5(f), and 5(g)). Indeed, although grip strength from 4 to 10 months of age show a slight decrease in all groups of animals (Figure 5(d)), the time-dependent decay of strength was significantly more pronounced in RYR1$^{Y522S/WT}$ mice (~−30%), compared to both WT (~−10%) and NAC-treated RYR1$^{Y522S/WT}$ (~−10%) mice (Figure 5(e)). Finally, *long-term* NAC treatment was also effective in restoring the kinetic-contractility properties (i.e., force frequency and tetanic force) of isolated EDL muscles from RYR1$^{Y522S/WT}$ mice, which were weaker than WT when untreated (Figures 5(f) and 5(g) and Supplementary Figure S2 B).

3.5. NAC Treatment Reduces 3-Nitrotyrosine (3-NT) and SOD2 Levels in Skeletal Muscle from RYR1$^{Y522S/WT}$ Mice. We measured in WT, and in untreated or NAC-treated RYR1$^{Y522S/WT}$ mice (both at 4 and 10 months of age), (i) levels of 3-Nitrotyrosine (3-NT), a product of nitration of tyrosine residues of proteins mediated by RNS such as peroxynitrite anion and nitrogen dioxide, which are indicators of oxidative protein damage and inflammation [31–34]; (ii) expression levels of superoxide dismutase types 1 and 2 (SOD1 and SOD2), the two main intracellular enzymes, respectively, localized in the cytoplasm and within mitochondrial matrix, that catalyze the dismutation of anion ($O_2^{\bullet-}$) into O_2 and hydrogen peroxide (H_2O_2) [35–37], the first step in the elimination of reactive species of oxygen (ROS). WB analyses (Figure 6(a and e)), performed on total hind limb muscle homogenates, revealed that the amount of 3-NT was significantly higher in RYR1$^{Y522S/WT}$ compared to WT mice, with a ~1.5-fold increase (Figure 6(b and f)). NAC treatment normalized 3-NT level to values similar to those of WT mice (Figure 6(a, b, e, and f)). In the same samples, we also measured SOD1 and SOD2 protein contents (Figure 6(a and e)): while there were no differences in SOD1 levels among the three groups of mice (Figure 6(a, c, e, and g)), SOD2 in RYR1$^{Y522S/WT}$ muscles was ~1.5 times higher than that in WT muscles (Figure 6(a, d, e, and h)); also, in this case, NAC treatment brought back SOD2 levels to values closer to those of WT (Figure 6(a, d, e, and h)).

4. Discussion

The substitution of a tyrosine with a serine in position 522 (Y522S) of RYR1 results in gain-of-function of the SR Ca^{2+} release channel linked, in humans, to MH with formation of *cores* [10]. The expression of this mutation in an animal model successfully reproduced the human phenotype, as heterozygous RYR1$^{Y522S/WT}$ knock-in mice are MH susceptible [15] and develop structural abnormalities resembling human CCD [17]. The formation of *unstructured* and *contracture cores* in RYR1$^{Y522S/WT}$ muscle fibers is initiated by mitochondrial damage, with abnormalities that then extend to sarcotubular system and contractile elements [17]. The mechanisms linking the RYR1 mutation to the mitochondrial damage in RYR1$^{Y522S/WT}$ muscle fibers are still not fully understood: one possibility is that Ca^{2+}-dependant overproduction of ROS and RNS plays a direct role in the destruction of mitochondria [16, 17].

4.1. Main Findings of the Present Paper: NAC Ameliorates Structure and Function of RYR1$^{Y522S/WT}$ Muscle by Reducing Oxidative Stress. NAC was previously used to reduce oxidative stress and normalize SR Ca^{2+} release in RYR1$^{Y522S/WT}$ mice and in [16] mice lacking calsequestrin-1 (CASQ1-null) [19, 38]. NAC treatment also reduced the rate of mortality [19] and prevented mitochondrial damage [39] in CASQ1-null mice that, similarly to RYR1$^{Y522S/WT}$ mice, triggers lethal MH episodes when exposed to halogenated anesthetics and heat [40, 41]. The results of the present paper demonstrate that NAC treatment in RYR1$^{Y522S/WT}$ mice (i) reduces formation of *unstructured* and *contracture*

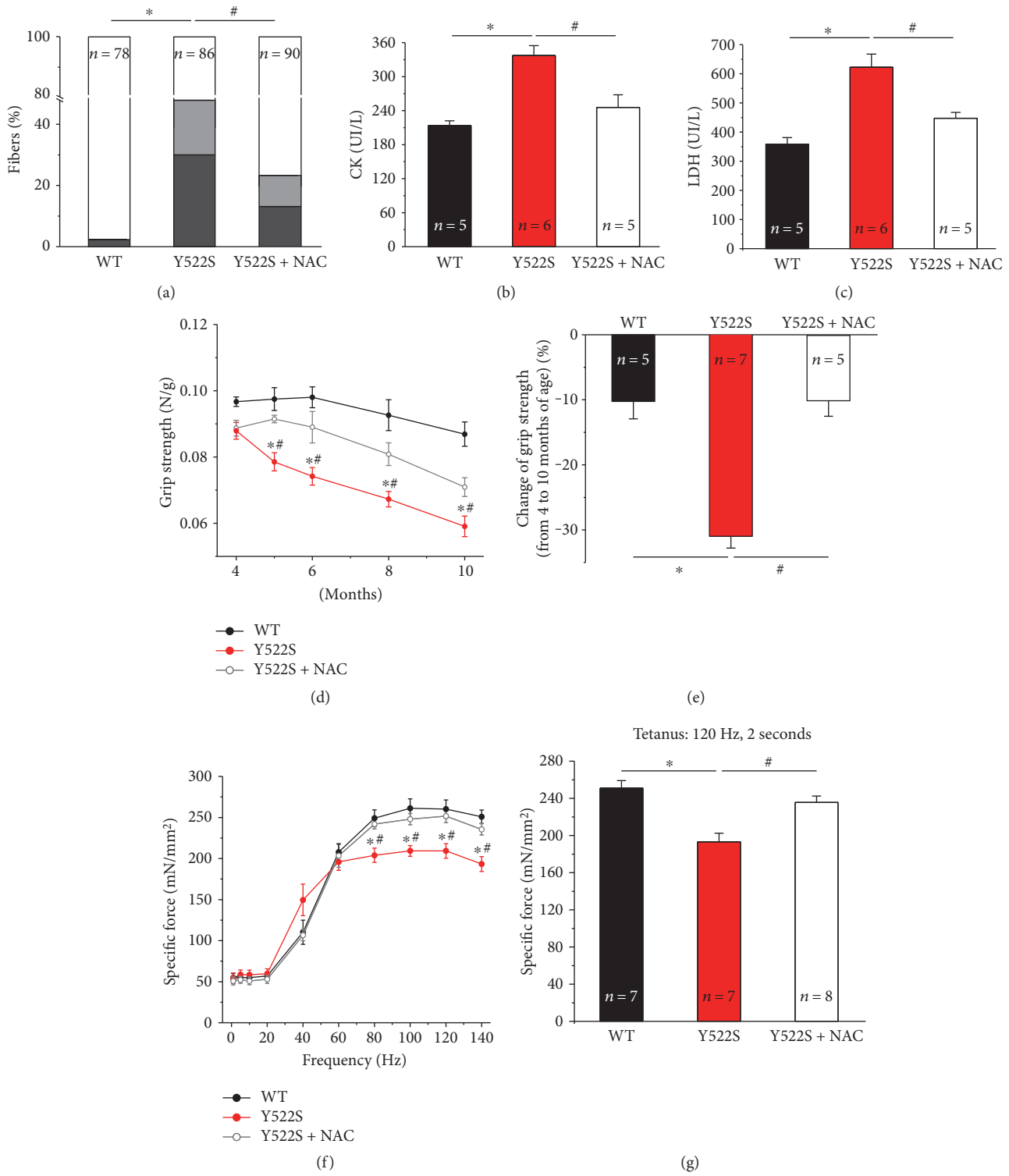

FIGURE 5: Effects of *long-term* NAC treatment at 10 months of age. (a) Quantitative analysis of EDL fibers presenting the features classified in Figures 1(a), 1(b), and 1(c) shown as percentage of fibers analyzed (white: *normal fibers*; grey: *fibers with unstructured cores*; and dark grey: *fibers with contracture cores*). See also Table S4. (b and c) Serum levels of creatine kinase (CK) and lactate dehydrogenase (LDH). (d) Time course of grip strength from 4 (beginning of *long-term* NAC treatment) to 10 months (end of *long-term* NAC treatment) of age expressed as force on body weight (N/g). (e) Change in grip strength from 4 to 10 months of age (shown as a percentage). (f and g) Force-frequency (1–140 Hz) relationship curves of specific force (f) and specific force during a single 2 s, 120 Hz stimulation train (g) recorded for the same EDL muscles. In s (b–g), data are given as mean ± SEM; $^{*}p < 0.05$, WT versus RYR1$^{Y522S/WT}$ mice; $^{\#}p < 0.05$, untreated RYR1$^{Y522S/WT}$ versus NAC-treated RYR1$^{Y522S/WT}$ mice. In (a), n = number of EDL fibers analyzed; in (b–e), n = number of mice; in (f and g), n = number of EDL muscles.

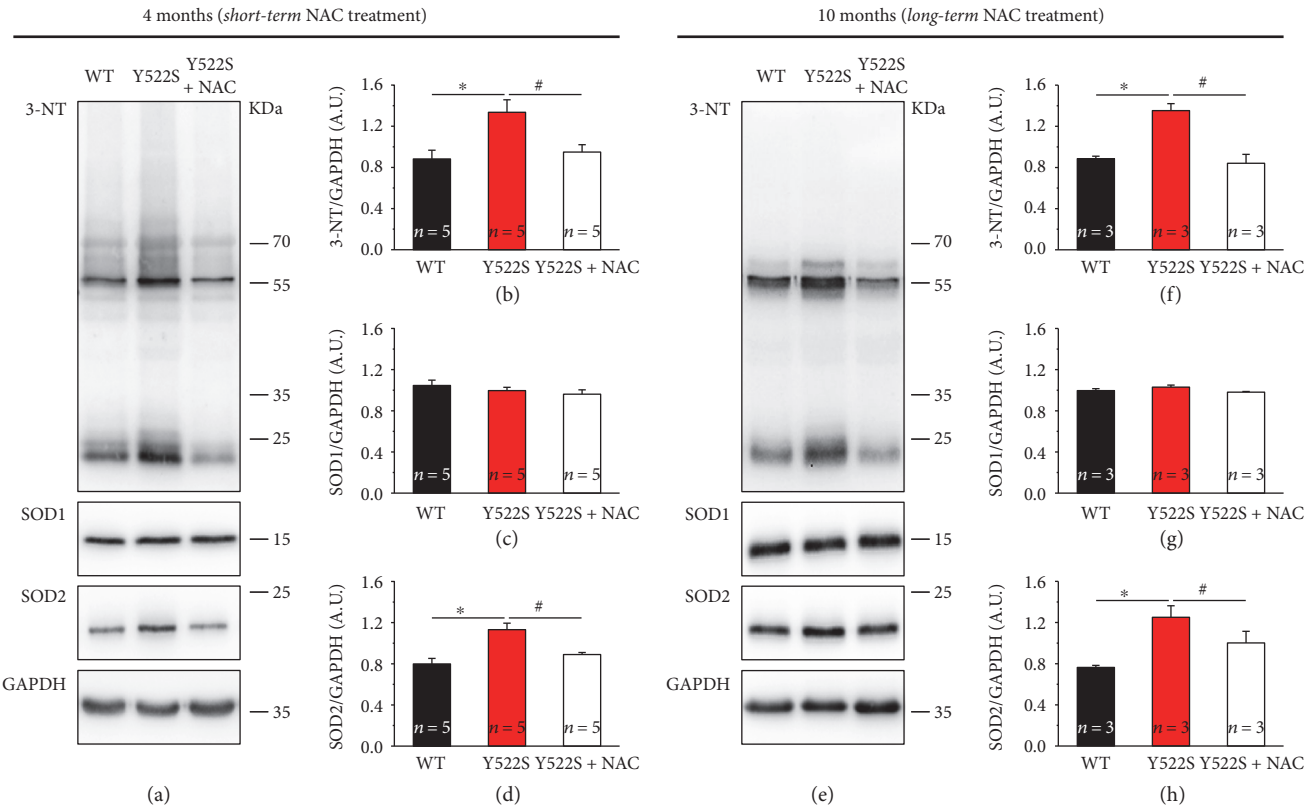

Figure 6: Oxidative stress markers at 4 and 10 months of age following either *short-* or *long-term* treatment. (a and e) Representative immunoblots showing expression of 3-Nitrotyrosine (3-NT), SOD1, and SOD2 in total hind limb muscle homogenates. (b–d) and (f–h) Relative band densities normalized to GAPDH levels. Data are given as mean ± SEM; $^{*}p < 0.05$, WT versus RYR1$^{Y522S/WT}$ mice; $^{\#}p < 0.05$, untreated RYR1$^{Y522S/WT}$ versus NAC-treated RYR1$^{Y522S/WT}$ mice. n = number of mice.

cores (Figures 1 and 2) and (ii) improves muscle function, both *in vivo* (grip strength) and ex vivo during electrical stimulation of isolated EDLs (Figure 3). The beneficial effect of NAC treatment on structure/function of RYR1$^{Y522S/WT}$ muscles is evident both when mice were treated starting at 2 months of age, that is, when mitochondrial and fiber damage was still minimal, but also in mice treated for extended periods (6 months of NAC administration; Figure 5) starting at 4 months of age when structural damage was already at an advanced stage, as quantitative analysis in Figure 4 points to significant protection from mitochondrial damage. The reduced formation of *cores* in NAC-treated RYR1$^{Y522S/WT}$ mice could result from the beneficial effect that this treatment exerts on mitochondrial morphology (Figure 4), as we have previously shown that mitochondrial damage plays a pivotal role in the formation of structural *cores* in this mouse model [17].

The role that oxidative stress plays in the events leading to mitochondrial damage and formation of *cores* in CCD has been long discussed. Our present data shows that in NAC-treated RYR1$^{Y522S/WT}$ mice, displaying improved fiber structure/function and reduced mitochondrial damage (Figures 1, 2, 3, 4, and 5), oxidative stress is significantly lower than that in untreated RYR1$^{Y522S/WT}$ mice (Figure 6). In line with these data, we have previously shown that treatment with antioxidants (NAC and Trolox) also lowered oxidative stress in mice with a similar phenotype [19, 39]. Specifically, levels of 3-NT and SOD2, but not of SOD1, which were significantly increased in RYR1$^{Y522S/WT}$ muscles, are reduced to levels more similar to WT following both *short-* and *long-term* NAC treatments (Figure 6). In general, the augmented expression of SOD1 and SOD2 likely reflects a compensatory response to excessive production of ROS [42], a finding in agreement with the observation that the expression of both isoforms increased under different physiopathological conditions in which oxidative stress is elevated [23, 43–46]. The fact that the SOD2 isoform, but not SOD1, is upregulated (Figure 6) suggests that (a) the $O_2^{\bullet-}$ generated in the mitochondrial matrix plays a central role in the elevated oxidative stress damaging mitochondria and fibers in RYR1$^{Y522S/WT}$ muscles [18] and (b) the effect of mitochondrial-targeted antioxidants should be tested in future studies.

4.2. Possible Molecular Mechanisms Linking Excessive SR Ca^{2+} Leak to Oxidative Stress, Mitochondrial Damage, and Formation of Cores. In RYR1$^{Y522S/WT}$ fibers, myoplasmic Ca^{2+} and oxidative stress are both chronically elevated [16, 18]. The Y522S gain-of-function mutation is directly responsible of excessive SR Ca^{2+} leak, whereas the elevated oxidative stress could result from (a) excessive mitochondrial Ca^{2+} uptake, which is known to stimulate the aerobic

metabolism [47, 48] and/or (b) increased ATP demand due to the constant need of actively removing excessive myoplasmic Ca^{2+} (by ATP-dependent reuptake into the SR or extrusion in the extracellular space). In turn, Ca^{2+} leak and oxidative stress are linked together in a loop where ROS/RNS results in oxidative modifications of RYR1 channel that enhances the opening probability of the channel and, thus, further Ca^{2+} release from the SR [16]. The accumulation of myoplasmic Ca^{2+} could also result from ROS/RNS-dependent decrease in the activity of both sarcoplasmic/endoplasmic reticulum Ca^{2+} ATPase (SERCA) [49] and plasma membrane Ca^{2+}-ATPase (PMCA). Although mitochondrial Ca^{2+} uptake in RYR1$^{Y522S/WT}$ fibers has not been directly measured, chronic elevation of myoplasmic Ca^{2+} could likely result in mitochondrial Ca^{2+} overload, loss of mitochondrial membrane potential, and swelling [50, 51]. The precise disposition of mitochondria next to CRUs (which contain RYR1) in skeletal muscle fibers [20], and their cross talk-based Ca^{2+} signaling [52–56], places these organelles in the unfortunate location to be directly exposed to the excessive Ca^{2+} leak through the mutated RYR1-Y522S channel. In ongoing experiments, we are currently investigating mitochondrial Ca^{2+} uptake in RYR1$^{Y522S/WT}$ fibers.

Chronic Ca^{2+} elevation and ROS/RNS overproduction are likely key players also in proteolysis of contractile elements and oxidation of proteins and lipids of intracellular organelles, such as CRUs and mitochondria. Increased intracellular Ca^{2+} concentration has been linked to muscle damage, mitochondrial swelling, and degeneration of myofibrils, [57–59] and activation of calpains, one of the most important nonlysosomal classes of proteases in skeletal muscle fibers, is indeed activated by increased Ca^{2+} levels [60–62] and by excessive oxidative stress [34, 63, 64]. Activation of calpains has been shown to promote degradation of specific sarcomeric proteins such as titin [24] and disruption of myofibrils [34, 65, 66]. We recently reported that RYR1$^{Y522S/WT}$ and CASQ1-null mice, both having altered Ca^{2+} handling and elevated oxidative stress, displayed levels of calpain activity significantly higher than WT [67]. Consistent with these data, results of the present study indicate that calpain activity is significantly elevated in RYR1$^{Y522S/WT}$ muscles, suggesting that the activation of this proteolytic system could contribute to the disruption of membrane organelles and myofibrillar architecture during formation of *cores*. In support of this hypothesis, our data showed that NAC treatment reduces calpain levels, formation of structural *cores*, and mitochondrial damage (Figures 1, 2, and 4).

4.3. Conclusions. The mechanism linking mutations in RYR1 to mitochondrial damage (and consequent formation of structural *cores*) in human CCD has been long discussed and still far from being unraveled. Our work provides some additional insights in the pathogenic mechanisms that underlie mitochondrial damage/disappearance in *cores* of RYR1$^{Y522S/WT}$ mice, supporting the idea that SR Ca^{2+} leak and oxidative stress do play a central role in these events. In addition, our results suggest that NAC administration (or more generally treatment with antioxidants) could be taken into consideration as a long-term therapeutic intervention to reduce the development of *cores* and improve muscle function in patients affected by CCD.

Abbreviations

CCD:	Central core disease
CM:	Confocal microscopy
CRU:	Calcium release unit
EC-coupling:	Excitation-contraction coupling
EDL:	Extensor digitorum brevis
EM:	Electron microscopy
NAC:	N-acetylcysteine
ROS and RNS:	Reactive oxygen and nitrogen species
RYR:	Ryanodine receptor
SR:	Sarcoplasmic reticulum
TT:	Transverse tubules
WT:	Wild type.

Disclosure

The abstract of the manuscript was presented in "XII annual meeting of the interuniversity Institute of Myology."

Conflicts of Interest

The authors declare that they have no conflicts of interest.

Authors' Contributions

Simona Boncompagni and Feliciano Protasi conceived and directed the study. Antonio Michelucci, Alessandro De Marco, Flavia A. Guarnier, and Simona Boncompagni performed the experimental work and data analysis. In detail, (a) Antonio Michelucci performed the spectrophotometric analysis of CK and LDH levels in blood samples and the *in vivo* grip strength and ex vivo force and contraction kinetics of intact EDL muscles; (b) Alessandro De Marco and Simona Boncompagni performed the qualitative and quantitative light and EM analysis; (c) Alessandro De Marco performed the western blot experiments; (d) Flavia A. Guarnier performed the measurements of the calpain activity and carbonyl protein content. Finally, Simona Boncompagni, Feliciano Protasi, and Antonio Michelucci wrote the manuscript. Antonio Michelucci and Alessandro De Marco are the cofirst authors. Feliciano Protasi and Simona Boncompagni are the cosenior authors.

Acknowledgments

The authors thank Dr. S. L. Hamilton (Baylor College of Medicine, Houston, TX, USA), who generated and kindly provided the RYR1$^{Y522S/WT}$ mouse line for this study. This study was supported by the following grants: (a) Italian Telethon ONLUS Foundation (Rome, Italy): GGP13213 to Feliciano Protasi; (b) Italian Ministry of Education, University and Research (Rome, Italy): RBFR13A20K to Simona Boncompagni; (c) Italian Ministry of Health, (Rome, Italy): GR-2011-02352681 to Simona Boncompagni; and (d) National Institute of Health (Bethesda, MD, U.S.A): AR053349-06 (subcontract to Feliciano Protasi).

References

[1] K. R. Magee and G. M. Shy, "A new congenital non-progressive myopathy," *Brain*, vol. 79, no. 4, pp. 610–621, 1956.

[2] H. Jungbluth, "Central core disease," *Orphanet Journal of Rare Diseases*, vol. 2, p. 25, 2007.

[3] V. Dubowitz and A. G. Pearse, "Oxidative enzymes and phosphorylase in central-core disease of muscle," *Lancet*, vol. 2, no. 7140, pp. 23-24, 1960.

[4] K. Hayashi, R. G. Miller, and A. K. Brownell, "Central core disease: ultrastructure of the sarcoplasmic reticulum and T-tubules," *Muscle & Nerve*, vol. 12, no. 2, pp. 95–102, 1989.

[5] D. H. Maclennan and E. Zvaritch, "Mechanistic models for muscle diseases and disorders originating in the sarcoplasmic reticulum," *Biochimica et Biophysica Acta*, vol. 1813, no. 5, pp. 948–964, 2011.

[6] C. Franzini-Armstrong and F. Protasi, "Ryanodine receptors of striated muscles: a complex channel capable of multiple interactions," *Physiological Reviews*, vol. 77, no. 3, pp. 699–729, 1997.

[7] M. F. Schneider, "Control of calcium release in functioning skeletal muscle fibers," *Annual Review of Physiology*, vol. 56, pp. 463–484, 1994.

[8] M. A. Denborough, K. C. Hopkinson, and D. G. Banney, "Firefighting and malignant hyperthermia," *British Medical Journal (Clinical Research Edition)*, vol. 296, no. 6634, pp. 1442-1443, 1988.

[9] D. H. MacLennan, K. Otsu, J. Fujii et al., "The role of the skeletal muscle ryanodine receptor gene in malignant hyperthermia," *Symposia of the Society for Experimental Biology*, vol. 46, pp. 189–201, 1992.

[10] K. A. Quane, J. M. Healy, K. E. Keating et al., "Mutations in the ryanodine receptor gene in central core disease and malignant hyperthermia," *Nature Genetics*, vol. 5, no. 1, pp. 51–55, 1993.

[11] M. A. Denborough, X. Dennett, and R. M. Anderson, "Central-core disease and malignant hyperpyrexia," *British Medical Journal*, vol. 1, no. 5848, pp. 272-273, 1973.

[12] G. D. Eng, B. S. Epstein, W. K. Engel, D. W. McKay, and R. McKay, "Malignant hyperthermia and central core disease in a child with congenital dislocating hips," *Archives of Neurology*, vol. 35, no. 4, pp. 189–197, 1978.

[13] G. B. Frank, "The current view of the source of trigger calcium in excitation-contraction coupling in vertebrate skeletal muscle," *Biochemical Pharmacology*, vol. 29, no. 18, pp. 2399–2406, 1980.

[14] A. Shuaib, R. T. Paasuke, and K. W. Brownell, "Central core disease. Clinical features in 13 patients," *Medicine (Baltimore)*, vol. 66, no. 5, pp. 389–396, 1987.

[15] M. G. Chelu, S. A. Goonasekera, W. J. Durham et al., "Heat- and anesthesia-induced malignant hyperthermia in an RyR1 knock-in mouse," *The FASEB Journal*, vol. 20, no. 2, pp. 329-330, 2006.

[16] W. J. Durham, P. Aracena-Parks, C. Long et al., "RyR1 S-nitrosylation underlies environmental heat stroke and sudden death in Y522S RyR1 knockin mice," *Cell*, vol. 133, no. 1, pp. 53–65, 2008.

[17] S. Boncompagni, A. E. Rossi, M. Micaroni et al., "Characterization and temporal development of *cores* in a mouse model of malignant hyperthermia," *Proceedings of the National Academy of Sciences of the United States of America*, vol. 106, no. 51, pp. 21996–22001, 2009.

[18] L. Wei, G. Salahura, S. Boncompagni et al., "Mitochondrial superoxide flashes: metabolic biomarkers of skeletal muscle activity and disease," *The FASEB Journal*, vol. 25, no. 9, pp. 3068–3078, 2011.

[19] A. Michelucci, C. Paolini, M. Canato et al., "Antioxidants protect calsequestrin-1 knockout mice from halothane- and heat-induced sudden death," *Anesthesiology*, vol. 123, no. 3, pp. 603–617, 2015.

[20] S. Boncompagni, A. E. Rossi, M. Micaroni et al., "Mitochondria are linked to calcium stores in striated muscle by developmentally regulated tethering structures," *Molecular Biology of the Cell*, vol. 20, no. 3, pp. 1058–1067, 2009.

[21] B. A. Mobley and B. R. Eisenberg, "Sizes of components in frog skeletal muscle measured by methods of stereology," *The Journal of General Physiology*, vol. 66, no. 1, pp. 31–45, 1975.

[22] A. V. Loud, "A method for the quantitative estimation of cytoplasmic structures," *The Journal of Cell Biology*, vol. 15, no. 3, pp. 481–487, 1962.

[23] L. Pietrangelo, A. D'Incecco, A. Ainbinder et al., "Age-dependent uncoupling of mitochondria from Ca^{2+} release units in skeletal muscle," *Oncotarget*, vol. 6, no. 34, pp. 35358–35371, 2015.

[24] D. E. Goll, V. F. Thompson, H. Li, W. Wei, and J. Cong, "The calpain system," *Physiological Reviews*, vol. 83, no. 3, pp. 731–801, 2003.

[25] A. Z. Reznick and L. Packer, "Oxidative damage to proteins: spectrophotometric method for carbonyl assay," *Methods in Enzymology*, vol. 233, pp. 357–363, 1994.

[26] D. Weber, M. J. Davies, and T. Grune, "Determination of protein carbonyls in plasma, cell extracts, tissue homogenates, isolated proteins: focus on sample preparation and derivatization conditions," *Redox Biology*, vol. 5, pp. 367–380, 2015.

[27] A. M. Connolly, R. M. Keeling, S. Mehta, A. Pestronk, and J. R. Sanes, "Three mouse models of muscular dystrophy: the natural history of strength and fatigue in dystrophin-, dystrophin/utrophin-, and laminin alpha2-deficient mice," *Neuromuscular Disorders*, vol. 11, no. 8, pp. 703–712, 2001.

[28] P. Brancaccio, G. Lippi, and N. Maffulli, "Biochemical markers of muscular damage," *Clinical Chemistry and Laboratory Medicine*, vol. 48, no. 6, pp. 757–767, 2010.

[29] J. Huang and N. E. Forsberg, "Role of calpain in skeletal-muscle protein degradation," *Proceedings of the National Academy of Sciences of the United States of America*, vol. 95, no. 21, pp. 12100–12105, 1998.

[30] J. Huang and X. Zhu, "The molecular mechanisms of calpains action on skeletal muscle atrophy," *Physiological Research*, vol. 65, no. 4, pp. 547–560, 2016.

[31] K. Ogino and D. H. Wang, "Biomarkers of oxidative/nitrosative stress: an approach to disease prevention," *Acta Medica Okayama*, vol. 61, no. 4, pp. 181–189, 2007.

[32] T. Grune, K. Merker, T. Jung, N. Sitte, and K. J. Davies, "Protein oxidation and degradation during postmitotic senescence," *Free Radical Biology & Medicine*, vol. 39, no. 9, pp. 1208–1215, 2005.

[33] T. Jung, M. Engels, B. Kaiser, D. Poppek, and T. Grune, "Intracellular distribution of oxidized proteins and proteasome in HT22 cells during oxidative stress," *Free Radical Biology & Medicine*, vol. 40, no. 8, pp. 1303–1312, 2006.

[34] S. K. Powers, J. Duarte, A. N. Kavazis, and E. E. Talbert, "Reactive oxygen species are signalling molecules for skeletal muscle adaptation," *Experimental Physiology*, vol. 95, no. 1, pp. 1–9, 2010.

[35] J. M. McCord and I. Fridovich, "The utility of superoxide dismutase in studying free radical reactions. I. Radicals generated by the interaction of sulfite, dimethyl sulfoxide, and oxygen," *The Journal of Biological Chemistry*, vol. 244, no. 22, pp. 6056–6063, 1969.

[36] S. Marklund and G. Marklund, "Involvement of the superoxide anion radical in the autoxidation of pyrogallol and a convenient assay for superoxide dismutase," *European Journal of Biochemistry*, vol. 47, no. 3, pp. 469–474, 1974.

[37] I. Fridovich, "Superoxide anion radical (O_2^-), superoxide dismutases, and related matters," *The Journal of Biological Chemistry*, vol. 272, no. 30, pp. 18515–18517, 1997.

[38] C. Paolini, M. Quarta, A. Nori et al., "Reorganized stores and impaired calcium handling in skeletal muscle of mice lacking calsequestrin-1," *The Journal of Physiology*, vol. 583, Part 2, pp. 767–784, 2007.

[39] C. Paolini, M. Quarta, L. Wei-LaPierre et al., "Oxidative stress, mitochondrial damage, and *cores* in muscle from calsequestrin-1 knockout mice," *Skeletal Muscle*, vol. 5, p. 10, 2015.

[40] M. Dainese, M. Quarta, A. D. Lyfenko et al., "Anesthetic- and heat-induced sudden death in calsequestrin-1-knockout mice," *The FASEB Journal*, vol. 23, no. 6, pp. 1710–1720, 2009.

[41] F. Protasi, C. Paolini, and M. Dainese, "Calsequestrin-1: a new candidate gene for malignant hyperthermia and exertional/environmental heat stroke," *The Journal of Physiology*, vol. 587, Part 13, pp. 3095–3100, 2009.

[42] F. A. Guarnier, A. L. Cecchini, A. A. Suzukawa et al., "Time course of skeletal muscle loss and oxidative stress in rats with Walker 256 solid tumor," *Muscle & Nerve*, vol. 42, no. 6, pp. 950–958, 2010.

[43] J. M. Gutteridge and B. Halliwell, *Radicals in Biology and Medicine*, Oxford University Press, Oxford, Fourth edition, 2007.

[44] M. H. Disatnik, J. Dhawan, Y. Yu et al., "Evidence of oxidative stress in mdx mouse muscle: studies of the pre-necrotic state," *Journal of the Neurological Sciences*, vol. 161, no. 1, pp. 77–84, 1998.

[45] J. M. Lawler, W. Song, and S. R. Demaree, "Hindlimb unloading increases oxidative stress and disrupts antioxidant capacity in skeletal muscle," *Free Radical Biology & Medicine*, vol. 35, no. 1, pp. 9–16, 2003.

[46] P. M. Abruzzo, S. di Tullio, C. Marchionni et al., "Oxidative stress in the denervated muscle," *Free Radical Research*, vol. 44, no. 5, pp. 563–576, 2010.

[47] R. M. Denton and J. G. McCormack, "The calcium sensitive dehydrogenases of vertebrate mitochondria," *Cell Calcium*, vol. 7, no. 5-6, pp. 377–386, 1986.

[48] P. R. Territo, S. A. French, and R. S. Balaban, "Simulation of cardiac work transitions, in vitro: effects of simultaneous Ca^{2+} and ATPase additions on isolated porcine heart mitochondria," *Cell Calcium*, vol. 30, no. 1, pp. 19–27, 2001.

[49] S. K. Powers and M. J. Jackson, "Exercise-induced oxidative stress: cellular mechanisms and impact on muscle force production," *Physiological Reviews*, vol. 88, no. 4, pp. 1243–1276, 2008.

[50] Q. Chen, Y. C. Chai, S. Mazumder et al., "The late increase in intracellular free radical oxygen species during apoptosis is associated with cytochrome c release, caspase activation, and mitochondrial dysfunction," *Cell Death and Differentiation*, vol. 10, no. 3, pp. 323–334, 2003.

[51] W. Wang, H. Fang, L. Groom et al., "Superoxide flashes in single mitochondria," *Cell*, vol. 134, no. 2, pp. 279–290, 2008.

[52] R. Rudolf, M. Mongillo, P. J. Magalhaes, and T. Pozzan, "In vivo monitoring of Ca^{2+} uptake into mitochondria of mouse skeletal muscle during contraction," *The Journal of Cell Biology*, vol. 166, no. 4, pp. 527–536, 2004.

[53] C. Caputo and P. Bolanos, "Effect of mitochondria poisoning by FCCP on Ca^{2+} signaling in mouse skeletal muscle fibers," *Pflügers Archiv*, vol. 455, no. 4, pp. 733–743, 2008.

[54] A. E. Rossi, S. Boncompagni, and R. T. Dirksen, "Sarcoplasmic reticulum-mitochondrial symbiosis: bidirectional signaling in skeletal muscle," *Exercise and Sport Sciences Reviews*, vol. 37, no. 1, pp. 29–35, 2009.

[55] A. E. Rossi, S. Boncompagni, L. Wei, F. Protasi, and R. T. Dirksen, "Differential impact of mitochondrial positioning on mitochondrial Ca^{2+} uptake and Ca^{2+} spark suppression in skeletal muscle," *American Journal of Physiology. Cell Physiology*, vol. 301, no. 5, pp. C1128–C1139, 2011.

[56] C. Franzini-Armstrong and S. Boncompagni, "The evolution of the mitochondria-to-calcium release units relationship in vertebrate skeletal muscles," *Journal of Biomedicine & Biotechnology*, vol. 2011, Article ID 830573, 9 pages, 2011.

[57] C. J. Duncan, "Role of intracellular calcium in promoting muscle damage: a strategy for controlling the dystrophic condition," *Experientia*, vol. 34, no. 12, pp. 1531–1535, 1978.

[58] D. G. Allen, N. P. Whitehead, and E. W. Yeung, "Mechanisms of stretch-induced muscle damage in normal and dystrophic muscle: role of ionic changes," *The Journal of Physiology*, vol. 567, no. 3, pp. 723–735, 2005.

[59] A. R. Burr and J. D. Molkentin, "Genetic evidence in the mouse solidifies the calcium hypothesis of myofiber death in muscular dystrophy," *Cell Death and Differentiation*, vol. 22, no. 9, pp. 1402–1412, 2015.

[60] D. E. Croall and G. N. DeMartino, "Calcium-activated neutral protease (calpain) system: structure, function, and regulation," *Physiological Reviews*, vol. 71, no. 3, pp. 813–847, 1991.

[61] P. Costelli, P. Reffo, F. Penna, R. Autelli, G. Bonelli, and F. M. Baccino, "Ca^{2+}-dependent proteolysis in muscle wasting," *The International Journal of Biochemistry & Cell Biology*, vol. 37, no. 10, pp. 2134–2146, 2005.

[62] H. Gissel, "The role of Ca^{2+} in muscle cell damage," *Annals of the New York Academy of Sciences*, vol. 1066, pp. 166–180, 2005.

[63] A. J. Smuder, A. N. Kavazis, M. B. Hudson, W. B. Nelson, and S. K. Powers, "Oxidation enhances myofibrillar protein degradation via calpain and caspase-3," *Free Radical Biology & Medicine*, vol. 49, no. 7, pp. 1152–1160, 2010.

[64] E. Dargelos, C. Brule, P. Stuelsatz et al., "Up-regulation of calcium-dependent proteolysis in human myoblasts under acute oxidative stress," *Experimental Cell Research*, vol. 316, no. 1, pp. 115–125, 2010.

[65] T. Tiago, P. S. Palma, C. Gutierrez-Merino, and M. Aureliano, "Peroxynitrite-mediated oxidative modifications of myosin and implications on structure and function," *Free Radical Research*, vol. 44, no. 11, pp. 1317–1327, 2010.

[66] M. Fedorova, N. Kuleva, and R. Hoffmann, "Identification, quantification, and functional aspects of skeletal muscle protein-carbonylation in vivo during acute oxidative stress," *Journal of Proteome Research*, vol. 9, no. 5, pp. 2516–2526, 2010.

[67] A. Michelucci, C. Paolini, S. Boncompagni, M. Canato, C. Reggiani, and F. Protasi, "Strenuous exercise triggers a life-threatening response in mice susceptible to malignant hyperthermia," *The FASEB Journal*, 2017.

Hindawi
Oxidative Medicine and Cellular Longevity
Volume 2017, Article ID 6936897, 15 pages
https://doi.org/10.1155/2017/6936897

Research Article

Estrogens Protect Calsequestrin-1 Knockout Mice from Lethal Hyperthermic Episodes by Reducing Oxidative Stress in Muscle

Antonio Michelucci,[1,2] Simona Boncompagni,[1,2] Marta Canato,[3] Carlo Reggiani,[3] and Feliciano Protasi[1,4]

[1]*CeSI-MeT, Center for Research on Ageing and Translational Medicine, University G. d'Annunzio of Chieti, 66100 Chieti, Italy*
[2]*Department of Neuroscience, Imaging, and Clinical Sciences (DNISC), University G. d'Annunzio of Chieti, 66100 Chieti, Italy*
[3]*Department of Biomedical Sciences, University of Padova, 35131 Padova, Italy*
[4]*Department of Medicine and Aging Science (DMSI), University G. d'Annunzio of Chieti, 66100 Chieti, Italy*

Correspondence should be addressed to Feliciano Protasi; feliciano.protasi@unich.it

Received 20 March 2017; Revised 11 July 2017; Accepted 20 July 2017; Published 10 September 2017

Academic Editor: Jose R. Pinto

Oxidative stress has been proposed to play a key role in malignant hyperthermia (MH), a syndrome caused by excessive Ca^{2+} release in skeletal muscle. Incidence of mortality in male calsequestrin-1 knockout (CASQ1-null) mice during exposure to halothane and heat (a syndrome closely resembling human MH) is far greater than that in females. To investigate the possible role of sex hormones in this still unexplained gender difference, we treated male and female CASQ1-null mice for 1 month, respectively, with Premarin (conjugated estrogens) and leuprolide (GnRH analog) and discovered that during exposure to halothane and heat Premarin reduced the mortality rate in males (79–27% and 86–20%), while leuprolide increased the incidence of mortality in females (18–73% and 24–82%). We then evaluated the (a) responsiveness of isolated muscles to temperature and caffeine, (b) sarcoplasmic reticulum (SR) Ca^{2+} release in single fibers, and (c) oxidative stress and the expression levels of main enzymes involved in the regulation of the redox balance in muscle. Premarin treatment reduced the temperature and caffeine sensitivity of EDL muscles, normalized SR Ca^{2+} release, and reduced oxidative stress in males, suggesting that female sex hormones may protect mice from lethal hyperthermic episodes by reducing both the SR Ca^{2+} leak and oxidative stress.

1. Introduction

Calsequestrin-1 (CASQ1) is an acidic protein which binds Ca^{2+} with moderate affinity, but high capacity, localized in the lumen of sarcoplasmic reticulum (SR) in proximity of ryanodine receptor type-1 (RYR1), the Ca^{2+} release channel of the SR [1–5]. CASQ1 and RYR1 are two main players in excitation-contraction (EC) coupling, the mechanism that links the depolarization of the transverse tubule (TT) membrane to the release of Ca^{2+} from the SR terminal cisternae which, in turn, activates muscle contraction [6]. In EC coupling, CASQ1 plays the dual role of intraluminal Ca^{2+} buffer and modulator of RYR1-mediated SR Ca^{2+} release [7–10].

We previously demonstrated that CASQ1 knockout mice (CASQ1-null) are vital under normal conditions [11], although the ablation of CASQ1 causes structural and morphological rearrangement of SR membranes at the triad junction, SR depletion, and abnormalities in SR Ca^{2+} release [11–14]. Interestingly, we also discovered that CASQ1-null mice trigger lethal hyperthermic episodes when exposed to both halothane and heat [15, 16], a phenotype that closely resembles that observed in *porcine stress syndrome* (*PSS*) [17, 18], and in knockin mice carrying point mutations in RYR1 gene linked to human malignant hyperthermia (MH) susceptibility, the $RYR1^{Y522S/WT}$ and $RYR1^{R163C/WT}$ mice [19, 20]. MH is a potentially lethal disorder triggered in humans by administration of halogenated/volatile anesthetics (i.e., halothane and isofluorane) and characterized by hyperthermia, rhabdomyolysis (i.e., the rupture of muscle fibers), and increased plasma/serum levels of K^+, Ca^{2+}, and creatine kinase (CK) [21, 22]. The widely accepted molecular mechanism underlying these crises is that the triggering

agents, commonly used during surgery interventions, trigger a sustained and uncontrolled release of Ca^{2+} from the SR of skeletal muscle fibers [23, 24].

In Dainese et al. [15], we also showed that incidence of mortality in CASQ1-null mice during exposure to both halothane and heat is significantly greater in males than in females, a finding in line with some epidemiological studies conducted in humans, which reported a male prevalence of ~3 : 1 to 4 : 1 [25–27]. To date, the reason for this gender difference in humans and in CASQ1-null mice remains unclear.

Durham et al. showed that in $RYR1^{Y522S/WT}$ mice the enhanced production of oxidative species of oxygen and nitrogen (ROS and RNS, resp.) results in RYR1 S-nitrosylation/glutathionylation, covalent modifications of RYR1 which further increase the opening probability of the mutated channel [28]. These findings suggested that excessive Ca^{2+}-dependent production of ROS/RNS likely plays a pivotal role in the cellular and molecular events leading to rhabdomyolysis of muscle fibers during MH reactions. In line with these findings, in Michelucci et al., [29] we reported that treatment of CASQ1-null male mice with antioxidants (i.e., N-acetylcysteine or Trolox) markedly reduced the rate of heat- and halothane-induced mortalities.

In the current study, we hypothesized that the difference in MH susceptibility between male and female CASQ1-null mice could reside in their different abilities to modulate oxidative stress. Indeed, it is well documented that female sex steroid hormones, that is, estrogens, have potent cellular antioxidant properties [30, 31], thanks to (i) their capability to upregulate the expression of several antioxidant enzymes; (ii) downregulate ROS-generating enzymes [32–34]; and (iii) their direct free-radical scavenging properties [35]. To investigate the possible role that estrogens play in gender difference in CASQ1-null mice, we treated for 1 month (3 to 4 months of age) male CASQ1-null mice with Premarin (a mixture of water-soluble-conjugated equine estrogens) and female CASQ1-null mice with leuprolide (a synthetic nonapeptide that functions as a potent gonadotropin-releasing hormone, or GnRH, analogue), to abolish estrogens production. Results of our experiments indicate that Premarin and leuprolide treatments reverse the halothane- and heat-induced mortalities of CASQ1-null mice, where Premarin exerted a striking protective effect in males while leuprolide increased significantly the MH susceptibility of females. Investigation of the possible molecular mechanisms indicates that estrogens reduce both SR Ca^{2+} leak and oxidative stress, two key events in MH crises.

2. Materials and Methods

2.1. Ethic Statement. All *in vivo* experiments/protocols on animals were conducted according to the Directive of the European Union 2010/63/UE and the National Institutes of Health Guide for the Care and Use of Laboratory Animals and approved by the Committee on the Ethics of Animal Experiments of the University of Chieti (15/2011/CEISA/COM).

2.2. Premarin and Leuprolide Treatments of CASQ1-Null Mice. CASQ1-null mice were generated as previously described [11]. Mice were housed in microisolator cages at 20°C in a 12 hrs light/dark cycle and provided free access to water and food. Three-month-old male and female CASQ1-null mice were randomly assigned to one of the three different experimental groups: control group, Premarin-treated male mice, and leuprolide-treated female mice.

Premarin (Wyeth Laboratories, Dallas, TX, USA) was dissolved in 0.9% NaCl solution and administered subcutaneously to CASQ1-null male mice at a final dose of 40 ng/g of body weight every day for 1 month. Leuprolide acetate salt (Sigma-Aldrich, Italy) was dissolved in 0.9% NaCl solution and also administered subcutaneously to CASQ1-null female mice at a final dose of 100 ng/g of body weight every day for 1 month.

2.3. Halothane Exposure and Heat Stress Protocol. To determine MH susceptibility to volatile halogenated anesthetics, mice were exposed to an air mixture containing halothane (Sigma-Aldrich, Italy) at concentrations sufficient to induce stage 3 anesthesia (2% halothane, with more added as necessary to induce and maintain this level of anesthesia) using an Isotec-3 evaporator (GE Healthcare, Milan, Italy), as previously described [15, 29]. During halothane exposure, mice were kept in a chamber at a constant temperature (32°C) to avoid a drop in body temperature during anesthesia. The maximum exposure time to halothane was 1 hr, and surviving mice were then recovered by suspension of anesthetic administration.

To determine MH susceptibility to high environmental temperature, mice were subjected to a heat stress protocol, performed in an environmental chamber at 41°C for 1 hr while their internal temperature was recorded, as previously described [15, 29]. Core body temperature was measured using a rectal thermometer (four channels thermometer TM-946, XS instruments, Modena, Italy) taped on the tails of the animals and recorded every 5 min throughout the duration of heat challenge, as in [15, 29].

2.4. Assessment of Rhabdomyolysis

2.4.1. Histologic Analysis. Immediately after heat stress, *extensor digitorum longus* (EDL) muscles were carefully dissected from CASQ1-null mice and fixed at room temperature in 3.5% glutaraldehyde 0.1 M Na cacodylate buffer, pH 7.2 overnight. Small bundles of fixed fibers were then postfixed in 2% OsO_4 in the same buffer for 2 hrs and then block-stained in aqueous saturated uranyl acetate. After dehydration, specimens were embedded in an epoxy resin (Epon 812). Semithin (800 nm) histological sections were cut with a Leica Ultracut R Microtome (Leica Microsystem, Vienna, Austria) using a Diatome diamond knife (Diatome Ltd., Biel, Switzerland). After staining with toluidine blue dye, the sections were viewed using a Leica DMLB light microscope (Leica Microsystem, Vienna, Austria). The percentage of fibers presenting signs of rhabdomyolysis was determined as previously described [29].

2.4.2. Immunofluorescence Analysis. EDL muscles were carefully dissected immediately after the heat stress protocol and fixed with 2% paraformaldehyde for 2 hrs, at room temperature. Small bundles of fixed fibers were processed for confocal microscopy (CM) acquisitions as previously described [36]. Briefly, samples were first exposed to a mouse monoclonal primary antibody which recognizes both RYR1 and RYR3 (34C, 1 : 20; Developmental Studies Hybridoma Bank, University of Iowa) and then to a Cy3 goat anti-mouse IgG secondary antibody (Jackson ImmunoResearch Laboratories, West Grove, PA, USA). Images were acquired using a LSM510 META laser scanning confocal microscope system (Zeiss, Jena, Germany) equipped with Zeiss Axiovert 200 inverted microscope and a Plan Neofluar oil-immersion objective (63X/1.3 NA).

2.4.3. Quantitative Plasma and Serum Analyses. For quantitative assessment of CK, K^+, and Ca^{2+} blood/serum markers of rhabdomyolysis, blood samples were collected from anesthetized mice following a brief exposure (30–35 min) to a nontriggering heat stress challenge. Blood samples were collected and processed as previously described [29]. Briefly, mice were anesthetized and 500–800 μl of blood was collected from the right ventricle with a 26-G needle. Approximately, half of this volume was placed in vials containing lithium heparin to prevent blood clotting and centrifuged at 2500g (4°C for 15 min) to isolate plasma. The other half of the blood was placed in a vial without anticoagulant, and serum was obtained by centrifugation at 4000g (4°C for 20 min). Spectrophotometrical measurements were performed using a Screen Touch Master spectrophotometer (Hospitex Diagnostic, Sesto Fiorentino, Italy).

2.5. Ex Vivo and In Vitro Experiments in Isolated Muscles and Single Fibers

2.5.1. Temperature and Caffeine Sensitivity of Intact EDL Muscles. Intact EDL muscles were dissected from hind limbs of mice, placed in a dish containing Krebs-Henseleit (KH) solution, pinned, and tied with fine silk sutures at each end. Muscles were then mounted vertically between two platinum electrodes immersed in an organ chamber filled with KH solution and attached to a servomotor and force transducer (model 1200A, Aurora Scientific, Aurora, ON, Canada). Before starting the experimental protocol, stimulation level and optimal muscle length (L_0) were determined using a series of 80 Hz tetani in order to adjust the muscle to the length that generated maximal force (F_0). Twitch and tetanic contractile properties, as well as force-frequency parameters, were measured and analyzed. During the experiments, temperature was kept constant at 25°C. To evaluate the development of contractures induced by increasing temperature, EDL muscles were electrically stimulated with a series of consecutive twitches (1 ms duration, 0.2 Hz for each twitch) applied every 5 seconds and exposed to an increase in temperature of 2°C every 5 min (from 25°C to 41°C) [15]. To determine caffeine sensitivity of resting tension and caffeine-dependent decay in twitch force, muscles were subjected to an *in vitro* contracture test (IVCT) protocol as previously described [29]. Briefly, while isolated EDL muscles were continuously stimulated at 0.2 Hz at 23–25°C, caffeine concentration in the bath was changed every 3 min (no wash between applications) as follows: 2, 4, 6, 8, 10, 14, 18, and 22 mM.

2.5.2. Cytosolic Ca^{2+} Measurements in Isolated Single FDB Fibers. Myoplasmic Ca^{2+} transients (60 Hz, 2 s) and caffeine-induced Ca^{2+} release were measured in fibers isolated from *flexor digitorum brevis* (FDB) according to a modified collagenase/protease method described previously [37]. Twenty-four hours after dissociation, FDB fibers were incubated with 5 μM Fura-2 acetoxymethyl ester (Fura-2 AM; Invitrogen, Eugene, OR, USA) for 30 min at 37°C, in a buffer containing the following: 125 mM NaCl, 5 mM KCl, 1 mM $MgSO_4$, 1 mM KH_2PO_4, 5.5 mM glucose, 1 mM $CaCl_2$, 20 mM HEPES, and 1% bovine serum albumin, pH 7.4. A minimum of 30 min was allowed for Fura-2 deesterification before the fibers were imaged. Intracellular Ca^{2+} transients were recorded at 25°C using a dual-beam excitation fluorescence photometry setup (IonOptix Corp., Milton, MA, USA), as previously described [11, 12]. Single fibers were subjected to 2 different stimulation protocols. (a) To evaluate tetanic transients, two trains of high-frequency stimulation (60 Hz for 2 s) were delivered with a recovery time of 5 min between trains. Fura-2 ratios were calculated and analyzed using IonWizard software (IonOptix Corp., Milton, MA, USA). Peak amplitude was calculated by subtracting basal fluorescence ratio values from peak ratio values. (b) To evaluate myoplasmic Ca^{2+} transients at increasing caffeine concentrations, fibers were continuously stimulated with a series of low frequency (0.5 Hz) trains in the presence of 10 mM of caffeine.

2.6. Measurements of Oxidative Stress Levels

2.6.1. Glutathione Assay. Reduced and oxidized levels of glutathione (GSH and GSSG, resp.) were measured as previously described [29]. Briefly, hind limb muscles were homogenized, and total GSH and GSSG levels were measured according to Rahman et al. [38]. 0.1 g of tissue from the hind limb muscles was homogenized and centrifuged, and intracellular GSH and GSSG levels were measured as previously described [39]; the assay was performed in 96-well plates (96 Well Tissue Culture Test Plate; Spl Life Sciences, Korea) using an Absorbance Microplate Reader SpectraMAX 190 (Molecular Devices, Sunnyvale, CA, USA). Data were normalized to a GSH standard curve with the GSH concentration in the samples determined from a linear regression from the GSH standard curve [38]. All reagents for these experiments were purchased from Sigma-Aldrich (Milan, Italy).

2.6.2. Western Blot Analyses. EDL muscles were homogenized in a lysing buffer containing 3% sodium dodecyl sulphate (SDS) (Sigma-Aldrich, Milan, Italy) and 1 mM EGTA (Sigma-Aldrich, Milan, Italy), using a mechanical homogenizer, and then centrifuged for 15 min at 900g at room temperature. Protein concentration was determined

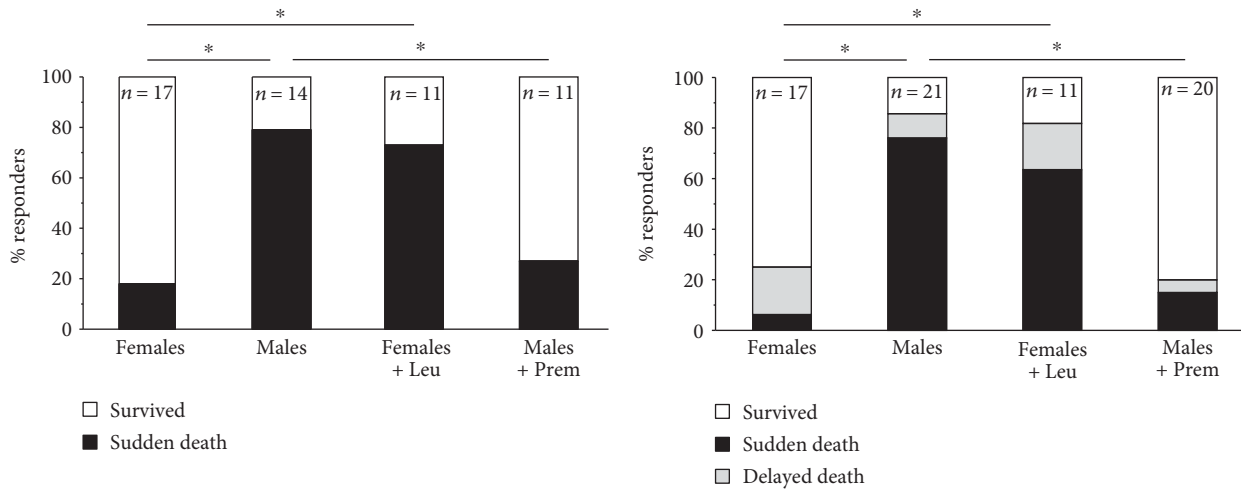

(a) Halothane sensitivity test

(b) Heat stress test

Figure 1: Mortality rate during exposure to halothane and heat stress protocols. Incidence of sudden and delayed (i.e., within 24 hrs after challenge) deaths during exposure to halothane (2% for 1 hr (a)) and to heat (41°C for 1 hr (b)) in male and female CASQ1-null mice, either untreated or treated with Premarin (males) or leuprolide (females). $^*p < 0.05$; n = number of mice. See also Tables S1 and S2.

spectrophotometrically using a modified Lowry method. 20–40 μg of total protein was resolved in 10–12% polyacrylamide electrophoresis gels, transferred to nitrocellulose membrane, and blocked with 5% nonfat dry milk (EuroClone, Milan, Italy) in Tris buffered saline and Tween 20 0.1% (TBS-T) for 1 hr. Membranes were then probed with primary antibodies diluted in 5% nonfat dry milk in TBS-T overnight at 4°C: (a) anticopper/zinc superoxide dismutase (SOD1) antibody (rabbit polyclonal 1 : 2000, Santa Cruz Biotechnology, Inc., Dallas, TX, USA); (b) antimanganese superoxide dismutase (SOD2) antibody (rabbit polyclonal, 1 : 5000; Santa Cruz Biotechnology, Inc., Dallas, TX, USA); (c) anti-3-nitrotyrosine (3-NT) antibody (mouse monoclonal, 1 : 500; Merck Millipore, Italy); (d) antineuronal nitric oxide synthase (nNOS) antibody (mouse monoclonal, 1 : 2000; BD Biosciences, Milan, Italy); (e) antiNADPH oxidase gp91phox membrane-bound subunit (NOX2) antibody (rabbit monoclonal, 1 : 3000; Abcam, Cambridge, UK); and (f) anticatalase (CAT) antibody (mouse monoclonal, 1 : 1000; Santa Cruz Biotechnology, Inc., Dallas, TX, USA). The antiglyceraldehyde-3-phosphate dehydrogenase (GAPDH) antibody (mouse monoclonal, 1 : 5000; OriGene Technologies, Inc., Rockville, MD, USA) was used as a loading control. Membranes were then incubated with the secondary antibody horseradish peroxidase-conjugated (1 : 10000, Merck Millipore, MA, USA), diluted in 5% nonfat dry milk in TBS-T, for 1 hr at room temperature. Proteins were detected by enhanced chemiluminescent liquid (Perkin-Elmer, Milan, Italy). Protein quantification was made using ImageJ software (National Institutes of Health, Bethesda, MA, USA).

2.7. Statistical Analyses. Statistical significance in experiments of halothane- and heat-induced mortalities was evaluated using a two-tailed Fisher's exact test. One-way ANOVA followed by post hoc Tukey test was used for statistical analyses of all other experiments except for the *in vivo* core temperature and the ex vivo temperature and caffeine sensitivity, in which statistical significance was determined using a repeated measures ANOVA followed by post hoc Tukey test for the pairwise comparisons. In all cases, differences were considered statistically significant at $p < 0.05$. Two-tailed Fisher's exact test was performed using GraphPad software, whereas one-way ANOVA and repeated measures ANOVA were performed using Origin 8.0 software.

3. Results

3.1. Estrogens Protect CASQ1-Null Mice from Halothane- and Heat-Induced Sudden Death by Reducing Hyperthermia. At four months of age, male and female control mice and mice treated with Premarin (males) or leuprolide (females) were exposed to either halothane (2%, 1 h at 32°C) or heat stress protocol (41°C, 1 h), as previously done in [15, 29].

Consistent with the previous results [15], in CASQ1-null mice, the mortality rate, during the administration of halothane and during heat stress protocol, was significantly lower in female mice (18% and 24%) than in male mice (79% and 86%) (Figure 1 and Supplementary Tables 1 and 2 available online at https://doi.org/10.1155/2017/6936897), with a male prevalence of ~4 : 1. The halothane and heat-induced hyperthermic crises exhibited a clinical presentation very similar to that observed during a classic anesthetic-induced MH reaction in humans: difficulty in breathing, tachypnea, impaired movements, and diffuse skeletal muscle rigidity (visual observation). Treatment of mice resulted in a clear reversion of the phenotype (Figure 1): Premarin had a striking protective effect in male mice with a significant reduction in the incidence of mortality (79–27% and 86–20%, resp., for halothane and heat exposure), while leuprolide caused a significant increase in the MH susceptibility of female mice (18–73% and 24–82%, resp., for halothane and heat stress).

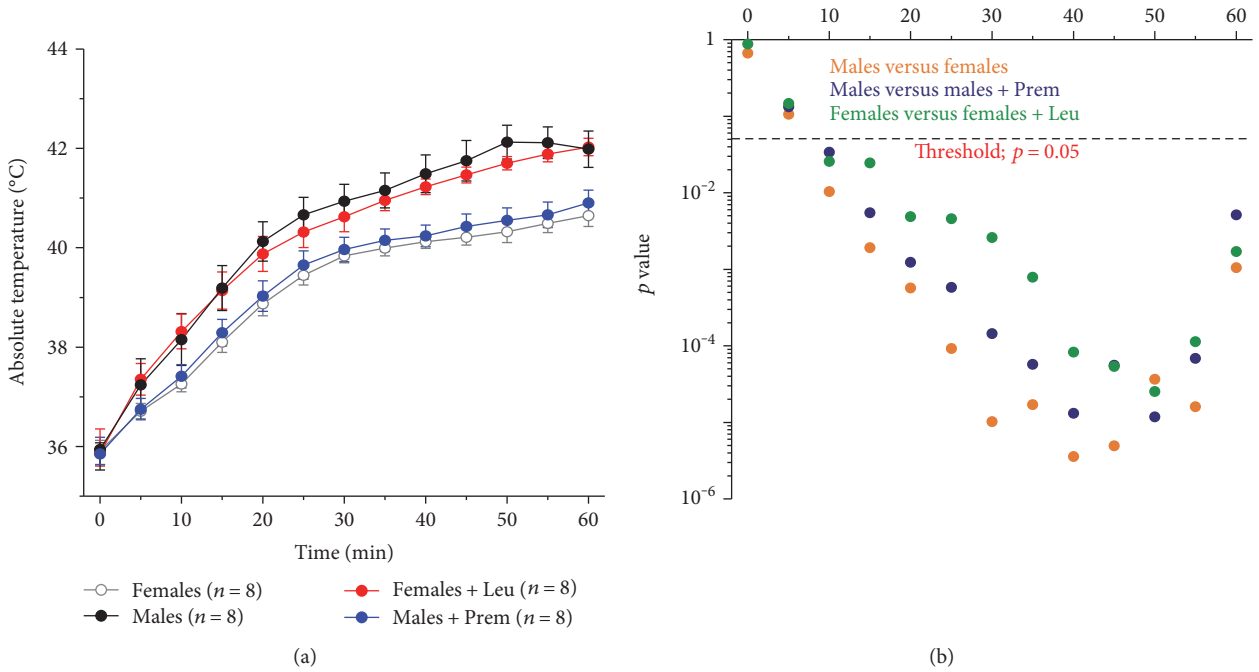

Figure 2: Changes in absolute core temperature in mice subjected to heat stress protocol. (a) Increase in absolute core temperature, recorded every 5 min, during exposure to heat stress protocol in male and female CASQ1-null mice, either untreated or treated with Premarin (males) and leuprolide (females). (b) Semilog plots showing results of repeated measures ANOVA with post hoc Tukey test. Data are given as mean ± SEM; n = number of mice. See also Table S3.

As a typical MH crisis is characterized by an abnormal and uncontrolled rise in body temperature, namely hyperthermia [40], we also recorded the rise in core temperature in all mice exposed to the heat stress protocol (Figure 2 and Supplementary Figure 1; see also Supplementary Table 3). Temperature was monitored throughout the entire duration of the experiment, and recorded every 5 min, and showed both as absolute (Figure 2) and relative (ΔT) (Supplementary Figure 1) temperature. The results indicate that, during heat stress protocol, the time-dependent increase in core temperature observed in female mice was significantly lower than that in male mice; specifically, at the end of the stress protocol, the core temperature recorded in females and males was 40.6 ± 0.2°C and 42.0 ± 0.4°C, respectively (Figure 2), with a temperature change from beginning to end of the experiment of ΔT = +4.7 ± 0.3°C and ΔT = +6.1 ± 0.3°C, respectively (Supplementary Figure 1). Following treatment with Premarin, the temperature recorded at the end of the protocol in male mice was 40.9 ± 0.3°C (Figure 2), with an increase of core temperature from beginning to end of the experiment quite similar to that in female mice (ΔT = +5.1 ± 0.2°C) (Supplementary Figure 1); conversely, treatment of female mice with leuprolide resulted in a significantly increased rise in core temperature to values similar to that of male mice, with an absolute temperature at the end of 42.1 ± 0.2°C (Figure 2) and relative increase of +6.4 ± 0.5°C (Supplementary Figure 1).

3.2. Estrogens Reduce Muscle Damage and Rhabdomyolysis in EDL Muscles of CASQ1-Null Mice during Heat Stress. Rhabdomyolysis, a typical clinical sign of MH episodes and exertional/heat strokes in humans [41, 42], is characterized by breakdown of skeletal muscle fibers with the release of the intracellular proteins and ions into the blood stream. We (a) analyzed histological sections to quantify the percentage of EDL fibers affected by structural damage following the heat stress protocol (Figures 3(a), 3(b), 3(c), 3(d), and 3(i); see also Supplementary Table 4); (b) labeled small bundles of EDL fibers with a primary antibody against RYR1, marking the position of calcium release units (CRUs) to visualize striation abnormalities (Figures 3(e), 3(f), 3(g), and 3(h)); (c) measured the blood levels of CK (in serum), K^+ (in plasma), and Ca^{2+} (in plasma), recognized markers of skeletal muscle damage and rhabdomyolysis (Figures 3(j), 3(k), and 3(l)). Following the heat stress protocol, while normal cross striation was well preserved in fibers from females (Figures 3(a) and 3(e)), fibers from males showed severe disarray of the internal organization, with large areas presenting loss of striation and hypercontracted myofibrils (Figures 3(b) and 3(f)). The effects of treatments were striking: pretreatment of male mice with Premarin strongly protected muscle fibers from heat stress-induced damage (Figures 3(d) and 3(h)), whereas treatment of female mice with leuprolide resulted in a clear increase in the number of fiber presenting loss of striation and contractures (Figures 3(c) and 3(g)).

In histological sections (Figures 3(a), 3(b), 3(c), and 3(d)), we also quantified the percentage of fibers presenting structural damage (Figure 3(i); see also Supplementary Table 4) following the heat stress challenge: 11.6 ± 5.4% of fibers presented signs of structural damage in female mice, while

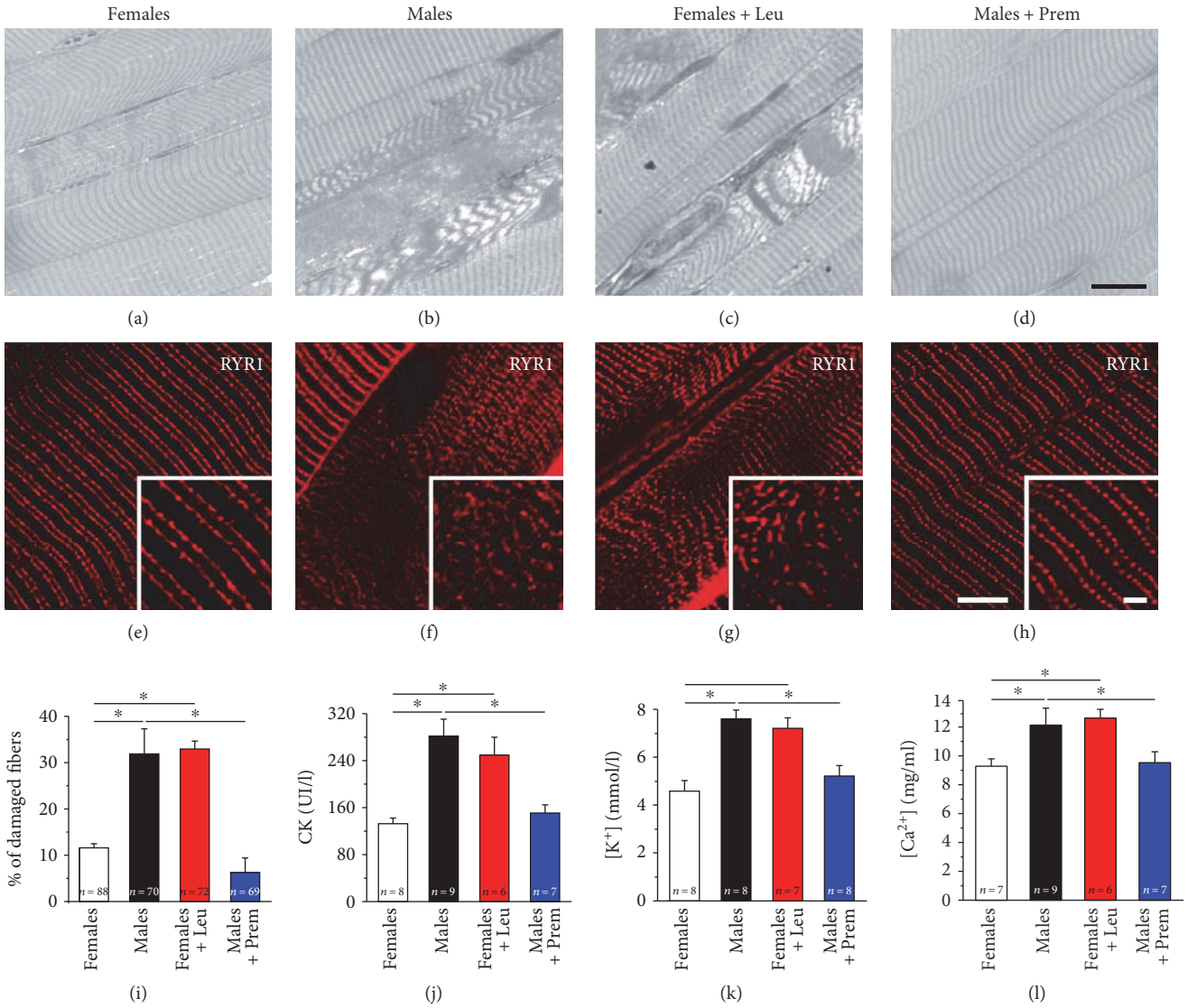

Figure 3: Assessment of muscle damage and blood levels of CK K^+, and Ca^{2+} following exposure to heat stress protocol. (a–h) Histological (a–d) and immunofluorescence of EDL fibers labeled with anti-RYR1 antibody (e–h) examination of EDL muscles after exposure to the heat stress protocol in male and female CASQ1-null mice, either untreated or treated with Premarin (males) and leuprolide (females). (i) Quantitative analysis of EDL fibers presenting structural damage and contractures. See also Table S4. (j–l) Blood levels of CK in serum (j), K^+, and Ca^{2+} in plasma (k and l) following heat stress protocol. Data are given as mean ± SEM; $^*p < 0.05$; n = number of mice. Scale bars in (a–e): 10 μm (insets 5 μm).

in males, this percentage was 31.9 ± 5.4%. Again, the effect of treatments was striking as EDL fibers from male mice treated with Premarin were protected from structural damage (6.3 ± 3.2%), while the percentage of altered fibers in EDL muscles dissected from leuprolide-treated female mice was increased (32.9 ± 1.7%).

In support of the structural evidence collected by analysis of histological sections (Figures 3(a), 3(b), 3(c), and 3(d)) and by confocal microscopy images (Figures 3(e), 3(f), 3(g), and 3(h)), biochemical analysis of blood samples revealed that the serum and plasma levels of markers of rhabdomyolysis (i.e., CK, K^+, and Ca^{2+}) were lower in female and Premarin-treated male mice (Figures 3(j), 3(k), and 3(l)), but higher in the other two groups of animals.

3.3. Estrogens Lower the Temperature and Caffeine Sensitivity of EDL Muscles Isolated from CASQ1-Null Mice. To evaluate the effect of increasing temperature on muscle contractility, we performed an *in vitro* heat stress protocol, based on exposure of isolated EDL muscles to increase steps of temperature of 2°C each. When exposed to this protocol, EDL muscles from female mice showed a slight increase in basal tension starting at ~33°C, with a more significant increase in tension only at temperatures above 37°C (Figure 4(a)). On the other hand, EDL muscles excised from male mice started to develop tension already at ~31°C, with the development of strong contractures toward the end of the protocol (Figure 4(a)). Premarin and leuprolide treatments, completely reverted this temperature sensitivity: specifically,

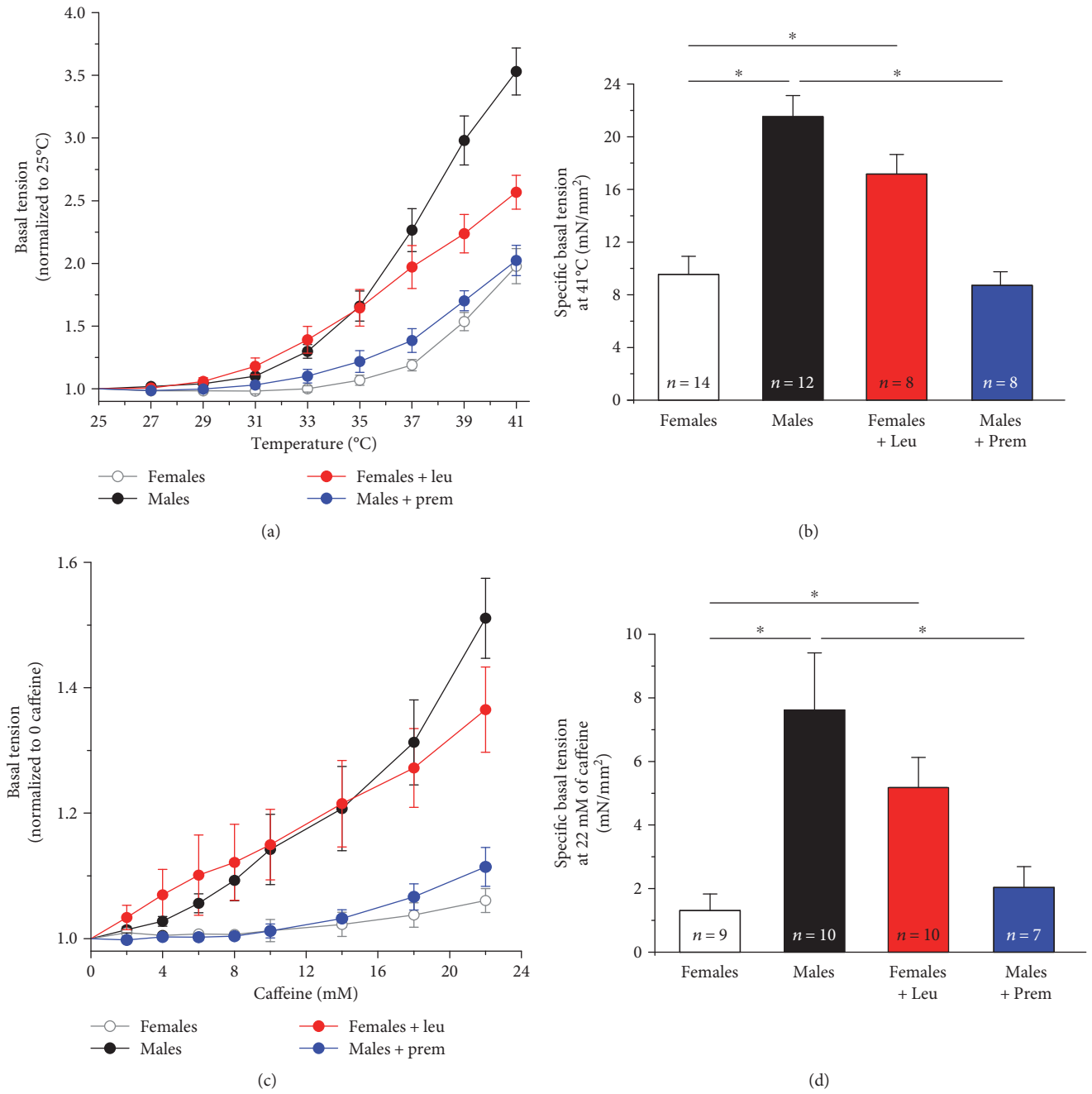

FIGURE 4: Temperature and caffeine dependence of basal tension in isolated EDL muscles. (a) Temperature dependence of basal tension in EDL muscles excised from male and female CASQ1-null mice, either untreated or treated with Premarin (males) and leuprolide (females). (b) Specific basal tension (expressed as mN/mm^2) calculated at the last experimental point (T = 41°C). (c) IVCT performed using increasing caffeine concentrations in EDL muscles. (d) Specific basal tension (expressed as mN/mm^2) calculated at the last experimental point (22 mM caffeine). Data are given as means ± SEM; $^*p < 0.05$; n = number of muscles.

Premarin reduced the rise in basal tension in male EDL muscles (Figure 4(a)), with a decrease of specific force calculated at the last experimental point (41°C) of ~40% (Figure 4(b)). Conversely, leuprolide treatment increased the temperature sensitivity of EDL muscles from female mice (Figure 4(a)) with a specific force at the end of the experiment (41°C), ~30% higher than that of EDLs from females (Figure 4(b)).

We then performed a classic caffeine-dose response experiment, mimicking the *in vitro contracture test* (IVCT) that is used in humans to test MH susceptibility [43, 44]. Caffeine is a potent agonist of RYR1 that triggers release of Ca^{2+} from the SR: MH susceptible patients usually display a lower threshold of response to caffeine [45, 46]. The contractile response during IVCT (Figure 4(c)) indicated that EDL muscles from female mice displayed a caffeine sensitivity

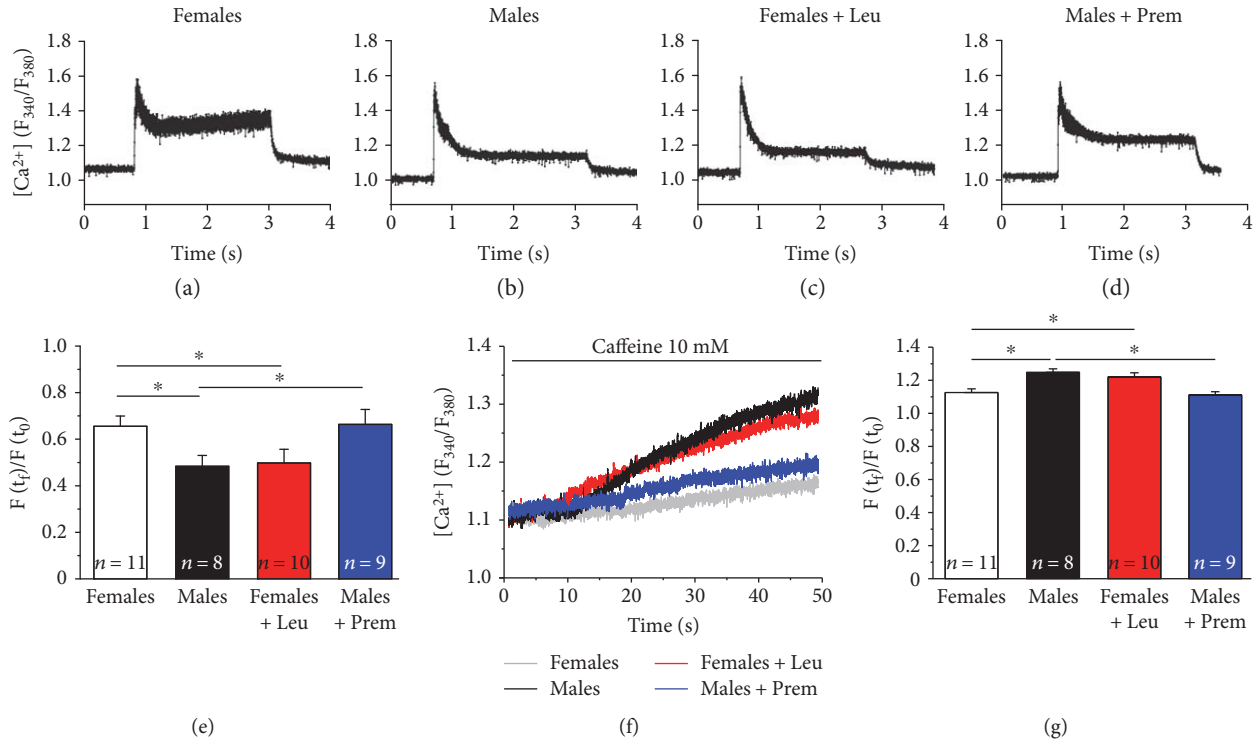

Figure 5: Cytosolic Ca^{2+} concentration during stimulation at 60 Hz and caffeine-induced Ca^{2+} release in single FDB fibers. (a–d) Representative traces of Fura-2 fluorescence obtained during sustained high-frequency electrical stimulation (60 Hz, 2 s) in single FDB fibers from male and female CASQ1-null mice, either untreated or treated with Premarin (males) and leuprolide (females). (e) Fractional Fura-2 ratio signal, calculated as the ratio between the fluorescence peaks at the end (F (t_f)) and at the beginning (F (t_0)) of the 60 Hz stimulation protocol. (f) Representative traces of Fura-2 fluorescence showing the increase of myoplasmic Ca^{2+} induced by 10 mM caffeine. (g) Fractional Fura-2 ratio signal calculated as the ratio between the fluorescence peaks at the end (F (t_f)) and at the beginning (F (t_0)) of the protocol. Data in (e) and (g) are given as means ± SEM; $^*p < 0.05$; n = number of fibers.

significantly lower than that from male mice, as clearly shown by the development of tension at lower caffeine concentrations in the latter (Figure 4(c)). Also in this case, Premarin and leuprolide treatments completely reverted the sensitivity of EDL muscles. Specifically, Premarin treatment of male mice (a) increased the threshold of response to higher caffeine concentrations; (b) reduced specific basal tension at 22 mM caffeine of ~73% compared to that recorded in control males; and (c) abolished the development of full contractures (Figures 4(c) and 4(d)) of EDL muscles. On the other hand, leuprolide treatment of female mice (a) lowered the threshold of response to caffeine, with tension that started to rise already at 2 mM caffeine; (b) increased the specific basal tension at 22 mM caffeine of ~75% compared to control females; and (c) caused development of full contractures (Figures 4(c) and 4(d)) of EDL muscles.

In the same muscles, we also evaluated twitch tension in response to increasing caffeine concentrations (Supplementary Figure 2). During the first steps of caffeine application (from 2 to 8 mM), while muscles from females showed an enhancement of twitch force, those from males displayed already a decay, likely due to a faster SR depletion [12]. Again, Premarin and leuprolide treatments completely inverted the ability of EDL muscles to produce force in dependence of caffeine (Supplementary Figure 2). Indeed, muscles from Premarin-treated males exhibited an increased capability to produce force, along the entire range of caffeine application, compared to those of control males, while muscles from leuprolide-treated females displayed a significant caffeine-dependent force decline, very similar to that of males.

3.4. Estrogens Normalize Electrical-Evoked Ca^{2+} Transients and Reduce the Caffeine-Induced Ca^{2+} Release in Single FDB Muscle Fibers. We have previously shown that single FDB fibers from male CASQ1-null mice undergo severe SR depletion when stimulated at high frequency [12]. Here, we measured myoplasmic Ca^{2+} during prolonged high-frequency stimulation (60 Hz, 2 s) and during low-frequency stimulation (0.5 Hz, 0.2 s) in the presence of 10 mM caffeine, in enzymatically dissociated single FDB fibers loaded with the ratiometric Ca^{2+} dye Fura-2. When exposed to a 60 Hz stimulus train for 2 seconds, FDB fibers from female mice displayed a myoplasmic Ca^{2+} transient with a lower decay compared to that observed in male fibers (Figures 5(a) and 5(b)). Specifically, the average residual Fura-2 fluorescence at the end of the 2 sec stimulus (calculated as the ratio between Fura-2 ratio at the end of the stimulation with that recorded at the beginning of the stimulation) was, respectively, 0.62 ± 0.02 and 0.44 ± 0.02 in FDB fibers from female and male mice (Figure 5(e)).

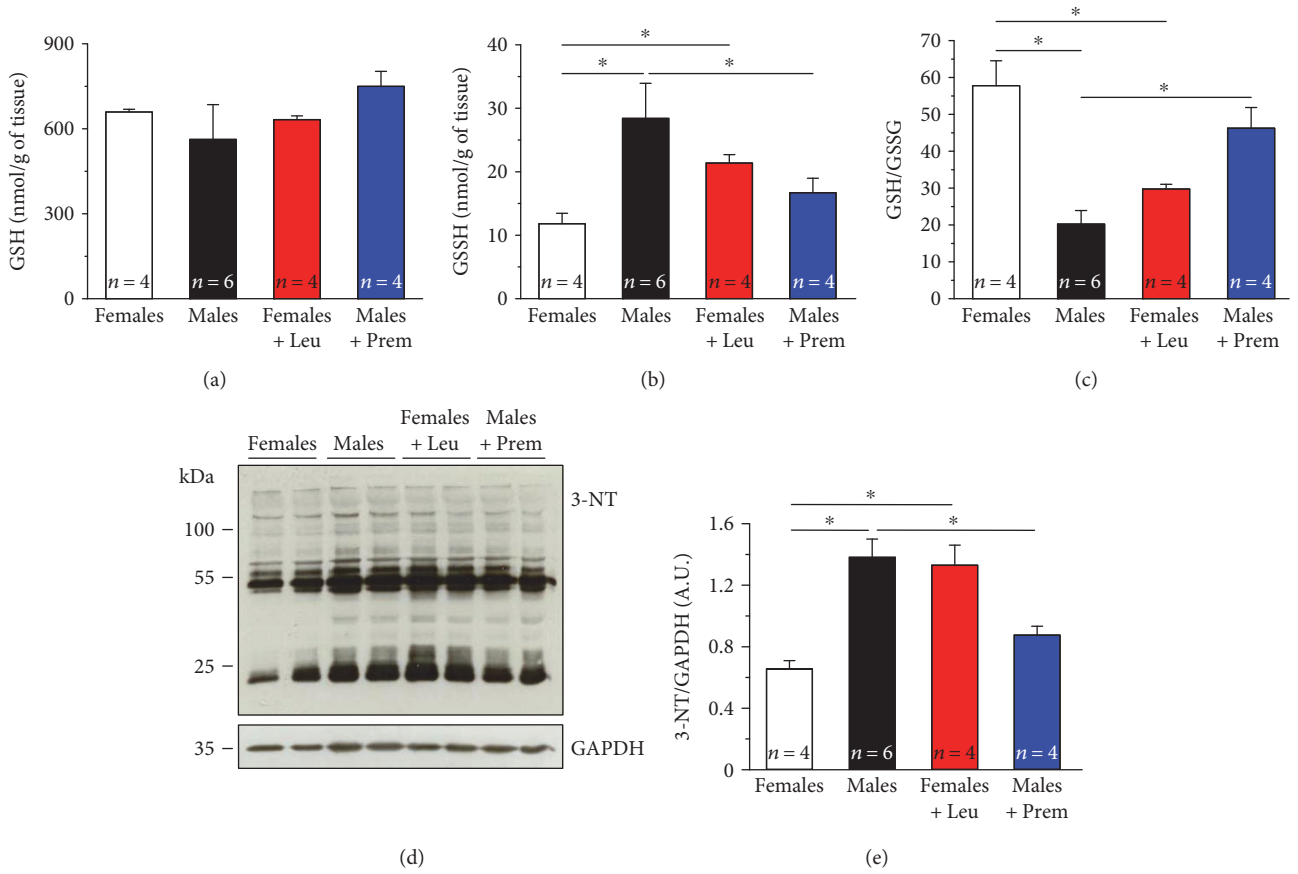

FIGURE 6: Levels of GSH, GSSG, and 3-nitrotyrosine (3-NT) in both total hind limb and EDL muscle homogenates. (a and b) Levels of reduced (GSH) and oxidized (GSSG) glutathione (both expressed as nmol/g of tissue), measured in control conditions in hind limb muscles from male and female CASQ1-null mice, either untreated or treated with Premarin (males) and leuprolide (females). (c) GSH/GSSG ratio measured in the same specimens. (d) Representative immunoblots showing levels of 3-NT measured in control conditions in EDL muscles from male and female CASQ1-null mice, either untreated or treated with Premarin (males) and leuprolide (females). (e) Relative band densities normalized to GAPDH in the same specimens. Data are given as mean ± SEM; $^*p < 0.05$; n = number of mice.

Interestingly, in FDB fibers from leuprolide-treated female mice (Figure 5(c)), the Ca^{2+} transient decay was significantly increased compared to that of females (but similar to that of males), with an average value of residual fluorescence of 0.45 ± 0.03 (Figure 5(e)). On the other hand, in FDB fibers from Premarin-treated male mice (Figure 5(d)), the Ca^{2+} transient decay was markedly reduced compared to that of males, with an average value of residual fluorescence of 0.63 ± 0.03 (Figure 5(e)).

As excessive basal tension and development of full contractures are both indicative of abnormally elevated Ca^{2+} levels, we also assessed the caffeine-induced SR Ca^{2+} release in single FDB fibers that were continuously stimulated at low frequency (0.5 Hz) (Figures 5(f) and 5(g)). Consistent with the results obtained during IVCT experiments (Figures 4(c) and 4(d)), FDB fibers from female mice showed a lower caffeine-dependent rise of myoplasmic Ca^{2+} concentration than that observed in FDB fibers from male mice (Figure 5(g)). As expected, while Premarin treatment in males strongly reduced the caffeine-induced SR Ca^{2+} release in FDB fibers, leuprolide treatment resulted in an enhanced elevation of myoplasmic Ca^{2+} concentration in female fibers (Figure 5(g)).

3.5. Estrogens Reduce Oxidative Stress in Muscles from CASQ1-Null Mice by Modulating Expression Levels of Either ROS/RNS-Generating or Antioxidant Enzymes. As excessive production of ROS and RNS has been proposed to be a key step in the cascade of molecular events that leads to rhabdomyolysis of muscle fibers and consequent death of MH susceptible mice [15, 28, 29], here, we measured markers of oxidative stress in EDL muscle homogenates. First, we assessed levels of GSH and GSSG (Figures 6(a) and 6(b)), a molecule synthesized from amino acids that is capable of reducing disulfide bonds to cysteines by serving as an electron donor [47, 48], and the GSH/GSSG ratio (Figure 6(c)), a parameter often used as a measure of cellular ROS reactivity [49]. GSH did not differ significantly in the four different groups of mice (Figure 6(a)), whereas GSSG levels were significantly higher in male and leuprolide-treated female mice than those in the other two groups (Figure 6(b)): as a consequence, the GSH/GSSG ratio in female mice was about 3-fold lower compared to male mice, suggesting that in females the global oxidative stress is markedly lower than that in males (Figure 6(c)). Noticeable, after 1 month of treatment, muscles from Premarin-treated male mice exhibited an increase of GSH/GSSG ratio compared to that

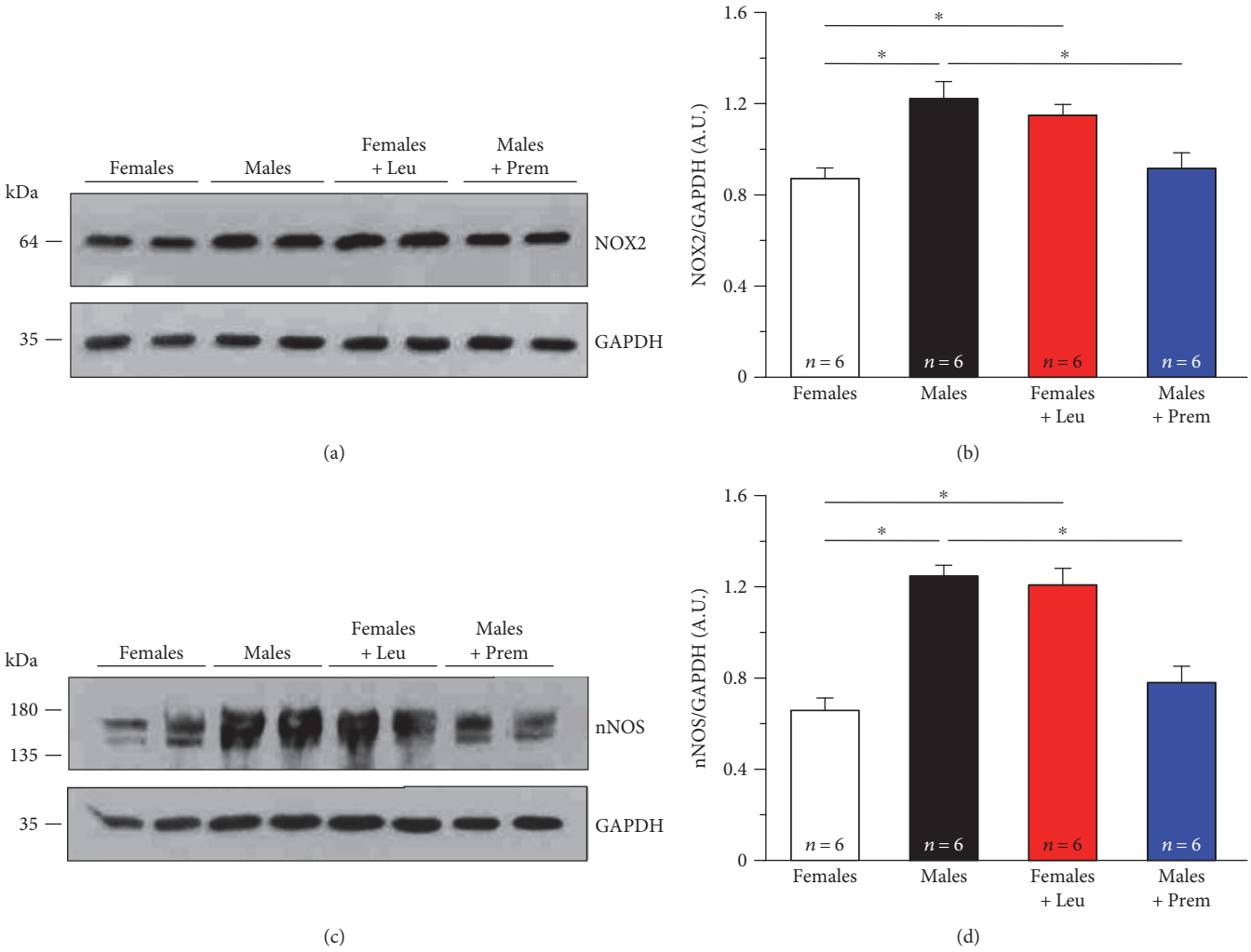

Figure 7: Levels of NOX2 and nNOS in EDL muscle homogenates. (a and c) Representative immunoblots showing levels of NOX2 gp91-phox subunit (a) and nNOS (c) in control conditions in EDL muscle homogenates from male and female CASQ1-null mice, either untreated or treated with Premarin (males) and leuprolide (females). (b and d) Relative band densities normalized to GAPDH. Data are given as mean ± SEM; $^*p < 0.05$; n = number of mice.

of males (more than doubled), while muscle homogenates of leuprolide-treated female mice showed a decrease of about 2-fold than those of female mice (Figure 6(c)).

We also measured by Western blot, again in EDL homogenates (Figures 6(d) and 6(e)), the amount of 3-nitrotyrosine (3-NT) (Figures 6(d) and 6(e)), a product of nitration of tyrosine residues of proteins mediated by RNS such as peroxynitrite anion and nitrogen dioxide, which is an indicator of oxidative stress and oxidative protein damage [50]. Whereas in females, 3-NT levels were significantly lower than those in males; after 1 month of Premarin treatment, male mice displayed a significant decrease of 3-NT levels compared to control males (~30%). Conversely, 1 month of leuprolide treatment of female mice determined an increase of 3-NT content of ~30% compared to control females.

To further dissect the molecular mechanisms by which estrogens modulate oxidative stress in muscle fibers from CASQ1-null mice, we then evaluated by Western blot the ability of estrogens to regulate expression of either ROS/RNS-generating enzymes or antioxidant enzymes. First, we measured (i) levels of NADPH oxidase $gp91^{phox}$ membrane-bound subunit (NOX2) (Figures 7(a) and 7(b)), belonging to a multiprotein enzyme complex which uses NADPH as a substrate to convert O_2 to superoxide anion (O_2^-) and hydrogen peroxide (H_2O_2) and which represents an important extramitochondrial source of ROS in skeletal muscle fibers [51–53] and (ii) levels of neuronal nitric oxide synthase (nNOS) (Figures 7(c) and 7(d)), one of the three isozymes responsible for the production of nitric oxide (NO) that is highly expressed in skeletal muscle [54, 55]. These analyses revealed that NOX2 and nNOS, respectively, responsible for the generation of ROS and RNS, were ~1.5- and 2.0-fold significantly higher in males compared to females (Figure 7), in line with the results showing that oxidative stress is lower in the latter (Figure 6).

Secondly, we evaluated expression levels of (i) copper/zinc superoxide dismutase (SOD1) (Figures 8(a) and 8(b)) and manganese superoxide dismutase (SOD2) (Figures 8(c) and 8(d)), the two main intracellular isoforms of a class of

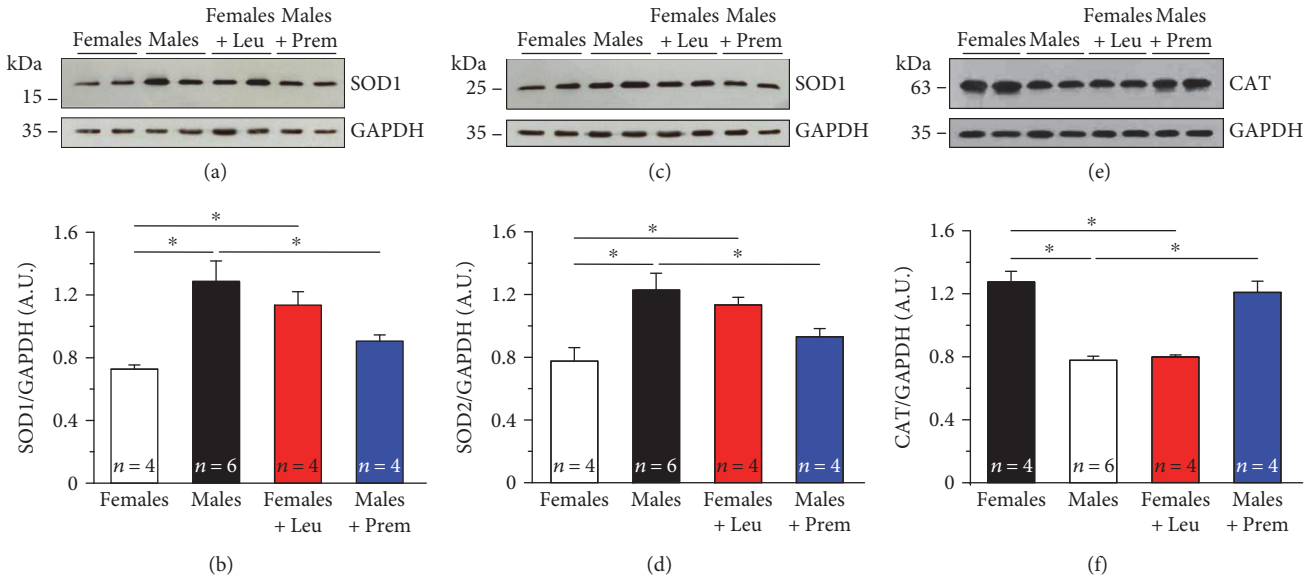

Figure 8: Levels of SOD1, SOD2, and CAT in EDL muscle homogenates. (a, c, and e) Representative immunoblots showing levels of SOD1 (a), SOD2 (c), and CAT (e) measured in control conditions in EDL muscle homogenates from male and female CASQ1-null mice, either untreated or treated with Premarin (males) and leuprolide (females). (b, d, and f) Relative band densities normalized to GAPDH. Data are given as mean ± SEM; $^*p < 0.05$; n = number of mice.

enzymes that catalyze the dismutation of O_2^- into O_2 and H_2O_2, the first step in the elimination of ROS [56] and of (ii) catalase (CAT) (Figures 8(e) and 8(f)), one of the most important antioxidant enzymes that catalyze the decomposition of H_2O_2 to H_2O and O_2 and that represent an important antioxidant defense for skeletal muscle [57]. We found that while SOD1 and SOD2 were significantly less expressed in female than in male muscles (Figures 8(a) and 8(b); Figures 8(c) and 8(d)), a completely opposite result was obtained for CAT, which was ~1.6-fold more expressed in females than males (Figures 8(e) and 8(f)). Also in these cases, Premarin and leuprolide treatments showed a potent effect in inverting the expression levels in the two genders, of both ROS/RNS-generating enzymes and antioxidant enzymes (Figures 7 and 8).

4. Discussion

4.1. Background. A review on the epidemiology of MH cases showed a male-to-female ratio of 2.2 : 1 for MHS in humans with males exhibiting a far greater fatality rate [25]. Later studies also found a similar disproportionate male susceptibility, with males representing 78% of the 181 MH cases in the North American MH Registry (NAMHR) [26] and 73% of the 308 NAMHR patients included in a recent MH recrudescence study [58]. Finally, a similar male prevalence (~4 : 1) was observed in 383 MH cases in Japan from 1961 to 2004 [59].

In 2009, we published a study showing that male mice lacking CASQ1 trigger lethal-hyperthermic episodes with a higher rate of mortality than females when exposed to both halothane and heat, a phenotype resembling human MHS [15]. Here, we hypothesized that female sex hormones may play a role in protecting CASQ1-null animals from MH-lethal episodes and treated male mice with Premarin, a mixture of equine water-soluble estrogens [60, 61], and female mice with leuprolide acetate, a GnRH analog that chronically abolish the hypothalamic-pituitary-gonadal axis [62].

4.2. Main Findings. Consistent with the previous work [15], when exposed to halothane and heat stress protocol, CASQ1-null male mice exhibited a higher rate of mortality than female mice, that is, ~4 : 1 ratio. Though, following treatment with Premarin and leuprolide, mortality rate was effectively reverted in the two genders: during exposure to halothane and heat stress, mortality in Premarin-treated males was greatly reduced, while mortality in leuprolide-treated females was significantly increased. The reduced mortality rate in Premarin-treated CASQ1-null male mice was strictly correlated to (a) reduced rise in core temperature; (b) protection from fiber damage; (c) reduced responsiveness of EDL muscles to both temperature and caffeine; and finally (d) reduced SR depletion and increased caffeine-induced Ca^{2+} release. Conversely, the increased mortality rate in leuprolide-treated CASQ1-null female mice was correlated to increased rise in core temperature and fiber damage, enhanced responsiveness of EDL muscles to both temperature and caffeine, and imbalanced Ca^{2+} handling. Our data also showed that EDL muscles from female and Premarin-treated male mice displayed increased GSH/GSSG ratio and reduced levels of nitrated proteins (3-NT) compared to the other two groups of mice, suggesting that estrogens affect global levels of oxidative stress.

4.3. Estrogens and Oxidative Stress Levels in Muscle. Durham et al. [28] demonstrated that excessive Ca^{2+}-dependent production of ROS and RNS plays a pivotal step in the cellular

and molecular events leading to rhabdomyolysis of muscle fibers during MH crises, in RYR1$^{Y522S/WT}$ mice. We also recently reported that treatment of CASQ1-null male mice with antioxidants (i.e., N-acetylcysteine and Trolox) markedly reduced the rate of heat- and halothane-induced mortalities [29]. Finally, the data presented here points to a strict correlation between estrogens, reduced oxidative stress, and protection from MH episodes, as mice with lower levels of oxidative stress also display a reduced mortality, lowered hyperthermia, and protection from fiber damage. The fact that estrogens have potent antioxidant properties is documented in the literature [30, 63], the molecular bases being genomic and nongenomic mechanisms involving their binding to nuclear receptors ERα or ERβ [32] and novel G-protein coupled receptors GPR30 and ER-X localized in the plasma membrane [64, 65]. Also documented is the fact that estrogens may have direct free-radical scavenging properties, because of the similarity in structure to vitamin E [35]. Also, a recent publication showed the protective role conferred by estrogens in the right ventricle function by showing improved contractile [66]. Specifically, reserve in animals with pulmonary hypertension associated with benefits of mitochondrial bioenergetics (these authors demonstrated that estrogens improve the right ventricle contractility by improving mitochondria structure and function and preventing excessive mitochondrial-induced ROS generation).

Although several data reported in the literature demonstrated potent antioxidant properties of estrogens [30–35], the precise mechanisms by which they could modulate oxidative stress in CASQ1-null mice remain unclear.

Our data show that estrogens possibly exert their antioxidant activity by regulating the expression of NOX2 and nNOS, responsible for the generation of ROS and RNS in muscle fibers. Less straight forward is the interpretation of data regarding SOD1 and SOD2, significantly less expressed in muscles from female and Premarin-treated male mice compared to the other two groups of animals, a result though opposite to that of CAT. Data about SOD1 and SOD2 are in agreement with (a) our previous work showing that male CASQ1-null mice exhibited higher levels of SOD1 than the normal [29] and (b) the literature demonstrating that SOD1 and/or SOD2 expression and activity are increased under conditions of high oxidative stress [67–70].

One possible interpretation of these findings could be that in the presence of estrogens, the reduced expressions of both NOX2 and nNOS (and possibly the consequent reduction in generation of O_2^- and NO) would prevent the upregulation of SOD1 and SOD2 expressions and the consequence accumulation of H_2O_2. This, together with the concomitant increase of CAT levels, could result in reduction of global oxidative stress (Figure 6).

4.4. Ca^{2+} Handling, Oxidative Stress, and Hormones: The Complicated Puzzle Leading to MH Crises in Male CASQ1-Null Mice. Muscle fibers from male CASQ1-null mice display an excessive leak of Ca^{2+} from the SR in basal conditions (i.e., already without exposure to environmental triggers) [15], possibly resulting from RYR1 hyperactivity due to lack of CASQ1 inhibition on the RYR1 open state [9, 10]. Although SR Ca^{2+} leak is clearly the starting event in MH reactions, also other important mechanisms seem to play a pivotal role during the cascade of events leading to rhabdomyolysis of skeletal fibers. Indeed, we have extensively discussed above the involvement of oxidative stress in MH reaction in both RYR1$^{Y552S/WT}$ and CASQ1-null mice [28, 29, 39]. In this puzzle involving imbalanced Ca^{2+} handling and excessive oxidative stress (which are likely not independent from one another), female sex hormones come into play by modulating both parameters. Indeed, in the current study, we showed that estrogens normalize SR Ca^{2+} release by reducing temperature and caffeine sensitivity of EDL muscles during IVCT experiments and decay of electrically evoked SR Ca^{2+} release and caffeine-induced SR Ca^{2+} release. Although the molecular mechanisms by which estrogens normalize intracellular Ca^{2+} handling are still unclear, based on the present and previous studies in MH susceptible mice [15, 28, 29], we are probably entitled to speculate that this could be the consequence of their ability to lower oxidative stress, possibly through the modulation of enzymes like NOX2 and nNOS, involved in the maintenance of redox balance within muscle fibers. Interestingly, it has been demonstrated that (i) both NOX2 and nNOS colocalize with RYRs at the triad junctions [52, 71, 72]; (ii) ROS, generated by NOX2 in the proximity of triads, stimulates SR Ca^{2+} release through RYR1 [52, 73]; and (iii) in cardiac muscle, nNOS is activated by increases in myoplasmic Ca^{2+} concentration, likely due to its colocalization with RYR2 [71, 72], although in skeletal muscle most nNOS localizes in the sarcolemma [74].

Thus, it is possible that, in CASQ1-null muscle fibers, the close positioning of either NOX2 or nNOS to RYR1 and the Ca^{2+}-dependent activation of nNOS could be responsible for the excessive production of ROS and RNS which in turn would lead to glutathionylation and nitrosylation of specific cysteine residues [52, 55], oxidative modifications that further increase the opening probability of the leaky RYR1 channel; the consequent excessive release of Ca^{2+} from the SR would promote the dangerous feed-forward mechanism already proposed to underlie MH reactions [28].

4.5. Closing Remarks. Although the molecular pathways that allow estrogens to protect skeletal fibers from rhabdomyolysis during MH crises deserve further investigation, the present work contains convincing evidence that female sex hormones do provide an effective protection for CASQ1-null mice against lethal MH-like events. Whether similar mechanisms may underlie also differences in MH incidence between males and females in humans could be worth of consideration.

Abbreviations

CASQ1: Calsequestrin type-1
CASQ1-null: CASQ1 knockout mice
CAT: Catalase
EC coupling: Excitation-contraction coupling
EDL: Extensor digitorum longus
FDB: Flexor digitorum brevis

GSH: Reduced glutathione
GSSG: Oxidized glutathione
H_2O_2: Hydrogen peroxide
IVCT: *In vitro* contracture test
NO: Nitric oxide
nNOS: Neuronal nitric oxide synthase
NOX2: NADPH oxidase $gp91^{phox}$ membrane-bound subunit
MH: Malignant hyperthermia
O_2^-: Superoxide anion
ROS: Reactive species of oxygen
RNS: Reactive species of nitrogen
RYR: Ryanodine receptor
SOD1: Copper/zinc superoxide dismutase
SOD2: Manganese superoxide dismutase
SR: Sarcoplasmic reticulum.

Conflicts of Interest

The authors declare that they have no conflict of interest.

Authors' Contributions

Feliciano Protasi conceived and directed the study. Antonio Michelucci, Simona Boncompagni, and Marta Canato performed the experimental work and data analysis. In detail, Antonio Michelucci performed (a) *in vivo* experiments of mortality rate (Figure 1); (b) internal temperature measurements (Figure 2); (c) blood analysis of CK, K^+, and Ca^{2+} levels (Figures 3(i), 3(j), 3(k), and 3(l)); (d) ex vivo experiments in isolated EDL muscles (Figure 4); and (e) measurements of oxidative stress (Figures 6 and 7); Simona Boncompagni performed confocal microscopy acquisitions and quantitative assessment of fiber damage in histological sections (Figures 3(a), 3(b), 3(c), 3(d), 3(e), 3(f), 3(g), and 3(h)); Marta Canato and Carlo Reggiani performed *in vitro* Ca^{2+} measurements in isolated FDB fibers (Figure 5). Finally, Antonio Michelucci, Simona Boncompagni, and Feliciano Protasi wrote the manuscript.

Acknowledgments

This study was supported by the following grants: (a) Italian Telethon ONLUS Foundation (Rome, Italy): GGP13213 to Feliciano Protasi and Carlo Reggiani; (b) National Institute of Health (Bethesda, MD, U.S.A): AR059646-06 (subcontract to Feliciano Protasi); (c) Italian Ministry of Education, University and Research (Rome, Italy): RBFR13A20K to Simona Boncompagni; and (d) Italian Ministry of Health (Rome, Italy): GR-2011-02352681 to Simona Boncompagni. The authors thank Dr. Alessandro De Marco for the technical assistance in the experiments of Figure 6. Finally, the abstract of the manuscript was presented in "XIII annual meeting of the interuniversity Institute of Myology, 2016."

References

[1] G. Meissner, "Isolation and characterization of two types of sarcoplasmic reticulum vesicles," *Biochimica et Biophysica Acta*, vol. 389, no. 1, pp. 51–68, 1975.

[2] K. P. Campbell, D. H. MacLennan, and A. O. Jorgensen, "Staining of the Ca^{2+}-binding proteins, calsequestrin, calmodulin, troponin C, and S-100, with the cationic carbocyanine dye "stains-all"," *The Journal of Biological Chemistry*, vol. 258, no. 18, pp. 11267–11273, 1983.

[3] K. Yano and A. Zarain-Herzberg, "Sarcoplasmic reticulum calsequestrins: structural and functional properties," *Molecular and Cellular Biochemistry*, vol. 135, no. 1, pp. 61–70, 1994.

[4] T. Imagawa, J. S. Smith, R. Coronado, and K. P. Campbell, "Purified ryanodine receptor from skeletal muscle sarcoplasmic reticulum is the Ca^{2+}-permeable pore of the calcium release channel," *The Journal of Biological Chemistry*, vol. 262, no. 34, pp. 16636–16643, 1987.

[5] J. S. Smith, T. Imagawa, J. Ma, M. Fill, K. P. Campbell, and R. Coronado, "Purified ryanodine receptor from rabbit skeletal muscle is the calcium-release channel of sarcoplasmic reticulum," *The Journal of General Physiology*, vol. 92, no. 1, pp. 1–26, 1988.

[6] M. F. Schneider, "Control of calcium release in functioning skeletal muscle fibers," *Annual Review of Physiology*, vol. 56, pp. 463–484, 1994.

[7] N. Ikemoto, M. Ronjat, L. G. Meszaros, and M. Koshita, "Postulated role of calsequestrin in the regulation of calcium release from sarcoplasmic reticulum," *Biochemistry*, vol. 28, no. 16, pp. 6764–6771, 1989.

[8] T. Kawasaki and M. Kasai, "Regulation of calcium channel in sarcoplasmic reticulum by calsequestrin," *Biochemical and Biophysical Research Communications*, vol. 199, no. 3, pp. 1120–1127, 1994.

[9] N. A. Beard, M. M. Sakowska, A. F. Dulhunty, and D. R. Laver, "Calsequestrin is an inhibitor of skeletal muscle ryanodine receptor calcium release channels," *Biophysical Journal*, vol. 82, no. 1, Part 1, pp. 310–320, 2002.

[10] N. A. Beard, D. R. Laver, and A. F. Dulhunty, "Calsequestrin and the calcium release channel of skeletal and cardiac muscle," *Progress in Biophysics and Molecular Biology*, vol. 85, no. 1, pp. 33–69, 2004.

[11] C. Paolini, M. Quarta, A. Nori et al., "Reorganized stores and impaired calcium handling in skeletal muscle of mice lacking calsequestrin-1," *The Journal of Physiology*, vol. 583, Part 2, pp. 767–784, 2007.

[12] M. Canato, M. Scorzeto, M. Giacomello, F. Protasi, C. Reggiani, and G. J. Stienen, "Massive alterations of sarcoplasmic reticulum free calcium in skeletal muscle fibers lacking calsequestrin revealed by a genetically encoded probe," *Proceedings of the National Academy of Sciences of the United States of America*, vol. 107, no. 51, pp. 22326–22331, 2010.

[13] C. Paolini, M. Quarta, L. D'Onofrio, C. Reggiani, and F. Protasi, "Differential effect of calsequestrin ablation on structure and function of fast and slow skeletal muscle fibers," *Journal of Biomedicine and Biotechnology*, vol. 2011, Article ID 634075, 10 pages, 2011.

[14] F. Protasi, C. Paolini, M. Canato, C. Reggiani, and M. Quarta, "Lessons from calsequestrin-1 ablation *in-vivo*: much more than a Ca^{2+} buffer after all," *Journal of Muscle Research and Cell Motility*, vol. 32, no. 4-5, pp. 257–270, 2011.

[15] M. Dainese, M. Quarta, A. D. Lyfenko et al., "Anesthetic- and heat-induced sudden death in calsequestrin-1-knockout mice," *The FASEB Journal*, vol. 23, no. 6, pp. 1710–1720, 2009.

[16] F. Protasi, C. Paolini, and M. Dainese, "Calsequestrin-1: a new candidate gene for malignant hyperthermia and exertional/environmental heat stroke," *The Journal of Physiology*, vol. 587, Part 13, pp. 3095–3100, 2009.

[17] T. E. Nelson, E. W. Jones, J. H. Venable, and D. D. Kerr, "Malignant hyperthermia of Poland China swine: studies of a myogenic etiology," *Anesthesiology*, vol. 36, no. 1, pp. 52–56, 1972.

[18] E. W. Jones, T. E. Nelson, I. L. Anderson, D. D. Kerr, and T. K. Burnap, "Malignant hyperthermia of swine," *Anesthesiology*, vol. 36, no. 1, pp. 42–51, 1972.

[19] M. G. Chelu, S. A. Goonasekera, W. J. Durham et al., "Heat- and anesthesia-induced malignant hyperthermia in an RyR1 knock-in mouse," *The FASEB Journal*, vol. 20, no. 2, pp. 329-330, 2006.

[20] T. Yang, J. Riehl, E. Esteve et al., "Pharmacologic and functional characterization of malignant hyperthermia in the R163C RyR1 knock-in mouse," *Anesthesiology*, vol. 105, no. 6, pp. 1164–1175, 2006.

[21] H. Rosenberg, N. Sambuughin, S. Riazi, and R. Dirksen, "Malignant hyperthermia susceptibility," 1993.

[22] D. H. MacLennan and M. S. Phillips, "Malignant hyperthermia," *Science*, vol. 256, no. 5058, pp. 789–794, 1992.

[23] T. E. Nelson, "Abnormality in calcium release from skeletal sarcoplasmic reticulum of pigs susceptible to malignant hyperthermia," *The Journal of Clinical Investigation*, vol. 72, no. 3, pp. 862–870, 1983.

[24] J. R. Mickelson, E. M. Gallant, L. A. Litterer, K. M. Johnson, W. E. Rempel, and C. F. Louis, "Abnormal sarcoplasmic reticulum ryanodine receptor in malignant hyperthermia," *The Journal of Biological Chemistry*, vol. 263, no. 19, pp. 9310–9315, 1988.

[25] K. P. Strazis and A. W. Fox, "Malignant hyperthermia: a review of published cases," *Anesthesia and Analgesia*, vol. 77, no. 2, pp. 297–304, 1993.

[26] B. W. Brandom and M. G. Larach, "Reassessment of the safety and efficacy of dantrolene," *Anesthesiology*, vol. 96, article A1199, 2002.

[27] T. Migita, K. Mukaida, M. Kawamoto, M. Kobayashi, I. Nishino, and O. Yuget, "Propofol-induced changes in myoplasmic calcium concentrations in cultured human skeletal muscles from RYR1 mutation carriers," *Anaesthesia and Intensive Care*, vol. 35, no. 6, pp. 894–898, 2007.

[28] W. J. Durham, P. Aracena-Parks, C. Long et al., "RyR1 S-nitrosylation underlies environmental heat stroke and sudden death in Y522S RyR1 knockin mice," *Cell*, vol. 133, no. 1, pp. 53–65, 2008.

[29] A. Michelucci, C. Paolini, M. Canato et al., "Antioxidants protect calsequestrin-1 knockout mice from halothane- and heat-induced sudden death," *Anesthesiology*, vol. 123, no. 3, pp. 603–617, 2015.

[30] A. D. Mooradian, "Antioxidant properties of steroids," *The Journal of Steroid Biochemistry and Molecular Biology*, vol. 45, no. 6, pp. 509–511, 1993.

[31] M. A. Gomez-Zubeldia, J. J. Arbues, G. Hinchado, A. G. Nogales, and J. C. Millan, "Influence of estrogen replacement therapy on plasma lipid peroxidation," *Menopause*, vol. 8, no. 4, pp. 274–280, 2001.

[32] C. Borras, J. Gambini, M. C. Gomez-Cabrera et al., "17β-oestradiol up-regulates longevity-related, antioxidant enzyme expression via the ERK1 and ERK2$^{[MAPK]}$/NFκB cascade," *Aging Cell*, vol. 4, no. 3, pp. 113–118, 2005.

[33] M. Florian, A. Freiman, and S. Magder, "Treatment with 17-beta-estradiol reduces superoxide production in aorta of ovariectomized rats," *Steroids*, vol. 69, no. 13-14, pp. 779–787, 2004.

[34] A. H. Wagner, M. R. Schroeter, and M. Hecker, "17beta-estradiol inhibition of NADPH oxidase expression in human endothelial cells," *The FASEB Journal*, vol. 15, no. 12, pp. 2121–2130, 2001.

[35] K. Sugioka, Y. Shimosegawa, and M. Nakano, "Estrogens as natural antioxidants of membrane phospholipid peroxidation," *FEBS Letters*, vol. 210, no. 1, pp. 37–39, 1987.

[36] L. Pietrangelo, A. D'Incecco, A. Ainbinder et al., "Age-dependent uncoupling of mitochondria from Ca^{2+} release units in skeletal muscle," *Oncotarget*, vol. 6, no. 34, pp. 35358–35371, 2015.

[37] E. Defranchi, E. Bonaccurso, M. Tedesco et al., "Imaging and elasticity measurements of the sarcolemma of fully differentiated skeletal muscle fibres," *Microscopy Research and Technique*, vol. 67, no. 1, pp. 27–35, 2005.

[38] I. Rahman, A. Kode, and S. K. Biswas, "Assay for quantitative determination of glutathione and glutathione disulfide levels using enzymatic recycling method," *Nature Protocols*, vol. 1, no. 6, pp. 3159–3165, 2006.

[39] C. Paolini, M. Quarta, L. Wei-LaPierre et al., "Oxidative stress, mitochondrial damage, and cores in muscle from calsequestrin-1 knockout mice," *Skeletal Muscle*, vol. 5, p. 10, 2015.

[40] A. Bouchama and J. P. Knochel, "Heat stroke," *The New England Journal of Medicine*, vol. 346, no. 25, pp. 1978–1988, 2002.

[41] M. Davis, R. Brown, A. Dickson et al., "Malignant hyperthermia associated with exercise-induced rhabdomyolysis or congenital abnormalities and a novel RYR1 mutation in New Zealand and Australian pedigrees," *British Journal of Anaesthesia*, vol. 88, no. 4, pp. 508–515, 2002.

[42] J. F. Capacchione, N. Sambuughin, S. Bina, L. P. Mulligan, T. D. Lawson, and S. M. Muldoon, "Exertional rhabdomyolysis and malignant hyperthermia in a patient with ryanodine receptor type 1 gene, L-type calcium channel alpha-1 subunit gene, and calsequestrin-1 gene polymorphisms," *Anesthesiology*, vol. 112, no. 1, pp. 239–244, 2010.

[43] European MH Group, "A protocol for the investigation of malignant hyperpyrexia (MH) susceptibility," *British Journal of Anaesthesia*, vol. 56, pp. 1267–1269, 1984.

[44] M. G. Larach, "Standardization of the caffeine halothane muscle contracture test. North American malignant hyperthermia group," *Anesthesia and Analgesia*, vol. 69, no. 4, pp. 511–515, 1989.

[45] J. R. Lopez, N. Linares, I. N. Pessah, and P. D. Allen, "Enhanced response to caffeine and 4-chloro-m-cresol in malignant hyperthermia-susceptible muscle is related in part to chronically elevated resting $[Ca^{2+}]_i$," *American Journal of Physiology-Cell Physiology*, vol. 288, no. 3, pp. C606–C612, 2005.

[46] V. Tegazzin, E. Scutari, S. Treves, and F. Zorzato, "Chlorocresol, an additive to commercial succinylcholine, induces contracture of human malignant hyperthermia-susceptible muscles via activation of the ryanodine receptor Ca^{2+} channel," *Anesthesiology*, vol. 84, no. 6, pp. 1380–1385, 1996.

[47] H. Sies, "Glutathione and its role in cellular functions," *Free Radical Biology & Medicine*, vol. 27, no. 9-10, pp. 916–921, 1999.

[48] A. Pompella, A. Visvikis, A. Paolicchi, V. De Tata, and A. F. Casini, "The changing faces of glutathione, a cellular protagonist," *Biochemical Pharmacology*, vol. 66, no. 8, pp. 1499–1503, 2003.

[49] M. Asensi, J. Sastre, F. V. Pallardo et al., "Ratio of reduced to oxidized glutathione as indicator of oxidative stress status and DNA damage," *Methods in Enzymology*, vol. 299, pp. 267–276, 1999.

[50] K. Ogino and D. H. Wang, "Biomarkers of oxidative/nitrosative stress: an approach to disease prevention," *Acta Medica Okayama*, vol. 61, no. 4, pp. 181–189, 2007.

[51] K. Bedard and K. H. Krause, "The NOX family of ROS-generating NADPH oxidases: physiology and pathophysiology," *Physiological Reviews*, vol. 87, no. 1, pp. 245–313, 2007.

[52] C. Hidalgo, G. Sánchez, G. Barrientos, and P. Aracena-Parks, "A transverse tubule NADPH oxidase activity stimulates calcium release from isolated triads via ryanodine receptor type 1 S -glutathionylation," *The Journal of Biological Chemistry*, vol. 281, no. 36, pp. 26473–26482, 2006.

[53] A. Espinosa, A. García, S. Härtel, C. Hidalgo, and E. Jaimovich, "NADPH oxidase and hydrogen peroxide mediate insulin-induced calcium increase in skeletal muscle cells," *The Journal of Biological Chemistry*, vol. 284, no. 4, pp. 2568–2575, 2009.

[54] L. Kobzik, M. B. Reid, D. S. Bredt, and J. S. Stamler, "Nitric oxide in skeletal muscle," *Nature*, vol. 372, no. 6506, pp. 546–548, 1994.

[55] J. S. Stamler and G. Meissner, "Physiology of nitric oxide in skeletal muscle," *Physiological Reviews*, vol. 81, no. 1, pp. 209–237, 2001.

[56] J. M. McCord and I. Fridovich, "The utility of superoxide dismutase in studying free radical reactions. I. Radicals generated by the interaction of sulfite, dimethyl sulfoxide, and oxygen," *The Journal of Biological Chemistry*, vol. 244, no. 22, pp. 6056–6063, 1969.

[57] S. K. Powers, L. L. Ji, A. N. Kavazis, and M. J. Jackson, "Reactive oxygen species: impact on skeletal muscle," *Comprehensive Physiology*, vol. 1, no. 2, pp. 941–969, 2011.

[58] J. M. Burkman, K. L. Posner, and K. B. Domino, "Analysis of the clinical variables associated with recrudescence after malignant hyperthermia reactions," *Anesthesiology*, vol. 106, no. 5, pp. 901–906, 2007.

[59] T. Migita, K. Mukaida, M. Kawamoto, M. Kobayashi, and O. Yuge, "Fulminant-type malignant hyperthermia in Japan: cumulative analysis of 383 cases," *Journal of Anesthesia*, vol. 21, no. 2, pp. 285–288, 2007.

[60] L. D. McCullough, N. J. Alkayed, R. J. Traystman, M. J. Williams, and P. D. Hurn, "Postischemic estrogen reduces hypoperfusion and secondary ischemia after experimental stroke," *Stroke*, vol. 32, no. 3, pp. 796–802, 2001.

[61] K. H. Shen, C. H. Lin, H. K. Chang, W. C. Chen, and S. H. Chen, "Premarin can act via estrogen receptors to rescue mice from heatstroke-induced lethality," *Shock*, vol. 30, no. 6, pp. 668–674, 2008.

[62] A. C. Wilson, S. V. Meethal, R. L. Bowen, and C. S. Atwood, "Leuprolide acetate: a drug of diverse clinical applications," *Expert Opinion on Investigational Drugs*, vol. 16, no. 11, pp. 1851–1863, 2007.

[63] M. A. Gomez-Zubeldia, G. Hinchado, J. J. Arbues, A. G. Nogales, and J. C. Millan, "Influence of estradiol on oxidative stress in the castrated rat uterus," *Gynecologic Oncology*, vol. 80, no. 2, pp. 227–232, 2001.

[64] C. M. Revankar, D. F. Cimino, L. A. Sklar, J. B. Arterburn, and E. R. Prossnitz, "A transmembrane intracellular estrogen receptor mediates rapid cell signaling," *Science*, vol. 307, no. 5715, pp. 1625–1630, 2005.

[65] T. Funakoshi, A. Yanai, K. Shinoda, M. M. Kawano, and Y. Mizukami, "G protein-coupled receptor 30 is an estrogen receptor in the plasma membrane," *Biochemical and Biophysical Research Communications*, vol. 346, no. 3, pp. 904–910, 2006.

[66] A. Liu, J. Philip, K. C. Vinnakota et al., "Estrogen maintains mitochondrial content and function in the right ventricle of rats with pulmonary hypertension," *Physiological Reports*, vol. 5, no. 6, 2017.

[67] M. H. Disatnik, J. Dhawan, Y. Yu et al., "Evidence of oxidative stress in mdx mouse muscle: studies of the pre-necrotic state," *Journal of the Neurological Sciences*, vol. 161, no. 1, pp. 77–84, 1998.

[68] J. M. Lawler, W. Song, and S. R. Demaree, "Hindlimb unloading increases oxidative stress and disrupts antioxidant capacity in skeletal muscle," *Free Radical Biology & Medicine*, vol. 35, no. 1, pp. 9–16, 2003.

[69] D. J. Mahoney, J. J. Kaczor, J. Bourgeois, N. Yasuda, and M. A. Tarnopolsky, "Oxidative stress and antioxidant enzyme upregulation in SOD1-G93A mouse skeletal muscle," *Muscle & Nerve*, vol. 33, no. 6, pp. 809–816, 2006.

[70] P. M. Abruzzo, S. di Tullio, C. Marchionni et al., "Oxidative stress in the denervated muscle," *Free Radical Research*, vol. 44, no. 5, pp. 563–576, 2010.

[71] J. M. Hare, "Nitric oxide and excitation-contraction coupling," *Journal of Molecular and Cellular Cardiology*, vol. 35, no. 7, pp. 719–729, 2003.

[72] L. A. Barouch, R. W. Harrison, M. W. Skaf et al., "Nitric oxide regulates the heart by spatial confinement of nitric oxide synthase isoforms," *Nature*, vol. 416, no. 6878, pp. 337–339, 2002.

[73] R. Xia, J. A. Webb, L. L. Gnall, K. Cutler, and J. J. Abramson, "Skeletal muscle sarcoplasmic reticulum contains a NADH-dependent oxidase that generates superoxide," *American Journal of Physiology-Cell Physiology*, vol. 285, no. 1, pp. C215–C221, 2003.

[74] K. E. Wells, S. Torelli, Q. Lu et al., "Relocalization of neuronal nitric oxide synthase (nNOS) as a marker for complete restoration of the dystrophin associated protein complex in skeletal muscle," *Neuromuscular Disorders*, vol. 13, no. 1, pp. 21–31, 2003.

Hindawi
Oxidative Medicine and Cellular Longevity
Volume 2017, Article ID 1987218, 10 pages
https://doi.org/10.1155/2017/1987218

Research Article

Increased Circulating Levels of Interleukin-6 Induce Perturbation in Redox-Regulated Signaling Cascades in Muscle of Dystrophic Mice

Laura Pelosi,[1] Laura Forcina,[1] Carmine Nicoletti,[1] Bianca Maria Scicchitano,[2] and Antonio Musarò[1,3]

[1]*DAHFMO-Unit of Histology and Medical Embryology, Sapienza University of Rome, Laboratory affiliated to Istituto Pasteur Italia-Fondazione Cenci Bolognetti, Rome, Italy*
[2]*Institute of Histology and Embryology, School of Medicine, Catholic University of the Sacred Heart, Rome, Italy*
[3]*Center for Life Nano Science@Sapienza, Istituto Italiano di Tecnologia, Rome, Italy*

Correspondence should be addressed to Antonio Musarò; antonio.musaro@uniroma1.it

Received 7 April 2017; Revised 31 May 2017; Accepted 7 June 2017; Published 6 August 2017

Academic Editor: Andrea Vasconsuelo

Duchenne muscular dystrophy (DMD) is an X-linked genetic disease in which dystrophin gene is mutated, resulting in dysfunctional or absent dystrophin protein. The pathology of dystrophic muscle includes degeneration, necrosis with inflammatory cell invasion, regeneration, and fibrous and fatty changes. Nevertheless, the mechanisms by which the absence of dystrophin leads to muscle degeneration remain to be fully elucidated. An imbalance between oxidant and antioxidant systems has been proposed as a secondary effect of DMD. However, the significance and precise extent of the perturbation in redox signaling cascades is poorly understood. We report that mdx dystrophic mice are able to activate a compensatory antioxidant response at the presymptomatic stage of the disease. In contrast, increased circulating levels of IL-6 perturb the redox signaling cascade, even prior to the necrotic stage, leading to severe features and progressive nature of muscular dystrophy.

1. Introduction

Duchenne muscular dystrophy (DMD) is an X-linked genetic disease caused by mutations in the dystrophin gene, leading to instability of the dystrophin-glycoprotein complex (DGC) with subsequent necrosis and fibrosis [1].

Although the genetic basis of DMD is known, the mechanisms by which the primary genetic defect leads to muscle wasting remain to be fully elucidated [2–4]. Among the potential factors involved in the pathogenesis of muscular dystrophy, oxidative stress [5, 6] might be responsible for the activation of degenerative processes and for the appearance and progress of pathologic changes in dystrophic muscles [4]. Nevertheless, the significance and precise role of excessive oxidant-related damage is poorly understood. The reactive oxygen species (ROS) are naturally and constantly formed inside of the organism, as a result of cell activity. It is plausible that under physiological conditions, skeletal muscle activates an endogenous program of antioxidant defense to maintain the ROS production at physiological levels [7]. Extreme or pathologic conditions generate much higher levels of ROS that overwhelm cellular antioxidant defenses, leading to protein carbonylation, DNA damage, and RNA oxidation. The excess of ROS production can also alter calcium handling, another pathogenic factor associated with muscular dystrophy, leading to the activation of proteolytic systems and muscle wasting [8, 9].

Different animal models of dystrophin deficiency are actively studied. The mdx mouse is the most widely used model for muscular dystrophy [2]. However, the mdx mouse presents some limitations, including the pathophysiology and clinical outcome criteria, compared to DMD patients, due to the fact that skeletal muscles of mdx mice undergo extensive necrosis only early in neonatal life. Thus, there is

a greater imperative towards improving the validity of animal models and the design of preclinical experimental therapeutic approaches. We recently generated a more severe animal model, the mdx/IL6 mouse, that closely approximates the human disease and more faithfully recapitulates the disease progression in humans [10]. In particular, we observed that forced expression of IL-6 in the adult mdx mice, increased necrosis, sustained inflammatory response, and repeated cycles of muscle degeneration and regeneration, leading to exhaustion of satellite cells [10].

In this study, we analysed whether the exacerbated phenotype induced by increased circulating levels of IL-6 involves a perturbation in redox signaling cascade, even prior to the necrotic phase. We revealed, in mdx/IL6 mice, a progressive reduction of the Nrf2-dependent antioxidant compensatory mechanism, a severe phenotypic feature observed in human DMD patients [11].

2. Materials and Methods

2.1. Mice and Treatments. Animal models used in the current study are 2-, 4-, and 24-week-old wild-type C57Bl/6J mice and mdx (Jackson Laboratories) and mdx/IL6 [10] transgenic mice. moAb-IL6R treatment: mdx mice were injected subcutaneously, starting at 15 days of age, with the neutralizing monoclonal antibody MR16-1 (kindly provided by Chugai Pharmaceutical Co., Ltd.) [3, 12] to the murine IL-6 receptor (moAb-IL6R) at a dose of 100 μg/g of body weight and then twice a week with 20 μg/g (for a total of 5 doses) in PBS [3]. Mice were sacrificed at 4 weeks of age. Animals were maintained according to the institutional guidelines of the animal facility of the unit of Histology and Medical Embryology. All the animal experiments were approved by the ethics committee of Sapienza University of Rome-Unit of Histology and Medical Embryology and were performed in accordance with the current version of the Italian law on the protection of animals.

2.2. Protein Extraction and Western Blot Analysis. Diaphragm muscles were isolated from 2-, 4-, and 24-week-old mdx and mdx/IL6 mice and immediately frozen in liquid nitrogen. Each sample (liquid nitrogen powdered diaphragm muscles) was homogenized in protein lysis buffer [Tris-HCl, pH 7.5/20 mM, EDTA/2 mM, EGTA/2 mM, sucrose/250 mM, DTT/5 mM, Triton-X/0.1%, PMSF/1 mM, NaF/10 mM, SOV4/0.2 mM, cocktail protease inhibitors/1X (Sigma Aldrich)]. Western blotting analysis was performed using 70 μg of protein extracts, and filters were blotted with antibodies against gp91phox (BD Transduction Laboratories), Nrf2 (Santa Cruz Biotechnology), NFκB p65 (ser536; Cell Signaling), NFκB (Cell Signaling), α-tubulin (Sigma Aldrich), β-tubulin (Cell Signaling), Glu-tubulin (detyrosinated α-tubulin; Abcam), and GAPDH (Santa Cruz Biotechnology). Signals derived from appropriate HRP-conjugated secondary antibodies (Bethyl Laboratories) were captured by Chemi DocTM XRS 2015 (Bio-Rad Laboratories), and densitometric analysis was performed using Image Lab software (version 5.2.1; Bio-Rad Laboratories©).

2.3. RNA Extraction and Quantitative Real-Time PCR Analysis. The total mRNA of 2-, 4-, and 24-week-old wild-type, mdx, and mdx/IL6 mice was extracted from liquid nitrogen powdered diaphragm muscle in TRI Reagent (Sigma-Aldrich) using Tyssue Lyser (Qiagen). To synthesize double-stranded cDNA, 1 μg of each RNA sample was reverse transcribed using the QuantiTect Reverse Transcription kit (Qiagen). For the analysis of IL-6, TNFα, IL-1β, IL-10, and IL6rα, cDNA from each sample was preamplified using the TaqMan PreAmp Master Mix (Applied Biosystem) according to the manufacturer's protocol. Quantitative real-time PCR was performed, with or without preamplification procedure, on ABI PRISM 7500 SDS (Applied Biosystem) using specific 6-carboxyfluorescein (FAM)-labeled TaqMan assays for SIRT1, Utrn, SOD1, SOD2, CAT-1, Gpx1, GCLC, GCLM, NQO1, HO-1, IL-6, TNFα, IL-1β, IL-10, IL6rα, and Hprt as housekeeping genes (Applied Biosystem). Data were analysed using the 2-DDCt method and reported as mean fold change in gene expression relative to wild type.

2.4. Dihydroethidium Staining and Confocal Analysis for ROS Detection. Muscles from wild-type, mdx, mdx/IL-6, and mdx-treated mice with the neutralizing monoclonal antibody to the IL-6 receptor (moAb-IL6R) were embedded in tissue freezing medium and snap frozen in nitrogen-cooled isopentane. Muscle frozen sections (30 μm) were incubated with 5 μM dihydroethidium (DHE) (Molecular Probes; #D23107) in PBS at 37°C for 30 min [13] and analysed at confocal microscopy (Laser-Scanning TCS SP2; Leica) to reveal ROS production. DHE fluorescence was analysed with LAS AF Lite software, measuring the total intensity of DHE fluorescence, which represents the full amount of fluorescence held within the entire z-axis of the series. 60 optical sections/genotype for three separate experiments were analysed.

2.5. Data and Statistical Analysis. Statistical analysis was performed using the GraphPad Prism software (San Diego, CA, USA). Statistically significant differences among groups were assessed using one-way ANOVA with a Bonferroni's posttest or Dunn's posttest and between pairs with Mann–Whitney test or Student's t-test for normally distributed variables. All data are presented as mean ± SEM; $p < 0.05$ is considered statistically significant. Sample size was predetermined based on the variability observed in preliminary and similar experiments. All experiments requiring animal models were subjected to randomization based on litter.

3. Results

3.1. Increased Levels of IL-6 Cytokine Contribute to Enhance Markers of ROS Production in mdx Mouse Model. The progress of the dystropathology in the mdx mouse model has been extensively described. A prenecrotic stage, characterized by normal myofibres with peripheral nuclei, intact sarcolemma, and nonfragmented sarcoplasm, is observed within the first 21 days of age. Necrosis peaks by 25-26 days and then significantly decreases to stabilize by 8 weeks of age to a relatively low level of active damage [2]. Among the

secondary processes that accompany muscle degeneration, the infiltration of inflammatory cells reflects the immune response to tissue damage.

To verify whether oxidative stress is a direct consequence of necrosis and inflammation or whether it can be induced in the prenecrotic stage, we analysed relevant markers of the redox signaling in the muscle of 2-week-old mdx mice. We found a strong upregulation of gp91phox (NOX2), the main source of ROS production [14, 15], in the diaphragm of 2-week-old mdx mice compared to wild-type littermates (Figure 1(a)), suggesting the presence of pro-oxidant conditions during the early disease stages. This was supported by a significant reduction in SIRT1 and Nrf2 expressions (Figures 1(b) and 1(c)), which are important mediators that promote the antioxidant response by activating several antioxidant enzymes [16–20].

It has been reported that, although with the absence of significant infiltration of mononuclear inflammatory cells within the dystrophic muscle, DMD patients display an increase in the plasma levels of proinflammatory cytokines at the presymptomatic stage of the disease [21]. Thus, the release of specific proinflammatory cytokines can stimulate ROS production, enhancing cellular damage in DMD [22]. To support this evidence, we analysed relevant markers of the oxidant and antioxidant signaling in the muscle of mdx/IL6 mice [10] at the prenecrotic stage. Increased IL-6 plasma levels induced a strong upregulation of gp91phox expression (Figure 1(a)) accompanied by a significant downregulation of SIRT1 and Nrf2 expressions (Figures 1(b) and 1(c)) in 2-week-old mdx/IL6 mice, compared to both wild-type and mdx littermates. This suggests that IL-6 promotes a perturbation of redox status in dystrophic muscles, modulating relevant factors of the redox signaling even in the prenecrotic phase.

To casually link IL-6 overexpression with ROS production in DMD pathology, we treated 2-week-old mdx mice with the neutralizing monoclonal antibody to the IL-6 receptor (moAb-IL6R), as previously described [3]. Fifteen days after the treatment, we analysed the ROS-sensitive dye DHE in the muscle of untreated and moAb-IL6R-treated mdx mice. Figure 1(d) shows a strong reduction of DHE fluorescence in moAb-IL6R-treated mdx compared to untreated mdx mice, indicating that IL-6 blockade prevents excessive ROS production in dystrophic muscles. Notably, the muscle of mdx/IL6 mice displayed a significant increase of DHE fluorescence compared to that of control mdx and moAb-IL6R-treated mdx littermates (Figure 1(d)), supporting the role of IL-6 in the induction of pathologic changes observed at prenecrotic stage.

Overexpression of utrophin (Utrn) is able to counteract the lack of dystrophin protecting the sarcolemma integrity in the dystrophic muscle [23, 24]. Thus, we evaluated the levels of Utrn mRNA in the diaphragm of 2-week-old wild-type, mdx, and mdx/IL6 mice and we found a significant upregulation of its expression in mdx mice, compared to both wild-type and mdx/IL6 mice (Figure 1(e)). Interestingly, IL-6 overexpression reduced Utrn expression compared to mdx littermates, further supporting the evidence that the mdx/IL6 mouse model closely approximates the human disease and more faithfully recapitulates the disease progression in humans.

3.2. Analysis of Nrf2 Antioxidant Genes in Muscle of Dystrophic Mice at Prenecrotic Stage. We have recently reported the central role of Nrf2 signaling pathway in the pathogenesis of DMD [11]. To better define the Nrf2-dependent antioxidant response in the prenecrotic dystrophic muscle, we analysed the expression of Nrf2 antioxidant enzymes in 2-week-old mdx mice (Figure 2). We found that the levels of several Nrf2-regulated gene expressions including SOD1/2, CAT-1, Gpx1, and GCL [25] were expressed at similar levels in both 2-week-old wild-type and mdx mice, whereas NAD(P)H quinone dehydrogenase 1 (NQO1), the enzyme catalyzing the reduction of quinones to hydroquinones, was reduced in mdx mice compared to wild-type littermates (Figure 2(a)). Of note, ROS-detoxifying enzymes, such as catalase-1 and Gpx1, were significantly reduced in mdx/IL6 compared to mdx mice, being consistent with the reduction in Nrf2 protein level (Figure 1(c)).

Interestingly, HO-1, another Nrf2-regulated gene and a modulator of the inflammatory response, was upregulated in both mdx and mdx/IL6 mice compared to wild-type littermates, although the expression of HO-1 resulted reduced in mdx/IL6 mice compared to mdx littermates (Figure 2(b)). It is plausible that the initial increase in IL-6 plasma levels induces an alteration in the redox signaling, which might stimulate the inflammatory response. To support this hypothesis, we analysed the expression of both proinflammatory cytokines such as IL-6, TNFα, and IL-1β and anti-inflammatory cytokine, such as IL-10, in 2-week-old dystrophic mice (Figures 2(c), 2(d), 2(e), and 2(f)). We found that increased plasma levels of IL-6 induced an upregulation of relevant markers of muscle wasting, such as IL6Rα (Figure 2(g)), IL-1β (Figure 2(e)), TNFα (Figure 2(d)), and NFκB (Figure 2(h)) [26, 27] in mdx/IL6 mice, compared to mdx littermates. This suggests that IL-6 triggers an alteration in the redox signaling, initiating degenerative process [22, 26, 27].

3.3. X-ROS Signaling Is Altered in Prenecrotic Dystrophic Diaphragm Muscle and Increases during the Progression of Pathology. In DMD, the primary defect leads to the alteration of microtubule network (MT network) that activates robust NOX2-dependent ROS production, a pathway called X-ROS [28]. A complete transcriptome analysis on biopsies of DMD patients has also revealed an upregulation of several X-ROS-related transcripts, including NOX2 and nine different tubulin isoforms [28]. Moreover, genetic silencing of Nrf2 enhances X-ROS signaling in a mild mouse model of DMD [29], suggesting a correlation between X-ROS signaling and Nrf2-dependent antioxidant response. The upregulation of NOX2's catalytic (gp91phox) subunit, which we observed in the prenecrotic dystrophic muscle (Figure 1(b)), suggests the presence of pro-oxidant conditions that could be dependent by the alteration of X-ROS signaling.

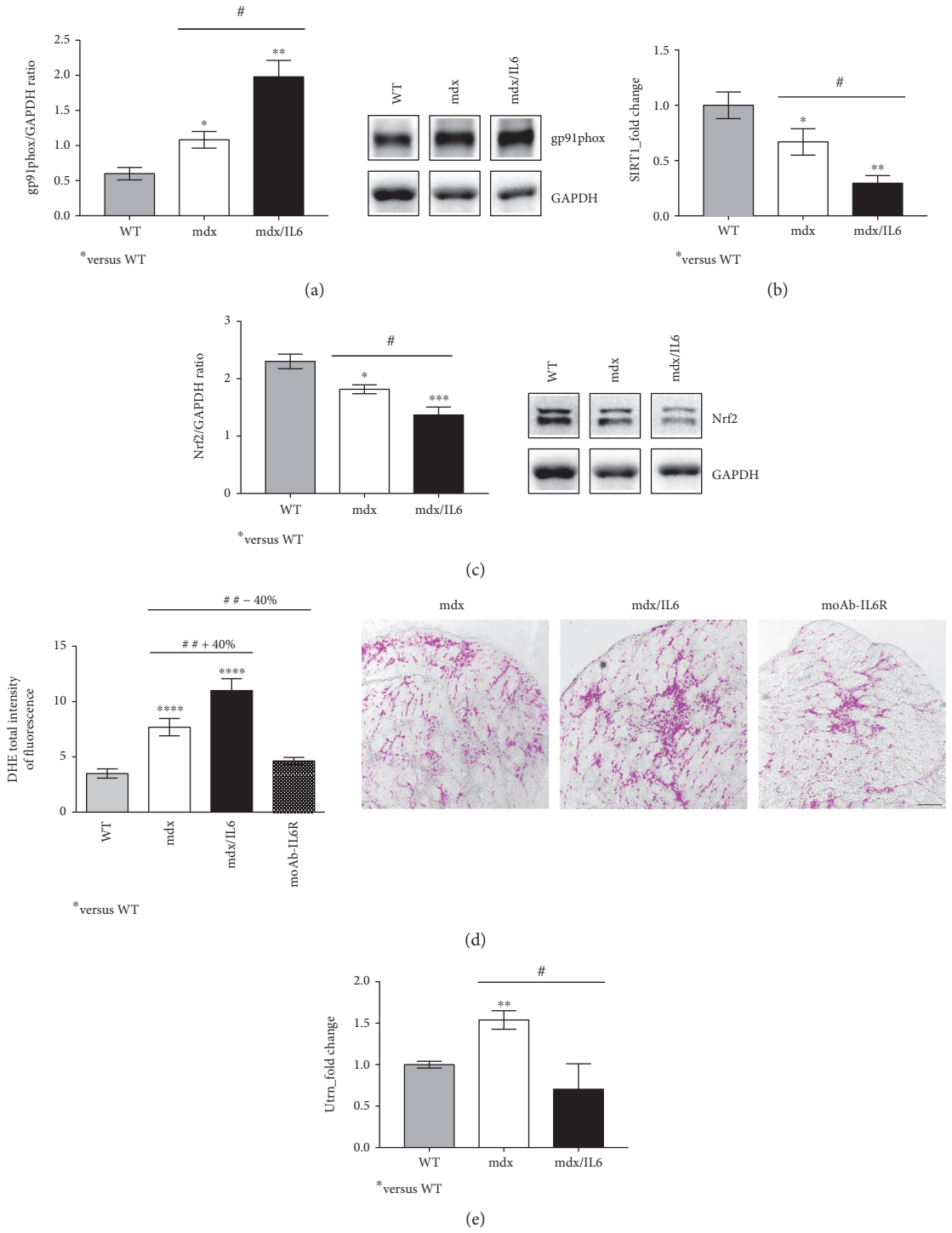

Figure 1: Analysis of redox-regulating signaling in the diaphragm muscle of 2-week-old dystrophic mice. Western blot analysis (right panels show representative images) for the expression of gp91phox (a) and Nrf2 (c) proteins in 2-week-old wild-type (WT), mdx, and mdx/IL6 mice. Values represent mean ± SEM; $n = 3$ to 6 mice per group. $^{*}p < 0.05$, $^{**}p < 0.005$, and $^{***}p < 0.0005$ compared to WT mice; $^{\#}p < 0.05$ between mdx and mdx/IL6 littermates by ANOVA. Real-time PCR analysis performed on diaphragm muscles from WT, mdx, and mdx/IL6 mice at 2 weeks of age for the expression of SIRT1 (b) and utrophin (Utrn) (e). Values are reported as fold change in expression and represent mean ± SEM; $n = 4$ to 12 per group. $^{*}p < 0.05$, $^{**}p < 0.005$ compared to WT mice; $^{\#}p < 0.05$ (by ANOVA). (d) Blockade of IL-6 receptor by moAb-IL6R neutralizing antibody reduces the amount of DHE-derived fluorescence in treated mdx compared to untreated mdx mice. Graphs (left panel) show the quantification of DHE total intensity in the muscles of indicated genotypes. The right panel shows representative images of DHE staining from the muscle sections of 4-week-old mdx/IL-6 and moAb-IL6R-treated and untreated mdx mice. Scale bar, 100 μm. Values represent mean ± SEM; $n = 3$ independent experiments. $^{****}p < 0.0001$, $^{\#\#}p < 0.005$ using ANOVA. In (a) and (c), the lanes were run on the same gel but were not contiguous.

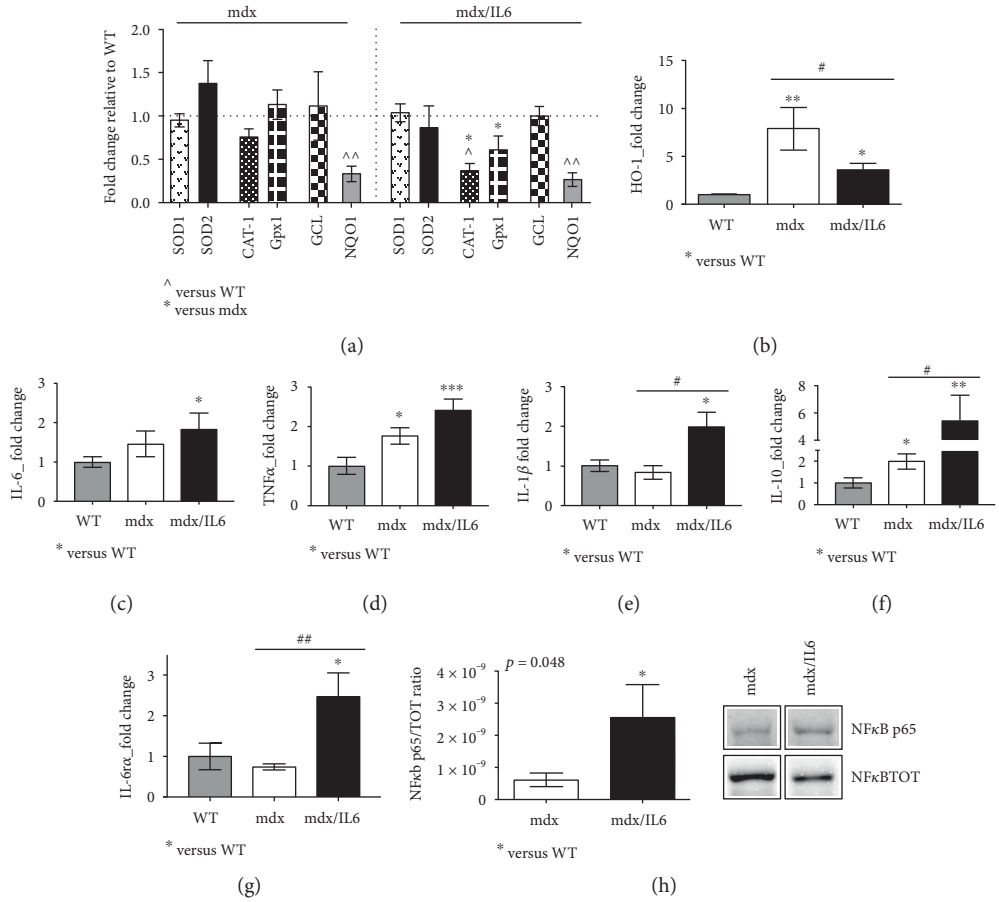

Figure 2: Nrf2 antioxidant genes are differently regulated in the prenecrotic dystrophic muscle. (a) Real-time PCR analysis of Nrf2-dependent genes (SOD1, SOD2, CAT-1, Gpx1, GCL, and NQO1) performed on the diaphragm muscle of 2-week-old WT, mdx, and mdx/IL6 mice. Values are reported as fold change in expression relative to the calibrator (WT, horizontal dot line) and represent mean ± SEM; $n = 3$ to 5 per group. p value by unpaired statistical tests. $^{\wedge}p < 0.05$, $^{\wedge\wedge}p < 0.005$. Analysis of HO-1 mRNA (b), IL-6 mRNA (c), TNFα mRNA (d), IL-1β mRNA (e), IL-10 mRNA (f), and IL6rα mRNA (g) expressions in the diaphragm of 2-week-old WT, mdx, and mdx/IL6 mice. Data are presented as the mean ± SEM; $n = 3$ to 6 mice per group. $^{*}p < 0.05$, $^{**}p < 0.005$, and $^{***}p < 0.0005$ compared to WT mice; $^{\#}p < 0.05$, $^{\#\#}p < 0.005$ between mdx and mdx/IL6 littermates (by ANOVA). (h) Densitometric analysis (left panel) and representative western blot (right panel) for NFκB active (NFκB p65) and total (NFκB TOT) protein expression in the diaphragm muscle of indicated genotypes. Values are reported as mean ± SEM; $n = 5$ to 7 per group. p using Student's two-tailed t-test. In (h), gels were simultaneously run under same experimental conditions.

To support this hypothesis, we analysed the density of MT network in terms of the abundance of α-, β-, and Glu-tubulin proteins, in dystrophic muscles at 2 weeks of age (Figures 3(a), 3(b), and 3(c)). We found an upregulation of the overall subunits in mdx and mdx/IL6 compared to wild type mice, indicating an alteration of microtubule network at this stage of pathology. Notably, we observed a significant increase in detyrosination of tubulin content (Glu-tubulin), but not of the α (Figure 3(a))- and β (Figure 3(b))-tubulin subunits, in the diaphragm of mdx/IL6 mice compared to mdx littermates (Figure 3(c)).

To verify whether ROS production parallels X-ROS signaling during the progression of DMD pathology, we analysed gp91phox expression and microtubule subunits' content in dystrophic mice at 4 and 24 weeks of age (Figures 3(d) and 3(e)). We found that the dystrophic muscle displayed per se increased levels of gp91phox and tubulin subunit expression at both 4 (Figure 3(d)) and 24 weeks of age (Figure 3(e)) compared to wild type, whereas increased levels of IL-6 significantly enhanced content of gp91phox and of α-, β-, and Glu-tubulin proteins compared to mdx mice, suggesting that IL-6 exacerbates the dystrophic phenotype acting also on the stimulation of X-ROS signaling.

3.4. Increased Levels of IL-6 Affect Nrf2 Antioxidant Response during the Progression of Pathology. In order to evaluate the correlation between the temporal progression of X-ROS signaling and Nrf2-dependent antioxidant response in muscular dystrophy and to better define the pathogenic role of IL-6 in muscular dystrophy, we analysed the Nrf2-mediated antioxidant enzyme expression in the diaphragm of mdx and mdx/IL6 mice at different stages of pathology (Figure 4). In particular, we evaluated the antioxidant response in dystrophic mice at two different ages and stages of disease, namely, at 4 weeks of age, in which a peak

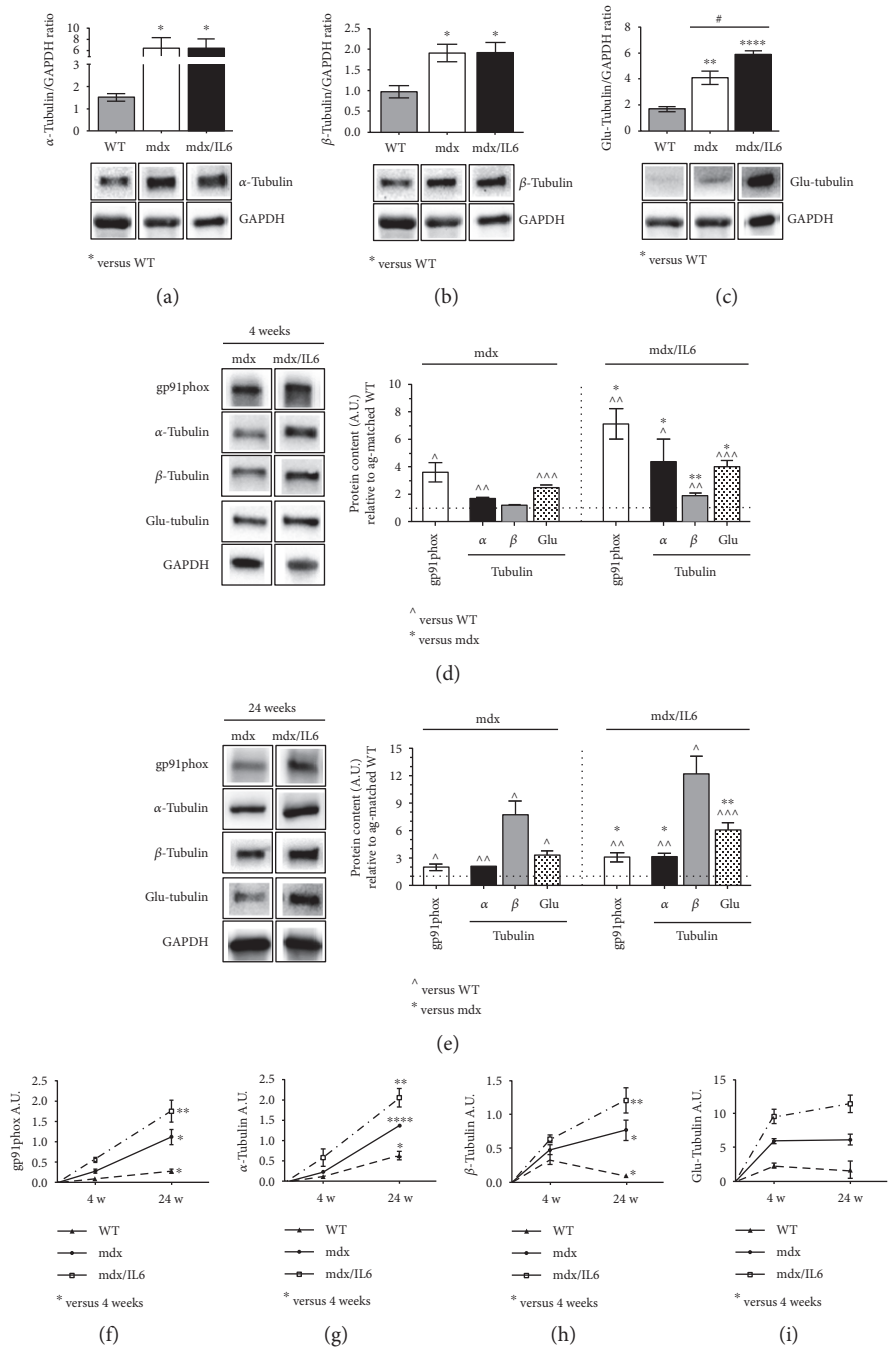

Figure 3: X-ROS signaling is altered in the prenecrotic dystrophic diaphragm muscle and increased during the progression of pathology. Densitometric analysis (upper panels) and representative images (bottom panels) of western blot analysis for the expression of α-tubulin (a), β-tubulin (b), and Glu-tubulin (c) proteins in the diaphragm muscle of 2-week-old WT, mdx, and mdx/IL6 mice. Values represent mean ± SEM; $n = 3$ to 7 mice per group. p value by ANOVA. X-ROS signaling components were analysed by western blot (left panels show representative images) at later stages of pathology in 4-week-old (d) and 24-week-old (e) diaphragm muscle from WT, mdx, and mdx/IL6 mice. Values are reported as protein content relative to age-matched WT (horizontal dot line) and represent mean ± SEM; $n = 3$ to 7 mice per group. $^{\wedge}p < 0.05$, $^{\wedge\wedge}p < 0.005$, and $^{\wedge\wedge\wedge}p < 0.0005$ compared to WT mice; $^{*}p < 0.05$, $^{**}p < 0.005$ with respect to mdx littermates (by ANOVA). Temporal progression of gp91phox (f), α-tubulin (g), β-tubulin (h), and Glu-tubulin (i) proteins between 4 weeks (4 w) and 24 weeks (24 w) of age in the diaphragm muscles of indicated genotypes. Graphs show an increase of the expression levels of tubulin subunits and of gp91phox protein during the progression of pathology. Values represent mean ± SEM. $^{*}p < 0.05$, $^{**}p < 0.005$, and $^{****}p < 0.0001$ by ANOVA.

of necrosis is observed, and at 24 weeks of age, a stage in which the affected muscle rapidly regenerates and regains structural and functional integrity [2].

We found that most of the antioxidant enzymes, including CAT-1, Gpx1, and GCL, were upregulated in 4-week-old mdx and mdx/IL6 mice compared to wild-type littermates

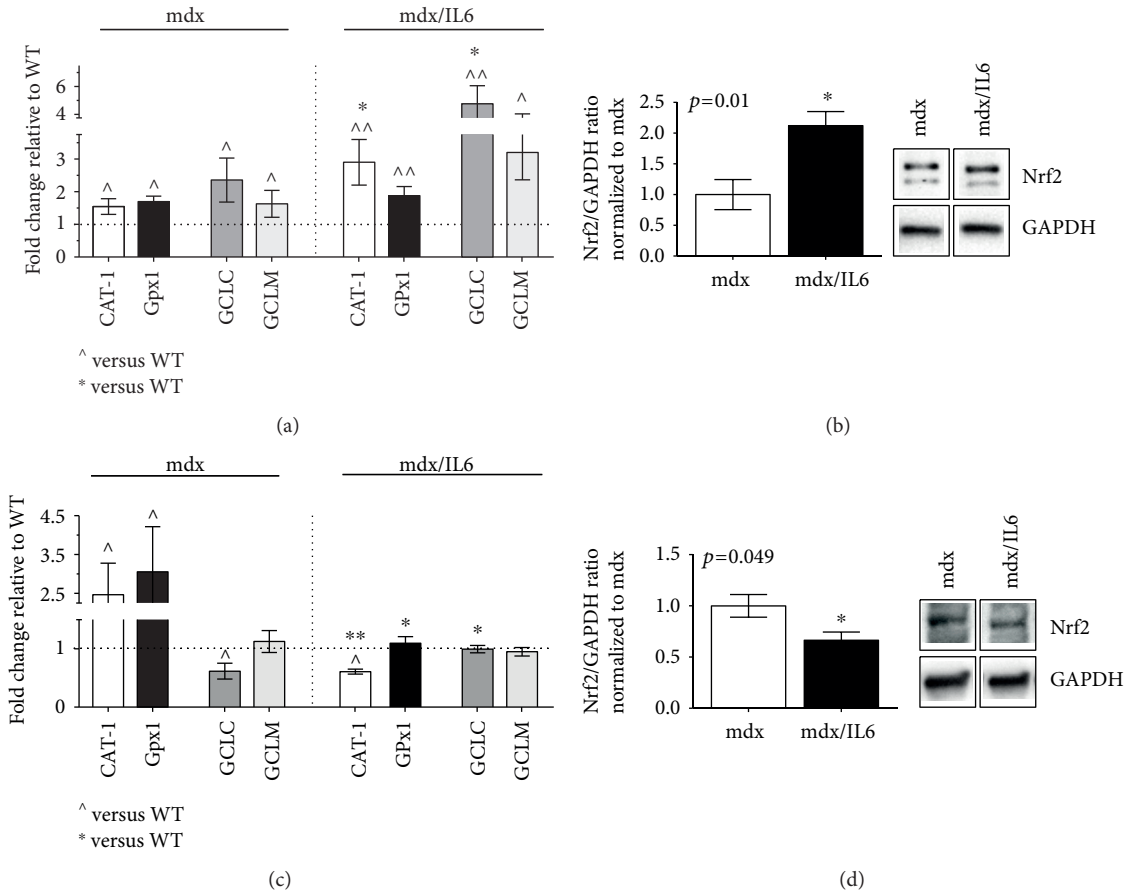

Figure 4: Time course analysis of Nrf2-dependent antioxidant response in dystrophic mice. Real-time PCR analysis performed on diaphragm muscles from wild-type (WT), mdx, and mdx/IL6 mice at 4 (a) and 24 (c) weeks of age for the expression of Nrf2-dependent genes involved in the antioxidant response. Values are reported as fold change in the expression relative to the calibrator (WT, horizontal dot line) and represent mean ± SEM; $n = 3$ to 6 mice per group. $^{\wedge}p < 0.05$, $^{\wedge\wedge}p < 0.005$ compared to WT mice; $^{*}p < 0.05$, $^{**}p < 0.005$ with respect to mdx littermates (by ANOVA). Nrf2 protein expression was evaluated by western blot analysis (right panels show representative images) in 4-week-old (b) and 24-week-old (d) diaphragms of indicated genotypes. Densitometric analyses (left panels) are expressed as values relative to age-matched mdx and represent mean ± SEM; $n = 4$ to 5 mice per group. p value using Student's two-tailed t-test.

(Figure 4(a)). Notably, the increased plasma levels of IL-6 induced a more significant upregulation of CAT-1 compared to mdx mice (Figure 4(a)). We also found that the levels of mRNAs that encode the components of gamma-glutamyl-cysteine ligase and the rate-limiting enzyme for glutathione biosynthesis (glutamyl-cysteine ligase modulator (GCLM) and glutamyl-cysteine ligase catalytic subunit (GCLC)) were expressed at higher levels in mdx/IL6 mice compared to mdx littermates, indicating that IL-6 overexpression induces a dysregulation of GSH synthesis in dystrophic muscles. These data suggest that the exacerbated muscle phenotype, induced by increased levels of IL-6 is associated with an imbalance between oxidant and antioxidant systems, as also suggested by increased expression of Nrf2 protein in 4-week-old mdx/IL6 mice compared to mdx littermates (Figure 4(b)).

Then, we analysed the expression pattern of the antioxidant enzymes in both mdx and mdx/IL6 mice of 24 weeks of age, a stage normally spared by the absence of dystrophin. We observed that CAT-1 and Gpx1, which catalyze the conversion of hydrogen peroxide to water and oxygen, were still upregulated in the diaphragm of 24-week-old mdx mice compared to both wild-type and mdx/IL6 mice (Figure 4(c)). This suggests that the antioxidant compensatory mechanism is still activated in adult mdx muscles and this might explain the mild muscle phenotype observed in mdx mice at this stage of pathology. In contrast, increased levels of IL-6 induced a significant downregulation of the ROS-detoxifying enzymes, compared to mdx mice, suggesting that IL-6 overexpression negatively affects the compensatory response in the dystrophic muscle. This evidence was supported by the significant reduction of Nrf2 protein expression in 24-week-old mdx/IL6 mice compared to mdx littermates (Figure 4(d)).

4. Discussion

In this study, we monitored relevant markers of the redox signaling in the dystrophic muscle and suggested a potential link between increased circulating levels of IL-6 and oxidative damage.

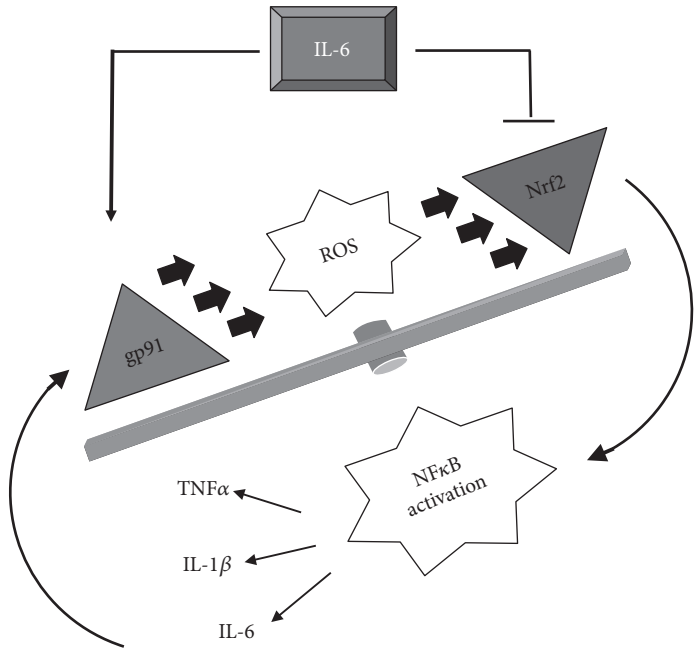

Figure 5: IL-6 exacerbates the oxidant-related damage in the dystrophic muscle. Increased levels of IL-6 could contribute to amplify degenerative processes in mdx mice by enhancing the expression of both gp91phox and NFκB and by reducing the Nrf2-antioxidant response.

Duchenne muscular dystrophy is an X-linked genetic disease due to mutations in the dystrophin gene, leading to alterations in intracellular signaling that causes an imbalance between protein synthesis and protein degradation, with subsequent necrosis and fibrosis [1].

Currently, there is no effective therapy for Duchenne muscular dystrophy. Although stem cells and exon skipping approach offer new tools for regeneration in muscle disease, the signaling and molecular pathway involved in the survival of the rescued phenotype is an important question that remains to be satisfactorily addressed. Among factors that might interfere with therapeutic approaches, the dystrophic environment represents an important determinant [30]. Thus, a better understanding of the hostile microenvironment should prove useful for producing new adjuvant treatments.

Potential candidates that contribute to sustain a hostile microenvironment in the dystrophic muscle include oxidative stress [4] and interleukin-6 (IL-6), a pleiotropic cytokine that is produced by different cell types and has the capacity to induce several different intracellular signaling pathways [3, 10, 31]. The skeletal muscle is able to activate, under physiological conditions, an endogenous program of antioxidant defense to maintain the ROS production at a functional level [7]. Nevertheless, damaging stimuli might alter the delicate balance between ROS production and antioxidant defense, leading to oxidative stress. The opposite effects exerted by different concentration of ROS can be justified considering the concept of hormesis [32], in which a low dose of a substance is stimulatory and a high dose is inhibitory. Thus, the muscle benefits from low doses of radicals while it is damaged by higher levels of ROS.

Our work supports the evidence that dystrophic muscle is able to activate a compensatory response to cope the negative effects of oxidative stress. Nevertheless, this compensatory mechanism is impinged by factors that are associated with the pathogenesis of muscular dystrophy, such as IL-6. Indeed, the persistent activation of IL-6 signaling impairs the antioxidant response during the progression of pathology, contributing to the severity of pathology.

In particular, we first verified whether relevant markers of the redox signaling are direct targets of necrosis and inflammation, which characterize the necrotic stage of the disease, or whether they can be induced in the prenecrotic stage. We found a strong upregulation of one of the relevant and critical factors for ROS production in the dystrophic muscle, namely, gp91phox (NOX2), and a significant reduction in SIRT1 and Nrf2 expression, important mediators of the antioxidant response, in the diaphragm muscle of 2-week-old mdx mice compared to wild-type littermates. This indicates that the activation of redox-regulated signaling precedes necrosis rather than resulting from it and supports oxidative stress as a primary pathogenetic mechanism in muscular dystrophy [4].

We also analysed the relevant markers of the X-ROS signaling at 4 weeks (necrotic stage) and 24 weeks (a stage normally spared by the absence of dystrophin) of age in mdx mice. We revealed that X-ROS signaling is already altered in the dystrophic diaphragm at the necrotic stage, whereas markers of the antioxidant compensatory mechanism were upregulated in adult mdx muscles.

To further support the evidence that the imbalance between oxidant and antioxidant mechanisms is a pathogenic factor associated with the severity of pathology, we analysed the markers of X-ROS signaling in the diaphragm muscle of mdx/IL6 mouse model, which recapitulates the severe phenotypic characteristics of DMD in

humans [3, 10]. Sustained increase in the levels of IL-6 alone is sufficient to exacerbate the dystrophic phenotype at a stage, 24 weeks of age, when only a mild muscle phenotype is apparent in mdx mice [10]. We revealed that increased levels of IL-6 induced a significant downregulation of the ROS-detoxifying enzymes, compared to mdx mice, and negatively affect the compensatory response in the dystrophic muscle.

5. Conclusion

Overall, our study is consistent with the model in which IL-6 could act as an important player in the crosstalk between ROS production and inflammatory response [22]. Increased levels of IL-6 enhance the expression of both gp91phox and NFκB and impinge the Nrf2-dependent antioxidant response in the dystrophic muscle, even at the prenecrotic stage (Figure 5). This altered redox-regulated signaling might trigger an inflammatory response, leading to muscle wasting.

Abbreviations

ANOVA: Analysis of variance
CAT-1: Catalase-1
DHE: Dihydroethidium
DMD: Duchenne muscular dystrophy
DTT: Dithiothreitol
EDTA: Ethylenediaminetetraacetic acid
EGTA: Ethylene glycol tetraacetic acid
GAPDH: Glyceraldehyde 3-phosphate dehydrogenase
GCL: Glutamate-cysteine ligase
GSH: Glutathione
GPx: Glutathione peroxidase
HO-1: Heme oxygenase 1
Hprt: Hypoxanthine guanine phosphoribosyl transferase
IL: Interleukin
IL-6Rα: Interleukin-6 receptor alpha
NaF: Sodium fluoride
NFκB: Nuclear factor kappa-light-chain-enhancer of activated B cells
NOX2: NAPDH oxidase 2
Nrf2: NF-E2-related factor 2
NQO1: NAD(P)H quinone dehydrogenase 1
PMSF: Phenylmethylsulfonyl fluoride
ROS: Reactive oxygen species
SEM: Standard error of the mean
SIRT1: Sirtuin 1
SOD: Superoxide dismutase
SOV4: Sodium orthovanadate
TNF: Tumor necrosis factor
Utrn: Utrophin.

Conflicts of Interest

The authors declare that they do not have any conflicts of interest.

Authors' Contributions

Laura Pelosi and Laura Forcina performed the gene and protein expression analysis. Bianca Maria Scicchitano performed the RNA extraction and real-time PCR analysis. Carmine Nicoletti managed the mouse models. Laura Pelosi, Laura Forcina, Bianca Maria Scicchitano, and Antonio Musarò designed the experiments and drafted the manuscript. Antonio Musarò designed the study and wrote the paper. All authors contributed to the acquisition, analysis, and interpretation of the data. Laura Pelosi and Laura Forcina contributed equally to this work. Bianca Maria Scicchitano and Antonio Musarò are co-senior authors.

Acknowledgments

The present research was supported by a grant from Fondazione Roma, Telethon, ASI, and Progetti Ateneo. The authors thank C. Miano for the technical support and Fabrizio De Benedetti for the IL-6 mice and scientific support.

References

[1] D. J. Glass, "Two tales concerning skeletal muscle," *The Journal of Clinical Investigation*, vol. 117, no. 9, pp. 2388–2391, 2007.

[2] M. D. Grounds, H. G. Radley, G. S. Lynch, K. Nagaraju, and A. De Luca, "Towards developing standard operating procedures for pre-clinical testing in the mdx mouse model of Duchenne muscular dystrophy," *Neurobiology of Disease*, vol. 31, no. 1, pp. 1–19, 2008.

[3] L. Pelosi, M. G. Berardinelli, L. De Pasquale et al., "Functional and morphological improvement of dystrophic muscle by interleukin 6 receptor blockade," *eBioMedicine*, vol. 2, no. 4, pp. 285–293, 2015.

[4] T. A. Rando, "Oxidative stress and the pathogenesis of muscular dystrophies," *American Journal of Physical Medicine & Rehabilitation*, vol. 81, 11 Supplement, pp. S175–S186, 2002.

[5] H. Sies, "Oxidative stress: a concept in redox biology and medicine," *Redox Biology*, vol. 4, pp. 180–183, 2015.

[6] H. Sies, C. Berndt, and D. P. Jones, "Oxidative stress," *Annual Review of Biochemistry*, vol. 86, pp. 715–748, 2017.

[7] A. Musaro, S. Fulle, and G. Fano, "Oxidative stress and muscle homeostasis," *Current Opinion in Clinical Nutrition and Metabolic Care*, vol. 13, no. 3, pp. 236–242, 2010.

[8] M. Sinha, P. Manna, and P. C. Sil, "Induction of necrosis in cadmium-induced hepatic oxidative stress and its prevention by the prophylactic properties of taurine," *Journal of Trace Elements in Medicine and Biology*, vol. 23, no. 4, pp. 300–313, 2009.

[9] B. M. Scicchitano, M. Faraldi, and A. Musaro, "The proteolytic systems of muscle wasting," *Recent Advances in DNA & Gene Sequences*, vol. 9, no. 1, pp. 26–35, 2015.

[10] L. Pelosi, M. G. Berardinelli, L. Forcina et al., "Increased levels of interleukin-6 exacerbate the dystrophic phenotype in mdx mice," *Human Molecular Genetics*, vol. 24, no. 21, pp. 6041–6053, 2015.

[11] S. Petrillo, L. Pelosi, F. Piemonte et al., "Oxidative stress in Duchenne muscular dystrophy: focus on the NRF2 redox pathway," *Human Molecular Genetics*, vol. 26, no. 14, pp. 2781–2790, 2017.

[12] M. Okazaki, Y. Yamada, N. Nishimoto, K. Yoshizaki, and M. Mihara, "Characterization of anti-mouse interleukin-6 receptor antibody," *Immunology Letters*, vol. 84, no. 3, pp. 231–240, 2002.

[13] N. P. Whitehead, C. Pham, O. L. Gervasio, and D. G. Allen, "N-Acetylcysteine ameliorates skeletal muscle pathophysiology in mdx mice," *The Journal of Physiology*, vol. 586, no. 7, pp. 2003–2014, 2008.

[14] N. P. Whitehead, E. W. Yeung, S. C. Froehner, and D. G. Allen, "Skeletal muscle NADPH oxidase is increased and triggers stretch-induced damage in the mdx mouse," *PLoS One*, vol. 5, no. 12, article e15354, 2010.

[15] M. Mittal, M. R. Siddiqui, K. Tran, S. P. Reddy, and A. B. Malik, "Reactive oxygen species in inflammation and tissue injury," *Antioxidants & Redox Signaling*, vol. 20, no. 7, pp. 1126–1167, 2014.

[16] H. Motohashi and M. Yamamoto, "Nrf2-Keap1 defines a physiologically important stress response mechanism," *Trends in Molecular Medicine*, vol. 10, no. 11, pp. 549–557, 2004.

[17] Y. S. Hori, A. Kuno, R. Hosoda et al., "Resveratrol ameliorates muscular pathology in the dystrophic mdx mouse, a model for Duchenne muscular dystrophy," *The Journal of Pharmacology and Experimental Therapeutics*, vol. 338, no. 3, pp. 784–794, 2011.

[18] A. Salminen, K. Kaarniranta, and A. Kauppinen, "Crosstalk between oxidative stress and SIRT1: impact on the aging process," *International Journal of Molecular Sciences*, vol. 14, no. 2, pp. 3834–3859, 2013.

[19] C. Sun, C. Yang, R. Xue et al., "Sulforaphane alleviates muscular dystrophy in mdx mice by activation of Nrf2," *Journal of Applied Physiology (1985)*, vol. 118, no. 2, pp. 224–237, 2015.

[20] A. Kuno and Y. Horio, "SIRT1: a novel target for the treatment of muscular dystrophies," *Oxidative Medicine and Cellular Longevity*, vol. 2016, Article ID 6714686, 11 pages, 2016.

[21] L. De Pasquale, A. D'amico, M. Verardo, S. Petrini, E. Bertini, and F. De Benedetti, "Increased muscle expression of interleukin-17 in Duchenne muscular dystrophy," *Neurology*, vol. 78, no. 17, pp. 1309–1314, 2012.

[22] V. Malik, L. R. Rodino-Klapac, and J. R. Mendell, "Emerging drugs for Duchenne muscular dystrophy," *Expert Opinion on Emerging Drugs*, vol. 17, no. 2, pp. 261–277, 2012.

[23] R. Gilbert, J. Nalbanoglu, J. M. Tinsley, B. Massie, K. E. Davies, and G. Karpati, "Efficient utrophin expression following adenovirus gene transfer in dystrophic muscle," *Biochemical and Biophysical Research Communications*, vol. 242, no. 1, pp. 244–247, 1998.

[24] J. Tinsley, N. Deconinck, R. Fisher et al., "Expression of full-length utrophin prevents muscular dystrophy in mdx mice," *Nature Medicine*, vol. 4, no. 12, pp. 1441–1444, 1998.

[25] K. Itoh, T. Chiba, S. Takahashi et al., "An Nrf2/small Maf heterodimer mediates the induction of phase II detoxifying enzyme genes through antioxidant response elements," *Biochemical and Biophysical Research Communications*, vol. 236, no. 2, pp. 313–322, 1997.

[26] M. D. Grounds and J. Torrisi, "Anti-TNFalpha (Remicade) therapy protects dystrophic skeletal muscle from necrosis," *FASEB Journal*, vol. 18, no. 6, pp. 676–682, 2004.

[27] J. G. Tidball and M. Wehling-Henricks, "Macrophages promote muscle membrane repair and muscle fibre growth and regeneration during modified muscle loading in mice in vivo," *The Journal of Physiology*, vol. 578, Part 1, pp. 327–336, 2007.

[28] R. J. Khairallah, G. Shi, F. Sbrana et al., "Microtubules underlie dysfunction in Duchenne muscular dystrophy," *Science Signaling*, vol. 5, no. 236, p. ra56, 2012.

[29] P. Kombairaju, J. P. Kerr, J. A. Roche et al., "Genetic silencing of Nrf2 enhances X-ROS in dysferlin-deficient muscle," *Frontiers in Physiology*, vol. 5, p. 57, 2014.

[30] A. S. Brack, M. J. Conboy, S. Roy et al., "Increased Wnt signaling during aging alters muscle stem cell fate and increases fibrosis," *Science*, vol. 317, no. 5839, pp. 807–810, 2007.

[31] J. A. Carson and K. A. Baltgalvis, "Interleukin 6 as a key regulator of muscle mass during cachexia," *Exercise and Sport Sciences Reviews*, vol. 38, no. 4, pp. 168–176, 2010.

[32] E. J. Calabrese and L. A. Baldwin, "Hormesis: the dose-response revolution," *Annual Review of Pharmacology and Toxicology*, vol. 43, pp. 175–197, 2003.

Hindawi
Oxidative Medicine and Cellular Longevity
Volume 2017, Article ID 9456163, 10 pages
https://doi.org/10.1155/2017/9456163

Research Article

Protective Effects of Dinitrosyl Iron Complexes under Oxidative Stress in the Heart

Valery I. Kapelko, Vladimir L. Lakomkin, Alexander A. Abramov, Elena V. Lukoshkova, Nidas A. Undrovinas, Asker Y. Khapchaev, and Vladimir P. Shirinsky

Russian Cardiology Research and Production Complex, Ministry of Healthcare of the Russian Federation, 3rd Cherepkovskaya St., Building 15a, Moscow 121552, Russia

Correspondence should be addressed to Vladimir P. Shirinsky; shirinsky@gmail.com

Received 6 January 2017; Accepted 27 February 2017; Published 21 March 2017

Academic Editor: Andrey J. Serra

Background. Nitric oxide can successfully compete with oxygen for sites of electron-transport chain in conditions of myocardial hypoxia. These features may prevent excessive oxidative stress occurring in cardiomyocytes during sudden hypoxia-reoxygenation. *Aim*. To study the action of the potent stable NO donor dinitrosyl iron complex with glutathione (Oxacom®) on the recovery of myocardial contractile function and Ca^{2+} transients in cardiomyocytes during hypoxia-reoxygenation. *Results*. The isolated rat hearts were subjected to 30 min hypoxia followed by 30 min reoxygenation. The presence of 30 nM Oxacom in hypoxic perfusate reduced myocardial contracture and improved recovery of left ventricular developed pressure partly due to elimination of cardiac arrhythmias. The same Oxacom concentration limited reactive oxygen species generation in hypoxic cardiomyocytes and increased the viability of isolated cardiomyocytes during hypoxia from 12 to 52% and after reoxygenation from 0 to 40%. Oxacom prevented hypoxia-induced elevation of diastolic Ca^{2+} level and eliminated Ca^{2+} transport alterations manifested by slow Ca^{2+} removal from the sarcoplasm and delay in cardiomyocyte relaxation. *Conclusion*. The potent stable NO donor preserved cardiomyocyte integrity and improved functional recovery at hypoxia-reoxygenation both in the isolated heart and in cardiomyocytes mainly due to preservation of Ca^{2+} transport. Oxacom demonstrates potential for cardioprotection during hypoxia-reoxygenation.

1. Introduction

Oxidative stress in cells occurs when reactive oxygen species (ROS) prevail over the means of antioxidant protection. Reoxygenation after a period of hypoxia is a classic model of oxidative stress. Cardiomyocytes in hypoxic conditions mobilize a number of protective mechanisms to enable them to retain integrity in this critical period and restore normal function at reoxygenation. A deep fall in contractile function allows them to conserve limited stores of ATP and phosphocreatine. This is realized by means of limiting Ca^{2+} entry into cells [1] due to the shortening of action potential and early release of K^+, which gradually reduces excitability of cardiomyocytes. Also, the activity of Ca^{2+}-ATPase of sarcoplasmic reticulum (SERCA2) declines quite rapidly [2], with further reduction in Ca^{2+} uptake in the reticulum and subsequent release into sarcoplasm. However, an increased level of sarcoplasmic Ca^{2+} in diastole [3], especially during reoxygenation, induces the opening of the mitochondrial pores [4] with the subsequent fall of the potential.

In the last decade, many aspects of altered redox regulation in hypoxia became more evident. Although oxygen consumption during hypoxia is reduced, the mitochondria continue to generate superoxide [5], although in smaller amounts, about one-third of normal production, according to some estimates [1]. Perhaps, this is due to incomplete use of oxygen, because activation of NO synthases, especially of NOS3 [6] that occurs during the initial period of hypoxia, changes the competition between oxygen and nitric oxide for cytochrome oxidase in favor of the latter [7]. Moreover, NO, as well as S-nitrosothiols, can inhibit complex I by S-nitrosylation. This effect can be blocked by reducing agents, nitrolases and thioredoxin [8]. Thus, NO accumulation plays a protective role, as it allows chelating iron released from

oxygen complexes to form NO-Fe^{2+} complexes in the presence of glutathione [9].

In light of these findings, elevated NO levels could potentially be useful during reoxygenation when the availability of oxygen to mitochondria suddenly multiplies. The well-known NO donors such as nitroglycerin, nitrosorbide, nitroprusside, and nitrite liberate NO in cells and tissues during their metabolism. However, some of these substances, such as sodium nitroprusside, contain cyanide anions, while other compounds including nitroglycerin can induce methemoglobinemia. As a result of decades-long research of professor Anatoly F. Vanin (Semenov Institute of Chemical Physics, Russian Academy of Sciences) and his colleagues, it was established that S-nitrosothiols present in cells can easily interact with iron ions released from the iron donor ferritin to form dinitrosyl iron complexes (DNIC) [10, 11]. The main feature of DNIC is that they serve as carriers of the "ready-to-use," iron-stabilized form of NO and do not contain toxic components. When local NO concentration decreases the DNIC release nitric oxide and chelate it while in excess, thus functioning as nitric oxide depot/buffer in cells.

This concept was embodied at the Russian Cardiology Research and Production Complex by creating a drug Oxacom (Patent RU2291880) which represents a DNIC with glutathione as a ligand. In preclinical studies, a dose-dependent hypotensive effect of Oxacom in conscious rats was observed [12]. Oxacom injection substantially increased nitric oxide content in various rat organs. Lungs and liver demonstrated 5-6-fold increase of NO content while in the heart NO levels rise 14-fold [13]. During phase 1 and 2 clinical trials Oxacom was tested in healthy volunteers and in patients with hypertensive crisis. In these groups, it consistently reduced arterial blood pressure by 15–20% for 8–10 hours [14]. In the present report, we provide evidence that DNIC in the form of Oxacom could be successfully used to protect cardiomyocytes from functional decline and damage associated with hypoxia-reoxygenation and oxidative stress. These results for the first time outline the novel possible therapeutic implication for Oxacom as antihypoxic cardioprotective drug.

2. Materials and Methods

2.1. Isolated Heart Experiments. Hearts were isolated from male Wistar rats ($n = 48$) anesthetized with ketamine (100 mg/kg). The protocol of experiments was approved by the Animal Ethics Committee of the Institute of Experimental Cardiology of the Russian Cardiology Research and Production Complex (# 3/15). Hearts were isolated from rats anesthetized with ketamine (100 mg/kg). Hearts were cannulated and coronary vessels were retrogradely perfused at 37°C using standard Krebs-Henseleit solution containing 11 mM glucose and presaturated with carbogen (95% O_2, 5% CO_2). A latex balloon was introduced into the left ventricle (LV) and isovolumic pressure in LV and ECG were monitored. The balloon was filled with liquid to set diastolic pressure at 10–12 mm Hg in order to achieve an optimal distension of LV. Retrograde perfusion was conducted at constant pressure of 70 mm Hg. Electrodes were placed on the right atrium for electrostimulation.

Heart perfusion was performed in a specialized Hugo Saks perfusion system. The LV pressure and ECG were recorded using Harvard Apparatus (USA) sensors and amplifiers. All signals (LV pressure and coronary perfusion rate) were transferred to the computer through the preliminary amplifiers and analog-to-digital converter (ADC:USB-6215, National Instruments, USA, using sampling rate of 1000 Hz). In addition to analog signals (maximum and minimum LV pressure, rates of pressure rise and drop, and heart rate) the heart work index (the product of developed pressure and heart rate), which characterizes the overall energy consumption, and relaxation index (LV $-dP/dt$ divided by LV developed pressure) were calculated.

In order to manage the ADC and record primary signals as binary files on the computer's hard drive, as well as for further analysis of signals, computer programs were developed by Dr. Lukoshkova using National Instruments LabVIEW graphical programming environment. These programs calculate functionally relevant parameters in each cardiocycle, average these parameters for every 2 seconds, record all estimated parameters into text files, and continuously display averaged values as trends on the monitor screen.

The program is designed for the analysis of records, primarily, of calculated values. It allows examine trends of functionally relevant parameters throughout the experiment and at any stage of the experiment. It provides options to remove artefact values and average the results of measurements in a variety of modes: (a) using averaging intervals from 6 s to 30 min; (b) linking the beginning of an averaged segment to the mark introduced by the operator during the experiment; (c) averaging between marks; and (d) combining averaging modes. The results of calculations can be written as text files or directly transferred to Excel spreadsheet using a ClipBoard function.

2.1.1. Experimental Protocol. After recording of the cardiac baseline function, stepwise electric stimulation with increasing rate exceeding the spontaneous rate was applied using increments of 0.5 Hz up to 12 Hz and pacing for 15 sec at each rate. Then electrostimulation was stopped and 10 minutes later the functional parameters were recorded before the start of hypoxic perfusion. The 30 min hypoxia (replacement of O_2 by N_2 in perfusate) was followed by 30 min reoxygenation. This protocol was chosen after the preliminary tests, which revealed that 20-minute hypoxia was insufficient to cause cardiac dysfunction and the degree of recovery was close to 100%. At the end of experiment, electric stimulation with increasing rate was repeated. Oxacom (30 nM) was added to perfusate during hypoxic perfusion and it was not added at reoxygenation.

An assessment of the heart dysfunction was performed by comparison of its functional parameters before, during, and after hypoxia. An indispensable component of this evaluation was the magnitude of LV diastolic pressure, which reflects the degree of myocardial stiffness occurring during hypoxia.

2.2. Determination of Glutathione Levels in Myocardial Tissue. Rat hearts were washed with phosphate buffered saline and

frozen in liquid nitrogen immediately after experimental procedures. The tissue was ground in liquid nitrogen, and three volumes of 5% 5-sulphosalicylic acid (SSA) were added to 0.1–0.3 mg of the powder. The tissue sample was extracted using a glass-glass homogenizer on ice and centrifuged at 10,000 ×g for 10 min at 4°C to pellet the proteins. The supernatant fraction (up to 10 μL) was used for measurements of total glutathione (GSH + GSSG) content using Glutathione Assay Kit (Sigma) according to the manufacturer's instructions in a buffer containing 95 mM KH_2PO_4, pH 7.0, 0.95 mM EGTA, 48 mM NADPH, 0.031 mg/mL 5,5′-dithiobis(2-nitrobenzoic acid) (DTNB), 0.115 U/mL glutathione reductase, and 0.24% SSA in a final volume of 200 μL. Kinetics of DTNB reduction to 5-thio-2-nitrobenzoic acid (TNB) were measured using a Victor X3 plate reader (Perkin Elmer) at 405 nm. The amount of glutathione was calculated using a standard curve of reduced glutathione. Data were expressed as a mean from at least triplicate measurements ± standard deviation (SD). Amount of reduced glutathione (GSH) was calculated from measurements where both NADPH and glutathione reductase were excluded from the assay mixture. Average relative amount of reduced glutathione in the heart was calculated based on determined values.

2.3. Isolation and Manipulation of Cardiomyocytes. Right before cardiomyocyte isolation all buffers were supplemented with 1000 U/L heparin, warmed to 37°C in a water bath, and bubbled with carbogen (95% O_2, 5% CO_2) for 30 min. Rat heart was cannulated through aorta and perfused for 10 min according to the method of Langendorf to remove blood with Krebs-Henseleit buffer supplemented with 1.2 mM Ca^{2+}. Next, heart was perfused with Ca^{2+}-free buffer for 30 min to remove Ca^{2+} from extracellular spaces. After washing steps, heart was perfused in a recirculation mode for 30 min with 10 mL of 0.5 mg/mL collagenase (CLS 2, Worthington, 325 U/mg) solution in a Ca^{2+}-free buffer. Following perfusion the heart was placed in a petri dish with 10 mL of fresh collagenase solution and minced in 1-2 mm^3 pieces using fine scissors. Tissue suspension was transferred in 50 mL tube and gently pipetted for 10–15 min using sterile 5 mL plastic pipette with wide opening. Digested tissue was filtered through the 200 micron Nylon mesh to separate isolated cardiomyocytes from undigested heart fragments. Cardiomyocyte suspension was left in a sterile 50 mL tube for 10 min to settle down live cells. Then the supernatant was removed and cardiomyocytes were gently resuspended in 10 mL of albumin solution (6 mg/mL) supplemented with 0.1 mM Ca^{2+} and left for 10 min to settle. This step was repeated several times by placing cells in an albumin solution with increasing concentration of Ca^{2+} using steps of 0.25 mM until 1 mM Ca^{2+} was set. Cardiomyocytes were kept at 4°C in Krebs-Henseleit solution supplemented with 1 mM Ca^{2+} and 6 mg/mL albumin no more than 12 hours after isolation.

In order to reproduce normoxic or hypoxic conditions during the experiment cardiomyocytes were placed in experimental chamber in the buffer bubbled with carbogen or hypoxic gas mixture (95% N_2, 5% CO_2), respectively, and the chamber space above the buffer was constantly flashed with the corresponding gas mixture.

2.4. Ca^{2+} Transient Measurements in Cardiomyocytes. Cardiomyocytes were loaded with fluorescent Ca^{2+} indicator Fluo-4 (Invitrogen) for 20 min in the dark and transferred in a 250 μL experimental chamber made of plastic walls and glass coverslip as the bottom. Two platinum electrodes are fixed at the opposite walls of the chamber. These electrodes are connected to Grass SD9 electrostimulator and are used to pace cardiomyocytes in the chamber by rectangular electric impulses at 38 V and 1 Hz. The chamber is mounted on the stage of an inverted AxioVert 200 M microscope (Zeiss) in a thermostat set at 37°C. Buffer is delivered in the chamber by gravity flow at 1–5 mL/min and removed from the chamber using a peristaltic pump. Cardiomyocytes are monitored through the coverslip using x63 oil objective and AxioCam HS high speed CCD camera (Zeiss). Fluorescence of Fluo-4 is excited using an HBO 103W/2 mercury lamp (Osram) and an appropriate filter cube for FITC-based fluorophores. Illumination intensity is kept low and exposure times are made short in order to prevent Fluo-4 bleaching and cardiomyocyte damage. Fluorescent signal from the individual cardiomyocytes is recorded at 50–200 frames/sec and images are streamlined to a terabyte hard drive for further processing using AxioVision Physiology software (Zeiss).

2.5. Reactive Oxygen Species Measurement in Cardiomyocytes. Fluorescent indicator Dihydrorhodamine 123 (Thermo Fisher Scientific) was used to assess reactive oxygen species (ROS) accumulation in isolated rat cardiomyocytes. The same experimental setup was used as described above for Ca^{2+}-transient measurements in cardiomyocytes. Cells were loaded with DHR 123 for 20 min. Electrostimulation of cardiomyocytes was done in parallel with fluorescence recording and between interventions cells were kept in the dark.

2.6. Statistics. Statistical processing of experimental data obtained in isolated heart and isolated cardiomyocyte studies was performed using Statistics Package in Microsoft Excel 2013 and Student's t-test. Values in the tables and text are given as M ± SEM unless indicated differently.

3. Results and Discussion

3.1. Isolated Perfused Heart Experiments

3.1.1. Selection of Oxacom Concentration. In order to determine an optimal concentration of Oxacom to be used during hypoxic perfusion, we studied this compound across the concentration range of 0.01–2.7 μM in oxygenated hearts. The coronary flow rate was monitored as the main parameter as the increased rate under constant perfusion pressure indicates a decreased tone of the coronary vessels. Coronary flow rate clearly increased from 16.0 ± 1.2 to 20.2 ± 1.2 mL/min, but the changes in LV developed pressure were modest, about +7–9%. Only Oxacom concentration of 2.7 μM caused a distinct decrease in LV developed pressure by 24%. In this

Table 1: Functional parameters of the isolated heart in the absence and in the presence of Oxacom in hypoxic perfusate.

	Before hypoxia		After hypoxia (30 min) and reoxygenation (30 min)	
	Control ($n = 15$)	Oxacom ($n = 9$)	Control ($n = 11$)	Oxacom ($n = 9$)
Heart rate, beats/min	267 ± 9	250 ± 10	267 ± 11	253 ± 9
LV developed pressure, mm Hg	183 ± 6	195 ± 6	61 ± 8	79 ± 6
$+dP/dt$max, mm Hg/s	4490 ± 200	4830 ± 160	1520 ± 167	2020 ± 169
$-dP/dt$max, mm Hg/s	2630 ± 96	2670 ± 116	1240 ± 196	1760 ± 93*
LV diastolic pressure, mm Hg	10 ± 1	9 ± 1	59 ± 5	45 ± 4
Coronary flow rate, mL/min	18.0 ± 1.7	18.1 ± 1.1	16.8 ± 4.3	13.3 ± 1.2

* $p < 0.05$ versus control after hypoxia-reoxygenation.

regard, for further work the concentration of Oxacom 30 nM was selected, which reliably increased coronary flow rate and the index of relaxation by 8-9%. Both these effects could be interpreted as facilitation of Ca^{2+} removal from smooth muscle cells and cardiomyocytes, the events compatible with the reduction of hypoxic injury to myocardium.

3.1.2. Hypoxia-Reoxygenation in Control Experiments. Baseline cardiac functional parameters are important for recovery of function after hypoxia-reoxygenation. It is known that lower intensity of oxidative metabolism at the beginning of hypoxia provides better recovery after reoxygenation. In this regard, the experiments where LV developed pressure was below 130 mm Hg and heart rate was below 230 beats/min were excluded from analysis.

Hypoxic perfusion of the heart resulted in a steep drop of LV developed pressure already in the first minutes of hypoxia along with increasing LV diastolic pressure that characterized myocardial contracture. Cardiac arrhythmias were observed in hypoxic period and they increased dramatically during reoxygenation. Arrhythmic events included extrasystoles, idioventricular rhythm, and fibrillation, which ceased spontaneously. Altogether, due to these reasons 4 hearts of 15 total did not restore function at the end of experiments.

By the end of reoxygenation the heart rate restored function completely while LV developed pressure restored function only by 27 ± 6% (by 34 ± 4% excluding experiments with zero recovery). The cardiac work changed accordingly. The LV diastolic pressure dramatically rose during hypoxia and slightly increased by the end of reoxygenation averaging 57 ± 5 mm Hg.

3.1.3. Action of Oxacom in Hypoxia-Reoxygenation. During 10–30 min period of hypoxia in the presence of Oxacom the plateau level of LV diastolic pressure was consistently lower by 12–20 mm Hg than in control and this difference was statistically significant (Figure 1). During reoxygenation step, this difference persisted throughout the period. The rate of LV diastolic pressure lowering was higher in these experiments than in controls, especially at the initial stage of

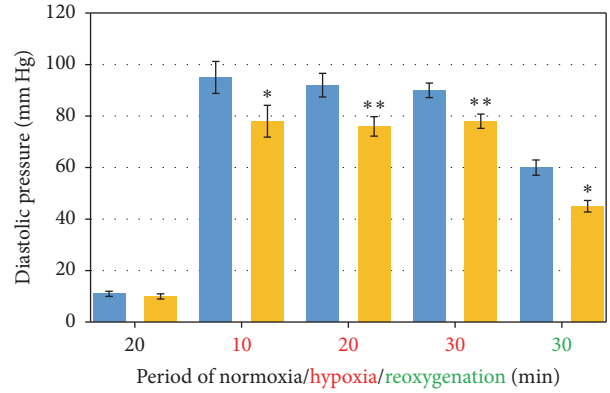

Figure 1: LV diastolic pressure after periods of normoxia (20 min), hypoxia (10–20–30 min), and reoxygenation (30 min) in the absence (blue) and in the presence of Oxacom (orange) in hypoxic perfusate. * $p < 0.05$; ** $p < 0.01$.

reoxygenation. Thus, Oxacom attenuated both hypoxia- and reoxygenation-induced myocardial contractures.

In both groups studied, the cardiac functional parameters before hypoxia were similar (Table 1). After hypoxia-reoxygenation the average values in Oxacom group tended to be better whereas $-dP/dt$max parameter was significantly higher than in control.

Recurrent arrhythmias were observed during both periods of hypoxia and reoxygenation in control and Oxacom experiments. Overall, the arrhythmias were observed in 10 out of 11 experiments in control group and in 7 out of 9 experiments in Oxacom group. The average integral length of arrhythmic events in control group was 14 ± 2 min, half of which originated from ventricular tachycardia (7 ± 1 min). In Oxacom group, the same distribution of arrhythmic events was observed; however, the values were significantly smaller, 4 ± 1 min and 2 ± 1 min ($p < 0.02$).

First NO-related effects on hypoxia- and reoxygenation-induced arrhythmias, especially ventricular arrhythmias, were reported in the 1970s when nitroglycerin was shown to be effective in these conditions (for review see [15]). Later

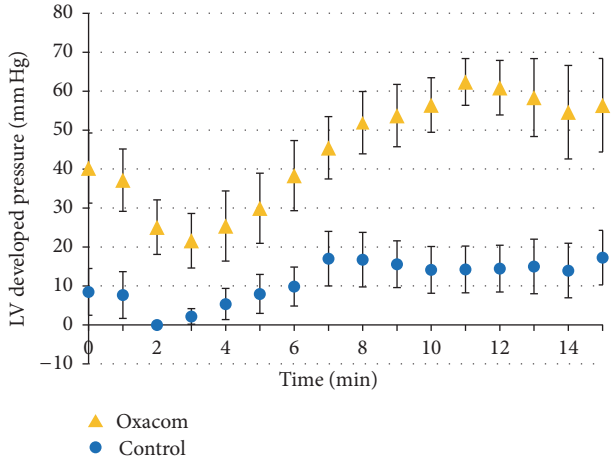

Figure 2: The time course of LV developed pressure during reoxygenation in groups in the absence and in the presence of Oxacom in hypoxic perfusate. Values in Oxacom group are significantly different from control group ($p < 0.05$).

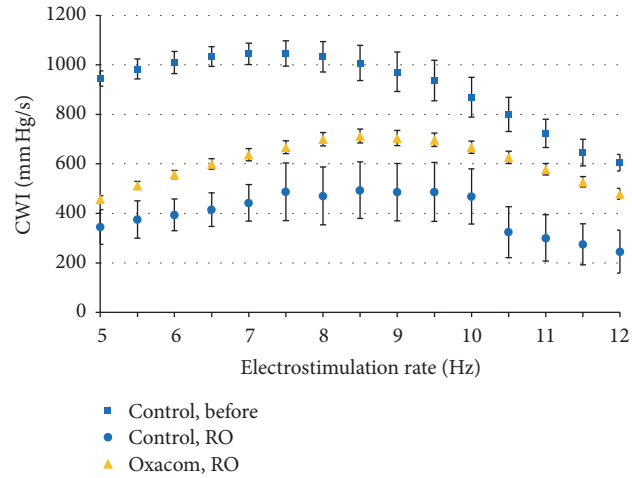

Figure 3: Dependence of cardiac work index (CWI) on the rate of heart electrostimulation before and after hypoxia-reoxygenation. CWI = LV developed pressure × heart rate; RO, reoxygenation. Difference between Oxacom and control after reoxygenation is statistically significant at 6-7 and 10–12 Hz ($p < 0.05$).

several groups used NO precursor L-arginine as well as L-arginine methyl ester to cope with experimental ventricular arrhythmia [16, 17]. Although these studies reported successful prevention of arrhythmia, the concentrations of substances used to achieve restoration of normal electric activity of the heart ranged from 5 mM to 100 mM exceeding estimated concentration of L-arginine in plasma 50–1000-fold [18].

The time course of LV developed pressure highly depended on arrhythmias because, during arrhythmic episodes, it dropped almost to zero. Still, in the presence of Oxacom LV pressure was maintained at higher levels throughout the hypoxic period and especially at the start of reoxygenation when arrhythmias in Oxacom group quickly ceased (Figure 2). The developed pressure in Oxacom group was also higher throughout reoxygenation period comprising 29 ± 4% of the initial value at 10 min (control 8 ± 4%, $p < 0.01$), 34 ± 6% at 20 min (control 15 ± 5%, $p < 0.05$), and 41 ± 3% at 30 min (control 33 ± 4%, $p < 0.01$, paired Student's t-test).

An attempt to restore cardiac function using L-arginine was undertaken by Agulló et al. [19]. They added 3 mM L-arginine to a perfusing solution for isolated hearts and improved recovery of the contractile function after reoxygenation from 2% to 12% of the initial value. An opposite effect was noticed when an inhibitor of soluble guanylate cyclase was used. Thus, the protective effect of arginine was apparently realized through the increased formation of cGMP.

Electrostimulation with increasing rate was performed before and after hypoxia-reoxygenation. The results shown in Figure 3 demonstrate that stimulation of normoxic hearts at the rate of 5.0–7.5 Hz was accompanied by the rise in cardiac work index. This increase was rather small due to the high levels of developed pressure in the group (183–195 mm Hg). At higher stimulation rates, the index declined smoothly; still, all the hearts successfully reproduced the highest rate of 12 Hz.

After reoxygenation cardiac work index in control group stimulated at initial 5 Hz rate was significantly lower than in Oxacom group ($p < 0.02$). Further increase of stimulation rate resulted in the failure of 3 out of 11 control hearts to reproduce the frequency above 10 Hz while two hearts failed at 8 Hz. In contrast, all the hearts in Oxacom group successfully reproduced the highest applied stimulation rate. Based on the heart performance, the average cardiac work index in Oxacom group was 1.5–2-fold higher than in control group ($p < 0.01$). At maximal rate of stimulation, the cardiac work index in Oxacom group accounted for approximately 75% of the CWI for untreated normoxic heart.

Thus, addition of 30 nM Oxacom to hypoxic perfusate reduced hypoxic and reoxygenation contracture, maintained steady cardiac work during the period of hypoxia, and increased the degree of functional recovery of the heart following reoxygenation. In addition, Oxacom supported the ability of the hearts to reproduce the highest rate of stimulation and significantly increased the LV developed pressure at any frequency compared to control group not exposed to this compound. It should be pointed out that the beneficial effect of Oxacom was realized at 30 nM while similar effects of L-arginine and L-arginine methyl ester were achieved at 3 mM–100 mM [16, 17, 19], that is, at several orders of magnitude higher concentrations.

3.2. Reduced Glutathione Content in the Hearts Subjected to Hypoxia-Reoxygenation. Reduced glutathione in control normoxic hearts comprised 79.9 ± 2.1% of the total glutathione whereas after hypoxia-reoxygenation it decreased to 62.1 ± 1.1% that is, by 22%. In the hearts subjected to hypoxia-reoxygenation in the presence of 30 nM Oxacom the level of GSH was 58.3 ± 1.5%. Thus, low dose of Oxacom did

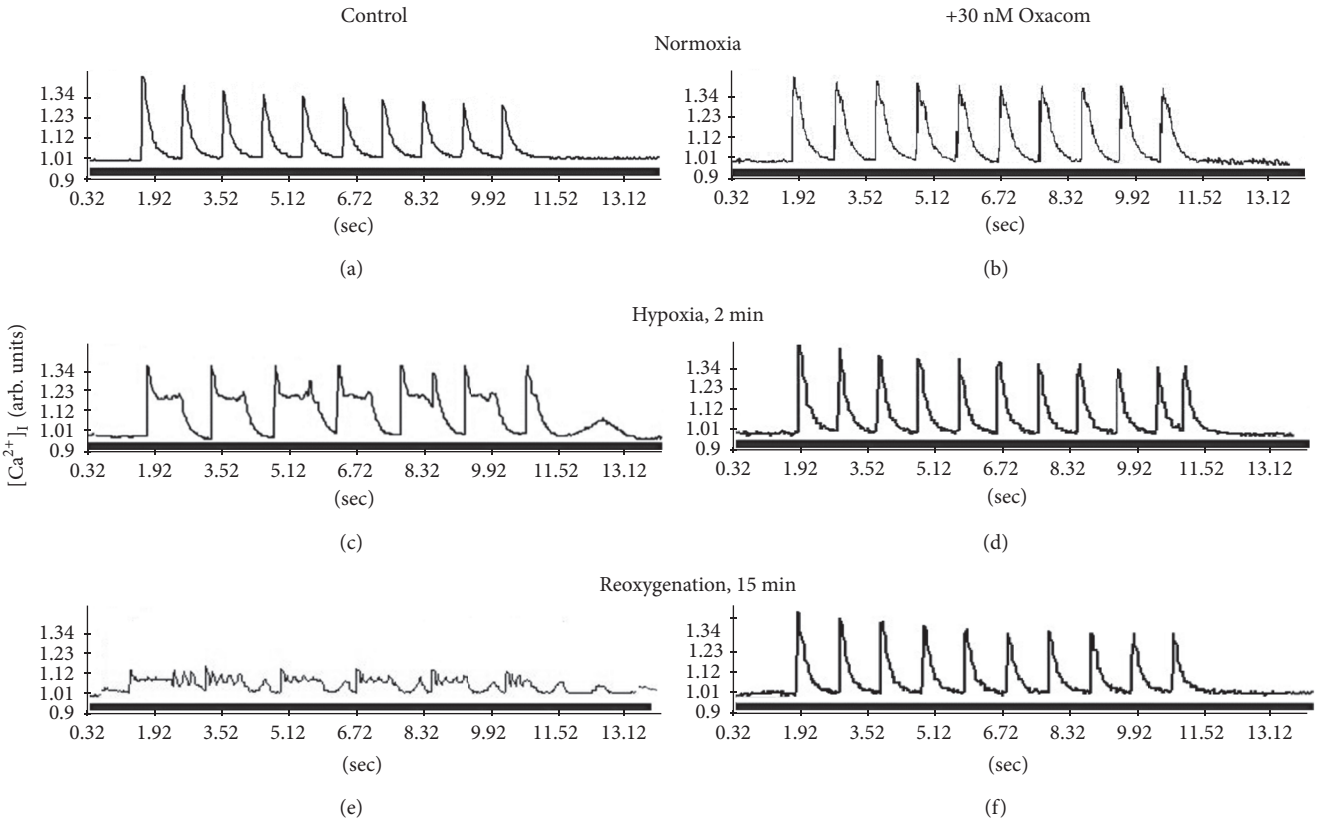

Figure 4: Effects of Oxacom on Ca^{2+} transients in isolated adult rat cardiomyocytes subjected to hypoxia-reoxygenation. Cardiomyocytes loaded with Fluo-4 were preincubated with 30 nM Oxacom for 30 min and electrostimulated by ten rectangular pulses at 1 Hz under conditions of normoxia, after 2 min of hypoxia produced by exchanging regular perfusion buffer saturated with carbogen (95% O_2, 5% CO_2) for hypoxic buffer saturated with 95% N_2 and 5% CO_2 and then after 15 min of reoxygenation. Typical recordings are shown. The legend for ordinate on the left applies to all graphs.

not significantly alter the content of GSH in our model of hypoxia-reoxygenation.

3.3. Effects of Oxacom on Ca^{2+} Transients in Isolated Rat Cardiomyocytes Subjected to Hypoxia-Reoxygenation. Control cardiomyocytes electrically paced at 1 Hz under normoxic conditions respond by the regular Ca^{2+} spikes produced simultaneously in all regions of sarcoplasm and generate no Ca^{2+} transients in the absence of electrostimulation (Figure 4). The shape of Ca^{2+} peaks is asymmetric with the steep upward shoulder and more shallow downward shoulder especially in its lower part. This shape of Ca^{2+} transient reflects molecular events underlying Ca^{2+} transport in cardiomyocytes. Fast rise in sarcoplasmic Ca^{2+} is achieved through the opening of Ca^{2+} channels and fast diffusion of Ca^{2+} ions in the sarcoplasm along the gradient. The reverse process of Ca^{2+} removal from the sarcoplasm into Ca^{2+} stores and across the sarcolemma outside the cell works against Ca^{2+} gradient and requires energy. This task is mainly fulfilled by Na/Ca exchanger (NCX) and Ca-ATPases such as SERCA2 and PMCA in cardiomyocytes. Working in direct mode NCX expels one Ca^{2+} ion from the sarcoplasm into extracellular space in exchange for three Na^+ ions using electrochemical gradient for Na^+ across sarcolemma generated by Na/K-ATPase. NCX has low affinity and high capacity for Ca^{2+} and is mostly active at peak Ca^{2+} concentration in the sarcoplasm. SERCA2 and PMCA have higher affinity and lower capacity for sarcoplasmic Ca^{2+} and are more effective at moderate to low Ca^{2+} concentrations.

Under normoxic conditions NCX and ion pumps promptly remove Ca^{2+} from the sarcoplasm to achieve its basal levels before the next electric stimulus arrives. The total length of Ca^{2+} transient under control normoxic conditions is 200–250 ms. During hypoxia the peak levels of free ionized Ca^{2+} entering cardiomyocytes modestly increase judging by the increase of Ca^{2+} transient amplitude (Figure 4(c)). At the same time the process of Ca^{2+} sequestration is retarded which is reflected by a "dome" on the downward shoulder of Ca^{2+} peak and about 1.5-fold increase in time required to reach basal Ca^{2+} level. Still, the initial removal of high Ca^{2+} from hypoxic cardiomyocytes is not altered in our model and the level of Ca^{2+} declines swiftly as in control cells suggesting that NCX function may not be critically affected in these conditions unlike the function of SERCA2 and PMCA. Additionally, cardiomyocytes become partially refractory

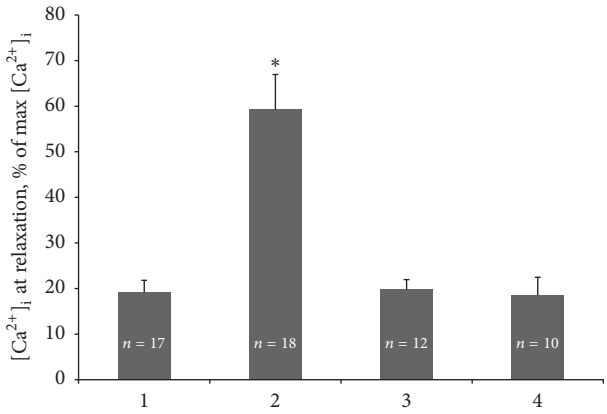

Figure 5: Quantitation of Oxacom effects on Ca^{2+} levels at relaxation in isolated adult rat cardiomyocytes subjected to hypoxia-reoxygenation. 1, control (normoxia); 2, hypoxia, 2 min; 3, hypoxia + 30 nM Oxacom, 2 min; 4, reoxygenation + 30 nM Oxacom, 15 min. *n*, number of cells for each condition. Mean ± SD. $^*p < 0.01$, 2 versus 1, 3, and 4.

and do not respond to every electric stimulus. Based on the "area under the curve" measurements using ImageJ software (NIH, USA) the average content of free ionized Ca^{2+} per Ca^{2+} peak is 3-fold higher in hypoxic than in normoxic cardiomyocytes indicating substantial Ca^{2+} overload. Noteworthily, in our experimental model cardiomyocytes hardly recover from more than 2 min of hypoxia and subsequent reoxygenation after this period of time does not improve their Ca^{2+} transients indicating irreversible damage to the molecular systems of Ca^{2+} transport (Figure 4(e)).

In contrast, these negative events are not developed when cardiomyocytes are preincubated with 30 nM Oxacom and this compound is present in the perfusate throughout the experiment (Figures 4(b), 4(d), and 4(f)). Oxacom does not alter Ca^{2+} transients in normoxic perfusion conditions and maintains normal parameters of Ca^{2+} peaks under both hypoxic and reoxygenation conditions. In the presence of Oxacom cardiomyocytes respond to each of ten electric stimuli in a packet by a single Ca^{2+} spike demonstrating no refractory behavior. Figure 5 shows the quantitative assessment of basal Ca^{2+} in rat cardiomyocytes averaged from the set of experiments such as those presented in Figure 4. It confirms that the level of basal Ca^{2+} in cardiomyocytes subjected to 2 min of hypoxia is 3-fold higher than in normoxic control cells and in cardiomyocytes preincubated with 30 nM Oxacom and subjected to hypoxia-reoxygenation. Because of the relatively small contribution of excessive extracellular Ca^{2+} entry in our model of acute hypoxia of cardiomyocytes we favor the hypothesis that observed Ca^{2+} overloading is mainly due to the failure of Ca^{2+} sequestration systems. In separate experiments, we found that 0.3 nM Oxacom was able to reproduce the effects of 30 nM Oxacom on Ca^{2+} transients in isolated cardiomyocytes subjected to hypoxia-reoxygenation (see supplemental figures S1 and S2 in Supplementary Material available online at https://doi.org/10.1155/2017/9456163). However, such low dose of Oxacom was not effective in isolated perfused heart model.

Thus, Oxacom prevents alterations induced by hypoxia-reoxygenation in Ca-ATPases and, perhaps, NCX and allows cardiomyocytes maintain normal Ca^{2+} transport in these stressful conditions.

3.4. Effects of Oxacom on Cardiomyocyte Contractility and Viability. Contractile activity of cardiomyocytes, based on their visual assessment under the microscope, was fully consistent with the parameters of Ca^{2+}-transport; each Ca^{2+} peak was followed by a single contraction of cellular body. Prolonged Ca^{2+} elevations in hypoxia were accompanied by the same lengthy cellular contractions. Thus, the effect of Oxacom on contractile activity of cardiomyocytes in our model was mainly determined by its impact on the process of Ca^{2+} removal from the sarcoplasm.

Oxacom improved viability of cardiomyocytes subjected to hypoxia-reoxygenation. Our isolation procedure typically yields about half of viable cardiomyocytes in the total cell isolate. These cells display characteristic elongated shape with sharp edges (Figure 6(a)). After two minutes of hypoxia elongated live cardiomyocytes comprised about 12% whereas other cells were rounded and supercontracted exhibiting irreversible damage (Figure 6(b)). Preincubation of cardiomyocytes with 30 nM Oxacom in normoxic conditions does not change the appearance of cell sample that contained 53% of viable cells.

Exposure of cardiomyocytes to 2 min hypoxia in the presence of Oxacom resulted in 52% elongated cells in the sample (Figure 6(c)) similar to normoxic control. After reoxygenation in the presence of Oxacom more that 40% of cardiomyocytes were viable (Figure 6(d)) while there were no viable cells in control sample. Similar results were obtained using quantitation of cells stained with Trypan Blue (data not shown). Thus, low doses of Oxacom protect isolated cardiomyocytes from profound damage and death caused by hypoxia-reoxygenation.

3.5. Effects of Oxacom on Reactive Oxygen Species Accumulation in Isolated Rat Cardiomyocytes Subjected to Hypoxia-Reoxygenation. The alterations of ion-transporting molecular systems of cardiomyocytes in conditions of hypoxia-reoxygenation and ischemia-reperfusion are often linked to the damage of ion transporters and regulatory proteins by reactive oxygen species (ROS) that accumulate in cells during the disturbances in oxygen supply. As shown in Figure 7, ROS levels are not significantly altered in cardiomyocytes under normoxic conditions (Figure 7(a), before hypoxia).

However, both hypoxia and electrostimulation lead to increased ROS in control cells. Reoxygenation initially increases the levels of ROS in cardiomyocytes whereas about 1 min after the start of reoxygenation further increase in ROS is blunted regardless of cardiomyocyte electrostimulation. Perhaps, this reflects the recovery of the normal redox state in cardiomyocytes following oxygen availability. Overall increase in ROS achieved in control cardiomyocytes during

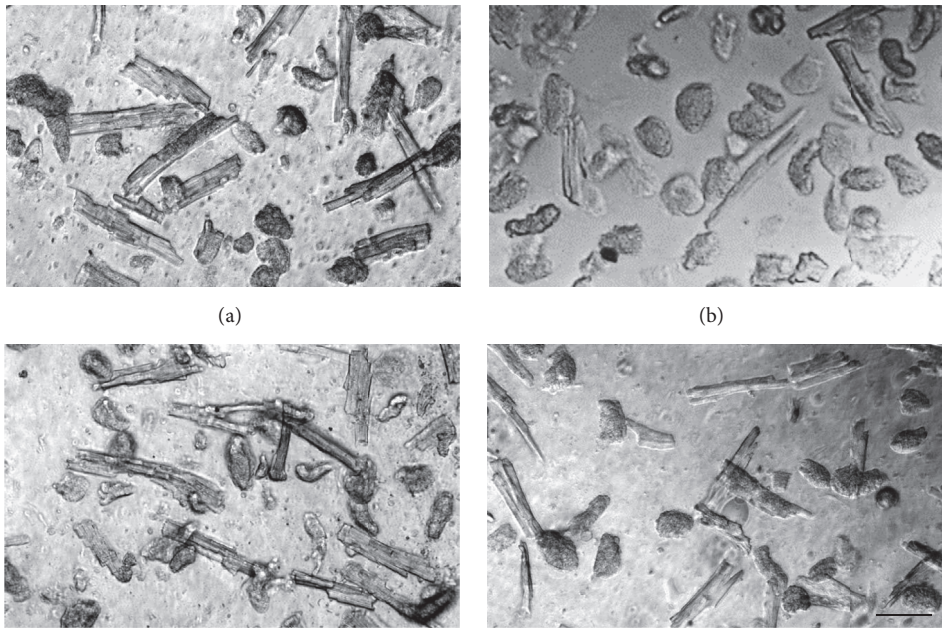

Figure 6: Effects of Oxacom on rat cardiomyocyte viability following hypoxia and reoxygenation. (a) Freshly isolated cardiomyocytes in normoxic buffer; (b) after 2 min of hypoxia; (c) after 2 min of hypoxia in the presence of 30 nM Oxacom; (d) after 15 min of reoxygenation in the presence of 30 nM Oxacom. Phase contrast. Bar, 50 μm.

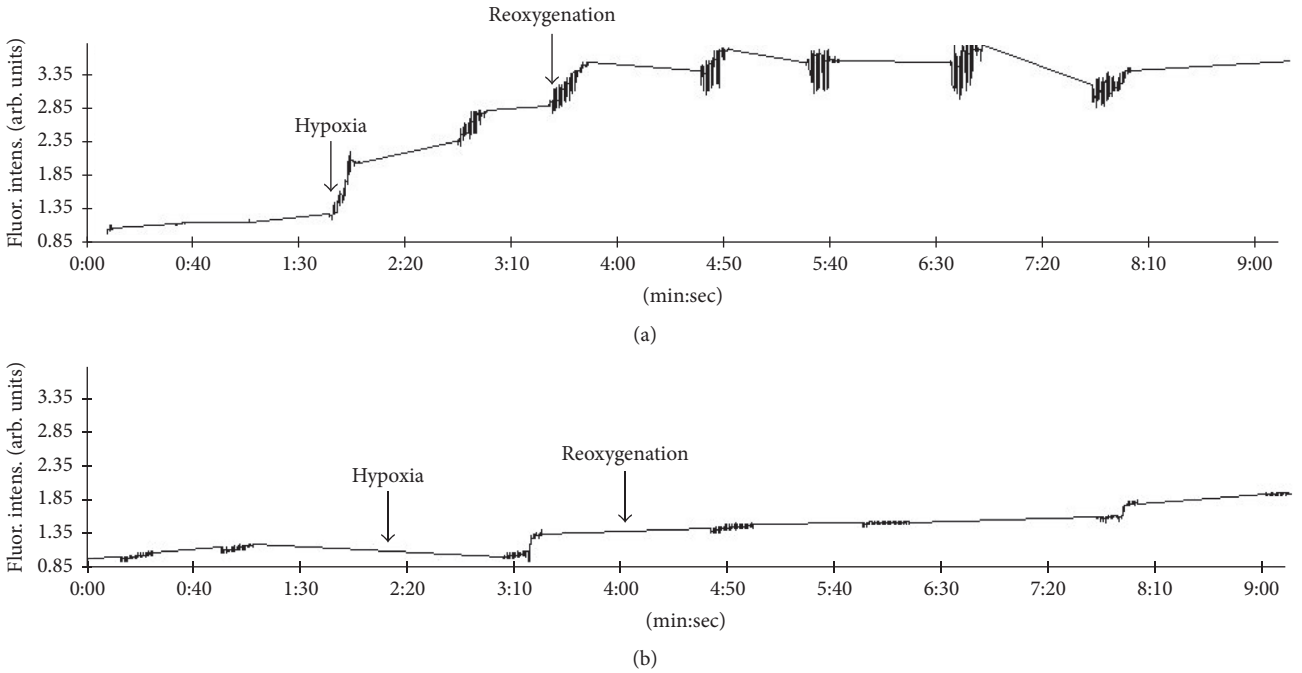

Figure 7: Effects of Oxacom on reactive oxygen species accumulation in adult rat cardiomyocytes subjected to hypoxia-reoxygenation. Cardiomyocytes loaded with DHR-123 fluorescent indicator for ROS were sequentially perfused with normoxic and hypoxic buffers (indicated by arrows) and electrostimulated by rectangular pulses as 1 Hz. "Noisy" fragments of the curve correspond to electrostimulation and fluorescence recording periods. (a) Control cardiomyocytes. (b) Cardiomyocytes preincubated with 30 nM Oxacom. Typical recordings are shown.

hypoxia-reoxygenation in our experiments was about 3.5-fold.

In the presence of 30 nM Oxacom cardiomyocytes demonstrated no significant increase of ROS compared to control cells when subjected to hypoxia/electrostimulation. Specifically, Oxacom attenuated the accumulation of ROS during the period of hypoxia 6-fold. Similarly, during the first minute of reoxygenation Oxacom limited ROS accumulation; however, noticeable increase in ROS was observed at a later time with no evidence for saturation. Overall increase in ROS was about 2-fold in cardiomyocytes treated with Oxacom, which is 75% less than in control cardiomyocytes. Thus, in the presence of Oxacom the accumulation of ROS in cardiomyocytes during hypoxia was markedly attenuated and the latter effect could be related to the better performance of Ca-ATPases and, perhaps, NCX/Na/K-ATPase in these cells.

It is possible that Oxacom acts to maintain the thiol groups of SERCA2 and other Ca^{2+}-transporters in reduced state and/or protects them through a reversible S-nitrosylation. It is known that cysteine residues of proteins located on the cytosolic side of sarcoplasmic reticulum membrane [20] may undergo redox modifications such as S-S bond formation, S-glutathionylation, and S-nitrosylation (SNO). Some of the cysteine residues are modified non-specifically whereas S-nitrosylation or S-glutathionylation of other cysteines may change the functional activity of affected proteins including SERCA2, RyR2 Ca^{2+}-channels, and L-Type Ca^{2+}-channels [21, 22]. Because superoxide and nitric oxide are constantly formed in cardiomyocytes these substances seem to act as endogenous regulators of Ca^{2+} transporting proteins [21]. In the case of RyR2, the direct relationship between the number of S-nitrosylated thiol groups and Ca^{2+}-channel activity was demonstrated [8]. Modification of 2 cysteines activates the channel; modification of 4 cysteines is accompanied by a moderate channel activation. S-nitrosylation of 11 cysteine residues (about 3 residues in each subunit) causes a significant activation of RyR2 whereas the modification of twice as many cysteines leads to irreversible channel activation.

Based on the current estimations of in vivo nitric oxide levels ranging from 100 pM or less up to 5 nM [23] one can assume that 30 nM Oxacom could release amounts of NO comparable to those produced by endogenous NO synthases and sufficient for protein S-nitrosylation. An alternative/additional pathway for Oxacom to influence SERCA2 activity in cardiomyocytes would be through the activation of cyclic GMP-dependent protein kinase (PKG) and phosphorylation of SERCA2 principal inhibitor phospholamban and, perhaps, other SERCA2 regulators, in particular, Hsp20 [24]. Our findings that 0.3 nM Oxacom was equally effective as 30 nM Oxacom in prevention of Ca^{2+} accumulation in hypoxic cardiomyocytes favor NO signaling pathway rather than the direct nitrosylation of the set of cellular proteins. Finally, the attenuation by Oxacom of ROS generation during the period of hypoxia suggests possible stimulatory effects of this compound on antioxidant defense systems of cardiomyocytes different from glutathione system. One possible scenario is that by direct scavenging of the hydroxyl and superoxide radicals NO could protect cardiac Na/K-ATPase from inactivation [25] and consequently prevent Ca^{2+} overload through NCX working in reverse mode. Outlined multiple possibilities warrant further studies to elucidate in detail the molecular basis of Oxacom action on Ca^{2+} transporters and ROS production; such experiments have already been initiated.

4. Conclusions

Obtained results demonstrate that Oxacom is an effective pharmacologic compound capable of reducing hypoxic contractures and promoting increase in the speed and extent of LV developed pressure recovery during reoxygenation. Its action to attenuate cardiac arrhythmias and to preserve the ability of the heart to reproduce high rate of contractions suggests that Oxacom can improve the function of calcium transport proteins in cardiomyocytes. This assumption was supported by direct experiments in isolated cardiomyocytes. Oxacom eliminated calcium transport alterations that took place in control experiments in the form of the slow Ca^{2+} removal from the sarcoplasm and delayed cardiomyocyte relaxation.

This corresponds well to the view that Ca^{2+} removal from the sarcoplasm by Ca^{2+}-ATPases of the sarcolemma and sarcoplasmic reticulum (PMCA and SERCA2) as well as by NCX/Na/K-ATPase tandem is energy-dependent process that slows down due to the depletion of high-energy phosphates during the shortage of oxygen. However, contractile process requires much more energy than the work of the membrane ion pumps. In this regard, the prevention by Oxacom of hypoxic contracture and more rapid recovery of the contractile function during reoxygenation in the presence of this compound suggest protective effects on mitochondria. Observed action of Oxacom to limit ROS generation in hypoxic cardiomyocytes additionally supports the mitochondrial vector for the future mechanistic studies of this novel cardiovascular drug.

Conflicts of Interest

The authors declare no conflicts of interest.

Acknowledgments

This study was supported by the Ministry of Education and Science of the Russian Federation (Contract 16.512.11.2281) and in part by the Russian Foundation for Basic Research (Grant 15-04-06571).

References

[1] L. C. Hool, C. A. Di Maria, H. M. Viola, and P. G. Arthur, "Role of NAD(P)H oxidase in the regulation of cardiac L-type Ca2+ channel function during acute hypoxia," *Cardiovascular Research*, vol. 67, no. 4, pp. 624–635, 2005.

[2] Z. Yang and D. S. Steele, "Effects of phosphocreatine on SR Ca^{2+} regulation in isolated saponin-permeabilized rat cardiac

myocytes," *The Journal of Physiology*, vol. 539, no. 3, pp. 767–777, 2002.

[3] Y. Kihara, W. Grossman, and J. P. Morgan, "Direct measurement of changes in intracellular calcium transients during hypoxia, ischemia, and reperfusion of the intact mammalian heart," *Circulation Research*, vol. 65, no. 4, pp. 1029–1044, 1989.

[4] S. M. Davidson, D. M. Yellon, M. P. Murphy, and M. R. Duchen, "Slow calcium waves and redox changes precede mitochondrial permeability transition pore opening in the intact heart during hypoxia and reoxygenation," *Cardiovascular Research*, vol. 93, no. 3, pp. 445–453, 2012.

[5] P. T. Schumacker, "Hypoxia, anoxia, and O2 sensing: the search continues," *American Journal of Physiology—Lung Cellular and Molecular Physiology*, vol. 283, no. 5, pp. L918–L921, 2002.

[6] H. Strijdom, S. Jacobs, S. Hattingh, C. Page, and A. Lochner, "Nitric oxide production is higher in rat cardiac microvessel endothelial cells than ventricular cardiomyocytes in baseline and hypoxic conditions: a comparative study," *The FASEB Journal*, vol. 20, no. 2, pp. 314–316, 2006.

[7] J. F. Turrens, "Mitochondrial formation of reactive oxygen species," *Journal of Physiology*, vol. 552, no. 2, pp. 335–344, 2003.

[8] L. Xu, J. P. Eu, G. Meissner, and J. S. Stamler, "Activation of the cardiac calcium release channel (ryanodine receptor) by poly-S-nitrosylation," *Science*, vol. 279, no. 5348, pp. 234–237, 1998.

[9] P. Korge, P. Ping, and J. N. Weiss, "Reactive oxygen species production in energized cardiac mitochondria during hypoxia/reoxygenation: modulation by nitric oxide," *Circulation Research*, vol. 103, no. 8, pp. 873–880, 2008.

[10] A. F. Vanin, V. P. Mokh, V. A. Serezhenkov, and E. I. Chazov, "Vasorelaxing activity of stable powder preparations of dinitrosyl iron complexes with cysteine or glutathione ligands," *Nitric Oxide*, vol. 16, no. 3, pp. 322–330, 2007.

[11] A. F. Vanin, A. P. Poltorakov, V. D. Mikoyan, L. N. Kubrina, and D. S. Burbaev, "Polynuclear water-soluble dinitrosyl iron complexes with cysteine or glutathione ligands: electron paramagnetic resonance and optical studies," *Nitric Oxide—Biology and Chemistry*, vol. 23, no. 2, pp. 136–149, 2010.

[12] V. L. Lakomkin, A. F. Vanin, A. A. Timoshin, V. I. Kapelko, and E. I. Chazov, "Long-lasting hypotensive action of stable preparations of dinitrosyl-iron complexes with thiol-containing ligands in conscious normotensive and hypertensive rats," *Nitric Oxide—Biology and Chemistry*, vol. 16, no. 4, pp. 413–418, 2007.

[13] A. A. Timoshin, V. L. Lakomkin, A. A. Abramov et al., "The hypotensive effect of the nitric monoxide donor Oxacom at different routs of its administration to experimental animals," *European Journal of Pharmacology*, vol. 765, pp. 525–532, 2015.

[14] E. I. Chazov, O. V. Rodnenkov, A. V. Zorin et al., "Hypotensive effect of Oxacom® containing a dinitrosyl iron complex with glutathione: animal studies and clinical trials on healthy volunteers," *Nitric Oxide*, vol. 26, no. 3, pp. 148–156, 2012.

[15] D. E. Burger, "Protective role of nitric oxide against cardiac arrhythmia—an update," *The Open Nitric Oxide Journal*, vol. 3, no. 1, pp. 38–47, 2011.

[16] C. Baccaro, F. Bennardini, G. Dini et al., "Cardiac hypoxia and subsequent reoxygenation: sensitivity to L-arginine methylester," *British Journal of Pharmacology*, vol. 87, no. 4, pp. 649–656, 1986.

[17] L. Fei, A. D. Baron, D. P. Henry, and D. P. Zipes, "Intrapericardial delivery of L-arginine reduces the increased severity of ventricular arrhythmias during sympathetic stimulation in dogs with acute coronary occlusion: nitric oxide modulates sympathetic effects on ventricular electrophysiological properties," *Circulation*, vol. 96, no. 11, pp. 4044–4049, 1997.

[18] N. Lüneburg, V. Xanthakis, E. Schwedhelm et al., "Reference intervals for plasma L-arginine and the L-arginine: asymmetric dimethylarginine ratio in the framingham offspring cohort," *Journal of Nutrition*, vol. 141, no. 12, pp. 2186–2190, 2011.

[19] L. Agulló, D. García-Dorado, J. Inserte et al., "L-arginine limits myocardial cell death secondary to hypoxia-reoxygenation by a cGMP-dependent mechanism," *American Journal of Physiology—Heart and Circulatory Physiology*, vol. 276, no. 5, pp. H1574–H1580, 1999.

[20] J. J. Marengo, C. Hidalgo, and R. Bull, "Sulfhydryl oxidation modifies the calcium dependence of ryanodine- sensitive calcium channels of excitable cells," *Biophysical Journal*, vol. 74, no. 3, pp. 1263–1277, 1998.

[21] S. Györke and D. Terentyev, "Modulation of ryanodine receptor by luminal calcium and accessory proteins in health and cardiac disease," *Cardiovascular Research*, vol. 77, no. 2, pp. 245–255, 2008.

[22] A. Z. Vielma, L. León, I. C. Fernández, D. R. González, M. P. Boric, and D. Laver, "Nitric oxide synthase 1 modulates basal and β-adrenergic-stimulated contractility by rapid and reversible redox-dependent S-nitrosylation of the heart," *PLoS ONE*, vol. 11, no. 8, Article ID e0160813, 2016.

[23] C. N. Hall and J. Garthwaite, "What is the real physiological NO concentration in vivo?" *Nitric Oxide*, vol. 21, no. 2, pp. 92–103, 2009.

[24] E. G. Kranias and R. J. Hajjar, "Modulation of cardiac contractility by the phopholamban/SERCA2a regulatome," *Circulation Research*, vol. 110, no. 12, pp. 1646–1660, 2012.

[25] K. Y. Xu, S. P. Kuppusamy, J. Q. Wang et al., "Nitric oxide protects cardiac sarcolemmal membrane enzyme function and ion active transport against ischemia-induced inactivation," *The Journal of Biological Chemistry*, vol. 278, no. 43, pp. 41798–41803, 2003.

Hindawi
Oxidative Medicine and Cellular Longevity
Volume 2017, Article ID 3868305, 17 pages
https://doi.org/10.1155/2017/3868305

Research Article

Tocotrienol-Rich Fraction Ameliorates Antioxidant Defense Mechanisms and Improves Replicative Senescence-Associated Oxidative Stress in Human Myoblasts

Shy Cian Khor, Wan Zurinah Wan Ngah, Yasmin Anum Mohd Yusof, Norwahidah Abdul Karim, and Suzana Makpol

Department of Biochemistry, Faculty of Medicine, Level 17, Preclinical Building, Universiti Kebangsaan Malaysia Medical Centre (UKMMC), Jalan Yaacob Latif, Bandar Tun Razak, 56000 Cheras, Kuala Lumpur, Malaysia

Correspondence should be addressed to Suzana Makpol; suzanamakpol@ppukm.ukm.edu.my

Received 18 October 2016; Revised 22 November 2016; Accepted 18 December 2016; Published 24 January 2017

Academic Editor: Andrea Vasconsuelo

During aging, oxidative stress affects the normal function of satellite cells, with consequent regeneration defects that lead to sarcopenia. This study aimed to evaluate tocotrienol-rich fraction (TRF) modulation in reestablishing the oxidative status of myoblasts during replicative senescence and to compare the effects of TRF with other antioxidants (α-tocopherol (ATF) and *N*-acetyl-cysteine (NAC)). Primary human myoblasts were cultured to young, presenescent, and senescent phases. The cells were treated with antioxidants for 24 h, followed by the assessment of free radical generation, lipid peroxidation, antioxidant enzyme mRNA expression and activities, and the ratio of reduced to oxidized glutathione. Our data showed that replicative senescence increased reactive oxygen species (ROS) generation and lipid peroxidation in myoblasts. Treatment with TRF significantly diminished ROS production and decreased lipid peroxidation in senescent myoblasts. Moreover, the gene expression of superoxide dismutase *(SOD2)*, catalase *(CAT)*, and glutathione peroxidase *(GPX1)* was modulated by TRF treatment, with increased activity of superoxide dismutase and catalase and reduced glutathione peroxidase in senescent myoblasts. In comparison to ATF and NAC, TRF was more efficient in heightening the antioxidant capacity and reducing free radical insults. These results suggested that TRF is able to ameliorate antioxidant defense mechanisms and improves replicative senescence-associated oxidative stress in myoblasts.

1. Introduction

Adult skeletal muscle contains a subpopulation of cells that readily proliferate and differentiate when required to maintain the structure and function of skeletal muscle [1]. These cells were first identified by Mauro in 1961 as quiescent cells located between the basal lamina and sarcolemma of myofibers, known as satellite cells [2]. Human satellite cells can be isolated and cultured in vitro with a limited proliferative capacity depending on the donor age. Proliferating satellite cells are known as myoblasts [3]. The proliferative lifespan of myoblasts remains stable during adulthood but decreases from infants to adolescents, and the cells ultimately reach replicative senescent [4].

During aging, a progressive loss of muscle mass and strength is observed, and this phenomenon is known as sarcopenia. Although the underlying mechanism is still uncertain, sarcopenia is believed to be the result of certain intrinsic or extrinsic factors, such as immobilization, chronic diseases, changes in hormone, and proinflammatory factors, as well as nutritional status in older adults [5]. Additionally, the accumulation of reactive oxygen species (ROS) has been suggested to play a vital role in this age-related muscle atrophy [6]. Redox imbalance observed in senescent satellite cells can be attributed to elevated ROS production or an impaired endogenous antioxidant defense system, leading to oxidative damage [7, 8]. The vulnerability of proliferating myoblasts to oxidative damage will affect muscle regeneration and contributes to the development of sarcopenia, suggesting that oxidative stress, satellite cells, and sarcopenia are interrelated [6, 7].

Oxidative stress in aged skeletal muscle can cause oxidative damage in cells, manifested as damaged DNA, lipid peroxidation, and protein carbonylation [9, 10]. In muscle fibers, free radicals can be produced intrinsically by mitochondria and regulate fundamental signaling pathways in skeletal muscle. The presence of reactive oxygen species (ROS) or reactive nitrogen species (RNS) can be counteracted by the antioxidant defense system, which includes antioxidant enzymes, vitamins, and glutathione, resulting in sustained redox balance [9]. If the antioxidant defense is overwhelmed by excess ROS or RNS, oxidative stress occurs which leads to muscle injury [8, 10].

In addition to the existing oxidative stress during aging, insufficient antioxidant intake among the elderly can contribute to the occurrence of sarcopenia [11]. Low antioxidant levels in older individuals were associated with poor muscle strength and low physical performance and can cause frailty in the elderly [12, 13]. An in vivo study demonstrated that vitamin E deficiency caused poor muscle performance and accelerated aging development [14]. Hence, introducing antioxidants such as vitamin E could be a relevant strategy to delay sarcopenia progression; however, more studies are needed [15].

Vitamin E is a lipid-soluble vitamin with two subclasses, tocopherols and tocotrienols [16]. A previous study reported that α-tocopherol was able to repair laser-induced disrupted myoblast membranes, indicating a therapeutic effect for vitamin E in the muscle [17]. However, the less-explored subtype of vitamin E is the class of tocotrienols. Similar to α-tocopherol, a potential therapeutic effect of tocotrienol-rich fraction (TRF) was proposed owing to its reversal effect on stress-induced presenescence (SIPS) model of myoblasts [18]. In our laboratory, we also found that TRF was superior to α-tocopherol in ameliorating replicative senescence-related aberration and promoting myogenic differentiation [19]. Thus, it would be of interest to elucidate the effects of tocotrienols on the dynamics of oxidative status in senescent myoblasts. Therefore, the aims of this study were to investigate the effects of tocotrienol-rich fraction (TRF) in reestablishing oxidative status during replicative senescence of myoblasts and to compare these effects with other antioxidants, such as α-tocopherol (ATF) and *N*-acetyl-cysteine (NAC), in young, presenescent, and senescent myoblasts followed by the measurement of cell viability and apoptosis as the final outcomes of antioxidant treatment.

2. Materials and Methods

2.1. Cell Culture. Human Skeletal Muscle Myoblasts (HSMM) were purchased from Lonza (Walkersville, MD, USA). Briefly, myoblasts were cultured in Skeletal Muscle Basal Medium (SkBM) that was supplemented with human epidermal growth factor, fetal bovine serum, dexamethasone, L-glutamine, and gentamicin sulfate/amphotericin B (Lonza, Walkersville, MD USA). Cells were cultivated at 37°C in a humid atmosphere containing 5% CO_2. The myoblasts then underwent serial passaging. The number of divisions was calculated for each passage using the formula $\ln(N/n)/\ln 2$, where N is the number of cells at the harvest stage and n is the number of cells at the seeding stage [20]. When cells reached replicative senescence, they were unable to proliferate within 10 days in culture. Myoblasts were divided into 3 different stages, young (<15 cell divisions), presenescent (18-19 cell divisions), and senescent (>20 cell divisions), based on their decreasing proliferative capacity which was represented by hyperbolic proliferative lifespan curve and diminishing percentage of BrdU incorporation. The presence of senescent cells was confirmed by SA-β-gal staining [19].

2.2. Antioxidants. Tocotrienol-rich fraction (TRF) was purchased from Sime Darby Sdn. Bhd., Selangor, Malaysia (TRF Gold TRI E 70), while alpha-tocopherol (ATF) was a gift from the Malaysian Palm Oil Board (MPOB) (Selangor, Malaysia). Both vitamin E subclasses are palm oil-derived. TRF consists of α-tocotrienol (ATT; 26.89%), β-tocotrienol (BTT; 3.64%), γ-tocotrienol (GTT; 31.66%), δ-tocotrienol (DTT; 13.66%), and α-tocopherol (ATF; 24.15%). Briefly, stock solutions of TRF were freshly prepared in 100% ethanol (1 : 1) and kept at −20°C for no longer than one month. A similar process was performed for ATF. TRF and ATF were then incubated overnight with fetal bovine serum at 37°C before use. Then, both TRF and ATF were diluted in culture medium and used at a final concentration of 50 μg/mL [19]. *N*-Acetyl-cysteine (NAC) was purchased from Sigma-Aldrich (St Louis, USA). NAC was freshly prepared in culture medium to the desired final concentration. A dosage of 1.0 mg/mL NAC was used for subsequent experiments, which was determined using a cell viability assay (Supplemental 1A in Supplementary Material available online at https://doi.org/10.1155/2017/3868305). A dosage of 25 μg/mL of TRF or ATF with 1.0 mg/mL NAC was used for combined treatment of TRF and NAC (TRF + NAC) and combination of ATF and NAC (ATF + NAC) (Supplemental 1B and C).

2.3. Cell Viability. The optimal concentrations of NAC, the combination of TRF and NAC (TRF + NAC), and the combination of ATF and NAC (ATF + NAC) were determined using a cell viability assay (Supplemental 1). The effects of H_2O_2 and antioxidants were also determined using cell viability assay. A CellTiter 96® Aqueous Nonradioactive Cell Proliferation Assay (MTS; Promega, Madison, USA) was used according to the manufacturer's instructions. Cells were incubated with several concentrations of antioxidants for 24 h and 45 min for H_2O_2. After that, the treatments were replaced by MTS for another 2 h of incubation. The absorbance of MTS formazan was measured at 490 nm with a microtiter plate reader (VersaMax Molecular Devices, USA). The optimum dosage of treatments was used for subsequent experiments.

2.4. Analysis of Cell Morphology. In brief, cells were plated and fixed with cold ethanol in μ-Slide 8 wells (ibidi, Martinsried, Germany) followed by incubation with an anti-Desmin antibody (dilution: 1 : 50) (D33; Dako, Produktionsvej, Denmark) and Alexa Fluor 488 goat anti-mouse (dilution: 1 : 500) (Molecular Probes, Eugene, OR, USA). Nuclei were visualized using Hoechst 33342 (Molecular Probes, Eugene, OR, USA). Slides were then observed under a Leica TCS SP5 II

Confocal Laser Scanning Microscope (Leica Microsystems, Wetzlar, Germany).

2.5. Senescence-Associated β-Galactosidase (SA β-gal) Staining. SA β-gal was evaluated using a Senescent Cell Histochemical Staining Kit (Sigma-Aldrich, St. Louis, Missouri, USA). Cells were stained according to the manufacturer's instructions. After the cells were incubated in staining solution for 8 h at 37°C in the absence of CO_2, at least 100 cells were observed under the microscope, and the percentage of blue stained cells was calculated.

2.6. Assessment of the Intracellular Production of Reactive Oxygen Species (ROS). ROS generation in myoblasts was determined using two dyes, dihydroethidium (DHE) and 5-(and-6)-carboxy-2′,7′-dichlorodihydrofluorescein diacetate (carboxy-H_2DCFDA) (Molecular Probes, Eugene, OR, USA). The fluorescence of DHE indicated oxidation by superoxide anions, while carboxy-H_2DCFDA is oxidized by hydrogen peroxide (H_2O_2), peroxynitrite, or hydroxyl radicals. Superoxide anions may contribute to carboxy-H_2DCFDA oxidation albeit to a lesser degree. Briefly, myoblasts were incubated in 20 μM DHE and 40 μM carboxy-H_2DCFDA for 45 min. After that, cells were washed with PBS and recovered in medium for 30 min. Then, we measured the intensity of the fluorescence using a flow cytometer (CytoFLEX, Beckman Coulter Pasadena, CA, USA) with the 585/42 bandpass and 525/40 bandpass channels. The percentage of cells that was positively labeled with a particular dye was reported independently. For observation, the same staining protocol was applied, followed by visualization of the nuclei using Hoechst 33342 (Molecular Probes, Eugene, OR, USA). Cells were then observed under a fluorescence microscope (EVOS FL digital inverted microscope, Thermo Fisher Scientific, USA).

2.7. Assessment of Lipid Peroxidation. Lipid peroxidation in myoblasts was measured using a dye, C11-BODIPY® (581/591) (Molecular Probes, Eugene, OR, USA), which is a lipid peroxidation sensor that can shift from red to green fluorescence emission upon oxidation of the polyunsaturated butadienyl segment of the fluorophore. Briefly, myoblasts were incubated in 10 μM C11-BODIPY for 30 min. After that, cells were washed with PBS, trypsinized, and reconstituted in PBS and the oxidized BODIPY was quantitated using a flow cytometer (CytoFLEX, Beckman Coulter Pasadena, CA, USA) with the 525/40 bandpass channel while reduced BODIPY was quantitated with 585/42 bandpass channel. The percentage of cells that was positively labeled with either oxidized or reduced BODIPY was obtained and the ratio of these percentages (oxidized/reduced BODIPY) was reported. For observation, the same staining protocol was applied, followed by visualization of the nuclei using Hoechst 33342 (Molecular Probes, Eugene, OR, USA). Cells were then observed under a fluorescent microscope (EVOS FL digital inverted microscope, Thermo Fisher Scientific, USA).

2.8. Cellular Uptake of Vitamin E. Vitamin E extraction was performed according to the protocol by Mazlan et al. [22]. After trypsinizing and counting the cells, 50 mg/mL butylated hydroxytoluene (BHT) was added to stop autooxidation. The hexane layer of supernatant was then collected, vacuum-dried, and stored at −80°C before analysis with HPLC. A total of 100 μL hexane was added before further dilution with hexane for HPLC analysis. The uptake of vitamin E was analyzed using an HPLC fluorescence detector (Ex/Em: 294 nm/330 nm) (RF-10A, Shimadzu, Japan). A TRF standard was used, and the concentrations of α-tocopherol (ATF), α-tocotrienol (ATT), β-tocotrienol (BTT), γ-tocotrienol (GTT), and δ-tocotrienol (DTT) uptake in cells were calculated in μg/mL per million cells.

2.9. Determination of Antioxidant Enzymes at the Transcriptional Level. Total RNA was extracted using TRI reagent and polyacryl carrier (Molecular Research Center Inc., Ohio, USA). For gene expression determination, quantitative real-time RT-PCR (qRT-PCR) was used. The expression of *SOD1*, *SOD2*, *CAT,* and *GPX1* mRNA was quantitatively analyzed using KAPA SYBR FAST One-Step qPCR kit (Kapa Biosystems, Boston, Massachusetts, USA). For RT-PCR, 400 nM of each primer was used, and the primer sequences are shown in Table 1 [21]. The master mix was prepared, and PCR reactions were carried out in a Bio-Rad iQ5 Cycler (Hercules, CA, USA). The program included cDNA synthesis for 5 min at 42°C; predenaturation for 4 min at 95°C; and PCR amplification for 40 cycles of 3 sec at 95°C and 20 sec at 60°C. These reactions were followed by a melt curve analysis of each targeted gene. The melt curve analysis of each pair of primers and agarose gel electrophoresis that was performed on the PCR products were used to determine the primer specificity (Supplemental 2). The expression level of each targeted gene was normalized to that of glyceraldehyde 3-phosphate dehydrogenase (*GAPDH*). The relative expression value (REV) was calculated using the $2^{-\Delta\Delta Ct}$ method of relative quantification and the following equation:

$$\text{REV} = 2^{\text{Ct value of GAPDH} - \text{Ct value of the gene of interest}}. \quad (1)$$

2.10. Activities of Antioxidant Enzymes. The activities of three antioxidant enzymes, superoxide dismutase (Sod), catalase (Cat), and glutathione peroxidase (Gpx), were determined. These enzymes were extracted in PBS by sonication following the 24-hour treatments.

A Sod assay was performed according to Beyer Jr. and Fridovich [23]. In brief, substrate solution was freshly prepared by mixing L-methionine, nitro blue tetrazolium (NBT), 1% Triton-X, and PBS, pH 7.8 (Sigma, St Louis, USA). Then, 20 μL of enzyme extract and 10 μL of 4 mg/100 mL riboflavin (Sigma, St Louis, USA) were added before incubation under 20-W Sylvania GroLux lamps in a cupboard for 7 min. Absorbance was measured using a UV/VIS spectrophotometer (Shimadzu, Kyoto, Japan) at 560 nm. Sod specific activity was expressed in mU/mg of protein.

A Cat assay was carried out using the method described by Aebi [24]. Enzyme extract was added to a quartz cuvette. The reaction was started by adding 30 mM H_2O_2 (Merck,

Table 1: The primer sequences of *SOD1*, *SOD2*, *CAT,* and *GPX1* [21].

Gene	Forward	Reverse	Product size
SOD1	GAAGGTGTGGGGAAGCATTA	ACATTGCCCAAGTCTCCAAC	174
SOD2	CGTCACCGAGGAGAAGTACC	CTGATTTGGACAAGCAGCAA	313
CAT	CGTGCTGAATGAGGAACAGA	AGTCAGGGTGGACCTCAGTG	119
GPX1	CCAAGCTCATCACCTGGTCT	TCGATGTCAATGGTCTGGAA	127
GAPDH	TCCCTGAGCTGAACGGGAAG	GGAGGAGTGGGTGTCGCTGT	218

Darmstadt, German), and absorbance was measured kinetically for 30 seconds using a UV/VIS spectrophotometer (Shimadzu, Kyoto, Japan) at 240 nm. Cat-specific activity was expressed in mU/mg of protein.

A Gpx assay was carried out according to Paglia and Valentine [25]. Substrate solution was freshly prepared by mixing reduced glutathione, PBS at pH 7.0, sodium azide, the reduced form of nicotinamide adenine dinucleotide phosphate (NADPH), and glutathione reductase (1 U/mL) (Sigma, St Louis, USA). Enzyme extract was added to the substrate solution, and the reaction was started by adding H_2O_2 (Merck, Darmstadt, German). The conversion of NADPH to $NADP^+$ was measured kinetically using a UV/VIS spectrophotometer (Shimadzu, Kyoto, Japan) at 340 nm for 5 min. Gpx-specific activity was expressed in mU/mg of protein.

The total protein was extracted using lysis buffer, and its concentration was determined using a Bio-Rad Protein Assay (Hercules, CA, USA) at 595 nm with a microtiter plate reader (VersaMax Molecular Devices, USA). The protein concentration was used to normalize the enzyme activity.

2.11. Measurement of Reduced to Oxidized Glutathione (GSH/GSSG) Ratio. The GSH/GSSG ratio was determined using a GSH/GSSG-Glo™ Assay Kit (Promega, Madison, WI), which is based on the firefly luciferase reaction. Based on the manufacturer's instructions, both the GSH and GSSG luminescent reaction schemes were performed and measured using a microplate reader with an integration time of 1 s/well (Infinite® 200, Tecan, USA). The ratio was calculated directly from Net RLU as stated in the technical manual.

2.12. Assessment of Apoptotic Events. Apoptosis profiles were determined using an Annexin V-FITC Apoptosis Detection Kit II (BD Pharmingen, CA, USA) according to the manufacturer's instructions. Two dyes were used, Annexin V-FITC, which was detected by FL1, and propidium iodide (PI), which was detected by FL3. The cells were analyzed with a FACS Calibur flow cytometer (Becton Dickinson, CA, USA). The percentage of cells that were negatively stained with both dyes ($FITC^{-ve}/PI^{-ve}$) was reported as viable cells, while percentage of cells that were positively stained with Annexin V-FITC only ($FITC^{+ve}/PI^{-ve}$) or both Annexin V-FITC and PI ($FITC^{+ve}/PI^{+ve}$) was reported as early and late apoptotic cells, respectively.

2.13. Statistical Analysis. Statistical analyses were performed using SPSS 22.0 software (IBM, NY, USA). All of the data are reported as the means ± standard deviation (SD) from at least three replicates. For all of the tests, $p < 0.05$ was considered statistically significant. To determine the significance between two treatment groups, comparisons were made using an independent t-test, while ANOVA was used to analyze multiple groups, followed by a post hoc Tukey's HSD or LSD (if equal variance was assumed) and Dunnett's T3 (if equal variance was not assumed) tests.

3. Results

3.1. Effects of Antioxidants on Senescent Myoblasts. To determine whether antioxidant properties alone are sufficient to ameliorate senescent myoblasts, in our study we tested a synthetic antioxidant, *N*-acetyl-cysteine (NAC), and its combination with TRF and ATF, besides treatment with TRF or ATF alone. Previously, the beneficial effects of TRF or ATF on senescent myoblasts were reported, where a concentration of 50 μg/mL TRF or ATF alone was able to increase cell viability, improve cellular morphology (more spindle-shaped cells were observed), and decrease the total of SA-β-gal staining positive cells during replicative senescence [19]. In the present study, we found that NAC was not toxic to cells up to the highest concentration used with a 24-hour incubation (Supplemental 1A). Thus, 1.0 mg/mL of NAC was used in the subsequent experiments. Different concentrations of TRF or ATF in combination with NAC were tested using cell viability assay (Supplemental 1B and 1C) in which a concentration of 25 μg/mL TRF or ATF was used with 1.0 mg/mL NAC in the subsequent experiment. NAC alone and in combination with TRF (TRF + NAC) or ATF (ATF + NAC) significantly improved the cellular morphology of senescent myoblasts (cells became spindle-shaped) and reduced the percentage of cells positive for a senescence biomarker (SA-β-gal staining) (Figures 1(a) and 1(b)).

3.2. Effects of Antioxidants on ROS Generation during Replicative Senescence. To elucidate the effects of aging on the oxidative status of myoblasts, we expanded cells in culture until replicative senescence was achieved. The generation of ROS was observed at all stages of cell culture using carboxy-H_2DCFDA (in green, H_2O_2, peroxynitrite, hydroxyl radicals, etc.) and DHE (in orange, superoxide anion) (Figures 2(a)–2(c)). The presence of carboxy-H_2DCFDA gradually increased in untreated control of young to senescent myoblasts (Figures 2(a)–2(c)). However, similar observations were not observed with DHE. Quantitative analysis showed that the amount of intracellular ROS was significantly

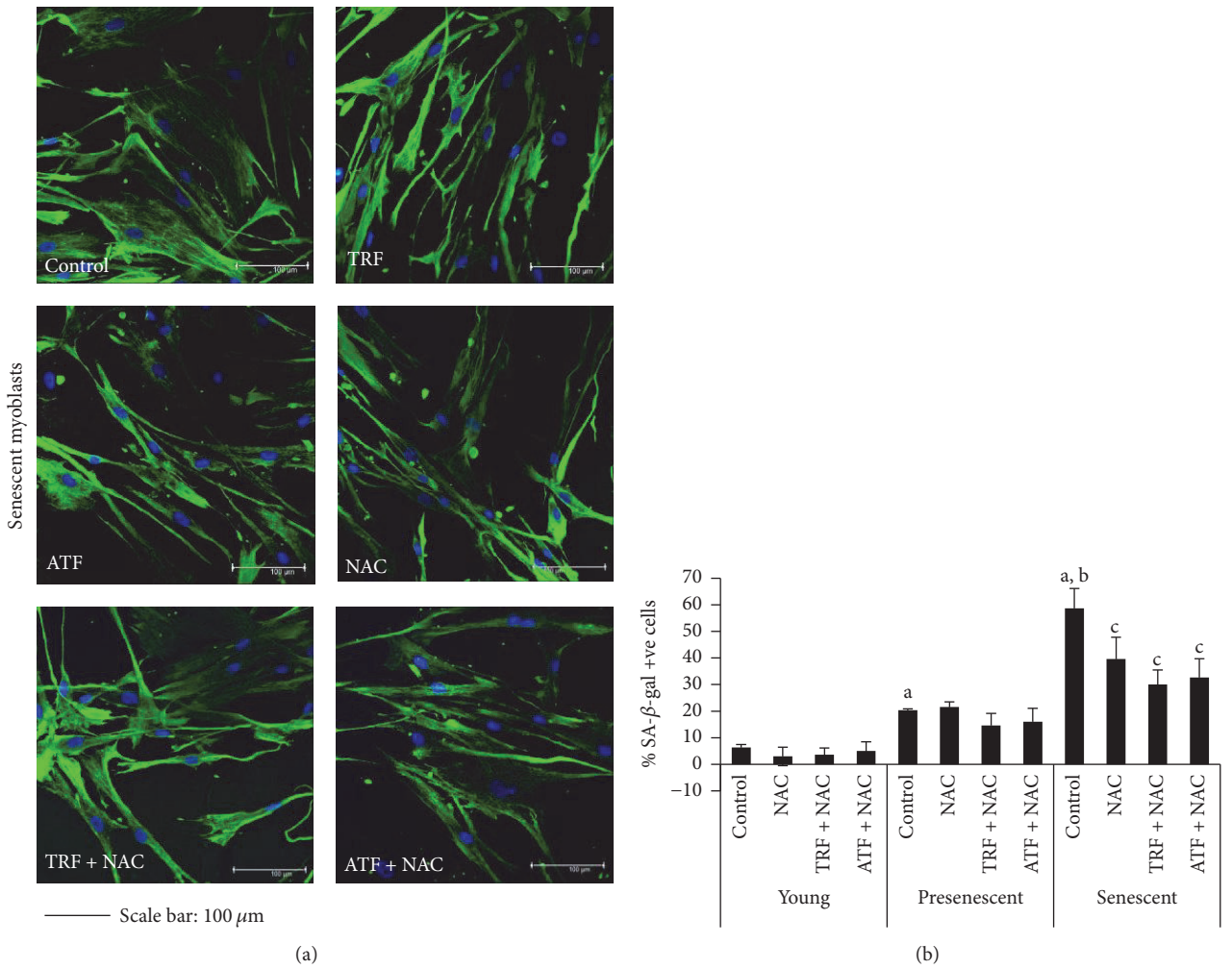

Figure 1: Protective effects of NAC alone and in combination with TRF and ATF on senescent myoblasts. (a) More spindle-shaped cells observed in senescent myoblasts after NAC, TRF + NAC, and ATF + NAC treatment, which were similar to the effect of TRF and ATF treatment alone on senescent myoblasts. Scale bar, 100 μm. (b) The percentage of SA-β-gal positive cells decreased in all treatment groups. [a]Denoting $p < 0.05$, significantly different compared to the young control, [b]$p < 0.05$, significantly different compared to the presenescent control, and [c]$p < 0.05$, significantly different compared to the senescent control. Data are presented as the mean ± SD, $n = 3$.

increased in presenescent and senescent myoblasts compared to young myoblasts ($p < 0.05$), and senescent myoblasts had the highest levels of ROS, suggesting that senescent cells experience more severe oxidant insults compared to young and presenescent cells (Figure 2(d)).

Both TRF and ATF treatments reduced the amount of intracellular ROS in senescent myoblasts, which was indicated by the decline in fluorescence intensity as well as the total number of positively stained cells (Figure 2(c)). The treatments were likely to diminish ROS in young and presenescent cells as well (Figures 2(a) and 2(b)). Quantitative analysis showed that both TRF and ATF significantly diminished intracellular H_2O_2 generation in presenescent and senescent myoblasts ($p < 0.05$) (Figure 2(d)). However, only ATF-treated senescent myoblasts had significantly lower intracellular superoxide anion levels compared to untreated senescent control cells ($p < 0.05$) (Figure 2(d)). Presenescent cells treated with TRF + NAC and ATF + NAC exhibited significantly lower ROS generation ($p < 0.05$) (Figure 2(d)). In senescent myoblasts only, TRF + NAC treatment caused a significant decrease in ROS generation ($p < 0.05$) (Figure 2(d)). A similar reduction in free radical generation was not observed in cells treated with NAC alone, indicating that the antioxidant effects observed were the result of TRF and ATF actions. The presence of ROS in all treatment groups in young, presenescent, and senescent myoblasts can be visualized in Figures 2(a), 2(b), and 2(c), respectively.

To confirm the effects of ROS on normal myoblasts, we measured the cell viability immediately after a short-term of H_2O_2 insult. Our results showed decreased cell viability at all stages of aging after 45 min of incubation with 1 mM, 1.5 mM, 2 mM, and 2.5 mM H_2O_2, $p < 0.05$ (Figure 2(e)). The steady

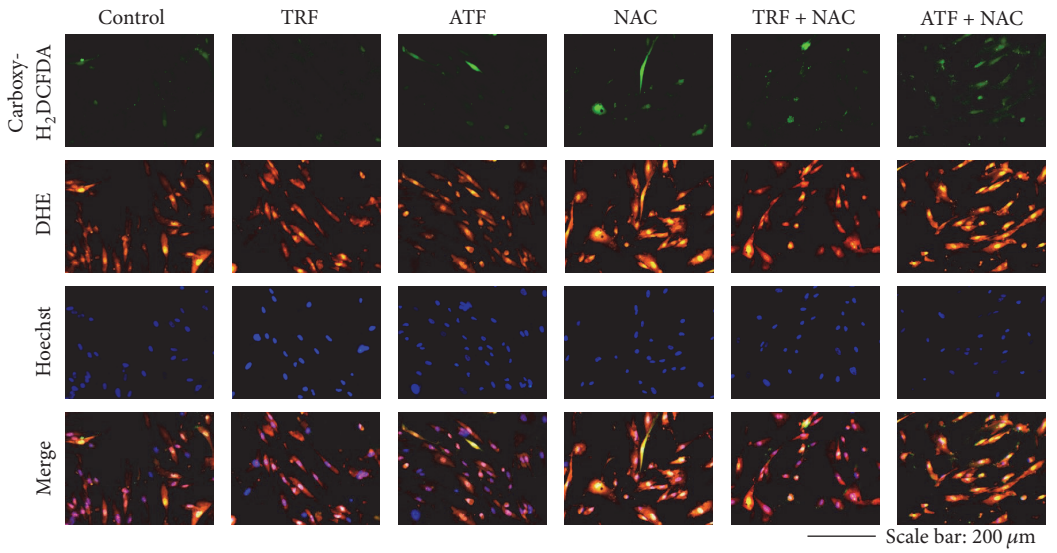

(a)

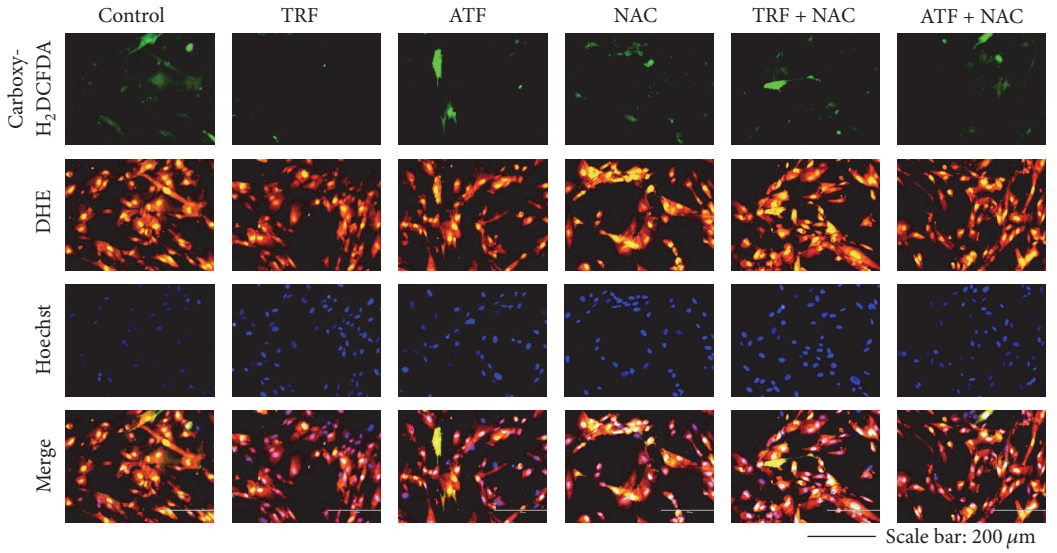

(b)

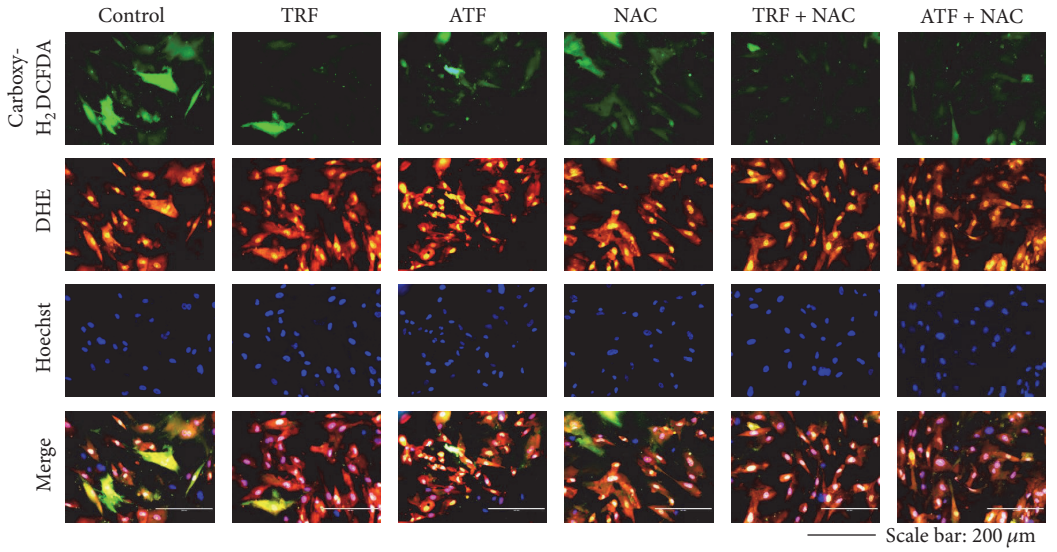

(c)

Figure 2: Continued.

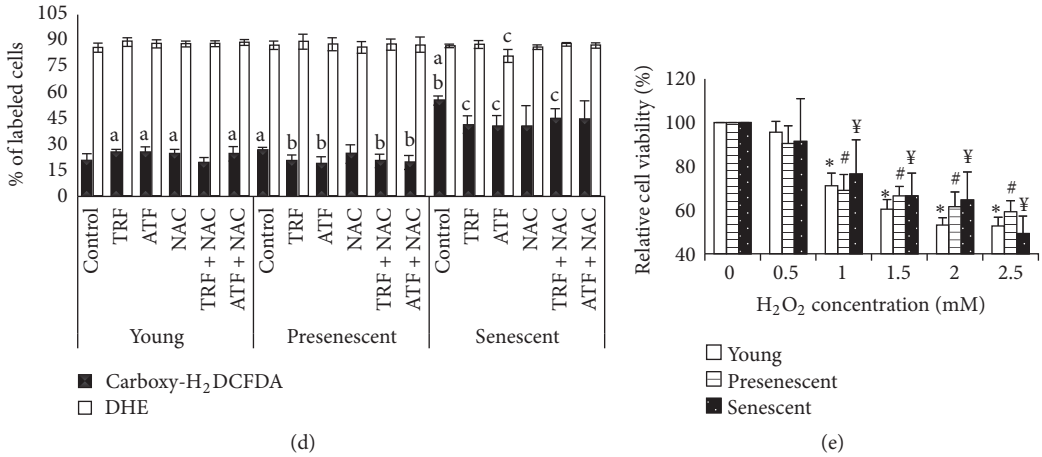

Figure 2: Effects of antioxidants treatment on the presence of ROS in myoblast cells. (a) Young, (b) presenescent, and (c) senescent myoblasts labeled with 20 μM DHE and 40 μM carboxy-H_2DCFDA to detect the presence of ROS which were observed under fluorescence microscope (magnification 200x, scale bar, 200 μm). TRF and ATF diminished the presence of ROS in senescent cells. (d) Quantitative analysis of ROS generation in myoblasts. The percentage of positively stained cells was significantly increased in presenescent and senescent myoblasts; however, the percentage was decreased in TRF-, ATF-, and TRF + NAC-treated senescent myoblasts. (e) A gradual decrease in cell viability with increasing concentrations of H_2O_2 was observed, indicating the vital role of redox balance maintenance in cells. [a]Denoting $p < 0.05$, significantly different compared to young control; [b]$p < 0.05$, significantly different compared to presenescent myoblasts; [c]$p < 0.05$, significantly different compared to senescent myoblasts; and $^{*\#¥}p < 0.05$, significantly different compared to 0 mM. Data are presented as the mean ± SD, $n = 3$.

decline in cell viability with increasing H_2O_2 concentration exposure may indicate the vital role of a maintained redox balance in muscle cells.

3.3. Effects of Antioxidants on Lipid Peroxidation during Replicative Senescence. To determine the oxidative damage in myoblasts, lipid peroxidation levels were measured with C11-BODIPY® (581/591), a sensitive fluorescent reporter for lipid peroxidation. The total number of cells that underwent a shift from red to green was gradually augmented from young to senescent cells (Figures 3(a)–3(c)). In senescent myoblasts, the amount of cells with lipid peroxidation, which was indicated by the percentage of cells with oxidized BODIPY (in green), was increased as represented in the right-shifted fluorescence intensity histogram (Figure 3(d)). Quantitative analysis showed that the ratio of cells with oxidized BODIPY to reduced BODIPY (in red) (oxidized/reduced BODIPY ratio) was significantly increased in presenescent and senescent myoblasts compared to young myoblasts ($p < 0.05$) (Figure 3(e)).

Evaluation of lipid peroxidation levels, which was performed after antioxidant treatment, showed that both TRF and ATF reduced the level of lipid peroxidation in young, presenescent, and senescent myoblasts (Figures 3(a), 3(b), 3(c), and 3(e)). The number of oxidized BODIPY-positive cells was decreased in both TRF- and ATF-treated senescent myoblasts (Figure 3(c)). Statistical analysis of the oxidized/reduced BODIPY ratio revealed that both TRF and ATF significantly reduced lipid peroxidation in presenescent and senescent myoblasts ($p < 0.05$) (Figure 3(e)). Surprisingly, NAC increased oxidized/reduced BODIPY ratio in presenescent myoblasts ($p < 0.05$) (Figure 3(e)). However, senescent cells treated with ATF + NAC and TRF + NAC showed significantly decreased lipid peroxidation (oxidized/reduced BODIPY ratio) compared to untreated control senescent myoblasts ($p < 0.05$) (Figure 3(e)).

3.4. Cellular Uptake of Vitamin E. To validate the cellular uptake of vitamin E, we determined the concentration of vitamin E isomers (ATF, ATT, BTT, GTT, and DTT) in all groups of cells (Figures 4(a) and 4(b)). Young, presenescent, and senescent TRF-treated myoblasts showed the presence of 5 vitamin E isomers, while a significantly inferior number of isomers were found in control cells (Figure 4(a)). A significantly higher concentration of ATF was observed in young, presenescent, and senescent ATF-treated myoblasts compared to untreated cells ($p < 0.05$) (Figure 4(a)). The NAC-treated cells contained the lowest concentrations of vitamin E isomers compared to its combination with TRF or ATF group (Figure 4(b)). TRF + NAC-treated cells contained high levels of all 5 isomers of vitamin E, while ATF + NAC cells only contained a high ATF concentration (Figure 4(b)).

3.5. TRF Treatment Modulates Antioxidant Capacity. The modulation of antioxidant capacity by TRF, ATF, NAC, TRF + NAC, and ATF + NAC during the replicative senescence of myoblasts was investigated by determining the mRNA expression of antioxidant enzymes *(SOD1, SOD2, CAT,* and *GPX1)* and activities of antioxidant enzymes (Sod, Cat, and Gpx), as well as the ratio of GSH/GSSG in young, presenescent, and senescent myoblasts (Figures 5 and 6). Overall, TRF treatment was more effective in modulating antioxidant enzymes expression, especially at transcriptional level, compared to other antioxidants in senescent myoblasts.

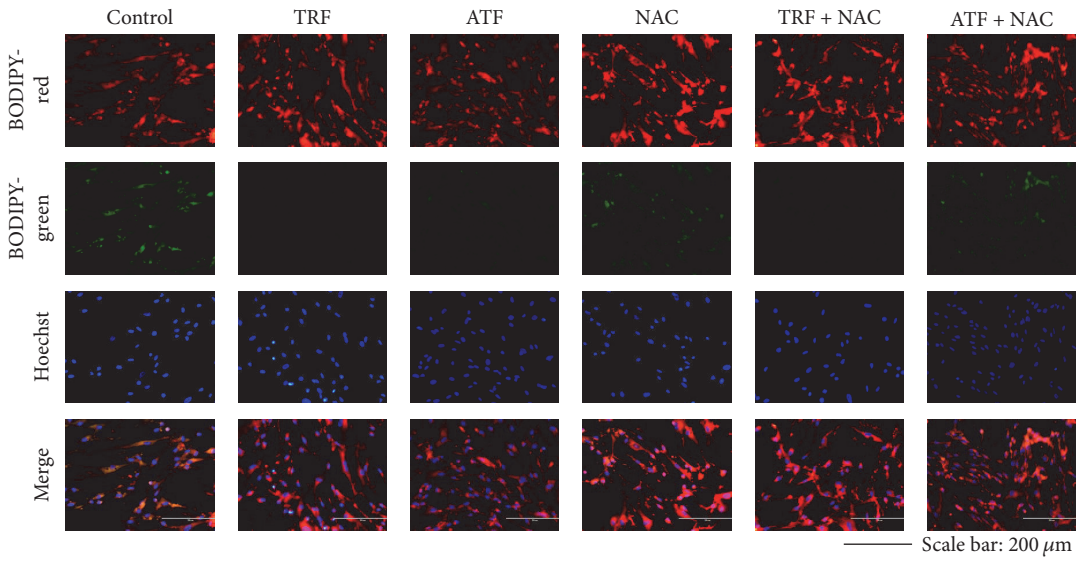

(a)

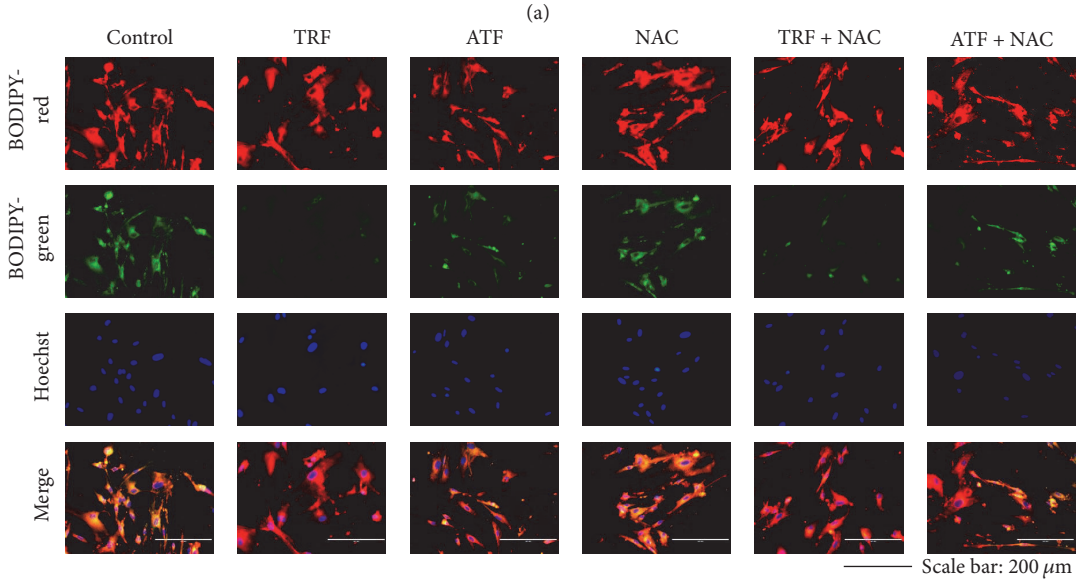

(b)

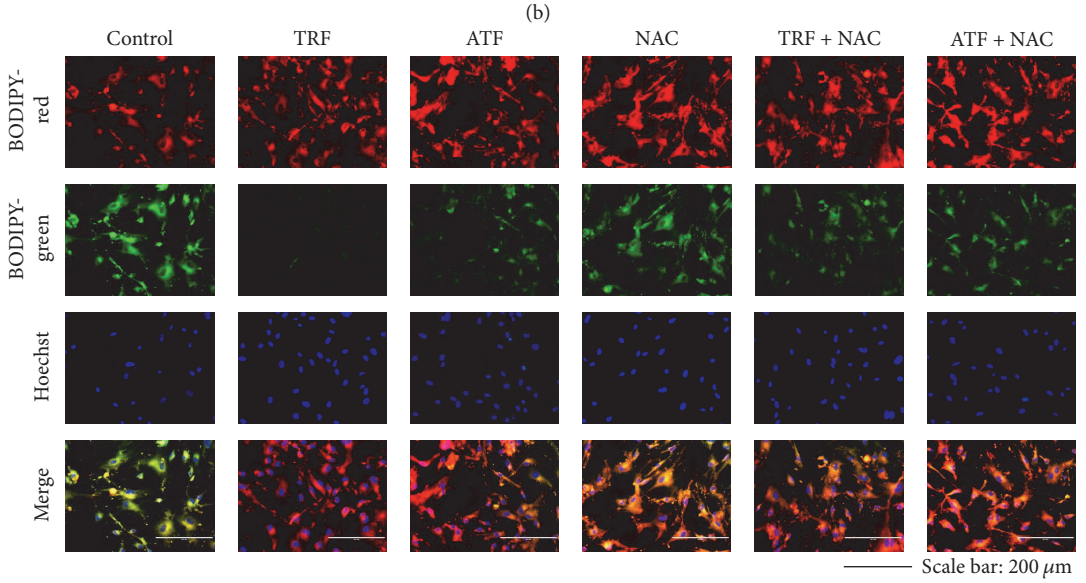

(c)

Figure 3: Continued.

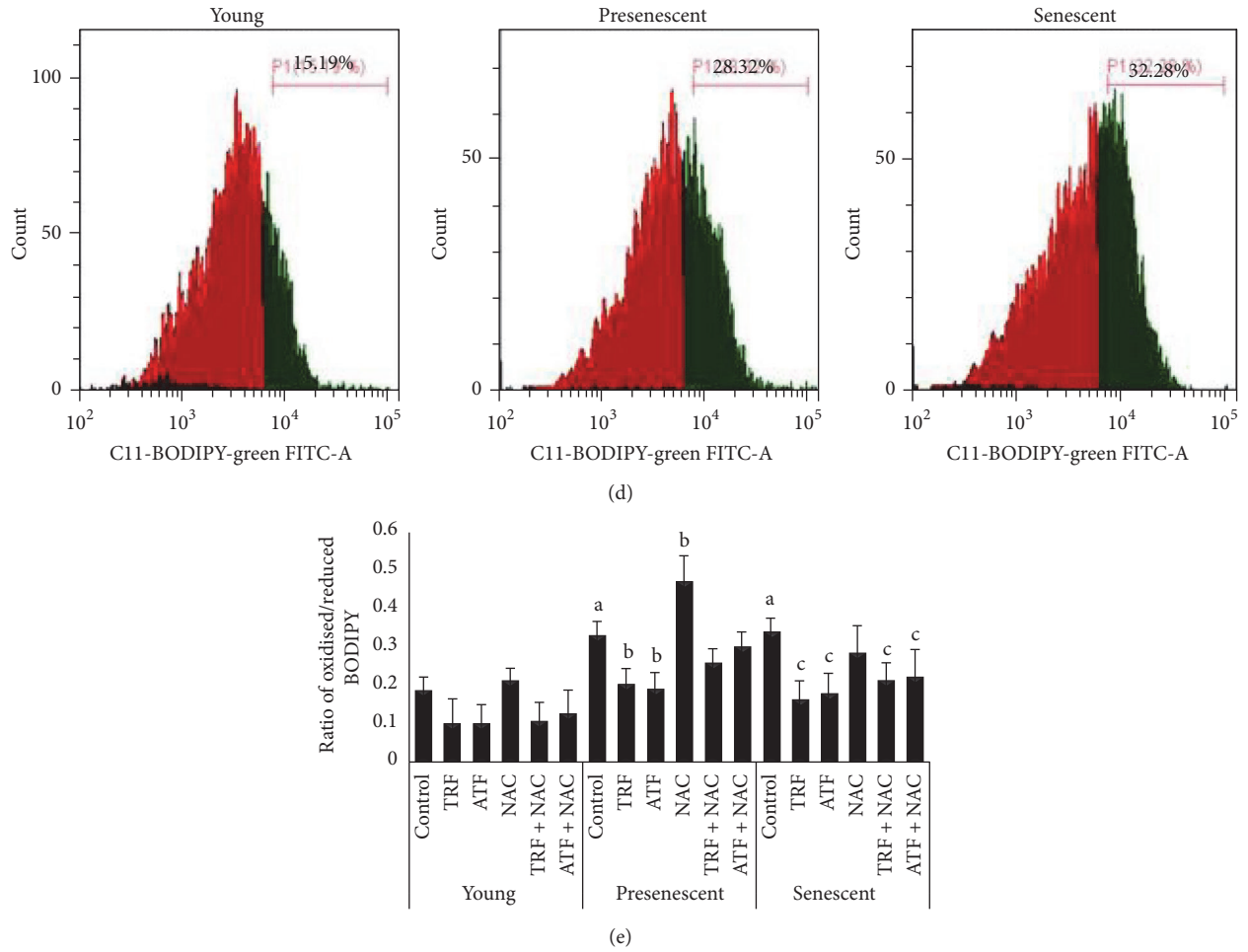

Figure 3: Effects of antioxidants treatment on lipid peroxidation levels of myoblasts. (a) Young, (b) presenescent, and (c) senescent myoblasts labeled with C11-BODIPY® (581/591) to detect lipid peroxidation which were observed under fluorescence microscope (magnification: 200x, scale bar, 200 μm). TRF and ATF treatment effectively reduced lipid peroxidation. (d) Representative histogram of myoblasts based on the oxidized BODIPY (in green, 525/40 bandpass channel). (e) Ratio of oxidized/reduced BODIPY virtually representing lipid peroxidation in myoblast cells. [a]Denoting $p < 0.05$, significantly different compared to young control; [b]$p < 0.05$, significantly different compared to presenescent myoblasts; [c]$p < 0.05$, significantly different compared to senescent myoblasts. Data are presented as the mean ± SD, $n = 3$.

There was no significant change in *SOD1* mRNA expression levels with aging and antioxidant treatment (Figure 5(a)). However, *SOD2* mRNA expression in the presenescent control was significantly increased compared to the young control ($p < 0.05$) (Figure 5(b)). TRF treatment upregulated *SOD2* mRNA expression in young, presenescent, and senescent myoblasts compared to their corresponding untreated controls ($p < 0.05$) (Figure 5(b)). Furthermore, our results showed that only TRF + NAC modulated the expression of *SOD2* mRNA, while NAC and ATF + NAC did not modulate any antioxidant enzymes at the transcriptional level (Figure 5(b)), suggesting that TRF exerted a modulatory effect at the transcriptional level. Moreover, Sod activity was increased in TRF-treated presenescent and senescent myoblasts compared to their untreated controls ($p < 0.05$) (Figure 6(a)). In senescent myoblasts, treatment with TRF + NAC significantly increased the activity of Sod compared to the senescent control ($p < 0.05$). However, similar increases in Sod activity were observed in young myoblasts treated with ATF + NAC, while, in presenescent myoblasts, treatment with NAC, TRF + NAC, and ATF + NAC decreased Sod activity.

In the presenescent control, *CAT* mRNA expression was significantly higher than the young control, $p < 0.05$ (Figure 5(c)). In contrast, Cat activity in the presenescent control was lower than in the young control ($p < 0.05$) (Figure 6(b)). Treatment with either TRF or ATF upregulated *CAT* mRNA expression in senescent myoblasts compared to untreated controls ($p < 0.05$) (Figure 5(c)), while only TRF increased Cat activity in senescent myoblasts and ATF increased Cat activity in presenescent myoblasts (Figure 6(b)). TRF + NAC significantly increased *CAT* mRNA expression in young myoblasts, in comparison to their untreated controls (Figure 5(c)). Treatment with NAC, TRF + NAC, and ATF + NAC increased Cat activity in presenescent myoblasts ($p < 0.05$), while, in young myoblasts, Cat activity was significantly increased with TRF + NAC and ATF + NAC treatment

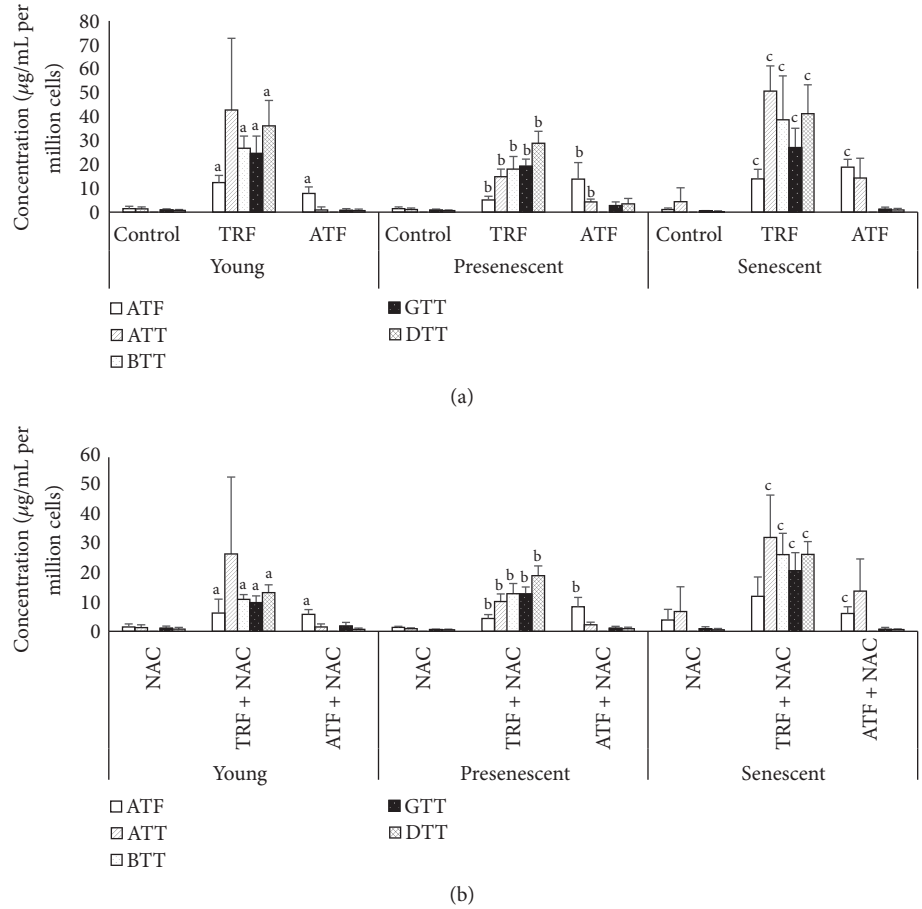

Figure 4: Cellular uptake of vitamin E isomers by myoblasts. (a) Untreated control, TRF- and ATF-treated young, presenescent, and senescent myoblasts. Cellular uptake of 5 vitamin E isomers was significantly higher in TRF-treated myoblasts. (b) NAC-, TRF + NAC-, and ATF + NAC-treated young, presenescent, and senescent myoblasts. Cellular uptake of 5 vitamin E isomers was significantly higher in TRF + NAC-treated myoblasts. [a]Denoting $p < 0.05$, significantly different compared to the young control, [b]$p < 0.05$, significantly different compared to the presenescent control, and [c]$p < 0.05$, significantly different compared to the senescent control. Data are presented as the mean ± SD, $n = 3$.

(Figure 6(b)). However, only ATF + NAC-treated senescent myoblasts demonstrated increased Cat activity.

No significant changes were observed in *GPX1* mRNA expression with aging in myoblasts, even though expression of this gene was modulated by TRF, which was evident by the upregulation of its mRNA expression in young, presenescent, and senescent cells ($p < 0.05$) (Figure 5(d)). However, a similar pattern of expression was not observed for the enzyme activity of Gpx. Gpx activity was significantly higher in the senescent control compared to both the young and presenescent controls ($p < 0.05$) (Figure 6(c)), while both TRF- and ATF-treated senescent myoblasts exhibited lower enzyme activities compared to the senescent control ($p < 0.05$) (Figure 6(c)). Gpx activity levels were increased in TRF + NAC-treated presenescent myoblasts but decreased in ATF + NAC-treated presenescent myoblasts (Figure 6(c)). NAC-, TRF + NAC-, and ATF + NAC-treated senescent myoblasts exhibited significantly lower Gpx activity compared to the untreated senescent control. A similar decrease in Gpx activity was observed in young myoblasts treated with NAC alone.

The GSH/GSSG ratio is always used as an indicator for antioxidant capacity. However, in our study, there was no significant change observed in the GSH/GSSG ratio between young, presenescent, and the senescent control (Figure 6(d)). In young and presenescent myoblasts, TRF treatment reduced the ratio significantly compared to untreated controls ($p < 0.05$) (Figure 6(d)). Determination of the GSH/GSSG ratio in myoblasts showed that treatment with NAC alone in young, presenescent, and senescent myoblasts resulted in a significantly increased GSH/GSSG ratio ($p < 0.05$) (Figure 6(d)). A similar increase in the GSH/GSSG ratio was observed in presenescent cells treated with TRF + NAC.

3.6. Effects of Antioxidants on Cell Viability and Apoptosis Profile. To evaluate the beneficial effects of TRF, ATF, NAC, and their combinations on oxidative status and its final outcome, cell viability (Figure 7(a)) and apoptosis profile (Figures 7(b)–7(d)) were measured. Our results showed that TRF, ATF, NAC, and their combinations significantly increased the number of viable cells in young, presenescent, and senescent

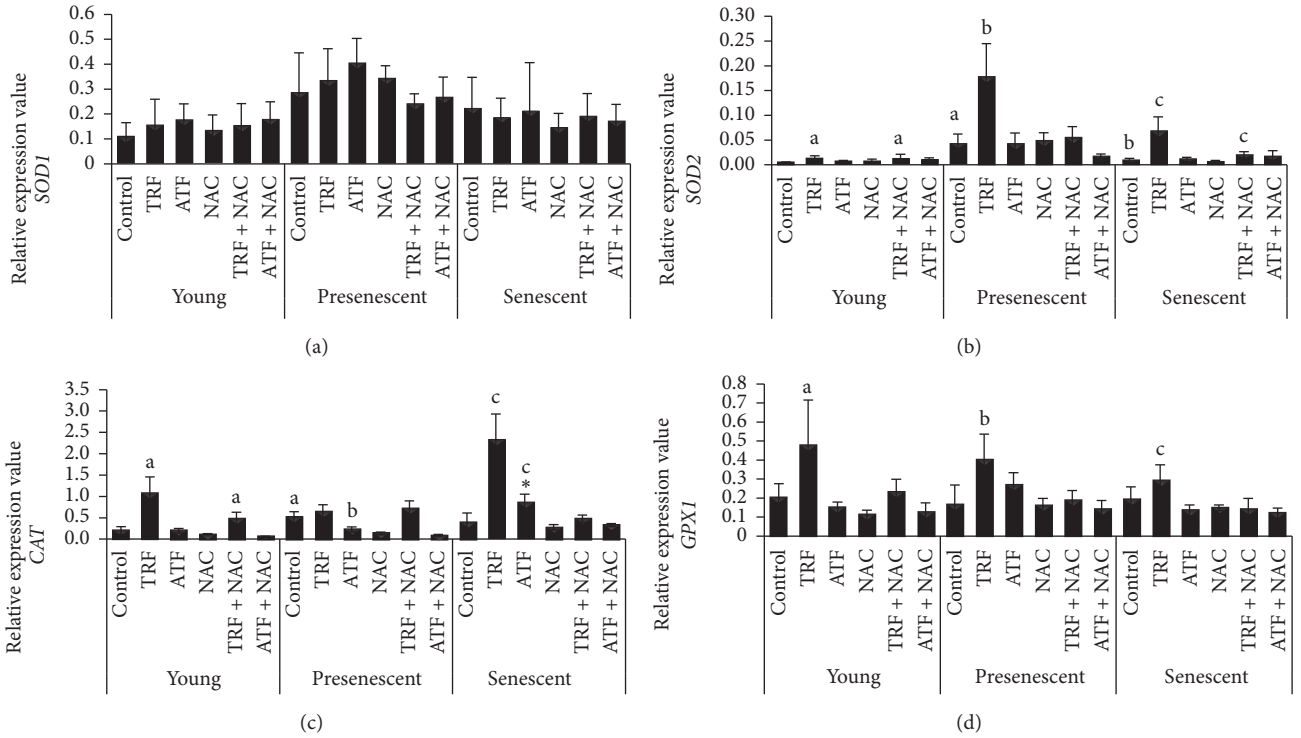

Figure 5: Effects of antioxidants treatment on antioxidant enzymes mRNA expression in young, presenescent, and senescent myoblasts. (a) *SOD1* mRNA, (b) *SOD2* mRNA, (c) *CAT* mRNA, and (d) *GPX1* mRNA expression. [a]Denoting $p < 0.05$, significantly different compared to the young control, [b]$p < 0.05$, significantly different compared to the presenescent control, [c]$p < 0.05$, significantly different compared to the senescent control, and $^{*}p < 0.05$, significantly different compared to TRF-treated senescent myoblasts. Data are presented as the mean ± SD, $n = 3$.

myoblasts compared to their corresponding untreated controls (Figure 7(a)).

Apoptotic changes were determined by Annexin V-FITC staining. Figure 7(b) shows the dot plot of FITC-Annexin V/PI double staining as determined by flow cytometry analysis. The three quadrants represent different cell conditions: the upper right quadrant (R1) indicates nonviable and late apoptotic cells ($FITC^{+ve}/PI^{+ve}$), the lower left quadrant (R2) indicates viable cells ($FITC^{-ve}/PI^{-ve}$), and the lower right quadrant (R3) indicates early apoptotic cells ($FITC^{+ve}/PI^{-ve}$), which is demonstrated by Annexin V binding and cytoplasmic membrane integrity. The quantitative data for the viable cells is shown in Figure 7(c). The percentage of viable cells in the presenescent and senescent controls was significantly lower than in the young control ($p < 0.05$). Treatment with TRF, ATF, TRF + NAC, or ATF + NAC was able to increase the number of viable cells during replicative senescence, signifying the protective role of antioxidant treatment against cell death. A similar increase in cell viability was observed in presenescent myoblasts treated with NAC, TRF + NAC, or ATF + NAC ($p < 0.05$).

Increases in early and late apoptotic events were observed in senescent myoblasts compared to young and presenescent cells ($p < 0.05$) (Figure 7(d)). Treatment with TRF, ATF, NAC, TRF + NAC, or ATF + NAC significantly reduced the number of early apoptotic cells in senescent myoblasts compared to untreated controls ($p < 0.05$). Only TRF, TRF + NAC, and ATF + NAC treatment significantly decreased the number of cells undergoing late apoptotic events ($p < 0.05$). Early and late apoptotic events were also increased in presenescent myoblasts and were reduced by TRF + NAC or ATF + NAC treatment ($p < 0.05$).

4. Discussion

Vitamin E is well known for its free radical-scavenging capacity, which plays an important role in antioxidant defense mechanisms. The lesser known form of vitamin E, tocotrienols, has been reported to possess greater antioxidant effects and better membrane penetration ability compared to tocopherols [26, 27]. These features contribute to their efficient uptake by targeted cells in addition to exhibiting higher scavenging power due to active recycling [26, 28]. The present study has demonstrated the effectiveness of TRF, a broad mixture of vitamin E, in combating oxidative stress and enhancing antioxidant defense mechanisms in senescent myoblasts, resulting in the improvement of senescence-associated oxidative stress as evidenced by decreased programmed cell death and increased cell viability.

In brief, increased oxidative stress as a result of redox imbalance during aging leads to increased susceptibility of satellite cells to apoptosis and affects muscle regeneration [6, 8, 29, 30]. The findings of this study showed that ROS generation was significantly increased in senescent myoblasts,

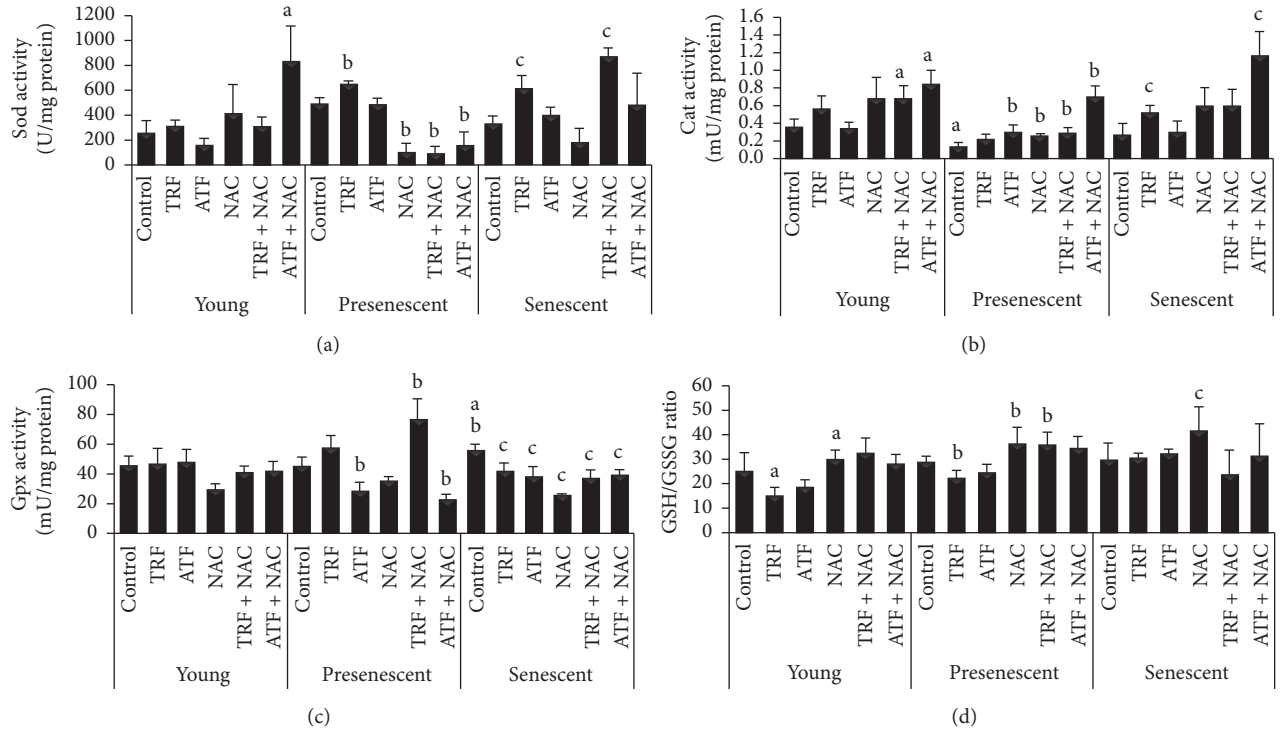

Figure 6: Effects of antioxidants treatment on antioxidant enzymes activities and GSH/GSSG ratio in young, presenescent, and senescent myoblasts. (a) Sod enzyme activity, (b) Cat enzyme activity, (c) Gpx enzyme activity, and (d) GSH/GSSG ratio. [a]Denoting $p < 0.05$, significantly different compared to the young control, [b]$p < 0.05$, significantly different compared to the presenescent control, and [c]$p < 0.05$, significantly different compared to the senescent control. Data are presented as the mean ± SD, $n = 3$.

resulting in higher levels of oxidative damage as indicated by elevated lipid peroxidation. Increased oxidative stress during replicative senescence has been reported to be similar to the conditions in satellite cells derived from aged individuals [8, 10]. Moreover, elevated ROS in myoblasts endangers cellular endurance as shown in our study. We found that the number of viable cells decreased with increasing exogenous H_2O_2 concentration [31].

The presence of free radicals in cells can be counteracted by antioxidant defense systems. However, antioxidant capacity decreases with advancing age, resulting in the accumulation of free radicals, which threaten cell viability [8]. As reported by Fulle and his coworkers [8], the levels of the antioxidant enzymes Cat and glutathione transferase in satellite cells isolated from the elderly were drastically decreased compared to cells from young donors. *SOD1* and *GPX1* mRNA expression were not significantly different across the cell stages. However, *SOD2* and *CAT* mRNA expression were upregulated in presenescent myoblasts, which was similar to Sod activity in a previous study [32]. Additionally, a decline in Cat activity was observed in presenescent myoblasts compared to young myoblasts. Because antioxidant enzymes are regulated in response to oxidative stress [33], we postulated that presenescent myoblasts were attempting to compensate for the decreased Cat levels by upregulating *CAT* mRNA expression to overcome the progressive increase in oxidative stress. Previous study reported that there is a compensatory machinery in antioxidant defense systems which maintains the integrity of muscle [34]. However, we found that senescent cells were less responsive to increased oxidative stress. The levels of *SOD2* mRNA in senescent cells were lower compared to presenescent cells. The expression of *SOD2* mRNA was critical because lack of gene *SOD2* can cause mitochondrial damage and lifespan shortening in *Drosophila* [35]. On the other hand, Gpx activity was increased in senescent myoblasts compared to young and presenescent myoblasts. A previous study also reported enhanced Cat and Gpx activity during aging, which could be an adaptive mechanism to the elevated H_2O_2 levels [36], but the response may be inadequate to counteract the existing ROS.

Our study also reports on the nonenzymatic antioxidants in senescent myoblasts, glutathione [9]. The GSH/GSSG ratio in our study remained unchanged at all ages, which is similar to data reported previously, suggesting that there is no alteration in GSH membrane transportation during aging [37]. Therefore, based on the intracellular ROS levels, lipid peroxidation, and enzymatic antioxidants, our results indicated that senescent myoblasts experience oxidant insults as a result of a less effective antioxidant defense system, which barely counteracted the elevated levels of cellular senescence-associated oxidative stress.

The vitamin E concentration in cells increased with vitamin E treatment (TRF or ATF alone), particularly in TRF-treated myoblasts, which contained all five isomers that were tested. NAC treatment did not affect vitamin E uptake by the cells, as shown by higher levels of vitamin E in myoblasts

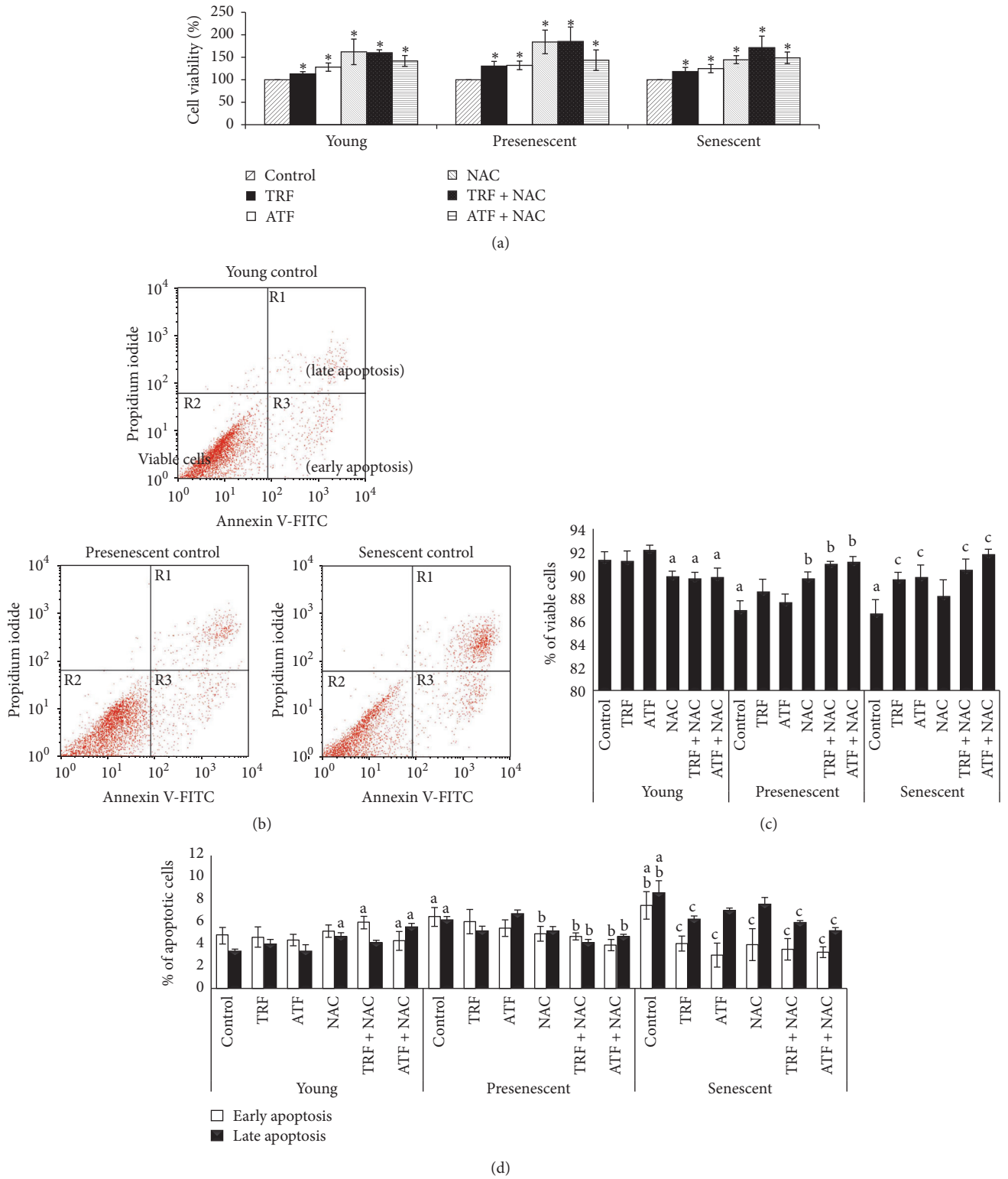

FIGURE 7: Effects of antioxidants treatment on cell viability and apoptosis. (a) The total number of viable cells after antioxidant treatment of young, presenescent, and senescent myoblasts. (b) Dot plot of Annexin V-FITC and PI double staining. Each quadrant represents different cell conditions, which are late apoptotic cells ($FITC^{+ve}/PI^{+ve}$; right upper quadrant; R1); viable cells ($FITC^{-ve}/PI^{-ve}$; left lower quadrant; R2); and early apoptotic cells ($FITC^{+ve}/PI^{-ve}$; right lower quadrant, R3). The cells shifted from the left lower quadrant to the right lower and upper quadrants when transitioning from young to senescent status. (c) The percentage of viable cells. (d) The apoptosis profile of myoblasts in response to all treatments during early and late apoptosis events. *Denoting $p < 0.05$, significantly different compared to respective control groups, $^{a}p < 0.05$, significantly different compared to young control, $^{b}p < 0.05$, significantly different compared to the presenescent control, and $^{c}p < 0.05$, significantly different compared to the senescent control. Data are presented as the mean ± SD, $n = 3$.

treated with TRF + NAC and ATF + NAC compared to cells treated with NAC alone. In brief, vitamin E can act as a nonenzymatic antioxidant to combat oxidative stress [9]. Thus, given its free radical-scavenging power, both TRF-treated and ATF-treated senescent myoblasts demonstrated reductions in their intracellular ROS generation and lipid peroxidation levels. Findings from a previous animal study reported a similar reduction in lipid peroxidation levels after TRF and ATF supplementation [38], revealing the protective effects of vitamin E against oxidative damage. TRF has been reported to improve senescence-associated phenotypes in H_2O_2-induced myoblasts [18]. In another study, ATF showed protective effects in H_2O_2-induced myoblasts [39]. Therefore, both TRF and ATF could potentially be used to protect cells against reactive oxidants.

Our data showed that TRF regulates the expression of antioxidant enzymes in young, presenescent, and senescent myoblasts. *SOD2* mRNA expression was upregulated in all TRF-treated cells, while Sod enzyme activity was upregulated in TRF-treated presenescent and senescent myoblasts. The *SOD2* mRNA encodes one of the Sod isoforms (MnSod), which is located in mitochondrial matrix [40]. Gianni et al. [41] suggested that a superoxide related mitochondrial stress is more apparent than cytosolic stress during aging. Previous studies also reported that increased mitochondrial DNA or RNA mutations were correlated with increasing age and abnormality of aged muscle [42, 43]. Hence, age-related oxidative stress is thought to lead to mitochondrial dysfunction, which eventually may lead to progressive loss of muscle mass and strength [44]. Instead of *SOD1* mRNA, TRF regulated *SOD2* mRNA; thus, we hypothesized that TRF may act on the mitochondria and potentially protect this organelle during aging. The upregulation of *SOD2* mRNA by TRF could be a compensatory mechanism to counteract elevated oxidative challenges in mitochondria during replicative senescence and prevent accumulation of oxidative damage that can trigger cellular aberration. Evidence demonstrated that γ-tocotrienol potentially protects renal proximal tubular cells from oxidant-induced mitochondria dysfunctional and cellular injury [45]. Increased Sod activity with TRF treatment further validated the ability of TRF to modulate the decomposition of superoxide anions to H_2O_2 [38]. However, neither *Sod* mRNA nor enzyme activity was modulated by ATF.

In addition to the significant regulation of Sod activity, TRF treatment also upregulated *CAT* and *GPX1* mRNA in young and senescent myoblasts. However, at the enzyme activity level, TRF increased Cat activity, whereas Gpx activity was reduced in senescent myoblasts. Cat and Gpx work in parallel to remove H_2O_2 in cells [9]. Gpx also catalyzes the elimination of hydroperoxides originated from unsaturated fatty acids at the expense of reduced glutathione [46]. However, the protective role of the glutathione redox cycle is limited at low levels of oxidative stress. During severe oxidant insults, Cat becomes more substantial [46]. Thus, increased Cat at the mRNA and enzyme activity revealed the effectiveness of TRF in enhancing the antioxidant defense system in senescent myoblasts. Because Gpx is involved in hydroperoxide degradation, decreased Gpx in TRF-treated senescent myoblasts may be attributable to decreased lipid peroxidation in cells as reported in this study. This explanation can also be applied to ATF-treated myoblasts, which exhibited decreased Gpx enzyme activity in both the presenescent and senescent stages. In addition, ATF treatment upregulated *CAT* mRNA in senescent cells but at levels that were significantly lower than TRF-treated cells. These findings indicate that TRF potentially improves the antioxidant defense system in senescent myoblasts, and this effect is better than that of ATF.

NAC is a precursor of cysteine that can sustain the production of glutathione, an important antioxidant in cells [47]. In this study, NAC treatment successfully increased the GSH/GSSG ratio in all myoblasts. NAC can scavenge ROS directly [47]. In a previous study, NAC showed protective effects against dystrophic muscle damage in the *mdx* mouse [48] and attenuates fatigue during prolonged exercise [49]. Our results showed that NAC ameliorated myoblast morphology and SA-β-gal staining during senescence, which is similar to the effects of TRF and ATF [19]. Similar effects were also observed in cells treated with combinations of TRF + NAC and ATF + NAC. However, intracellular ROS and lipid peroxidation levels were not modulated by NAC treatment alone during senescence. The rate constants of NAC in reaction with superoxide anion, H_2O_2, and peroxynitrite were comparatively low [47]; consequently, the influence of NAC on the dyes used in this study would be limited. In our study, lipid peroxidation levels were not improved by NAC, as supported by a previous study that measured malondialdehyde (MDA) as a product of lipid peroxidation in the *mdx* mouse [48]. As expected, both combined treatment with TRF + NAC and ATF + NAC lowered lipid peroxidation levels. On the other hand, intracellular ROS levels were only ameliorated by TRF + NAC treatment in senescent myoblasts, suggesting that TRF is better than ATF in scavenging ROS, even at lower concentrations, compared to the concentration used for TRF treatment alone.

The effects of NAC on antioxidant enzymes were only observed for Gpx activity in senescent myoblasts, although a previous study showed that NAC was able to increase antioxidant enzymes in cocaine-induced hepatocytes [50]. We found that NAC modulated the antioxidant enzyme activity in presenescent myoblasts as shown by decreased Sod activity and increased Cat activity with NAC treatment. Treatment of senescent myoblasts with the combination of TRF + NAC resulted in a stronger antioxidant defense response, which involves the upregulation of *SOD2* mRNA expression and the increment in Sod activity, as well as a decrease in Gpx activity, compared to treatment with NAC alone. These results were similar to those observed for TRF-treated senescent myoblasts. Regarding ATF, the combination of ATF + NAC exerted greater effects on antioxidant enzymes compared to treatment with ATF alone. Both Sod activity and Gpx activity decreased whereas Cat activity increased in presenescent myoblasts with ATF + NAC treatment. Increased Cat activity and decreased Gpx activity were also observed in ATF + NAC-treated senescent myoblasts. From the results, both TRF + NAC and ATF + NAC treatment were more effective than NAC alone in ameliorating the

antioxidant defense system, which is similar to previous study that showed combination of NAC and vitamin E has better effect on gentamycin-induced nephrotoxicity compared to NAC alone [51]. Therefore, the improved antioxidant defense mechanisms observed in this study may be attributable to the modulatory effects of vitamin E treatment.

Satellite cells play very important roles in regenerating injured muscle fibers [1]. Despite the availability of satellite cells, which decline with increasing age [52, 53], they may not be the sole reason underlying the impaired regenerative response to injury during aging. Decreased satellite cell proliferative capacity was reported with increased susceptibility to apoptosis, signifying the fact that programmed cell death may also play a part in age-related muscle regeneration impairment [29]. Under stressful stimuli, more satellite cells in old animals underwent apoptosis, thereby distorting skeletal muscle regeneration [29]. However, in a previous study, vitamin E was reported to be able to protect against cell death induced by low doses of oxidants [39]. In another study, it was reported that antioxidant levels were interrelated with the regenerative capacity of muscle stem cells [30]. In short, viable senescent myoblasts were preserved, and the amount of cell death was diminished with TRF treatment, which may be attributed to the improvement of the oxidative status in senescent cells. This may indicate that TRF ameliorates regenerative capacity during aging in human myoblasts [19].

Adequate supply of vitamin E is essential for muscle health. Conversely, vitamin E deficiency can lead to poor muscle performance [12, 14]. A study showed that the antioxidant properties alone are insufficient to repair the injured myoblasts [17]. Lipid-soluble vitamin E can easily diffuse into the hydrophobic membrane and act as a "stabilizer" for lipid membranes to facilitate ROS scavenging activity [17]. Accordingly, the findings of our study showed that both TRF and ATF produced greater effects than NAC in oxidative damage prevention. However, ATF, which is a well-known representative of vitamin E, was not as effective as TRF in protecting against replicative senescence in myoblasts. Although ATF improved the oxidative damage to a similar degree as TRF, TRF is superior in enhancing antioxidant defense mechanism. Previous findings showed that TRF-treated rats exhibited better physical performance and oxidative status than ATF-treated rats [38]. Unlike ATF, TRF is a broad mixture of vitamin E that contains all four isomers of tocotrienol and ATF; thus it should be more potent in scavenging free radicals. The distinctive antioxidant properties of each isomer have been attributed mainly to their chemical structure [54]. For instance, the unsaturated isoprenoid side chain of tocotrienols accounts for a higher peroxyl radical-scavenging potential compared to tocopherols [54]. As a result, even at a lower concentration, TRF is able to improve antioxidant defense mechanism and ameliorate the oxidative status of senescent myoblasts. Previous report suggested that, at low concentrations, γ-tocotrienol can protect cells against H_2O_2-induced apoptosis, while a higher concentration is required for ATF to produce the similar outcome [22]. Our results showed the modulatory effect of TRF is distinguishable compared to other treatments. Previous findings reported that tocotrienols can target a broad range of molecules that might play a role in aging or degenerative diseases [55]. Hence, we suggest that TRF is better than ATF in modulating antioxidant enzymes, particularly at the transcriptional level, to reestablish redox balance in senescent myoblasts.

In summary, our study highlights the effects of TRF on oxidative status in myoblasts during replicative senescence. The results of our study showed increased oxidative stress in senescent myoblasts with reduced antioxidant capacity and increased susceptibility towards programmed cell death or apoptosis, which were distinguishable from young myoblasts. Treatment with TRF in senescent myoblasts resulted in diminished ROS and lipid peroxidation in addition to reinforcing the antioxidant defense system by augmenting antioxidant enzymes levels in senescent myoblasts, which ultimately maintained the number of myoblast cells. In conclusion, TRF is a useful antioxidant that can counteract oxidative stress and improve cellular survival during replicative senescence of myoblasts, and thereby, it can potentially be used to ameliorate muscle regeneration such as sarcopenia, although further experiments should be carried out.

Competing Interests

The authors declare no conflict of interests.

Authors' Contributions

Shy Cian Khor performed the experiments, analyzed the data, and drafted the manuscript. Wan Zurinah Wan Ngah and Norwahidah Abdul Karim participated in designing the study and provided a critical analysis of the manuscript. Yasmin Anum Mohd Yusof provided a critical analysis of the manuscript. Suzana Makpol designed the study, interpreted the data, and revised the manuscript. All of the authors read and approved the final manuscript.

Acknowledgments

This research study was financially supported by Universiti Kebangsaan Malaysia Grants AP-2012-012 and UKM-FF-2013-259. The authors would like to express gratitude to all researchers and staff of the Biochemistry Department, Faculty of Medicine, Universiti Kebangssan Malaysia Medical Centre.

References

[1] S. B. P. Chargé and M. A. Rudnicki, "Cellular and molecular regulation of muscle regeneration," *Physiological Reviews*, vol. 84, no. 1, pp. 209–238, 2004.

[2] A. Mauro, "Satellite cell of skeletal muscle fibers," *The Journal of Biophysical and Biochemical Cytology*, vol. 9, no. 2, pp. 493–495, 1961.

[3] H. Yin, F. Price, and M. A. Rudnicki, "Satellite cells and the muscle stem cell niche," *Physiological Reviews*, vol. 93, no. 1, pp. 23–67, 2013.

[4] V. Mouly, A. Aamiri, A. Bigot et al., "The mitotic clock in skeletal muscle regeneration, disease and cell mediated gene therapy," *Acta Physiologica Scandinavica*, vol. 184, no. 1, pp. 3–15, 2005.

[5] A. J. Cruz-Jentoft, J. P. Baeyens, J. M. Bauer et al., "Sarcopenia: European consensus on definition and diagnosis: report of the European Working Group on Sarcopenia in Older People," *Age and Ageing*, vol. 39, no. 4, pp. 412–423, 2010.

[6] A. Vasilaki and M. J. Jackson, "Role of reactive oxygen species in the defective regeneration seen in aging muscle," *Free Radical Biology and Medicine*, vol. 65, pp. 317–323, 2013.

[7] B. Szczesny, G. Olah, D. K. Walker et al., "Deficiency in repair of the mitochondrial genome sensitizes proliferating myoblasts to oxidative damage," *PLOS ONE*, vol. 8, no. 9, Article ID e75201, 2013.

[8] S. Fulle, S. Di Donna, C. Puglielli et al., "Age-dependent imbalance of the antioxidative system in human satellite cells," *Experimental Gerontology*, vol. 40, no. 3, pp. 189–197, 2005.

[9] E. Doria, D. Buonocore, A. Focarelli, and F. Marzatico, "Relationship between human aging muscle and oxidative system pathway," *Oxidative Medicine and Cellular Longevity*, vol. 2012, Article ID 830257, 13 pages, 2012.

[10] G. Fanò, P. Mecocci, J. Vecchiet et al., "Age and sex influence on oxidative damage and functional status in human skeletal muscle," *Journal of Muscle Research and Cell Motility*, vol. 22, no. 4, pp. 345–351, 2001.

[11] J. P. Chaput, C. Lord, M. Cloutier et al., "Relationship between antioxidant intakes and class I sarcopenia in elderly men and women," *Journal of Nutrition, Health and Aging*, vol. 11, no. 4, pp. 363–369, 2007.

[12] M. Cesari, M. Pahor, B. Bartali et al., "Antioxidants and physical performance in elderly persons: the invecchiare in Chianti (InCHIANTI) study," *American Journal of Clinical Nutrition*, vol. 79, no. 2, pp. 289–294, 2004.

[13] A. Ble, A. Cherubini, S. Volpato et al., "Lower plasma vitamin E levels are associated with the frailty syndrome: the InCHIANTI study," *Journals of Gerontology—Series A Biological Sciences and Medical Sciences*, vol. 61, no. 3, pp. 278–283, 2006.

[14] R. Rafique, A. H. V. Schapira, and J. M. Cooper, "Mitochondrial respiratory chain dysfunction in ageing; influence of vitamin E deficiency," *Free Radical Research*, vol. 38, no. 2, pp. 157–165, 2004.

[15] S. C. Khor, N. Abdul Karim, W. Z. W. Ngah, Y. A. M. Yusof, and S. Makpol, "Vitamin E in sarcopenia: current evidences on its role in prevention and treatment," *Oxidative Medicine and Cellular Longevity*, vol. 2014, Article ID 914853, 16 pages, 2014.

[16] C. K. Sen, S. Khanna, and S. Roy, "Tocotrienols: vitamin E beyond tocopherols," *Life Sciences*, vol. 78, no. 18, pp. 2088–2098, 2006.

[17] A. C. Howard, A. K. McNeil, and P. L. McNeil, "Promotion of plasma membrane repair by vitamin E," *Nature Communications*, vol. 2, article no. 597, 2011.

[18] J. J. Lim, W. Z. Wan Ngah, V. Mouly, and N. Abdul Karim, "Reversal of myoblast aging by tocotrienol rich fraction post-treatment," *Oxidative Medicine and Cellular Longevity*, vol. 2013, Article ID 978101, 11 pages, 2013.

[19] S. C. Khor, A. M. Razak, W. Z. Wan Ngah, Y. A. Mohd Yusof, N. Abdul Karim, and S. Makpol, "The tocotrienol-rich fraction is superior to tocopherol in promoting myogenic differentiation in the prevention of replicative senescence of myoblasts," *PLoS ONE*, vol. 11, no. 2, Article ID e0149265, 2016.

[20] A. Bigot, V. Jacquemin, F. Debacq-Chainiaux et al., "Replicative aging down-regulates the myogenic regulatory factors in human myoblasts," *Biology of the Cell*, vol. 100, no. 3, pp. 189–199, 2008.

[21] T. A. F. T. Ahmad, Z. Jubri, N. F. Rajab, K. A. Rahim, Y. A. M. Yusof, and S. Makpol, "Gelam honey protects against gamma-irradiation damage to antioxidant enzymes in human diploid fibroblasts," *Molecules*, vol. 18, no. 2, pp. 2200–2211, 2013.

[22] M. Mazlan, T. Sue Mian, G. Mat Top, and W. Zurinah Wan Ngah, "Comparative effects of α-tocopherol and γ-tocotrienol against hydrogen peroxide induced apoptosis on primary-cultured astrocytes," *Journal of the Neurological Sciences*, vol. 243, no. 1-2, pp. 5–12, 2006.

[23] W. F. Beyer Jr. and I. Fridovich, "Assaying for superoxide dismutase activity: some large consequences of minor changes in conditions," *Analytical Biochemistry*, vol. 161, no. 2, pp. 559–566, 1987.

[24] H. Aebi, "Catalase *in vitro*," *Methods in Enzymology*, vol. 105, pp. 121–126, 1984.

[25] D. E. Paglia and W. N. Valentine, "Studies on the quantitative and qualitative characterization of erythrocyte glutathione peroxidase," *The Journal of Laboratory and Clinical Medicine*, vol. 70, no. 1, pp. 158–169, 1967.

[26] E. Serbinova, V. Kagan, D. Han, and L. Packer, "Free radical recycling and intramembrane mobility in the antioxidant properties of alpha-tocopherol and alpha-tocotrienol," *Free Radical Biology and Medicine*, vol. 10, no. 5, pp. 263–275, 1991.

[27] Y. J. Suzuki, M. Tsuchiya, S. R. Wassall et al., "Structural and dynamic membrane properties of α-tocopherol and α-tocotrienol: iimplication to the molecular mechanism of their antioxidant potency," *Biochemistry*, vol. 32, no. 40, pp. 10692–10699, 1993.

[28] Y. Saito, Y. Yoshida, K. Nishio, M. Hayakawa, and E. Niki, "Characterization of cellular uptake and distribution of vitamin E," *Annals of the New York Academy of Sciences*, vol. 1031, pp. 368–375, 2004.

[29] S. S. Jejurikar, E. A. Henkelman, P. S. Cederna, C. L. Marcelo, M. G. Urbanchek, and W. M. Kuzon Jr., "Aging increases the susceptibility of skeletal muscle derived satellite cells to apoptosis," *Experimental Gerontology*, vol. 41, no. 9, pp. 828–836, 2006.

[30] K. L. Urish, J. B. Vella, M. Okada et al., "Antioxidant levels represent a major determinant in the regenerative capacity of muscle stem cells," *Molecular Biology of the Cell*, vol. 20, no. 1, pp. 509–520, 2009.

[31] V. Renault, L.-E. Thornell, G. Butler-Browne, and V. Mouly, "Human skeletal muscle satellite cells: aging, oxidative stress and the mitotic clock," *Experimental Gerontology*, vol. 37, no. 10-11, pp. 1229–1236, 2002.

[32] S. Makpol, T. W. Yeoh, F. A. C. Ruslam, K. T. Arifin, and Y. A. M. Yusof, "Comparative effect of *Piper betle*, *Chlorella vulgaris* and tocotrienol-rich fraction on antioxidant enzymes activity in cellular ageing of human diploid fibroblasts," *BMC Complementary and Alternative Medicine*, vol. 13, article 210, 2013.

[33] A. A. Franco, R. S. Odom, and T. A. Rando, "Regulation of antioxidant enzyme gene expression in response to oxidative stress and during differentiation of mouse skeletal muscle," *Free Radical Biology and Medicine*, vol. 27, no. 9-10, pp. 1122–1132, 1999.

[34] M. J. Sullivan-Gunn and P. A. Lewandowski, "Elevated hydrogen peroxide and decreased catalase and glutathione peroxidase protection are associated with aging sarcopenia," *BMC Geriatrics*, vol. 13, no. 1, article 104, 2013.

[35] I. Martin, M. A. Jones, D. Rhodenizer et al., "*Sod2* knockdown in the musculature has whole-organism consequences in

Drosophila," *Free Radical Biology and Medicine*, vol. 47, no. 6, pp. 803–813, 2009.

[36] M. E. Inal, G. Kanbak, and E. Sunal, "Antioxidant enzyme activities and malondialdehyde levels related to aging," *Clinica Chimica Acta*, vol. 305, no. 1-2, pp. 75–80, 2001.

[37] B. Marzani, O. Pansarasa, and F. Marzatico, "'Oxidative stress' and muscle aging: influence of age, sex, fiber composition and function," *Basic and Applied Myology*, vol. 14, pp. 37–44, 2004.

[38] S.-P. Lee, G.-Y. Mar, and L.-T. Ng, "Effects of tocotrienol-rich fraction on exercise endurance capacity and oxidative stress in forced swimming rats," *European Journal of Applied Physiology*, vol. 107, no. 5, pp. 587–595, 2009.

[39] V. A. Nunes, A. J. Gozzo, I. Cruz-Silva et al., "Vitamin E prevents cell death induced by mild oxidative stress in chicken skeletal muscle cells," *Comparative Biochemistry and Physiology Part C: Toxicology & Pharmacology*, vol. 141, no. 3, pp. 225–240, 2005.

[40] I. N. Zelko, T. J. Mariani, and R. J. Folz, "Superoxide dismutase multigene family: a comparison of the CuZn-SOD (SOD1), Mn-SOD (SOD2), and EC-SOD (SOD3) gene structures, evolution, and expression," *Free Radical Biology and Medicine*, vol. 33, no. 3, pp. 337–349, 2002.

[41] P. Gianni, K. J. Jan, M. J. Douglas, P. M. Stuart, and M. A. Tarnopolsky, "Oxidative stress and the mitochondrial theory of aging in human skeletal muscle," *Experimental Gerontology*, vol. 39, no. 9, pp. 1391–1400, 2004.

[42] A. Cormio, F. Milella, J. Vecchiet, G. Felzani, M. N. Gadaleta, and P. Cantatore, "Mitochondrial DNA mutations in RRF of healthy subjects of different age," *Neurobiology of Aging*, vol. 26, no. 5, pp. 655–664, 2005.

[43] V. Pesce, A. Cormio, F. Fracasso et al., "Age-related mitochondrial genotypic and phenotypic alterations in human skeletal muscle," *Free Radical Biology and Medicine*, vol. 30, no. 11, pp. 1223–1233, 2001.

[44] C. M. Peterson, D. L. Johannsen, and E. Ravussin, "Skeletal muscle mitochondria and aging: a review," *Journal of Aging Research*, vol. 2012, Article ID 194821, 20 pages, 2012.

[45] G. Nowak, D. Bakajsova, C. Hayes, M. Hauer-Jensen, and C. M. Compadre, "γ-tocotrienol protects against mitochondrial dysfunction and renal cell death," *Journal of Pharmacology and Experimental Therapeutics*, vol. 340, no. 2, pp. 330–338, 2012.

[46] J. M. Matés, "Effects of antioxidant enzymes in the molecular control of reactive oxygen species toxicology," *Toxicology*, vol. 153, no. 1–3, pp. 83–104, 2000.

[47] Y. Samuni, S. Goldstein, O. M. Dean, and M. Berk, "The chemistry and biological activities of N-acetylcysteine," *Biochimica et Biophysica Acta (BBA)—General Subjects*, vol. 1830, no. 8, pp. 4117–4129, 2013.

[48] J. R. Terrill, H. G. Radley-Crabb, M. D. Grounds, and P. G. Arthur, "N-Acetylcysteine treatment of dystrophic mdx mice results in protein thiol modifications and inhibition of exercise induced myofibre necrosis," *Neuromuscular Disorders*, vol. 22, no. 5, pp. 427–434, 2012.

[49] I. Medved, M. J. Brown, A. R. Bjorksten et al., "N-acetylcysteine enhances muscle cysteine and glutathione availability and attenuates fatigue during prolonged exercise in endurance-trained individuals," *Journal of Applied Physiology*, vol. 97, no. 4, pp. 1477–1485, 2004.

[50] A. Zaragoza, C. Díez-Fernández, A. M. Alvarez, D. Andrés, and M. Cascales, "Effect of N-acetylcysteine and deferoxamine on endogenous antioxidant defense system gene expression in a rat hepatocyte model of cocaine cytotoxicity," *Biochimica et Biophysica Acta—Molecular Cell Research*, vol. 1496, no. 2-3, pp. 183–195, 2000.

[51] H. M. A. El-Fattah and N. M. El-Sheikh, "Evaluation of chemoprotective role of N-acetylcysteine and vitamin E on gentamicininduced nephrotoxicity," *Australian Journal of Basic and Applied Sciences*, vol. 6, no. 3, pp. 263–270, 2012.

[52] V. Renault, L.-E. Thorne, P.-O. Eriksson, G. Butler-Browne, and V. Mouly, "Regenerative potential of human skeletal muscle during aging," *Aging Cell*, vol. 1, no. 2, pp. 132–139, 2002.

[53] C. A. Collins, P. S. Zammit, A. Pérez Ruiz, J. E. Morgan, and T. A. Partridge, "A population of myogenic stem cells that survives skeletal muscle aging," *Stem Cells*, vol. 25, no. 4, pp. 885–894, 2007.

[54] L. Müller, K. Theile, and V. Böhm, "In vitro antioxidant activity of tocopherols and tocotrienols and comparison of vitamin E concentration and lipophilic antioxidant capacity in human plasma," *Molecular Nutrition & Food Research*, vol. 54, no. 5, pp. 731–742, 2010.

[55] B. B. Aggarwal, C. Sundaram, S. Prasad, and R. Kannappan, "Tocotrienols, the vitamin E of the 21st century: its potential against cancer and other chronic diseases," *Biochemical Pharmacology*, vol. 80, no. 11, pp. 1613–1631, 2010.